Photophysical Exploration of Rigidly Coupled Dimers for Singlet Fission and Triplet-Triplet Annihilation Upconversion

by

Alexander Thomas Gilligan

B.S., University of North Carolina at Chapel Hill, 2015

A thesis submitted to the

Faculty if the Graduate School of the

University of Colorado in partial fulfillment

of the requirement for the degree of

Doctor of Philosophy

Department of Chemistry

2023

Committee Members:

Niels Damrauer

Justin Johnson

Garry Rumbles

Tarek Sammakia

Gordana Dukovic

Gilligan, Alexander Thomas (Ph.D., Physical Chemistry)

Photophysical Exploration of Rigidly Coupled Dimers for Singlet Fission and Triplet-Triplet Annihilation Upconversion

Thesis directed by Professor Niels Damrauer

Abstract

The Sun is a nearly unlimited source of energy that can be used on Earth to power society without substantial impact to the broader environment that humanity depends on. Decades of work by the scientific community have gone into understanding the science of solar energy and engineering it for useful application. Fundamental limits prevent taking full advantage of available solar energy. Exciton downconversion/upconversion in organic systems, also known as singlet fission (SF) and triplet-triplet annihilation (TTA), are photophysical processes that can potentially overcome these limits. The acene series are a group of organic chromophores that fulfill the strict energetic requirements to perform SF and TTA via there singlet (S_1) and triplet (T_1) states.

A series of rigidly coupled acene dimers were photophysically characterized to probe fundamental aspects of SF and TTA. Tetracene and pentacene based dimers were both shown to undergo SF on the ultrafast timescale based on the observed rate constant (k_{SF}). While the pentacene dimer measured a unity SF yield the tetracene dimer was only ~50 % due to differences in the SF driving force (ΔG). Studies of the tetracene dimer were also performed in a polar solvent environment to measure the impact of the charge-transfer (CT) state, an important intermediate state in the SF process. They showed that CT state formation to be parasitic to productive SF.

Another tetracene dimer paired with a metal phthalocyanine sensitizer were used to generate anti-Stokes emission to study TTA upconversion (TTA-UC). Compared to a monomer reference the dimer demonstrated increased upconversion photoluminescence. Kinetic modeling

of upconversion system showed this result to be due to enhancement of the TTA rate constant (k_{TTA}).

Acknowledgements

To Niels: Simply put, this work wouldn't exist without you. During the time working for you I've been astounded by your ability to think deeply and ask questions about scientific work. In doing so you always pushed to achieve excellent work and grow as scientists as a result. On a personal note, you asked an even more fundamental question. Can we grow to become more than we are presently? It's one of the big questions in life and I'll always be thankful for you daring to ask more.

To Jasper, Sam, Thomas and Steve: I could not have asked for a better group of graduate students to learn under. Every day with y'all was both an opportunity to learn something from y'all and have fun doing so. Starting graduate school, you quickly learn how much you don't know and that you need to ask questions to what you do need to know. Thank you answering the million questions I asked, especially the dumb ones, and contributing to all the knowledge in this work.

To Steven, Ryan and Izzy: Y'all were the best group of coworkers/friends anyone could ask for. Coming into the office everyday and working with y'all was always a source of inspiration, even when things weren't working the way they should. Even the times we'd just hang out in the office and have fun were always a great source of relief to me. To journey with y'all was a privilege that I'm thankful for every day.

To Ethan: You made a lot of the molecules here and I'd study them (and try to destroy them). The work in this dissertation is as much yours as it is mine. Watching from the outside you're a MasterChef of organic chemistry. You also seemed to enjoy my interests of obscure history, strategy games, pop culture and current events. Through the easy times and tough ones you've been a great companion. Having a friend like you is a rare privilege.

To Nick, Jenny, Raythe, Arindam and Angelina: Watching y'all grow over the years has been an incredible experience. In one moment, I'm a teacher and then the next moment y'all are for me. The lab is in a good place with y'all at the helm. I envy what discoveries you'll find and can't wait to see them.

To friends made along the way: Peyton, from the days of Game of Thrones to today, I look forward to every Sunday. Andrew, from sharing tips on lasers to BBQ you've been a true friend. Thank you. Will, your dedication excellence in your chemistry was something I always admired as well as your friendship. Eric, I will miss all the great conversations had over coffee/lunch breaks with you

To the Papanikolas Family: Micah, Carribeth and John, y'all are immensely responsible for both nurturing my interest in chemistry in my high school/undergraduate studies and selecting Boulder as the place to continue them for my Ph.D. Thank you for guiding me all these years.

To Mom and Dodie: From my very first days on Earth to today I'm thankful to y'all for raising me be both a good scientist and a good person. The past year has been the toughest of my life and the support and love you've given over that time is something I'm thankful for every day of my life. Hopefully I remember to tell y'all that often enough.

To Dad: You've been my biggest supporter for my time in graduate school, offering advice and support when times were tough. I wish you could be here for the final result. I've got Bennie and Tris and they're happy as can be. I'm thankful every day for being your son and I'll love you forever Dad.

Table of Contents

List of Tables

List of Figures

Chapter 1: Introduction

1.1 Global Industrialization and Global Consequences

Global industrialization has led to an unprecedented demand for electrical power and majority of this demand has been supplied by the combustion of fossil fuel resources, leading to anthropogenic global warming.[1] Fig. 1.1 shows the steady increase in greenhouse gas emissions principally due to carbon dioxide over the past three decades. Projections of global warming show significant impact on society as soon as 2050 and have already begun to manifest in the form of extreme climate events.[2] To combat this global warming while providing for current energy needs, national governments are exploring alternative, renewable sources of energy (hydroelectric, wind, geothermal, solar).[3] Particular attention has been paid to the field of solar energy, which has increased from less than 1 GW in 2010 to over 70 GW in 2020 in the United States.[4] Solar energy has made significant progress over the past decade towards parity, both with fossil fuels and other renewable sources such as wind power.[3]

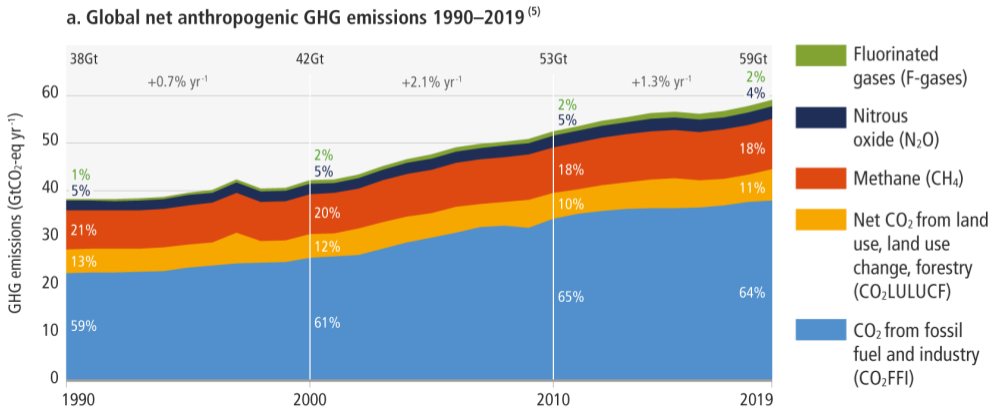

Figure 1.1 Breakdown of greenhouse gas emissions contributing to anthropogenic global warming. Courtesy of IPCC Sixth Assessment Report: Climate Change 2022: Mitigation of Climate Change (ref. 3).

While significant effort on the part of the scientific community has gone into developing new materials capable of increased solar harvesting efficiency, the vast majority of solar cell production is single junction silicon devices due to their ever lowering cost.[5] All single junction semiconductors face a fundamental limit in their efficiency for solar energy conversion based on their bandgap. Shockley and Queisser reported that the maximum efficiency of a silicon solar cell under typical Earth conditions was only ~30 %, based on its bandgap of 1.1 eV, meaning ~70 % of potential energy is lost.[6] The same work also determined that with an ideal bandgap the maximum efficiency of a single junction cell is only ~33 % at 1.3 eV.[6] Current silicon technology is approaching this limit as shown in Fig. 1.2. This wastes the majority of potential of many photons to provide useable energy. The primary losses in single bandgap solar cells are 1. the thermal relaxation of photoexcited electron-hole pairs from above-bandgap photons to the bandgap of the semiconductor material and 2. sub-bandgap photons that are unable to produce charge carriers. Maximizing photovoltaic efficiency requires designing systems that can overcome these limitations.

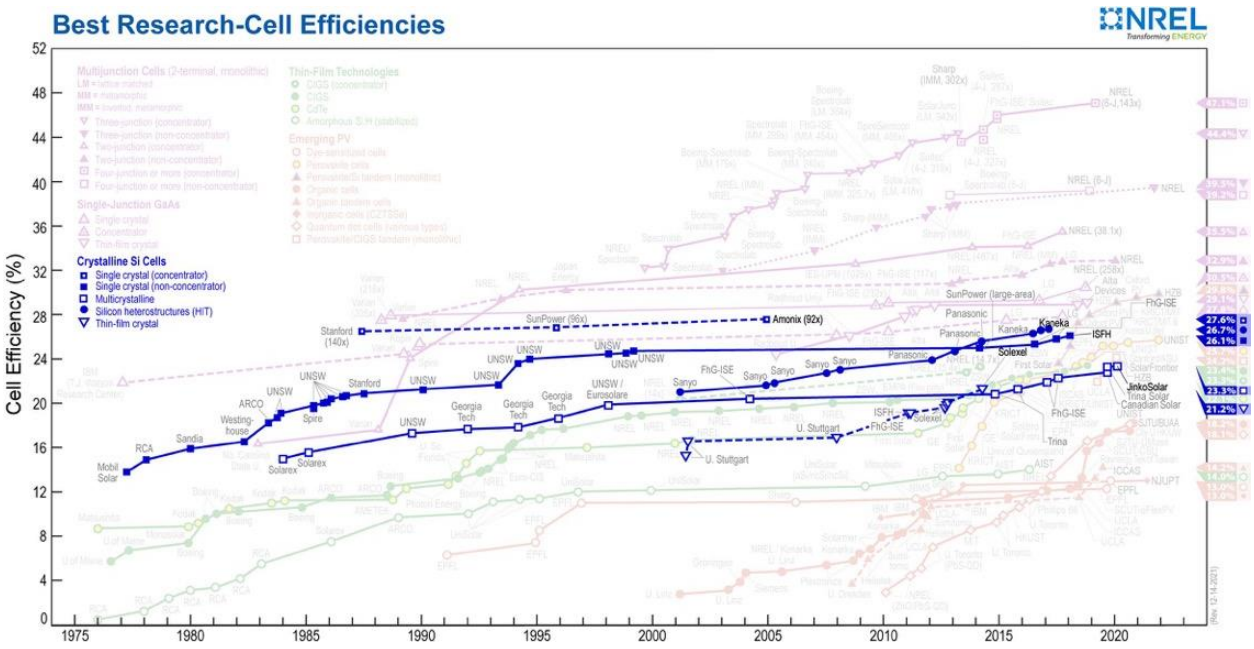

Figure 1.2 Silicon solar cell efficiencies as reported by the National Renewable Energy Laboratory as of September 2022.

To overcome the limits of the Shockley-Queisser analysis, either a multi-junction platform needs to be used, which can be expensive and technologically complex, or an alternative cell architecture is needed that allows for the efficient capture of above and sub-bandgap photons. We'll start with above bandgap photons since they contribute the larger share of loss in efficiency for lower bandgap materials (in silicon the efficiency loss from above bandgap photons is ~40 %).[7] An alternative exists that allows for the utilization of other bandgap materials while maintaining the effective cost basis of already established solar cell technology and construction. This alternative is multiple-exciton generation (MEG) where higher-energy photons are absorbed by the material and split into several lower-energy excited states that can be extracted into useful photocurrent.[8] Ideally the energy of the newly split lower-energy excitons can then be matched to the bandgap of an existing cell material, allowing for the extraction of photocurrent from the primary cell and the MEG cell simultaneously.[9,10] This combination MEG cell is capable of

increasing the solar conversion efficiency (SCE) limit from 33 % up to 48 % depending on the MEG-cell combination.[11]

1.2 Singlet Fission and Triplet-Triplet Annihilation

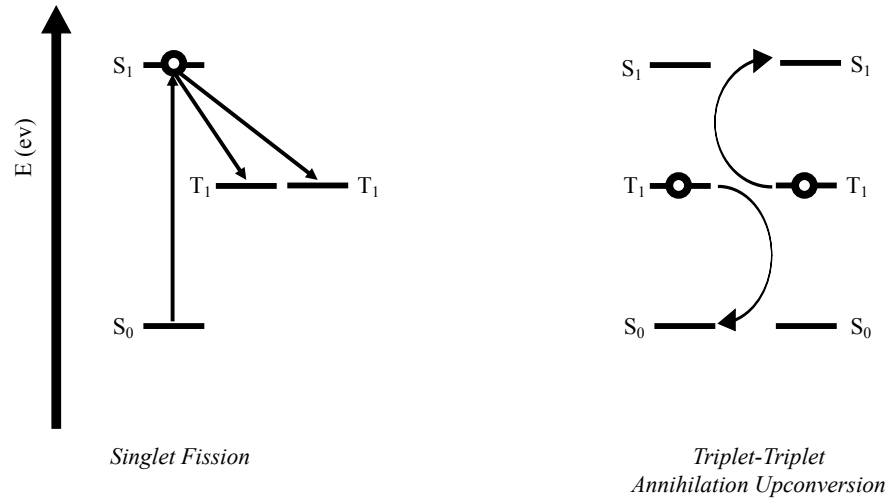

Figure 1.3 Energy diagrams for singlet fission and triplet-triplet annihilation.

A subset of multi-exciton generation is the process known as singlet fission, where a singlet exciton is split into two lower energy triplet excitons (for a maximum yield of 200 %). This photophysical process has been observed primarily in organic chromophores. Singlet fission was discovered in the 1960's, but there has been a resurgence of interest starting in the early 2000's due to both interest in improving solar energy conversion and interest in expansion in materials/experiments that can be used to probe the underlying photophysics.[9,11] Work by Nozik et al. showed that with an ideal singlet fission material in conjunction with a silicon solar cell could increase the SCE from 30 % to 45 %, a half again increase achieved by adding a viable singlet

fission material onto a photovoltaic cell that absorbs and splits high energy photons into two excitons close to the band-gap of the solar cell, minimizing thermalization losses.[9]

In organic chromophores, intersystem crossing (the nonradiative transition between two states of different spin-multiplicity) is often a slow process due to low spin-orbit coupling, such that triplet yields are often small. Intersystem crossing rate constants can be increased, to allow for large triplet yields via methods such as the heavy atom effect or transitioning to an energetically higher lying triplet before relaxing to the T_1, the lowest energy triplet. Singlet fission has been observed to form triplets on ultrafast timescales (on the order of 10^{-15} to 10^{-12} seconds), significantly faster than compared to most instances of intersystem crossing in organic chromophores (cases of the heavy-atom effect and higher energy triplet intermediates can also perform intersystem crossing on ultrafast timescales but are still limited to 100 % triplet yields). The rapid formation of triplet products in SF materials after photoexcitation suggests an intermediate state that maintains spin conservation while allowing for triplet excited state character. This intermediate state (hereafter referred to as the multiexcitonic coupled-triplet TT state) allows for the rapid formation of triplet electronic character in SF chromophores and has been the focus of intense study due to its essential but elusive role in the SF process. The basic singlet fission process is shown in Equation 1.

$$S_1 + S_0 \rightarrow {}^1TT \rightarrow T_1 + T_1 \qquad (1.1)$$

In order for singlet fission to occur in an experimental system, several requirements must be met beforehand.[11] The initially excited singlet state (S_1) should have an approximate energy that is twice the lowest triplet energy or $E(S_1) \geq 2 \times E(T_1)$. This is to ensure that there is sufficient energetic driving force to favor product formation. Additionally, there must be sufficient electronic

coupling between the initial S_1 and the ^{1}TT to allow for the rapid formation of the desired triplet products before decay to the ground-state or intersystem crossing occurs.

Of additional importance is the spin-dephasing from the TT state into independent triplets as the final product of singlet fission. The multiexcitonic TT has been the focus of significant efforts due to its importance in the singlet fission process.[12] While Equation 1 presents the TT state as a simple intermediate in singlet fission, in reality it masks the complex nature of the coupled triplet manifold. The coupled triplet state itself is composed of multiple states, based on their spin configuration, the ^{1}TT, ^{3}TT and ^{5}TT. Low electronic state couplings between the S_1 and ^{1}TT have suggested an additional intermediate state may be important, a charge-transfer state, that allows for energy transfers to occur.[13]

Singlet fission has since been studied in a variety of systems, from concentrated monomeric solutions of suitable chromophores[14,15] to prepared thin films.[16–18] Work by Bardeen first demonstrated the use of organic dimers as a viable framework to interrogate the singlet fission process itself.[19] Solution-based dimers offer the advantage of reducing a viable SF system to the fewest required components, two closely space chromophores, while concentrated solutions and thin film systems can introduce additional processes into the system, such as excimer formation that can obscure the SF event.[20]

Triplet-triplet annihilation (TTA) on the other hand is fundamentally the reverse process of singlet fission. Like singlet fission, it too was discovered in the 1960's in anthracene crystals.[21] In TTA two low energy triplet states are energetically upconverted into a singlet state that photoluminesces a higher energy photon. Similar to singlet fission, TTA has been investigated as a means of improving SCE by harvesting sub-bandgap photons.[22] In this scenario the two annihilated triplets are generated by sensitization from a sub-bandgap source, making the process

triplet-triplet annihilation upconversion (TTA-UC). A theoretical upconversion solar cell was shown to have a maximum possible SCE of ~48 %.[23] This is comparable to the optimized output from SF-silicon tandem cell and represents a significant gain over traditional single junction cells. It should be noted that these maximum efficiencies for SF & TTA-UC are heavily dependent on the bandgap of the base material. Moving to higher-energy bandgaps compared to Si, such as perovskite materials, will necessitate focusing on capturing sub-bandgap photons via TTA-UC compared with SF.

TTA-UC systems consist of two chromophores, referred to as the sensitizer and the annihilator species. The process of TTA-UC is described here briefly. Photoexcitation of the sensitizer species generates the initial excited population. This initial population undergoes intersystem crossing to generate long-lived triplet states. In the triplet state a sensitizer molecule can undergo energy transfer through a Dexter mechanism to transfer a triplet state onto the annihilator species. Two annihilator triplets can then collide to form an encounter complex, and energy is then transferred from one annihilator to the other, yielding one ground-state species and one with an excited singlet state. This excited singlet state can fluoresce photons of a higher energy than those of the initial excitation.

Just as with singlet fission, TTA-UC requires that several conditions be met for efficiency.[24] In TTA-UC the annihilator S_1 should be slightly less than approximately twice the energy of its T_1 $E(S_1) \leq 2 \times E(T_1)$, the opposite of the SF condition described previously). Additionally, a large fluorescence quantum yield is necessary to efficiently extract the upconverted photons. TTA-UC faces the additional challenge of selecting a sensitizer with favorable photophysical characteristics. A sensitizer should have a T_1 energy slightly greater than that of the annihilator so that triplet energy transfer proceeds efficiently. While not strictly necessary for

upconversion to occur, an efficient sensitizer will also have a high intersystem crossing yield with a long triplet lifetime (of at least 1 μs) to maximize the triplet energy transfer yield.

As with singlet fission the spin manifold of the resulting products after the triplet-triplet annihilation event must be considered. A collision of two triplets can result in up to 9 different spin microstates. This resulting encounter spin complex will result in a net singlet in 1/9th of all collisions, a triplet in 3/9th and a quintet complex in 5/9th. Of these only the singlet produces the photoluminescence desired in TTA-UC, suggesting upconversion can have a maximum efficiency of only ~11 %. Upconversion quantum yields larger than this limit have been observed in many systems suggesting that either triplets aren't simply quenched during the formation of this spin complex and are allowed to attempt triplet-triplet annihilation again before the triplet decays to the ground state or that interconversion is occurring in the spin manifold, allowing for the productive singlet to be formed eventually.[24] Unraveling details of the spin mechanics and populations occurring in TTA-UC has been the focus of many experimental and theoretical studies.

As a final note on singlet fission and triplet-triplet annihilation upconversion with regards to SCE, the previous discussion has demonstrated the viability for SF to harvest above bandgap photons more efficiently and for TTA-UC to harvest sub-bandgap photons. The combination of these two processes into a single solar cell architecture would maximize the efficiency of solar energy conversion.

1.3 The Acene Series

Singlet fission and triplet-triplet annihilation upconversion have been studied in a wide variety of organic chromophores, such as diimides[25–28] and isobenzofurans,[16,29,30] but the primary class of molecules examined is that of linear polycyclic aromatic hydrocarbons, in particular the

acene series. Acenes are a class of molecules where multiple aromatic rings are fused together to create highly conjugated systems. The simplest of these molecules is naphthalene, consisting of two fused benzene rings. It should be noted that in TTA-UC systems the organic chromophore is most often used as the annihilator species that produces the useful photoproduct.

While the family of isolated acene derivatives has been extended up to nonacene (number of rings, n = 9)[31] the fields of SF and TTA-UC focus on the molecules anthracene, tetracene and pentacene (n = 3, 4, 5) and various derivatives with chemical modifications to tune desired photophysical properties.[11,32] Polycyclic aromatic hydrocarbons possess many qualities that make them ideal systems for the study of singlet fission and triplet-triplet annihilation. They are good photoabsorbers with molecular attenuation coefficients on the order of ~10,000 $M^{-1}cm^{-1}$ in the visible spectrum range of light (~400 – 700 nm). With regards to both SF and TTA-UC their most important quality is the large energetic splitting between their S_1 and T_1 states, that produces the favorable condition of $E(S_1) \cong 2 \times E(T_1)$ necessary for both singlet fission and triplet-triplet annihilation. This arises from the large exchange energy due to their status as alternant hydrocarbons.[33] This exchange energy stays fairly consistent as the acene system is extended so that larger acenes will have relatively greater S_1 - T_1 gaps.[11] Fig. 1.4 shows the relative energetic spacing for S_1 and T_1 with regards to anthracene, tetracene and pentacene along with the Si bandgap.

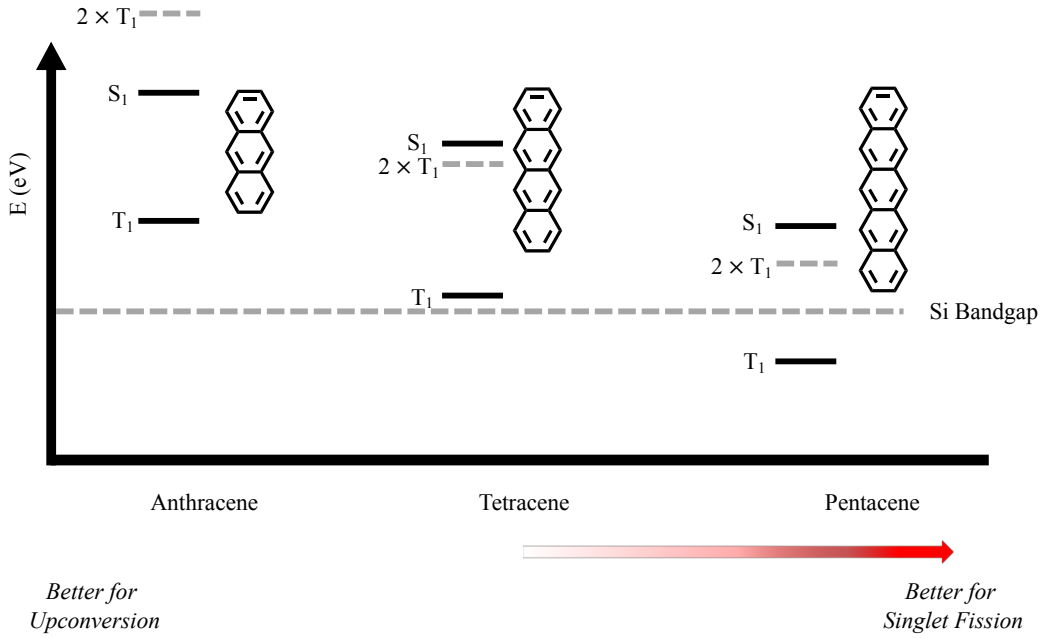

Figure 1.4 Comparison of relevant state energies for three acenes that characterize the study of SF and TTA-UC. State energies are measured solution-phase values.[34]

Anthracene (n = 3) is observed to have an S_1 of 3.30 eV with a T_1 of 1.84 eV. This gives $2\times T_1$ a value of 3.68 eV, presenting a 500 meV energetic barrier for singlet fission that makes it unlikely, but provides substantial driving force for triplet-triplet annihilation to occur. Indeed, one of the most common annihilator used in upconversion studies is a derivative of anthracene, 9,10-diphenylanthracene (DPA).[35–38] The phenyl substitutions in this case improve the TTA-UC performance over anthracene by reducing the otherwise competitive intersystem crossing quantum yield. Tetracene (n = 4) has an S_1 of 2.63 eV with a T_1 of 1.28 eV based on solution phase measumrents.[34] A $2\times T_1$ energy of 2.56 eV makes singlet fission energetically favorable. Indeed, tetracene has been shown to have a SF triplet yield of ~200 % (the maximum possible triplet yield through singlet fission), although these results came from crystals of tetracene.[11] The slight bias in favor of $2\times T_1 < S_1$ suggests that tetracene will also be capable of performing TTA-UC, albeit with a 50 meV energetic barrier. It should be noted at this point that the T_1 energy, 1.28 eV, is slightly

above the silicon bandgap (1.1 eV), making it an ideal material to use in conjunction with the most common solar cell material. Pentacene (n = 5) has a S_1 of 2.12 eV with a reported T_1 of 0.78 eV, the lowest of the discussed acene series.[34] In the case of pentacene a $2\times T_1$ energy of 1.56 eV would be insufficient driving force for upconversion to occur but would greatly favor singlet fission. Indeed, pentacene has been observed to undergo SF in <100 fs.[39] Broadly speaking of the acene molecules discussed so far, increasing the conjugated system decreases the lowest excited S_1 through electronic delocalization and increases the strength of the exchange interaction, decreasing the T_1 energy relative to that of the S_1. This makes singlet fission more favorable proceeding along the molecular series while disfavoring TTA-UC as shown in Fig. 1.4.

One challenge with acenes is their susceptibility to oxidation as the number of rings is increased. The electron rich π systems of acenes can undergo a Diels-Alder cycloaddition with oxygen that interrupts the conjugated π system.[40] To mitigate this the field has turned to the electron withdrawing substitutions on the polyacene such as the triisopropylsilyl acetylene groups (shortened to TIPS-acetylene groups).[41] The electron withdrawing effect of the acetylene groups reduces the susceptibility of the core conjugated system to cycloaddition by oxidation. The central ring of the polyacene is most vulnerable to oxidation due to greater HOMO density. Placement of TIPS-acetylene groups at this central location maximizes their effectiveness. These functionalizations have the added benefit of enhancing the solubility of the species, which are otherwise prone to aggregation at even low concentrations.

While providing additional stability to the acene, the electron withdrawing nature of the TIPS groups will have an impact on state energies that must be considered. The electron withdrawing effect of TIPS-acetylene on the acene will reduce the HOMO-LUMO gap leading to a corresponding decrease in the energy of the first excited state. This orbital reduction will also

impact the T_1 state due to it having the same orbital construction as the S_1, leading to a reduction in the triplet state energy as well. An equivalent reduction in the S_1 and T_1 state energies will make a chromophore more favorable to perform SF, while making TTA-UC unfavorable. In the chromophore tetracene it's reported S_1 energy is 2.63 eV while its T_1 energy is 1.28 eV, presents a favorable 50 meV driving force for SF to occur. The TIPS functionalized version of tetracene (TIPS-Tc) by contrast has an S_1 of 2.30 eV and a T_1 of 1.21 eV. This now presents an ~100 meV barrier to SF occurring, but now makes TTA favorable compared to unfunctionalized tetracene.

1.4 Rigidly Coupled Dimers for Photophysical Investigation of SF & TTA

Both SF & TTA-UC can be reduced to a two-chromophore system at its simplest. Molecular dimers of organic chromophores offer a powerful tool to study the underlying photophysics of SF & TTA-UC. Dimers offer a means of covalently coupling the chromophores together to allow for the study of SF & TTA-UC. While this can lock the interchomophore distance between the two molecules it still permits their free rotation that can result in sampling an orientational distribution. This can impact important parameters such as electronic coupling due to the significant dependence of chromophore orientation. Rigid coupling seeks to lock interchromophore distance while also maintaining chromophore orientation. Maintaining structural rigidity is important as it allows for mechanistic insight to the multi-exciton manifold that can impact product formation for both SF & TTA.

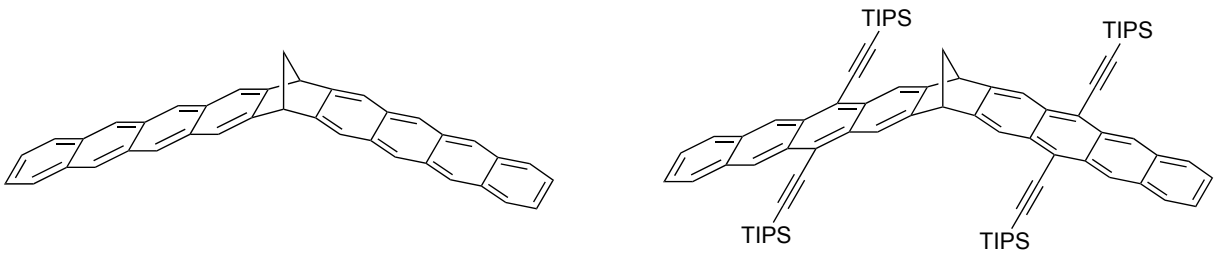

Figure 1.5 Geometric structures of previous dimer studied within the Damrauer Group. Referred to as BT1 (left) and TIPS-BT1 (right).

Previous work in the Damrauer Group has concerned the synthesis and photophysical study of two rigidly coupled tetracene dimers, referred to as BT1 and TIPS-BT1 (as shown in Fig. 1.5). The synthesis of these molecules was guided by theoretical work of Paddon-Row[42–46] that showed bridging via a norbornyl bridge provide sufficient electronic through-bond and through-space coupling for long-range electron transfer between the two chromophores. Such well-defined control of electronic coupling is desired for studying the SF and TTA-UC processes. The primary findings are briefly summarized as the following. BT1 was shown to undergo biexponential decay to the ground state monitoring the fluorescent S_1 via TCSPC, compared to the monomeric norbornyl-bridge tetracene which only showed single exponential decay.[47] Kinetic analysis determined the establishment of an equilibrium between S_1 and ^{1}TT resulting in small (~6 %) shift to ^{1}TT. Further analysis calculated an equilibrium constant of K = ~0.05, corresponding to a $\Delta G_{fiss} = \sim 25\ meV$. The endoergic nature of singlet fission in BT1 introduces a significant barrier to achieving unity ^{1}TT yield. Due to difficulties in synthesis and sample preparation the synthetic scheme for BT1 was modified to introduce TIPS-acetylene groups into the dimer. This new dimer, TIPS-BT1, was photophysically characterized in non-polar toluene and the polar solvent benzonitrile.[48] In toluene, TIPS-BT1 after photoexcitation returned to the ground state. In the polar benzonitrile, TIPS-BT1 showed a bifurcation from the Franck-Condon state into a minorly

populated dimer arm-localized state and a majorly populated dimer delocalized state. From this dimer delocalized state TIPS-BT1 was able to populate a solvent stabilized charge-transfer state due to the polar benzonitrile. In the initial analysis it was concluded that there was no apparent formation of ^{1}TT in TIPS-BT1 in either toluene or benzonitrile. Despite showing low or negligible triplet yields these dimers demonstrated the potential of rigid coupling by allowing in-depth photophysical investigation without concerns about position dependent chromophore orientations that can influence parameters such as electronic coupling. Much of the work in this thesis builds on these previous results.

1.5 Scope of Work & Summary of Chapters

Chapter 2 provides a summary of experimental methods used in the photophysical characterization of systems in **Chapters 3-5**. In **Chapter 3** a photophysical investigation of TIPS-acetylated tetracenic (TIPS-BT1′) & pentacenic (TIPS-BP1′) dimers is performed to study their viability as singlet fission materials. These results are compiled, analyzed and contrasted to previously studied tetracenic dimers studied with the Damrauer Group. **Chapter 4** continues the study of the TIPS-BT1′ from **Chapter 3** in the polar solvent benzonitrile to elucidate the role of the charge-transfer state in the singlet fission process. Finally, **Chapter 5** is an investigation of a new tetracenic dimer (TIPS-BTX′) as a platform for studying TTA-UC. Results show a significant enhancement of the TTA process compared to the monomeric TIPS-Tc.

1.6 References

(1) IPCC, 2021: *Climate Change 2021: The Physical Science Basis. Contribution of Working Group I to the Sixth Assessment Report of the Intergovernmental Panel on Climate Change*[Masson-Delmotte, V., P. Zhai, A. Pirani, S.L. Connors, C. Péan, S. Berger, N. Caud, Y. Chen, L. Goldfarb, M.I. Gomis, M. Huang, K. Leitzell, E. Lonnoy, J.B.R. Matthews, T.K. Maycock, T. Waterfield, O. Yelekçi, R. Yu, and B. Zhou (eds.)]. Cambridge University Press, Cambridge, United Kingdom and New York, NY, USA, In press, doi:10.1017/9781009157896.

(2) IPCC, 2018: Summary for Policymakers. In: *Global Warming of 1.5°C. An IPCC Special Report on the impacts of global warming of 1.5°C above pre-industrial levels and related global greenhouse gas emission pathways, in the context of strengthening the global response to the threat of climate change, sustainable development, and efforts to eradicate poverty* [Masson-Delmotte, V., P. Zhai, H.-O. Pörtner, D. Roberts, J. Skea, P.R. Shukla, A. Pirani, W. Moufouma-Okia, C. Péan, R. Pidcock, S. Connors, J.B.R. Matthews, Y. Chen, X. Zhou, M.I. Gomis, E. Lonnoy, T. Maycock, M. Tignor, and T. Waterfield (eds.)]. Cambridge University Press, Cambridge, UK and New York, NY, USA, pp. 3-24, doi:10.1017/9781009157940.001.

(3) IPCC, 2022*:* Summary for Policymakers. In: *Climate Change 2022: Mitigation of Climate Change. Contribution of Working Group III to the Sixth Assessment Report of the Intergovernmental Panel on Climate Change* [P.R. Shukla, J. Skea, R. Slade, A. Al Khourdajie, R. van Diemen, D. McCollum, M. Pathak, S. Some, P. Vyas, R. Fradera, M. Belkacemi, A. Hasija, G. Lisboa, S. Luz, J. Malley, (eds.)]. Cambridge University Press, Cambridge, UK and New York, NY, USA. doi: 10.1017/9781009157926.001.

(4) Electric Power Annual 2020. *Energy Information Administration, U.S.* **2022**.

(5) Woodhouse, M.; Feldman, D.; Fu, R.; Horowitz, K.; Chung, D.; Jordan, D.; Kurtz, S.; Jones-Albertus, R.; Department of Energy, U. On the Path to SunShot: The Role of Advancements in Solar Photovoltaic Efficiency, Reliability, and Costs. **2015**.

(6) Shockley, W.; Queisser, H. J. Detailed Balance Limit of Efficiency of P-n Junction Solar Cells. *J. Appl. Phys.* **1961**, *32* (3), 510–519.

(7) Heidarzadeh, H.; Rostami, A.; Dolatyari, M. Management of Losses (Thermalization-Transmission) in the Si-QDs inside 3C–SiC to Design an Ultra-High-Efficiency Solar Cell. *Mater. Sci. Semicond. Process.* **2020**, *109*, 104936.

(8) De Vos, A.; Desoete, B. On the Ideal Performance of Solar Cells with Larger-than-Unity Quantum Efficiency. *Sol. Energy Mater. Sol. Cells* **1998**, *51* (3–4), 413–424.

(9) Hanna, M. C.; Nozik, A. J. Solar Conversion Efficiency of Photovoltaic and Photoelectrolysis Cells with Carrier Multiplication Absorbers. *J. Appl. Phys.* **2006**, *100* (7), 074510.

(10) Zhu, X. Exceeding the Limit in Solar Energy Conversion with Multiple Excitons. *Acc. Chem. Res.* **2013**, *46* (6), 1239–1241.

(11) Smith, M. B.; Michl, J. Singlet Fission. *Chem. Rev.* **2010**, *110* (11), 6891–6936.

(12) Miyata, K.; Conrad-Burton, F. S.; Geyer, F. L.; Zhu, X.-Y. Triplet Pair States in Singlet Fission. *Chem. Rev.* **2019**, *119* (6), 4261–4292.

(13) Alvertis, A. M.; Lukman, S.; Hele, T. J. H.; Fuemmeler, E. G.; Feng, J.; Wu, J.; Greenham, N. C.; Chin, A. W.; Musser, A. J. Switching between Coherent and Incoherent Singlet Fission via Solvent-Induced Symmetry Breaking. *J. Am. Chem. Soc.* **2019**, *141* (44), 17558–17570.

(14) Walker, B. J.; Musser, A. J.; Beljonne, D.; Friend, R. H. Singlet Exciton Fission in Solution. *Nat. Chem.* **2013**, *5*, 1019–1024.

(15) Stern, H. L.; Musser, A. J.; Gelinas, S.; Parkinson, P.; Herz, L. M.; Bruzek, M. J.; Anthony, J.; Friend, R. H.; Walker, B. J. Identification of a Triplet Pair Intermediate in Singlet Exciton Fission in Solution. *Proc. Natl. Acad. Sci. U. S. A.* **2015**, *112* (25), 7656–7661.

(16) Johnson, J. C.; Nozik, A. J.; Michl, J. High Triplet Yield from Singlet Fission in a Thin Film of 1,3-Diphenylisobenzofuran. *J. Am. Chem. Soc.* **2010**, *132* (46), 16302–16303.

(17) Jundt, C.; Klein, G.; Sipp, B.; Le Moigne, J.; Joucla, M.; Villaeys, A. A. Exciton Dynamics in Pentacene Thin Films Studied by Pump-Probe Spectroscopy. *Chem. Phys. Lett.* **1995**, *241* (1–2), 84–88.

(18) Le, A. K.; Bender, J. A.; Roberts, S. T. Slow Singlet Fission Observed in a Polycrystalline Perylenediimide Thin Film. *J. Phys. Chem. Lett.* **2016**, *7* (23), 4922–4928.

(19) Müller, A. M.; Avlasevich, Y. S.; Müllen, K.; Bardeen, C. J. Evidence for Exciton Fission and Fusion in a Covalently Linked Tetracene Dimer. *Chem. Phys. Lett.* **2006**, *421* (4–6), 518–522.

(20) Dover, C. B.; Gallaher, J. K.; Frazer, L.; Tapping, P. C.; Petty, A. J.; Crossley, M. J.; Anthony, J. E.; Kee, T. W.; Schmidt, T. W. Endothermic Singlet Fission Is Hindered by Excimer Formation. *Nat. Chem.* **2018**, *10*, 305–310.

(21) Singh, S.; Jones, W. J.; Siebrand, W.; Stoicheff, B. P.; Schneider, W. G. Laser Generation of Excitons and Fluorescence in Anthracene Crystals. *J. Chem. Phys.* **1965**, *42* (1), 330–342.

(22) Schulze, T. F.; Schmidt, T. W. Photochemical Upconversion: Present Status and Prospects for Its Application to Solar Energy Conversion. *Energy Environ. Sci.* **2014**, *8* (1), 103–125.

(23) Trupke, T.; Green, M. A.; Würfel, P. Improving Solar Cell Efficiencies by Up-Conversion of Sub-Band-Gap Light. *J. Appl. Phys.* **2002**, *92* (7), 4117.

(24) Singh-Rachford, T. N.; Castellano, F. N. Photon Upconversion Based on Sensitized Triplet-Triplet Annihilation. *Coordination Chemistry Reviews*. **2010**, *254* (21–22), 2560–2573.

(25) Chen, M.; Bae, Y. J.; Mauck, C. M.; Mandal, A.; Young, R. M.; Wasielewski, M. R. Singlet Fission in Covalent Terrylenediimide Dimers: Probing the Nature of the Multiexciton State Using Femtosecond Mid-Infrared Spectroscopy. *J. Am. Chem. Soc.* **2018**, *140* (29), 9184–9192.

(26) Basel, B. S.; Zirzlmeier, J.; Hetzer, C.; Reddy, S. R.; Phelan, B. T.; Krzyaniak, M. D.; Volland, M. K.; Coto, P. B.; Young, R. M.; Clark, T.; et al. Evidence for Charge-Transfer Mediation in the Primary Events of Singlet Fission in a Weakly Coupled Pentacene Dimer. *Chem* **2018**, *4* (5), 1092–1111.

(27) Margulies, E. A.; Miller, C. E.; Wu, Y.; Ma, L.; Schatz, G. C.; Young, R. M.; Wasielewski, M. R. Enabling Singlet Fission by Controlling Intramolecular Charge Transfer in π-Stacked Covalent Terrylenediimide Dimers. *Nat. Chem.* **2016**, *8* (12), 1120–1125.

(28) Mandal, A.; Chen, M.; Foszcz, E. D.; Schultz, J. D.; Kearns, N. M.; Young, R. M.; Zanni, M. T.; Wasielewski, M. R. Two-Dimensional Electronic Spectroscopy Reveals Excitation Energy-Dependent State Mixing during Singlet Fission in a Terrylenediimide Dimer. *J. Am. Chem. Soc.* **2018**, 140 (51), 17907–17914.

(29) Johnson, J. C.; Akdag, A.; Zamadar, M.; Chen, X.; Schwerin, A. F.; Paci, I.; Smith, M. B.; Havlas, Z.; Miller, J. R.; Ratner, M. A.; et al. Toward Designed Singlet Fission: Solution Photophysics of Two Indirectly Coupled Covalent Dimers of 1,3-Diphenylisobenzofuran. *J. Phys. Chem. B* **2013**, *117* (16), 4680–4695.

(30) Buchanan, E. A.; Kaleta, J.; Wen, J.; Lapidus, S. H.; Císařová, I.; Havlas, Z.; Johnson, J. C.; Michl, J. Molecular Packing and Singlet Fission: The Parent and Three Fluorinated 1,3-Diphenylisobenzofurans. *J. Phys. Chem. Lett.* **2019**, *10* (8), 1947–1953.

(31) Kaur, I.; Jazdzyk, M.; Stein, N. N.; Prusevich, P.; Miller, G. P. Design, Synthesis, and Characterization of a Persistent Nonacene Derivative. *J. Am. Chem. Soc.* **2010**, *132* (4), 1261–1263.

(32) Zhou, J.; Liu, Q.; Feng, W.; Sun, Y.; Li, F. Upconversion Luminescent Materials: Advances and Applications. *Chem. Rev.* **2015**, *115* (1), 395–465.

(33) Michl, J.; Thulstrup, E. W. Why Is Azulene Blue and Anthracene White? A Simple Mo Picture. *Tetrahedron* **1976**, *32* (2), 205–209.

(34) Murov, S., Carmichael, I., Prodi, L., & Hug, G.L. Handbook of Photochemistry (2nd ed.). CRC Press. **1993**, DOI: 10.1201/9781420015195.

(35) Haefele, A.; Blumhoff, J.; Khnayzer, R. S.; Castellano, F. N. Getting to the (Square) Root of the Problem: How to Make Noncoherent Pumped Upconversion Linear. *J. Phys. Chem. Lett.* **2012**, *3* (3), 299–303.

(36) Olesund, A.; Gray, V.; Mårtensson, J.; Albinsson, B. Diphenylanthracene Dimers for Triplet-Triplet Annihilation Photon Upconversion: Mechanistic Insights for Intramolecular Pathways and the Importance of Molecular Geometry. *J. Am. Chem. Soc.* **2021**, *143* (15), 5745–5754.

(37) Matsui, Y.; Kanoh, M.; Ohta, E.; Ogaki, T.; Ikeda, H. Triplet–Triplet Annihilation-Photon Upconversion Employing an Adamantane-Linked Diphenylanthracene Dyad Strategy. *J. Photochem. Photobiol. A Chem.* **2020**, *387*, 112107.

(38) Fan, C.; Wei, L.; Niu, T.; Rao, M.; Cheng, G.; Chruma, J. J.; Wu, W.; Yang, C. Efficient

Triplet-Triplet Annihilation Upconversion with an Anti-Stokes Shift of 1.08 EV Achieved by Chemically Tuning Sensitizers. *J. Am. Chem. Soc.* **2019**, *141* (38), 15070–15077.

(39) Rao, A.; Wilson, M. W. B.; Albert-Seifried, S.; Di Pietro, R.; Friend, R. H. Photophysics of Pentacene Thin Films: The Role of Exciton Fission and Heating Effects. *Phys. Rev. B - Condens. Matter Mater. Phys.* **2011**, *84* (19), 195411.

(40) Arbuzov, Y. A. THE DIELS–ALDER REACTION WITH MOLECULAR OXYGEN AS DIENOPHILE. *Russ. Chem. Rev.* **1965**, *34* (8), 558.

(41) Anthony, J. E.; Brooks, J. S.; Eaton, D. L.; Parkin, S. R. Functionalized Pentacene: Improved Electronic Properties from Control of Solid-State Order [20]. *J. Am. Chem. Soc.* **2001**, *123* (38), 9482–9483.

(42) Scholes, G. D.; Ghiggino, K. P.; Oliver, A. M.; Paddon-Row, M. N. Through-Space and Through-Bond Effects on Exciton Interactions in Rigidly Linked Dinaphthyl Molecules. *J. Am. Chem. Soc.* **1993**, *115* (10), 4345–4349.

(43) Gerson, F.; Wellauer, T.; Oliver, A. M.; Paddon-Row, M. N. Long-Range Intramolecular Electron Transfer between Two Naphthalene Π-Moieties Attached to a Rigid Norbornylogous Spacer of Variable Length: An ESR and ENDOR Study. *Helv. Chim. Acta* **1990**, *73* (6), 1586–1601.

(44) Clayton, A. H. A.; Scholes, G. D.; Ghiggino, K. P.; Paddon-Row, M. N. Through-Bond and Through-Space Coupling in Photoinduced Electron and Energy Transfer: An *Ab Initio* and Semiempirical Study. *J. Phys. Chem.* **1996**, *100* (26), 10912–10918.

(45) Paddon-Row, M. N.; Shephard, M. J. Through-Bond Orbital Coupling, the Parity Rule, and the Design of "superbridges" Which Exhibit Greatly Enhanced Electronic Coupling: A Natural Bond Orbital Analysis. *J. Am. Chem. Soc.* **1997**, *119* (23), 5355–5365.

(46) Kroon, J.; Verhoeven, J. W.; Oliver, A. M.; Paddon-Row, M. N. Observation of a Remarkable Dependence of the Rate of Singlet-Singlet Energy Transfer on the Configuration of the Hydrocarbon Bridge in Bichromophoric Systems. *J. Am. Chem. Soc.* **1990**, *112* (12), 4868–4873.

(47) Cook, J. D.; Carey, T. J.; Damrauer, N. H. Solution-Phase Singlet Fission in a Structurally Well-Defined Norbornyl-Bridged Tetracene Dimer. *J. Phys. Chem. A* **2016**, *120* (26), 4473–4481.

(48) Cook, J. D.; Carey, T. J.; Arias, D. H.; Johnson, J. C.; Damrauer, N. H. Solvent-Controlled Branching of Localized versus Delocalized Singlet Exciton States and Equilibration with Charge Transfer in a Structurally Well-Defined Tetracene Dimer. *J. Phys. Chem. A* **2017**, *121* (48), 9229–9242.

Chapter 2: Experimental Materials and Methods

2.1 Experimental Materials

All compounds in sections 2.1.1-3 were synthesized by Dr. Thomas Carey, Ethan Miller and Nicholas Pompetti.

2.1.1 TIPS-Tc & TIPS-Pc

Monomer analogues of tetracenic and pentacenic dimers (referred to ad TIPS-Tc & TIPS-Pc respectively) were prepared via tips-alkynylation of 5,12-napthacenequinone and 5,12-anthracenequinone. Sample purity was checked via NMR.

2.1.2 TIPS-BT1′ & TIPS-BP1′

Synthetic procedures for TIPS-BT1′ & TIPS-BP1′ have been previously described.[1]

2.1.3 TIPS-BTX′

TIPS-BTX′ was synthesized through parallel CANAL reaction of two norbornyl TIPS-tetracene-quionone arms to 1,4-dibromo-2,5-dimethylbenzene.[2] The asymmetric nature of norbornyl TIPS-Tc arms means that synthesis of the final dimeric product will produce two constitutional isomers, a syn-variant with both tetracene arms on the same relative side of the central dimethylbenzene ring and an anti-variant where they’re on opposing sides. X-ray diffraction studies showed a 95:5 distribution between the two isomers with the syn-variant being the favored product.

2.1.4 Miscellaneous

The upconversion sensitizer used in **Chapter 5** (palladium(II) 1,4,8,11,15,18,22,25-octabutoxyphthalocyanine, shortened to PdPc) was purchased from Frontier Specialty Chemicals, with purity checked by NMR. In **Chapters 3, 4 & 5** spectroscopic grade toluene from Sigma-Aldrich and Alfa Aesar was used to prepare all samples. Molar absorptivity measurements in **Chapter 3** used spectroscopic grade chloroform form Sigma-Aldrich due to chloroform's larger solvent window compared to toluene to allow for measurement of near UV features. In **Chapter 4** samples were prepared with spectroscopic grade benzonitrile from Sigma-Aldrich.

2.2 Sample Preparation

Samples for absorption, steady-state emission, time-resolved emission and photoluminescence quantum yield measurements were prepared to have an absorbance of ~ 0.1 in 1 cm quartz cuvettes equipped with Kontes HI-VAC vacuum-valves and bubbled with argon for ~30 minutes to deoxygenate the sample prior to measurement. Femtosecond (**Chapter 3 & 4**) and nanosecond (**Chapters 3 & 4**) transient absorption samples were prepared in 2 mm quartz cuvettes using the same sample preparation methodology. Nanosecond TA samples in **Chapter 5** used 1 cm quartz cuvettes. Sample integrity after experiments was monitored via steady-state absorption. Upconversion samples were prepared so that the sensitizer absorption at the pump wavelength was ~ 0.13 in 1 cm quartz cuvettes (corresponding to a sensitizer concentration of ~ 1.3 μM). For the annihilator in upconversion samples, a stock solution was prepared and used to make several upconversion samples with varying annihilator concentrations. Annihilator concentrations were selected to cover a range of triplet energy transfer efficiencies with the PdPc sensitizer $\Phi_{TET} = \sim 0.14 - 0.8$ (determined via Stern-Volmer quenching experiments and equation 5.6.4 with

associated triplet lifetimes) for TIPS-Tc and $\Phi_{TET} = \sim 0.05 - 0.35$ for TIPS-BTX'. This corresponded to an annihilator concentration range of ~0.09 – 1.7 mM for monomer samples and ~0.03 – 0.4 mM for dimer samples. Upconversion samples were deoxygenated for ~45 minutes by bubbling argon through the sample. Sample integrity was checked via steady-state absorption measurements after the performed experiment.

2.3 Absorption & Emission Spectra and Photoluminescence Quantum Yield

Absorption experiments were performed using an Agilent Cary 5000 UV-Vis-NIR absorption spectrophotometer. Steady-state photoluminescence measurements were performed using an Olis SLM 8000 fluorometer. Photoluminescence quantum yields were determined via comparison to a reference sample of known quantum yield. Coumarin 540A in spectroscopic grade methanol was used as the reference sample for tetracenic species. In **Chapter 4** temperature dependent measurements were performed using a Quantum Northwest temperature control unit and sample holder.

2.4 Time-Correlated Single Photon Counting (TCSPC)

Fluorescence lifetime measurements were performed using a DeltaFlex Modular Fluorescence Lifetime System from Horiba Scientific Ltd. Two separate instruments of the same make and model were used to measure fluorescence lifetimes in **Chapter 4** and **Chapter 5**. Access to one instrument was provided by owner Prof. Gordana Dukovic. Access to the second instrument was provided by Dr. Molly Larson at the CU Boulder chemistry department shared instrumentation room. The sample was excited with a Horiba NanoLED-405L (402 nm, <200 ps) and emission

was collected at magic angle polarization. Collected data were fit to a sum of decaying exponentials with the lowest number of exponentials used that produced a reasonable fit.

2.5 Nanosecond Transient Absorption Spectroscopy (nsTA)

Nanosecond transient absorption measurements were performed on two sets of instruments. In **Chapter 3**, a spectrometer at the National Renewable Energy Laboratory was used. Therein, ultrafast pulses were generated using a Coherent Libra Ti:Sapphire amplifier with tunable wavelength selection provided by a TOPAS-C optical parametric amplifier. Generated pulses were ~100 fs, 1 kHz, ~200 nJ with a center wavelength of 530 nm for TIPS-BT1′ and 588 nm for TIPS-BP1′. The beam diameter at the sample holder was measured to have a full-width half maximum of ~240 μm. Data was recorded using an Ultrafast Systems EOS sub-nanosecond resolution TA Spectrometer.

The second nanosecond TA instrument was used for measurements in **Chapter 5** and to determine the anthracene triplet lifetime in **Chapter 4**. The pump source was a Nd:YAG (Continuum Surelite II) 10 Hz pulsed laser with 355 nm central wavelength output and ~5 ns pulse duration. Output was used either as the direct excitation sourced or used to pump a Continuum Surelite optical parametric oscillator to obtain variable wavelength selection. Power was attenuated with neutral density filters to achieve pulse energies of ~150 μJ/pulse at the sample. The probe source was a 100 W Xenon arc lamp that generated a broadband probe and sent into the sample at a perpendicular angle relative to the excitation beam. Probe light after the sample was sent into a monochromator to separate probe wavelengths. Wavelength selected kinetic traces were then measured on a negatively biased PMT (Hamamatsu R928-07) and recorded with a digital oscilloscope (Picoscope 5444D).

2.6 Femtosecond Transient Absorption Spectroscopy (fsTA)

Measurements in **Chapters 3 & 4** were carried out using two separate home-built tables. The first (where most of the data were collected) uses a Coherent Verdi G-7 to pump a Ti:sapphire oscillator (~800 nm, ~100 fs at 94 MHz, Clark NJA-5). The output is directed into a CPA-1000 regenerative amplifier to generate ~800 nm ~1.2 mJ pulses at 1 kHz. The second table (used for one measurement for each molecule TIPS-BP1′ and TIPS-BT1′) uses a Coherent Verdi V-7 to pump a Ti:sapphire oscillator (~800 nm, ~50 fs at 94 MHz, K&M Labs) whose output is directed into a Quantronix Odin multi-pass amplifier to generate ~800 nm ~1 mJ pulses at 1 kHz. On both tables, pump pulses were generated by first directing a portion of the fundamental into a home-built non-collinear optical parametric amplifier (NOPA) with output pulses centered at either 530 nm (for TIPS-BT1′) or 588 nm (for TIPS-BP1′). These were then passed through a prism compressor, mechanically chopped at 500 Hz, attenuated to tens of nJ/pulse with a spot size at the sample of ~ 200 μm FWHM, and set to magic angle polarization (54.7°) relative to the probe. Most of the experiments utilized a fluence of ~ 150 μJ/cm^2 although a lower fluence (~50 μJ/cm^2) was tested for both TIPS-BT1′and TIPS-BP1' and the ensuing dynamics showed no notable differences relative to the larger fluence measurements. Probe continuum light was generated from a small portion of the 800 nm amplifier output focused into a continuously translated (elliptically) CaF_2 crystal. After passing through the sample, probe light was band-pass filtered to remove excess fundamental and sent into a spectrograph (Chromex for CPA-1000 setup & Acton for Quantronix Odin) that directed the light onto an Andor; DU920P-OE charge-coupled device. The experiment was controlled through a home built LabView (National Instruments) software program.

2.7 Steady-State Upconversion

In **Chapter 5**, upconversion samples were pumped with a Thorlabs diode laser. A Thorlabs HL7302M 730 nm diode in a diode mount was controlled was a LD205C current controller and TED200C temperature monitor. A LTC56M collimating lens was used to collimate the diode output. Reference samples were pumped with a Thorlabs 405 nm diode. Beam power and area for fluence measurements was characterized with an Ophir 2A-BB-9 power meter and an Ophir SF928 Beam Profile Camera. The detection setup was the same described previously in **Section 2.3** with the addition of a 460 ± 170 nm bandpass filter.

2.8 Upconversion Decay and Pulsed Diode Excitation

The triplet lifetime of the annihilator used in TTA is a critical component for rationalizing the behavior of upconversion systems but can be difficult to measure due to artificial quenching caused by either excess concentration, laser excitation, or the fact that they can undergo TTA on their own. All of these factors can lead a shorter observed lifetime. Equation 2.1 is an expression derived by Albinsson et al to determine both the triplet lifetime and if second order quenching is occurring.[3]

$$I(t) \propto [^3An^*(t)]^n = \left([^3An.^*]_0 \frac{1-\beta}{e^{(t/\tau_T)} - \beta} \right)^n \tag{2.1}$$

I(t) is the time-resolved emission signal that is being monitored in the sample and is a measure of the excited triplet annihilator concentration [^{3}An*] at time t. While normally the triplet states of common organic annihilators are not phosphorescent and cannot be observed with photoluminesence, the TTA process generates an emissive singlet that can be. The parameter *n* speaks to how the emission intensity depends on the concentration of the triplet annihilator species. In TTA, since two excited annihilators are required to form an emissive state, that makes it a

second order process with $n = 2$. The triplet lifetime of the annihilator is τ_T. The parameter β is the fraction of triplet annihilator states that are decaying through the second order channel, in this case TTA. This experiment is traditionally performed at several different fluences to change the excited triplet concentration. Since the triplet lifetime shouldn't be changing, only β will vary, generally increasing at higher fluences as a greater proportion of excited triplet start decaying through TTA versus just relaxing down to the ground state.

To monitor the second order decay attributed to upconversion, a time-resolved pulsed diode experiment was performed on all upconversion samples. The experimental setup, also first developed by Albinsson et al for the study of upconversion, is briefly described here.[4,5] Using the same diode setup described for steady-state upconversion, a 100 Hz square wave pulse train with 50 ms pulses was generated from a computer controlled DAQ card to control the laser diode. This was done to ensure the upconversion sample had reached its steady-state and that the excited state concentrations for both sensitizer and annihilator were constant. The diode was turned off and the emissive decay was monitored via PMT and recorded on the same Picoscope used for nsTA. Laser power was attenuated with a neutral density wheel and recorded to cover an approximately a two order of magnitude fluence regime. Kinetic traces were then globally analyzed with custom MATLAB code to retrieve the global triplet lifetime and the corresponding value for β. Fig. 2.1 demonstrates observed second-order decay through upconversion in a sample of zinc(II) octaethylporphyrin (ZnOEP) and DPA in toluene collected at several different fluences. ZnOEP/DPA was chosen due DPA's history of excellent upconversion performance. Kinetic traces in Fig. 2.1 were fit to equation 2.1 with a τ of 4 ms and β allowed to float. β increased as fluence was increased representing increased decay through the second-order channel. The excellent fit without the need to vary τ or include additional exponential terms demonstrates ability

of the pulsed diode experiment and equation 2.1 to monitor and analyze photophysical dynamics, especially at early time where significant deviation from first-order kinetics is observed (dashed line in Fig. 2.1).

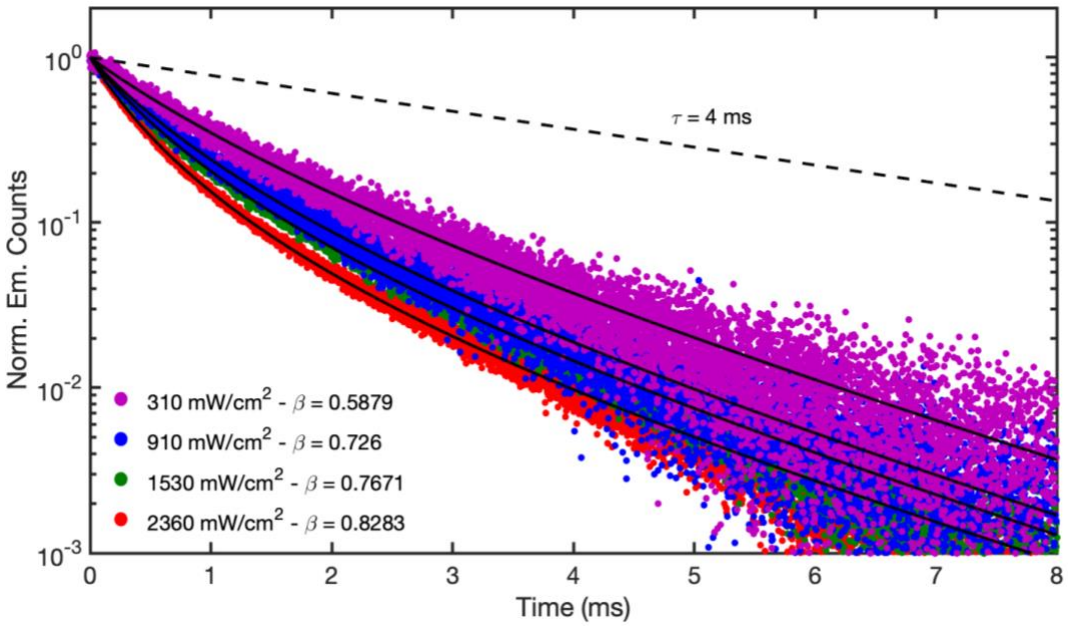

Figure 2.1 Kinetic traces from steady-state decay experiment of ZnOEP/DPA in toluene. Solid lines represent fits to expression 2.1. Dashed line is first-order 4 ms exponential decay for reference.

2.9 References

(1) Carey, T. J.; Snyder, J. L.; Miller, E. G.; Sammakia, T.; Damrauer, N. H. Synthesis of Geometrically Well-Defined Covalent Acene Dimers for Mechanistic Exploration of Singlet Fission. *J. Org. Chem.* **2017**, *82* (9), 4866–4874.

(2) Miller, E. G.; Singh, M.; Parkin, S. R.; Sammakia, T.; Damrauer, N. Preparation of a Rigid and Nearly Coplanar Bis-Tetracene Dimer through Application of the CANAL Reaction. *ChemRxiv* Cambridge: Cambridge Open Engage; **2021**; This content is a preprint and has not been subject to peer review.

(3) Edhborg, F.; Olesund, A.; Albinsson, B. Best Practice in Determining Key Photophysical Parameters in Triplet–Triplet Annihilation Photon Upconversion. *Photochem. Photobiol. Sci.* **2022**, *21* (7), 1143–1158.

(4) Olesund, A.; Johnsson, J.; Edhborg, F.; Ghasemi, S.; Moth-Poulsen, K.; Albinsson, B. Approaching the Spin-Statistical Limit in Visible-to-Ultraviolet Photon Upconversion. *J. Am. Chem. Soc.* **2022**, *144* (8), 3706–3716.

(5) Olesund, A.; Gray, V.; Mårtensson, J.; Albinsson, B. Diphenylanthracene Dimers for Triplet-Triplet Annihilation Photon Upconversion: Mechanistic Insights for Intramolecular Pathways and the Importance of Molecular Geometry. *J. Am. Chem. Soc.* **2021**, *143* (15), 5745–5754.

Chapter 3: Using Structurally Well-Defined Norbornyl-Bridged Acene Dimers to Map a Mechanistic Landscape for Correlated Triplet Formation in Singlet Fission

This chapter is adapted from: Gilligan, A. T.; Miller, E. G.; Sammakia, T.; Damrauer, N. H. Using Structurally Well-Defined Norbornyl-Bridged Acene Dimers to Map a Mechanistic Landscape for Correlated Triplet Formation in Singlet Fission. J. Am. Chem. Soc. 2019, 141 (14), 5961−5971.

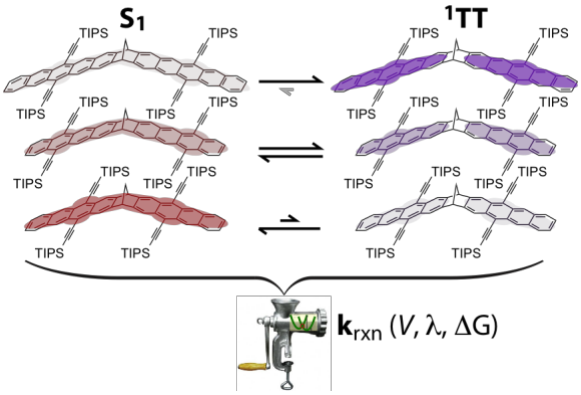

3.1 Introduction

Molecular dimers have emerged as key platforms for the mechanistic exploration of singlet fission (SF),[1,2] and in particular initial photophysics wherein a photoinduced singlet exciton is transformed into a multiexciton state, which is characterized as a singlet-coupled pair of triplets (^{1}TT). Understanding how to control such dynamics is motivated by the premise that SF may serve as a means to down-convert higher energy solar photons into multiple electronic excitations rather than into a single excitation plus waste heat.[3] Dimer and small oligomer systems using acenes,[4-20] but also diimides,[21] and isobenzofurans[22,23] are enabling the interrogation of numerous

fundamental issues affecting SF rates and yields, including reaction thermodynamics,[6,16-18,24] state couplings,[8,9,22,25,26] charge transfer intermediates,[10,19,21,22] the role of entropy,[8] spin dynamics,[15,27] and exciton binding.[8,23,28]

Within the overall body of dimer work in the literature, a leading role has been played by pentacene-based systems[5-7,10-12,14,15,17-19] where the $S_1 \rightarrow {}^1TT$ reaction driving force is significant at -200 to -300 meV and where ^1TT yields are commonly high, even in the first systems reported.[5-7] A variety of structural motifs have been explored which fall loosely into two groups. In one of these, dimer connectivity occurs via the chromophore ends either using single bonds through the acene 2 position[5,11] or using bicyclic moieties that connect simultaneously through the 2 and 3 positions.[14,17,18] This latter group includes the [2.2.1]-bridge dimer TIPS-BP1′ (see Fig. 3.1) discussed herein whose synthesis and preliminary photophysics were recently reported by us.[18] In the second group, connectivity occurs at the acene middle, through the 6 position directly[6,10] or via acetylene substituents that then link to a common bridge.[7,12,15,19] While the scope of systems is relatively large and growing, there is not yet consensus about factors controlling important mechanistic details, such as the rate constant for the $S_1 \rightarrow {}^1TT$ forward process. For example, there remain questions about electronic coupling for the photoreaction and whether it is dominated by terms that (a) directly connect the single and double exciton states[29] or (b) demand participation by virtual charge transfer states as is the more common assumption, or (c) entirely system specific. We believe that structurally well-defined dimer systems – including our [2.2.1]-bridge approach and the [2.2.2] and spiropyran approaches of Campos and Sfeir[14] – can play an important clarifying role in the field. By reducing conformational freedom, such systems limit configuration interaction with low energy singlet excimer states.[8,16] As well, they limit uncertainties about state coupling magnitudes and mechanisms that depend on relative chromophore orientation and orientation with

respect to bridging moieties. From this vantage point, we would argue that structural definition in dimers provides an opportunity to connect with theory through powerful few-parameter rate expressions such as Marcus theory.[30,31] If this is the case, and if computational tools can be employed to accurately predict physical quantities such as diabatic state couplings, then unifying design principles may have a better chance of emerging.

Although to a lesser extent than the pentacenic systems discussed above, tetraceneic dimers have also been explored and contribute to an overall mechanistic understanding. Early work by Bardeen and coworkers considered phenylene-spaced tetracene dimers.[4] They saw evidence in delayed fluorescence for involvement of the $S_1 \rightarrow {}^1TT$ photoreaction (and its reverse) although they concluded that the ^1TT yield was low, of order 3%; notably, that yield can be substantially increase in related systems by introduction of small oligomers such as trimers and tetramers.[32,33] By contrast, Bradforth, Thompson, and coworkers studying highly through-space coupled tetracene dimer systems, saw quantitative conversion of the singlet exciton to a new state that bears both excimer and multiexcitonic (^1TT) character.[8] In a related system modified to engage only through-bond coupling, they later report rapid formation of a triplet signature that lives for ~ 100 ps, consistent with ^1TT participation in the overall photoreaction.[20] In more rigid and weakly coupled dimers, we initially reported photoluminescence dynamics in room temperature toluene for our [2.2.1]-bridge parent BT1[9] (Fig. 3.1) and like Bardeen and coworkers concluded that the ^1TT yield was low. Our subsequent photophysical studies of a more soluble dimer TIPS-BT1 (Fig. 3.1) in toluene showed single-exponential singlet-exciton loss concomitant with ground state recovery on the 24 ns time scale and we concluded that the $S_1 \rightarrow {}^1TT$ photoreaction was not operable in that system.[13] We understood this as being a manifestation of point group symmetry properties in the dimer, and specifically a plane of symmetry that passes through both

chromophores of the dimer, that limits electronic coupling in the photoreaction (this symmetry plane can be understood easily in the diabatic state picture as obviating non-horizontal electron transfer couplings between virtual CT states and the ^{1}TT).[25,34,35] Interestingly, Saito and coworkers recently studied a bent cyclooctatetraene-bridged TIPS-tetracenic dimer with comparable symmetry called FLAP2, and while it has poor photostability compared to its anthracenic and pentancenic analogues, it offers compelling evidence for engaging the $S_1 \rightarrow {}^1$TT photoreaction on a ps time scale.[17] Those workers note that FLAP2 would have substantially more conformational flexibility about the bridge compared to TIPS-BT1 and suggest that this could lead to the stark dynamical differences between the two dimer systems.

In the work that follows, we explore excited state dynamics for a constitutional isomer of TIPS-BT1 called TIPS-BT1′ (Fig. 3.1), where the acetylene substitution pattern on each chromophore is moved outwards by a ring relative to the bridge, comparable to what is seen in FLAP2. Transient spectral data offer compelling evidence for the $S_1 \rightarrow {}^1$TT photoreaction as part of a picosecond timescale equilibration between these states. These data then suggest that the photoreaction energetics are highly sensitive to subtle changes in substitution patterns, for example between TIPS-BT1 and TIPS-BT1′ and lead to marked changes in ^{1}TT yield. Overall, Marcus theory offers a unifying explanation of dynamics in the full set of substituted dimers – TIPS-BT1, TIPS-BT1′, and the pentacenic TIPS-BP1′ – with vibronic coupling derived from symmetry-breaking motions being sufficient to engender fast dynamics.

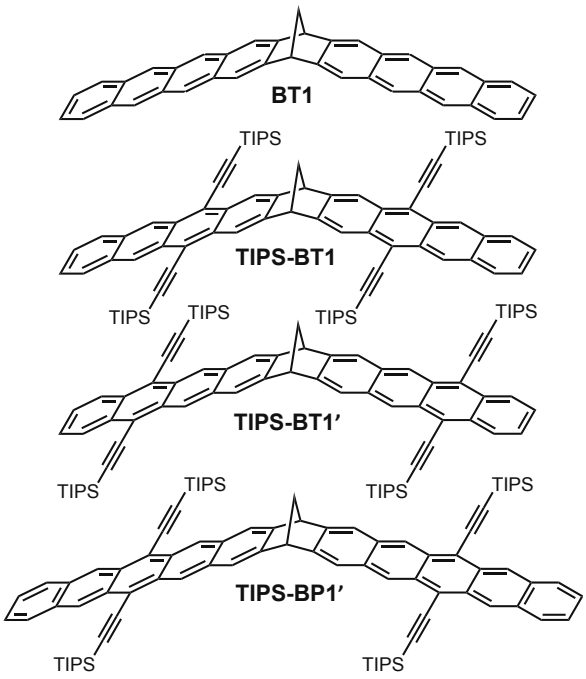

Figure 3.1 Norbornyl-bridged acene dimers discussed in text. BT1 is the conceptual parent.[9] The photophysics of triisopropylsilyl(TIPS)-acetylene substituted bis-tetracene TIPS-BT1 has been explored extensively elsewhere.[9,13] This current work focuses on the constitutional isomer TIPS-BT1′ and the bis-pentacene dimer TIPS-BP1′.[18]

3.2 Characterization of Pentacene Dimer

It is useful to start by characterizing the photoinduced dynamics of TIPS-BP1′ (Fig. 3.1), a molecule whose reaction driving force is expected to facilitate rapid formation of ^{1}TT based on results from a growing number of pentacene-based systems in the literature.[5-7,10-12,14,15,17-19] For example, in phenylene-bridged TIPS-pentacene dimers studied by Guldi, Tykwinski, and coworkers, phosphorescence measurements identified a T_1 energy of 0.8 eV.[7] Given the S_1 energy of 1.9 eV (ours is measured at 1.93 eV, vide infra) their systems were thermodynamically competent for singlet fission with a driving force of -0.3 eV. It is noted that in the communication of our synthetic methodology, we showed preliminary spectral evidence for ^{1}TT in TIPS-BP1′ at 10 ps following photoexcitation.[18] However, that work did not establish time constants or yields. Beginning with ground state absorption, Fig. 3.2(a) shows a normalized spectrum collected for

TIPS-BP1′ in room temperature toluene in a wavelength region that is coincident with our TA measurements described below. To the red is a vibronic progression characteristic of TIPS-Pentacene (TIPS-Pc) moieties, with the 0-0 band peaking at 638 nm. As we have previously described for related systems, the symmetry of this dimer and the fact that the $S_1 \leftarrow S_0$ is acene short-axis polarized, means that only the higher-energy excitonic transition in a Davydov-split pair is bright.[9,13,18] In other words, this system exhibits H-type coupling with respect to the $S_1 \leftarrow S_0$ transition of each chromophore arm. To the blue and peaked at 444 nm is a second progression that is also observed in monomer models such as TIPS-Pentacene (TIPS-Pc).[14] Not observed in toluene due to its UV cutoff is the characteristic Davydov splitting associated with coupling the individual-chromophore long axis transitions. As we have shown elsewhere,[18] this feature is seen for the compound in chloroform with intense absorption bands at 308 nm and 333 nm indicating a peak splitting of 0.30 eV. The relative intensity of these two features is readily understood[9,13,18] given the geometry of the dimer (and in particular the obtuse angle of 113° between chromophores) where the more intense lower energy transition at 333 nm arises due to the in-phase addition of the transition dipole moments (x-polarization; where dimer is oriented in the xz plane) whereas the less-intense higher energy transition at 308 nm is due to the subtraction of the transition dipole moments (z-polarization; where the z-axis coincides with the C_2 symmetry element.) A molar extinction spectrum collected in chloroform is shown in Fig. 3.10.1. The dimer exhibits very weak photoluminescence (Figs. 3.10.2 and 3.10.16) with an emissive quantum yield of ~ 0.5% (compared with 72% for TIPS-BT1 and TIPS-BT1′). Given rate constant and driving force arguments for ^{1}TT formation in TIPS-BP1′ (vide infra) we suspect this emission arises from an impurity not detected in the ^{1}H NMR baseline[18] where one of the two arms has been oxidized while the second arm remains acene-like and photoluminescent.

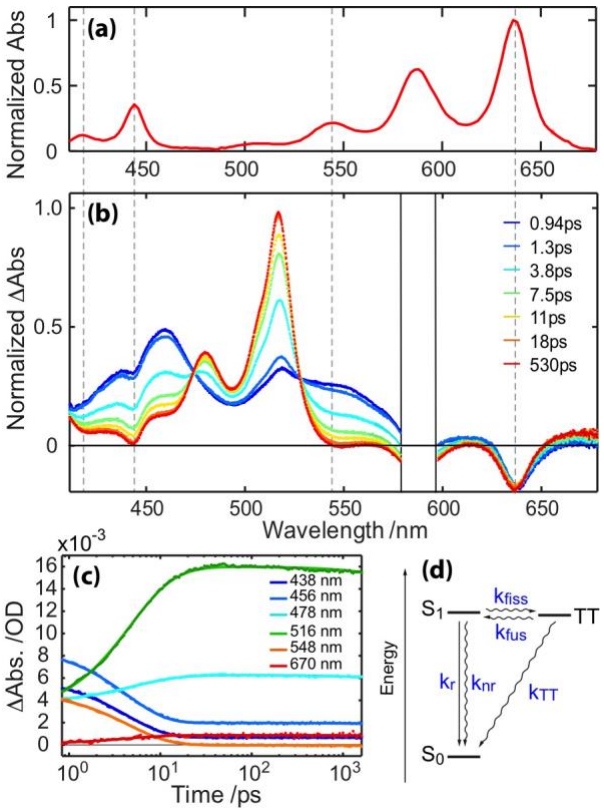

Figure 3.2 (a) Steady-state electronic absorption spectrum of TIPS-BP1′ in toluene at room temperature. (b) Transient absorption spectra of TIPS-BP1′ in room temperature toluene (normalized at Δt = 530 ps). The region surrounding the excitation wavelength of 588 nm is removed due to pump scatter. (c) Selected single wavelength kinetics traces (data points) for TIPS-BP1′ with applied model fits (lines) retrieved from global analysis. (d) Kinetic model of decay pathways of TIPS-BP1' after initial excitation.

Transient absorption (TA) dynamics were collected for TIPS-BP1′ in room temperature toluene following photoexcitation with ~ 50 fs laser pulses at a center wavelength of 588 nm (Fig. 3.2(b)). The early transient spectrum resembles the lowest energy singlet exciton in a monomer model TIPS-Pc[36] (see Fig. 3.10.17) including the excited-state absorption (ESA) at ~ 440 – 470 nm. That spectrum rapidly gives way to a new one that is characterized by the strong ESA at 517 nm along with a vibronic shoulder at 480 nm. These features, which do not further evolve out to the ~ 1 ns limit of this experiment, herald a state with triplet electronic character as seen in a

number of SF-active systems involving TIPS-acetylene substituted pentacene chromophores.[5,7] In line with other studies, the speed of the reaction is highly suggestive that the product state is not T_1 produced through intersystem crossing, but rather the ^{1}TT produced with spin conserving internal conversion. The data over the time range of 0.5 to 1500 ps are readily fit with a global A→B model with a time constant of 4.4 ps (Fig. 3.10.4). It is noted that the strong ESA feature shows a small ~1 nm blueshift over the course of its formation. Although not definitively assigned at this point, it is our expectation that the reactant singlet exciton (state A) is delocalized over both acene arms as was indicated in detailed time-resolved emission studies of TIPS-BT1.[13] In order to estimate the yield of ^{1}TT (state B), a sensitization experiment was undertaken to determine the molar extinction of the triplet in TIPS-BP1′, using photoexcited (360 nm) anthracene as a collisional triplet-triplet energy transfer partner (see details in the Chapter 3 S.I., section 3.10.5 and Fig. 3.10.13). Here, the assumption is made that that the spectral character of T_1 (observed lifetime τ_{obs} = 55 μs in room temperature toluene; see Fig. 3.10.11) is a suitable surrogate for each of the two chromophores in the ^{1}TT of TIPS-BP1′. This situation is enabled by the structural rigidity of this dimer, which limits conformational relaxation that might permit significant admixture by other states in the singlet manifold such as excimers.[8,10] With this analysis (see details in the Chapter 3 S.I.) we find a yield of 97 ± 11% from the perspective of the ^{1}TT or 194 ± 22% from the perspective of triplet excitons (see Chapter 3 SI, section 3.10.6 for a description of how error was propagated). These values are in line with those seen in other pentacenic dimer systems.[5,10,12,14]

A longer time delay TA spectroscopy was used to interrogate the fate of the transient described above that was produced in 4.4 ps. As shown in Fig. 3.10.6, the large majority of the signal decays towards baseline with single exponential character and a lifetime of 102 ns. This

shortened lifetime for a species that has triplet spectral character (vide supra) is further support for the assignment to ^{1}TT.[5,6,15] It is noted that a minor 3.5 % shelf is observed in the time window whose eventual decay to baseline requires 56 μs, thus suggesting assignment to T_1. Power-dependent studies did not show a percentage change in the magnitude of the shelf thereby arguing against production of T_1 by collision between ^{1}TT and ground state species (Fig. 3.10.10). It is possible that the shelf manifests as the spin-entangled ^{1}TT mixes with the ^{5}TT and eventually undergoes decoherence within the dimer into uncorrelated triplets.[15,27] If this is the case, the shelf would correspond to a dissociated triplet yield of 7 % of a possible 200 % as an upper limit on independent triplet formation. Another possibility is the presence half-oxidized dimers (dimers where one chromophore has been irreversibly oxidized, most likely by oxygen, leaving one functional chromophore that could undergo intersystem crossing to produce triplets). A single functional arm closely resembles the monomer species (TIPS-Pc being the monomer base for TIPS-BP1′). FsTA measurements of TIPS-Pc show no formation of triplets after initial excitation (Fig. 3.10.17). This makes intersystem crossing from half-oxidized dimers unlikely to be the source of the long-lived triplet shelf in TIPS-BP1′. Full assignment will require spin-sensitive measurements such as time-resolved EPR.[15,27,37,38] Regarding the 102 ns lifetime tied to the ^{1}TT $\rightarrow$ GS decay, it is acknowledged that this timescale is considerably lengthened compared to observations in initial highly coupled pentacene dimer systems (e.g. BP0 from Campos/Sfeir,[5] DP-Mes and DP-TIPS from Musser and coworkers,[10] and the pheny-ethynyl-bridged systems of Guldi/Tykwinski[7]). However, a number of systems have now been reported with >100 ns TT lifetimes in a variety of solvents.[5,14,15]

3.3 Discussion of a Common Model

As these TIPS-BP1′ studies will help us to understand data in the full series of molecules (Fig. 3.1), it is useful to present a common framework for analyzing kinetics at this point in the chapter. Because of the structural definition of these types of dimers, along with the weakly polar solvent environment that precludes significant participation by CT states (vide infra), a relatively simple three-state model can be utilized (Fig. 3.2(d)).[8,9,21] This includes a singlet exciton state, the TT, and the ground state. The singlet exciton state is coupled directly to the ground state via both radiative and non-radiative pathways (k_r and k_{nr}) and it can also be lost due to formation of the TT via k_{fiss} or reformed via the fusion process encompassed in k_{fus}. The last rate constant component in this model is the loss pathway linking the TT directly to the ground state, which is referred to as k_{TT}. In our understanding of these systems at this time, we assume that TT is primarily the pure singlet ^{1}TT produced in the spin-allowed k_{fiss} process, but recognize that this is not an eigenstate of the system[1,39] and that spin mixing with the ^{5}TT will begin to occur during the TT lifetime. In a related vein, the model ignores processes leading to the singlet fission product $T_1 + T_1$, which is presumed to occur in conjunction with spin mixing and decoherence, via the ^{5}TT. As a common model for each of the dimers explored this is reasonable given that for TIPS-BP1′ the long-time shelf corresponding to this product is relatively small (<3.5 %) and for TIPS-BT1′ it is nearly undetectable.

With this model we can now establish rate constants for the photophysical behavior in TIPS-BP1′. Recalling that the measured ^{1}TT yield determined using sensitization experiments is approximately quantitative, a large equilibrium constant $K = k_{fiss}/k_{fus}$ ($K \geq 100$) is expected such that the observed exponential decay of 4.4 ps reflects $1/k_{fiss}$ with little contamination (< 1 %) from k_{fus}. Note that K = 100 at room temperature for a system with a modest $S_1 \rightarrow {}^1$TT reaction driving

force of -0.12 eV. If the driving force were -0.34 eV as estimated in a related system[7] the equilibrium constant K would be greater than 5×10^5. The large equilibrium constant K also means that the observed 102 ns lifetime of the TA signal has little contamination from k_r and k_{nr} and rather reflects, almost exclusively, $1/k_{TT}$. The values of k_{fiss} and k_{TT} obtained for TIPS-BP1′ are listed in Table 3.1.

Table 3.1: Summary of room temperature photophysical properties for dimer species in toluene.

	TIPS-BT1 [a]	TIPS-BT1′ [b]	TIPS-BP1′ [b]
Φ_{em} [c]	0.72 ± 0.09	0.72 ± 0.09	< 0.01
$\tau_{obs\text{-}fast}$ /ps	0.85	2.5 ± 0.3	4.4 ± 0.2
k_{fiss} /s^{-1}	1.1×10^{11}	$(2.0 \pm 0.2)\times10^{11}$	$(2.3 \pm 0.1)\times10^{11}$
k_{fus} /s^{-1}	1.1×10^{12}	$(2.0 \pm 0.2)\times10^{11}$	$< (2.2 \pm 0.1)\times10^{9}$
τ_{obs} /ns	24.3	36 ± 3	102 ± 3 [d]
k_{TT} /s^{-1}	-	-	$(9.8 \pm 0.3)\times10^{6}$
ϕ (^{1}TT)	≤ 0.1	0.50 ± 0.08	≥ 0.97 ± 0.11
S_1 /eV	2.33	2.32	1.93
$K = k_{fiss}/k_{fus}$	0.1	1.0 ± 0.1	10^2 - 10^5 [e]

Table 3.1: [a]TIPS-BT1 taken from known value.[13] [b]Reported error is 2σ of three independent measurements. [c]TIPS-BT1′ measured relative to coumarin 540A (coumarin 153) in methanol (Φ_{em} = 0.45),[40] TIPS-BP1′ measured relative to oxazine 720 (oxazine 170) in methanol (Φ_{em} = 0.63).[41] [d]Lifetime represents decay of 97 % of initial signal. The remaining signal decays with a lifetime of 56 ± 10 μs. [e]See text for discussion of this range of K.

3.4 Characterization of Tetracene Dimers

We next consider the photoinduced dynamics of TIPS-BT1′ whose synthesis follows the same general approach used to prepare the larger acene dimer TIPS-BP1′.[18] As described in the Introduction, we had previously concluded that the close tetracene dimer analog TIPS-BT1 is inactive towards ^{1}TT formation as studied in weakly polar toluene.[13] As such, our assumption at the outset was that TIPS-BT1′ would also be inactive towards these photophysics due to their structural similarity. This assumption is called into question below.

Steady-state absorption for TIPS-BT1′ in room temperature toluene is shown in Fig. 3.3 in a spectral region highlighting properties of the lowest energy allowed vibronic transition. TIPS-BT1′, like TIPS-BP1′ exhibits H-type coupling with an optically allowed higher energy transition and a dark energetically lower but proximal transition. Also shown in Fig. 3.3 is the emission spectrum collected for TIPS-BT1′ in the same solvent. The spectrum mirrors the absorption and shows Stokes shifting of 8 nm. From the average of the 0-0 absorption and emission peaks, the value of the optically bright S_1 is determined to be 2.32 eV (see Table 3.1).

As was also the case for TIPS-BP1′, the toluene solvent UV absorption cutoff precludes observation of Davydov coupling between chromophore long-axis transitions. An absorption spectrum collected for TIPS-BT1′ in room temperature chloroform that does show this splitting is presented elsewhere[18] (the molar extinction spectrum is also presented in Fig. 3.10.1). In those data, the splitting is 0.47 eV; i.e. a value substantially larger than what is observed for TIPS-BP1′ (0.30 eV, vide supra). It is understood that a significant fraction of the Davydov splitting occurs via Coulomb interaction between individual chromophore transition dipole moments[34,42] and in the case of TIPS-BT1′ those moments have a smaller separation than in TIPS-BP1′.

We next consider a comparison of steady state photophysical data collected for TIPS-BT1′ versus the substitutional isomer TIPS-BT1. Of note, there is very little wavelength shift between these two molecules. The 0-0 transition in TIPS-BT1′ is red-shifted relative to TIPS-BT1 in both absorption and emission data with the bathochromic shift being small (3 nm and 4 nm, respectively). Averaging 0-0 absorption and emission peaks, the optically bright S_1 in TIPS-BT1 was determined to be 2.33 eV[13] (see Table 3.1) or 10 meV higher than what is found in TIPS-BT1′. There are subtle spectral differences between these two molecules that are also worth noting. For TIPS-BT1′, the ratio of 0-0 to 0-1 peak heights in *both* absorption and emission experiments is larger than what is found in TIPS-BT1. For the S_1 manifold this is an indication that the two chromophores in TIPS-BT1′ are more weakly interacting than what is seen in TIPS-BT1.[43] Stated a different way, it can be said that in TIPS-BT1′ where the silyl-acetylene groups of the two chromophores are further separated from one-another, the absorptive and emissive transitions are more characteristic of monomer-like line shapes.

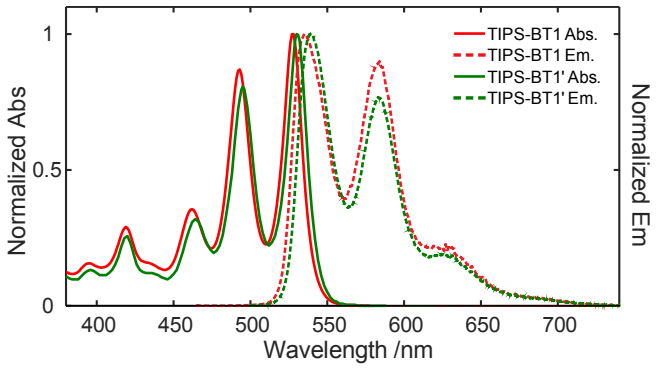

Figure 3.3 Normalized steady-state electronic absorption (solid) and emission (dashed) spectra for TIPS-BT1 (red) & TIPS-BT1' (green) in room temperature toluene.

Time-correlated single photon measurements at 539nm and 584nm, the primary spectral features in Fig. 3.3, were employed to determine photoluminescence lifetime properties for

TIPS-BT1′. The data sets can be modeled using a single exponential decay function with time constant τ_{obs} = 36 ± 3 ns (see Fig. 3.10.3). Notably this observed lifetime is larger than the value recorded for TIPS-BT1 (τ_{obs} = 24.3 ns[13]) in the same solvent and temperature. Both values are larger than the lifetime collected for the monomer TIPS-Tc (τ_{obs} = 12.5 ns[13]). We will come back to the lifetime difference between TIPS-BT1′ and TIPS-BT1 as it relates to interpretation of an overall decay model for these types of systems.

In our previous communication of synthetic approach to TIPS-BT1′ and TIPS-BP1′, we reported initial TA spectra collected for these dimers at Δt = 1 ps and 10 ps after photoexcitation over a probe spectral range of 450 nm – 650 nm chosen to interrogate the larger dimer TIPS-BP1′.[18] In that probe range no substantial changes were observed for TIPS-BT1′, and this led us to a preliminarily conclusion that SF dynamics are inactive, in line with our interpretation of photophysics for TIPS-BT1.[13] However, that TA experiment has now been revisited with finer time resolution and using a bluer probe spectrum inspired by the band shape changes observed for TIPS-BP1′ in Fig. 3.2.

TA dynamics for TIPS-BT1′ following ~ 50 fs pulse excitation at a center wavelength of 530 nm are shown in Fig. 3.4(b). Unlike previous measurements for TIPS-BT1 where spectral dynamics were not observed,[13] these new data for TIPS-BT1′ show striking evolution within the first ~ 15 ps in spectral regions blue of 450 nm. In particular, rapid loss of intensity is seen for a band in the vicinity of 425 nm, whose line shape is modified by ground state bleach features (see comparison with Fig. 3.4(a)), but otherwise heralds the S_1. Dynamics are seen at other wavelengths as well including significant modification of the magnitude of stimulated emission monitored at ~ 584 nm. Single wavelength kinetic traces extracted from the full spectral data indicate changes in the first 15 ps followed by a lack of further evolution on the 100 ps time scale. The full data set

for TIPS-BT1′ inclusive of spectra from Δt = 500 fs to 1.5 ns can be modeled using two single exponentially decaying basis functions, one of which has a time constant of 2.5 ps while the second is longer but poorly determined given the time limit of this TA experiment (see modeling discussion in Chapter 3 SI, section 3.10.8 and species associated spectra in Fig. 3.10.5). We will return to the faster dynamics later and discuss the slower decay first.

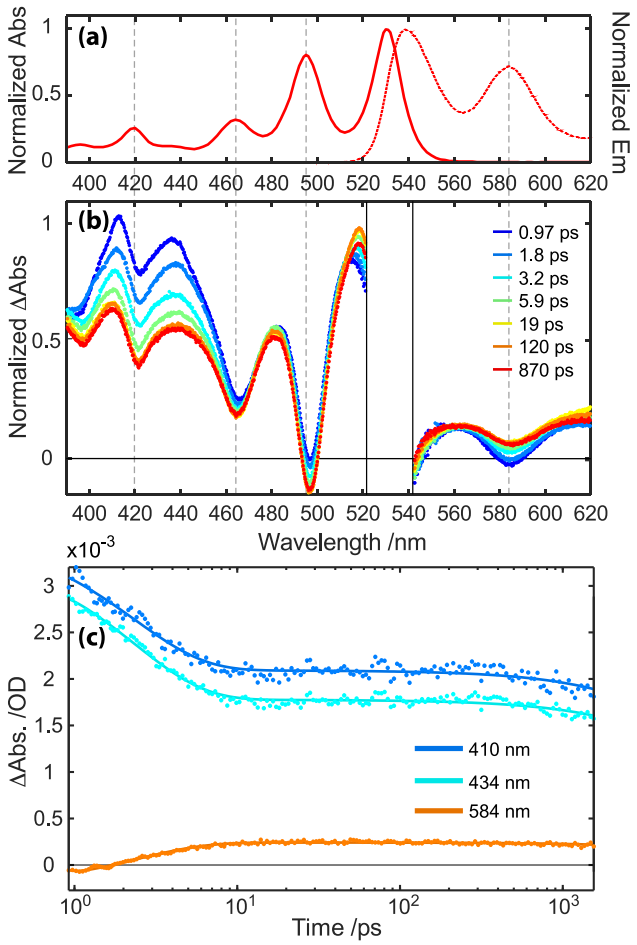

Figure 3.4 (a) Steady-state electronic absorption (solid) and emission (dashed) spectra of dimer TIPS-BT1′ in toluene at room temperature. (b) Transient absorption spectra of TIPS-BT1′ in toluene following ultrafast excitation at 530 nm. The spectral region around the excitation wavelength is removed due to pump scatter. (c) Selected single wavelength kinetics traces (data points) taken from the full-spectrum data with applied model fits (lines) retrieved from global analysis.

To better resolve the slower dynamics, the second TA spectrometer with longer time resolution was again employed. Transient spectral features of TIPS-BT1′ decay to < 1% of baseline and are globally modeled using a single exponential decay with a time constant of 35.8 ns (see Fig. 3.10.8). The spectral profile is identical to the second retrieved global fit basis spectrum. This time constant matches the 35 ns lifetime determined from the time-correlated single photon counting studies well (vide supra) and represents ground state recovery.

Returning to the faster 2.5 ps spectral dynamics in Fig. 3.4, it is noted that the observed changes *cannot* be rationalized by invoking the participation of an intramolecular charge transfer (CT) state formally reducing one chromophore arm of the dimer while oxidizing the other. Whereas population of such a state was previously observed in TIPS-BT1, that measurement required solvation in a polar benzonitrile medium and the results highlighted that excited state equilibrium is established between the CT and a dimer-delocalized singlet exciton at 2.29 eV above ground state.[13] For the same compound in less polar toluene, where the singlet exciton state is at a similar energy of 2.33 eV, no charge transfer excited state properties are observed.[13] From the perspective of TA spectral changes, the observation of CT for TIPS-BT1 in benzonitrile was very clearly indicated by a transient increase in the magnitude of features tied to the ground-state bleach. This was particularly noticeable at probe wavelengths between ~ 460 nm and 525 nm where singlet exciton ESA features overlap strongly with loss of $S_1 \leftarrow S_0$ absorption: as the singlet exciton ESA is lost in populating the CT, the bleach-related features grow in magnitude with large -ΔA variations. Such changes are absent in TIPS-BT1′ in toluene (Fig. 3.4(b)) and in fact at a wavelength of 515 nm we observe a small positive change in ΔA as the dynamics unfold.

On the other hand, it is possible to rationalize the transient spectral changes observed for TIPS-BT1′ in Fig. 3.4(b) if the state being populated has triplet electronic character. Fig. 3.5(a)

presents the $\Delta\varepsilon$ spectrum collected for TIPS-BT1′ following triplet sensitization (see Chapter 3 SI, section 3.10.5 for experimental details and Fig. 3.10.9) which shows two important qualities: first, weak ESA to the blue of 450 nm and second, stronger ESA between 450 nm and 550 nm that is highly modulated with ground-state bleach features leading to the appearance of several positive and negative TA features. The importance of the former is tied to that fact that in in TIPS-BT1′ and in other acetylene-substituted tetracene dimers, the singlet exciton state produced by visible light absorption has a strong ESA in the 400 - 450 nm region. As time evolves and population leaves this state, a weak ESA in the product can accommodate observation of transient loss in ΔA, consistent with what is seen in the first 10 ps (Fig. 3.4(b)). The importance of the latter ties to our ΔA observations between 460 nm and 550 nm, where changes during the dynamics are actually muted. In TIPS-BT1′, both the nascent singlet exciton and the triplet observed in this region have a strong ESA that is highly modulated by negative peaks associated with ground state bleach (see $\Delta t = 1$ ps in Fig. 3.4(b)). Thus, during interconversion from excited state reactant to product, overall changes in ΔA in this spectral region may in principle be subtle.

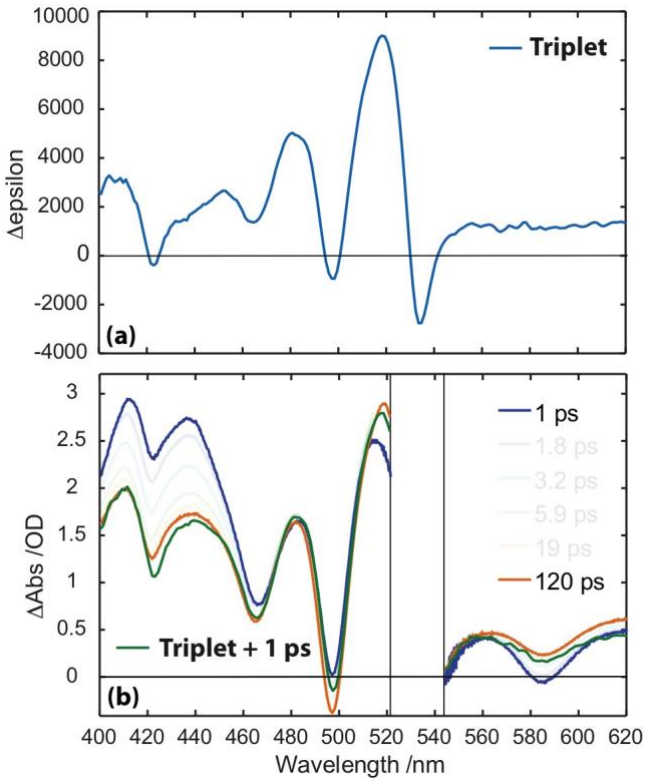

Figure 3.5 (a) Triplet Δε spectrum for TIPS-BT1′ from sensitization experiment in toluene (see Chapter 3 SI, section 3.10.5 for sensitization experiment details and Fig. 3.10.13) (b) Selected spectral slices for TIPS-BT1′ at 1 ps (blue) and 120 ps (red) along with a reconstructed TA spectrum (green) that is comprised of a superposition between the 1 ps TA spectrum and the sensitized triplet Δε spectrum from (a).

A more quantitative analysis begins by treating later-time spectra – described by the second component retrieved from the global analysis – in terms of two basis functions. The first is a ΔA spectrum collected at early time (Δt = 1 ps) where the dominant contribution is from the singlet exciton whose excited state concentration can be quantified by taking into account the laser power, spot size, and sample absorbance (see Chapter 3 SI for details). The second is the triplet Δε spectrum discussed above (Fig. 3.5(a)). Using a superposition of these two basis functions (50 % singlet exciton and 100 % triplet) we are able to recreate the Δt = 120 ps spectrum with high fidelity as shown in Fig. 3.5(b). There are two clear implications. The first is that the early dynamics serve to establish an equilibrium between the singlet exciton and a state with triplet character. Given the

timescale for the dynamics, that product state cannot be the T_1 and rather, is very likely the ^{1}TT where the structural integrity of the bridging norbornyl group enables the two chromophores to essentially preserve their triplet electronic character. This behavior in a tetracene dimer is different than a case where face-to-face interchromophore contact is more intimate leading to significant electronic perturbations.[8] On the other hand it is similar to observations by Saito and coworkers where the chromophores are separated by a bridge derived from cyclooctatetraene.[17,44] Note that in reference 44 we discuss our conclusion that these workers overestimate their triplet yield and that their results are more closely aligned with ours than has been reported.[17, 44] The second implication has to do with the basis function percentages needed to reproduce the later-time spectra. The 100% triplet yield needed should be thought of as a 50% TT so the overall population remains conserved in the experiment (50% S_1 and 50% ^{1}TT). Thus the equilibrium constant established with the 2.5 ps time scale is K = 1. In terms of energetics this means that the ^{1}TT lies in close energetic proximity to 2.32 eV where we measure the optically bright S_1 (Table 3.1).

3.5 Disentangling Dynamics in TIPS-BT1'

Kinetic modeling using the framework presented in Fig. 3.2(d) was undertaken for the TIPS-BT1′ data. There are too few independent measurements to uniquely determine each of the rate constants and we choose to draw from information obtained with the other dimers TIPS-BP1′ and TIPS-BT1 in order to gain insight. A starting point is the final decay rate constant k_{TT}. In TIPS-BT1′, ground state recovery is strongly influenced by the three rate constants k_r, k_{nr}, and k_{TT}, such that lifetime measurement – even with inclusion of radiative quantum yield information – is insufficient for independent determination of k_{TT}. We thus rely on insight from the larger dimer TIPS-BP1′ where k_{TT} was determined to be 1×10^7 s^{-1} (Table 3.1). While useful for modeling

purposes, this value is likely an overestimate for TIPS-BT1′. First, ^{1}TT → GS is highly exergonic for both dimers (> -1.5 eV) with values that are significantly larger than what would be expected for the reorganization energy of the electronic transformation in each corresponding system. Thus ^{1}TT → GS for either TIPS-BP1′ or TIPS-BT1′ is expected to take place in the Marcus inverted region where the reaction should slow as the driving force is increased from TIPS-BP1′ to TIPS-BT1′. Indeed Sanders et al. have observed energy gap law behavior for this decay process in a series of heterodimers.[24] Unfortunately, estimating the extent of the effect in TIPS-BT1′ is further challenged because reorganization energy is also impacted as the acene size is changed. Notably, however, the conclusions reached below are relatively insensitive to the precise value of k_{TT} and we are comfortable setting the value for TIPS-BT1′ at the value measured for TIPS-BP1′.

The next consideration is k_r and k_{nr}. Here the dimer system TIPS-BT1 is useful as it is a close structural analog to TIPS-BT1′ but one where ^{1}TT formation is minor (K is small) such that the previously reported values of k_r and k_{nr} ($k_r = 3.0 \times 10^7$ s^{-1} and $k_{nr} = 1.2 \times 10^7$ s^{-1}) are the dominant decay paths. A minor point about these rate constants is discussed in reference 45. Using these k_r and k_{nr} values along with k_{TT} obtained from TIPS-BP1′, the three-state model predicts an observed lifetime for TIPS-BT1′ – that of the $S_1 \leftrightarrows {}^1$TT equilibrium – of 38 ns. This is, in our view, remarkably similar to the kinetic observation of 36 ns (Table 3.1), thus providing strong support that we understand this TIPS-BT1′ system and that simple three-state model is appropriate.

The final consideration is k_{fiss} and k_{fus}. The observed 2.5 ps dynamics in TIPS-BT1′ represents establishment of the $S_1 \leftrightarrows {}^1$TT equilibrium, which then decays in 36 ns. Because of the large separation in these time scales, the rate constant for establishing the equilibrium is simply the sum of k_{fiss} and k_{fus} ($k_{obs\text{-}fast} = k_{fiss} + k_{fus} = 4.0 \times 10^{11}$ s^{-1}). Given K = 1, ^{1}TT is both formed and lost with a time constant of 5 ps ($k_{fiss} = k_{fus} = 2.0 \times 10^{11}$ s^{-1}). These rate constants were able to

accurately reproduce the dynamics of the S_1 and ^{1}TT populations present in TIPS-BT1′ (see example in Fig. 3.10.14). The large k_{fiss} in TIPS-BT1′ was initially surprising to us given aforementioned symmetry issues for this class of dimers.[25] However, diabatic coupling arguments can serve as basis for understanding this rate constant magnitude. In theoretical explorations of vibronic coupling in BT1 – explored because many vibrations break the aforementioned plane of symmetry – we predicted diabatic couplings (V_{eff}) between a singlet exciton state and the ^{1}TT of order 5.5 meV.[25] Such a quantity is not insignificant inasmuch as it approximately matches what is predicted[25] for tetracene dimer pairs (7.3 meV) germane to the crystal environment where singlet fission is known to take place on the picosecond time scale and be quantitative.[39] Although we have not calculated a comparable V_{eff} value for a TIPS-BT1′ model, we apply the 5.5 meV from the structurally similar BT1 to make rate constant estimates with non-adiabatic Marcus theory (see Chapter 3 S.I. for the equation and a schematic in Fig. 3.10.15 showing the parameters). Using this 5.5 meV V_{eff} as the state coupling, along with a reaction driving force ΔG = 0 meV that is appropriate for a system where K=1, one matches the $k_{fiss} = 2\times10^{11}$ s^{-1} of TIPS-BT1′ when the reorganization energy of the reaction is small, but not unreasonable, at λ = 0.18 eV (note that λ = 0.13 eV has been used in the description of ^{1}TT formation in solid-state acene systems[31]). These V_{eff} and λ parameter values justify the use of non-adiabatic Marcus theory. First the electronic coupling between reactant and product states (V_{eff}) is weak and less than kT. More importantly, its value is significantly smaller (by a factor of > 30) than the nuclear reorganization in the reaction (λ) meaning that structural and solvent fluctuations are required to bring the singlet and ^{1}TT states into resonance for rare electron tunneling events transforming reactant to product states. In other words, electron/phonon coupling is large by comparison to electron/electron couplings between states such that $S_1 \rightarrow {}^1$TT is best considered as an incoherent hopping process.

There is an issue that should be discussed at this point for the sake of completeness. Namely, we have previously argued for BT1 that λ for the diabatic $S_0S_1 \rightarrow {}^1TT$ may be larger, of order 0.5 eV.[9] The origin of this prediction is in calculations we made using structures from DFT and TD-DFT with gradients, that predicted a significant intramolecular (inner-sphere) reorganization energy λ_i = 0.43 eV ($S_1 \rightarrow Q$). Given the current results, this may be an overestimation. A potential origin of this overestimation can be understood in the following way. In our hands, TD-DFT as applied to BT1 and related systems – including use of a toluene solvent continuum model – finds an optimized singlet excited state that is arm-localized. This is true not only for BT1, but also when acetylene substituents are added in respective TIPS-BT1 and TIPS-BT1′models. However, arm localization contradicts spectroscopic findings for TIPS-BT1[13] where it is apparent that the singlet exciton state for the molecule in toluene is dimer delocalized. It's surmised that λ_i would be smaller for a dimer-delocalized exciton compared to the arm-localized state found using TD-DFT and additional theory is needed to explore this point. If a lower value of λ is operative as is now expected, then we also need to rationalize biexponential photoluminescence behavior observed for BT1.[9] One reasonable explanation, given the poor solubility of BT1 that precluded exploration with TA in the first place, is that aggregation effects contribute to multiexponential decay behavior. Given that TIPS-BT1′ readily dissolved into solution aggregation is not expected to be present to a significant degree.

3.6 Comparing TIPS-BT1' with TIPS-BP1'

We were initially rather surprised by the overall finding that k_{fiss} for TIPS-BT1′ (2.0×10^{11} s^{-1}) is similar to that of the larger and more exoergic TIPS-BP1′ (2.3×10^{11} s^{-1}; vide supra). As noted earlier for TIPS-BP1′, the $S_1 \rightarrow {}^1TT$ reaction driving force is substantial and expected to be in the

-0.2 to -0.35 eV range.[7] However, at the same time the reaction reorganization energy is expected to be smaller in TIPS-BP1′ than the $\lambda = 0.18$ eV suggested above for TIPS-BT1′ given the larger and more highly delocalized chromophores of the pentacenic dimer. Thus for TIPS-BP1′, $S_1 \rightarrow {}^1TT$ conversion is likely to take place in the Marcus inverted region in contrast to the analogous reaction for TIPS-BT1′ and this should contribute to reaction slowing, contrary to our initial assumption. Additionally, whereas the vibronic coupling theory mentioned above predicted diabatic coupling values of order $V_{eff} = 5.5$ meV for BT1, there is reason to expect it would be smaller in pentacene-based systems where exciton location from the perspective of the individual chromophores of the dimer is moved further away from the bridge linking the two. Qualitatively in support of this, we note our previous observation (vide supra) that Davydov splitting manifest in the UV is smaller for TIPS-BP1′ (0.30 eV) than it is for TIPS-BT1′ (0.47 eV). Factoring each of these things for TIPS-BP1′ – inverted region reactivity and smaller V_{eff} compared to TIPS-BT1′ – it is straightforward to come up with reasonable conditions that give $k_{fiss} = 2.3\times10^{11}$ s^{-1} (an example of possible values is given in reference 46). However, given that each Marcus theory parameter is expected to change on going from TIPS-BT1′ to TIPS-BP1′, it is difficult to make specific predictions without further constraints that may come from theory and experiment. Nonetheless, we can emphasize at this point that Marcus theory readily describes the set of behaviors seen in these types of dimer systems. It is also our hope that such a parametric rate theory can be useful comparing the behavior of other known systems. To this end, consistent treatments of diabatic coupling, reorganization energy, and driving force are needed.

Revisiting TIPS-BT1. As discussed in the Introduction, our published interpretation of TIPS-BT1 photophysics in toluene was that it did not engage in ${}^1TT$ formation and only decayed to ground state via k_r and k_{nr}.[13] This was based primarily the lack of spectral evolution in the TA

region (~ 420 nm) where there is a strong ESA attributed to the singlet exciton. In that published work, however, we did note a subtle (< 10%) exponential decay of the singlet exciton feature in single-wavelength data (λ_{probe} = 429 nm) that was fit with an 850 fs time constant. While the chance of ^{1}TT involvement was discussed, it was ultimately dismissed given the stark timescale difference to our BT1 data,[9] and because the absence of spectral evolution argued against it. However, based on the findings herein for TIPS-BT1′, it seems prudent to revisit these conclusions for TIPS-BT1. With the findings for TIPS-BT1′ as a quantitative guide (vide supra), the ~ 10% decay of the S_1 magnitude in TIPS-BT1 at λ_{probe} = 429 nm is consistent with establishment of a $S_1 \leftrightarrows {}^1$TT equilibrium, but one where the equilibrium constant is small at K ~ 0.1. Using this value in the framework of the three-state kinetic model (Fig. 3.2(d)), S_1 would decay in 850 fs (~10% of signal) as observed if $k_{fiss} = 1.07\times10^{11}$ s^{-1} (9.3 ps). This corresponds to an expected slowing relative to TIPS-BT1′ ($k_{fiss} = 2.0\times10^{11}$ s^{-1}; 5 ps), consistent with the more endergonic driving force of 59 meV (to accommodate K= 0.1). Again Marcus theory is adequate for understanding these results. For example, if λ and V_{eff} are respectively held fixed at the previously discussed values of 0.18 eV and 5.5 meV, the time scale for ^{1}TT formation in TIPS-BT1 is predicted to be 18 ps; i.e., of the right order of magnitude compared with the 9.3 ps time constant discussed above. Full agreement is achieved if V_{eff} is increased to 7.7 meV. An increase in V_{eff} for TIPS-BT1 relative to TIPS-BT1′ appears to us reasonable, given that the position of the TIPS-acetylene groups influences where the exciton resides, from the perspective of each chromophore relative to the bridge. Qualitative support for a coupling increase is the stronger excitonic interaction observed in TIPS-BT1 compared to TIPS-BT1′ based on vibronic features in the $S_1 \leftarrow S_0$ manifold (vide supra; Fig. 3.3). It is also worth noting the possibility that these subtle side-group perturbations impact electronic coupling for SF (increase it in TIPS-BT1 compared to TIPS-BT1′) in ways similar to those

observed by Lukman, Musser, and coworkers.[10] In their pentacene dimer systems, swapping TIPS-acetylene for mesityl side groups serves to increase the charge-transfer state character in the adiabatic reactant singlet state with profound impacts on dynamics and mechanism. In our systems, it is possible that TIPS-BT1 has slightly more CT character in the reactant adiabatic singlet compared to TIPS-BT1′. As noted earlier (Table 3.1), the S_1 in TIPS-BT1 is modestly higher in energy and this could facilitate more mixing with an otherwise isoenergetic higher-lying CT state. As well, the CT state could be lower in TIPS-BT1 compared to TIPS-BT1′ if, as expected, the cation and anion charge densities exploit the acetylene side groups. In TIPS-BT1, the side groups on the opposing chromophores are physically closer to each other and this would increase the Coulombic attraction between that cation and anion, thus stabilizing the CT. These issues may be factored in dimer design, but care must be taken to control relative reactant versus product energetics as discussed extensively in the next section.

3.7 TIPS-BT1 versus TIPS-BT1'

As a final point of discussion, we consider how the subtle structural side-group changes that have been implemented manifest in the equilibrium shift from TIPS-BT1 (K = 0.1) to TIPS-BT1′ (K = 1), recalling that this corresponds to a 59 meV exoergic shift for the $S_1 \rightarrow {}^1TT$ photoreaction between these two dimers. Some of this could come from state energetics based on observations already discussed. As shown in Fig. 3.3 and Table 3.1, the S_1 in TIPS-BT1 is slightly higher in energy compared to TIPS-BT1′, by 10 meV. One potential origin of this has to do with electronic perturbations to the acene chromophores that arise from linear attachment to the bicyclic alkyl bridge. In the consideration of monomer models, we have previously shown that the electron-

rich bridge serves to modestly destabilize S_1 and T_1 states relative to pure tetracene, presumably due to electron donating properties of the bridge and their preferential impact on the acene LUMO.[34] In the context of the current dimers, it is reasonable to expect that the position of the TIPS-acetylene substituents will impact the S_1 energy, and that this state will be higher for TIPS-BT1 because the acetylene substituents – which participate in determining the average position of the exciton – are closer to the destabilizing bridge. At first glance, the higher S_1 might appear to suggest that K would be larger in TIPS-BT1. Importantly however, the same argument applies to the T_1 states; i.e., more destabilization in TIPS-BT1 compared to TIPS-BT1′. Assuming the energy perturbation in the triplet manifold is similar to that of the S_1,[34] the $S_1 \rightarrow {}^1TT$ photoreaction is expected to be more uphill for TIPS-BT1 compared to TIPS-BT1′, given that the energy of the ^1TT is approximately twice the energy of the T_1. However, the extent should be small – of order 10 meV – and while it can contribute, it does not appear significant enough to explain the equilibrium shift observations in total. We have also briefly considered an explanation based on S_1 energies. In principle, observed differences in excitonic interactions for TIPS-BT1 versus TIPS-BT1' would manifest in larger energy splitting (ΔE_{S1}) between the higher energy optically bright S_1 and the lower energy dark S_1. Given that the photoreaction of interest will occur primarily from the lower energy dark S_1, the more excitonically coupled TIPS-BT1 could be preferentially disadvantaged. However, in order for this effect to meaningfully lower the equilibrium constant of interest, the difference in ΔE_{S1} for TIPS-BT1 versus TIPS-BT1' (i.e., $\Delta\Delta E_{S1}$) needs to be a substantial percentage of 59 meV. We do not think this is the case for these dimers. When considering Davydov splitting in the $S_3 \leftarrow S_0$ region, TIPS-BT1 exhibits a larger value (0.499 eV[13]) compared to TIPS-BT1' (0.472 eV)(see SI) but this represents a 5% difference out of ~ 0.5 eV of splitting. If we apply this percentage difference to the much smaller Davydov splitting expected for the $S_1 \leftarrow S_0$

transition in the visible (of order 30 meV[34]), we find only 1.5 meV to work with. This is not enough to substantively impact the $S_1 \leftrightarrows {}^1TT$ equilibrium.

A final source of energy perturbation that intrigues us has to do with the biexcitonic TT manifold. As discussed recently by Greenham, Behrends, and coworkers in their electron spin resonance studies of singlet fission in TIPS-tetracene films, triplet interactions in biexciton states are dominated, not by dipolar coupling, but by exchange interactions.[38] The perturbation to the energies of the different state multiplicities that emerge – including the ^1TT, ^3TT, and ^5TT – depends on the extent to which relevant orbitals in the individual chromophore triplets share common space. Unlike dipolar coupling, exchange interactions can account for significant amounts of energy, of order eV, when the extent of common orbital space is extensive as it is in individual acenes; i.e., the reason they are useful for SF problems. Thus even if common orbital space is not large, as one might expect for two acene chromophores juxtaposed relative to one another across a bridge, it is not unreasonable to obtain the 10s of meV contributions needed to shift the $S_1 \leftrightarrows {}^1TT$ equilibrium between the two dimers. This would occur by utilizing a combination of through-space interactions as well as through-bond pathways mediated by the norbonyl-bridge σ and $\sigma\times$ system. Such pathways are known to be effective for coupling π-chromophore systems in both electron and energy transfer problems.[42,47-49] In order for this exchange effect to contribute to the observations in the dimer systems, the sign of the TT exchange interaction needs to be controlled such that ^1TT is destabilized at the same time that ^5TT is stabilized. This is the same direction one would expect for Hund's rule. In TIPS-BT1′ where the acetylene substituents draw the two triplet excitons further away from one another, exchange interactions would decrease, leading to smaller energy splitting between ^1TT and ^5TT and less energetic cost to populating the ^1TT from the S_1 as has been observed. On the other hand, in TIPS-

BT1 where the position of the acetylene substituents favors stronger exchange interactions in the TT manifold, the ^{1}TT would be pushed to higher energy thus decreasing its relative population within $S_1 \leftrightarrows {}^1$TT equilibrium, again consistent with our observations. Temperature dependent TA measurements have been used previously to interrogate ^{5}TT dynamics.[49] Given the small amplitude TA signal observed background noise will likely obscure meaningful amplitude changes. High level electronic structure theory is likely needed to confirm the sign of the exchange interaction and to determine the magnitude of the effect in these systems.

3.8 Conclusions

These studies have focused on two structurally well-defined acene dimers for exploration of excited state dynamics tied to singlet fission. Our emphasis has been on understanding time scales for formation of the multiexcitonic ^{1}TT state as well as its loss to the ground state either directly or via pathways involving re-formation and decay of the singlet exciton state. The first dimer system – TIPS-BP1′ – is pentacenic in nature such that ^{1}TT formation is exoergic and seen to be efficient with ~ unit quantum yield. The second of these systems – TIPS-BT1′ – is tetracenic and is a close constitutional isomer of a dimer recently studied by our group called TIPS-BT1. The two differ only in the placement of solubilizing TIPS-acetylene side groups. They are energetically quite similar, as borne out using static absorption and emission spectroscopies, and yet they exhibit markedly different evolution of transient absorption features including strong evidence in TIPS-BT1′ for the rapid emergence of significant ^{1}TT population.

There are several notable individual findings that are summarized below. However, we first emphasize the general conclusion that in this class of pentacenic and tetracenic dimer systems, where structural definition is by design, we have achieved a unifying understanding of dynamics

in terms of the few-parameter rate constant expression of Marcus theory. This allows us to assess appropriate magnitudes for diabatic coupling, reorganization energy λ, and driving force that enables efficient ^{1}TT formation in these and related systems. The overall mechanistic understanding means that these systems can provide benchmarks upon which subsequent variations that alter structure, energetics, and symmetry can be judged.

The first notable specific finding concerns TIPS-BT1′ where we observe rapid formation of the ^{1}TT (τ_{fiss} = 5 ps) in concert with establishment of an excited state equilibrium of equal proportions (K ~ 1) with the singlet exciton state S_1 that resides 2.3 eV above the ground state. The established equilibrium means that the ^{1}TT resides at a highly similar energy. This speed is initially surprising given the absence of reaction driving force and given the unfavorable structural symmetry in this dimer (a long-axis reflection plane) expected to limit diabatic coupling between reactant and product.[25,34] However, we conclude that we have the framework to rationalize this time constant. Theory we previously applied to the parent norbornyl-bridged tetracene dimer BT1, that factors vibronic coupling through symmetry-breaking vibrational motions (normal modes within the A_2 and B_2 irreducible representations), predicts an effective diabatic coupling V_{eff} of order 5.5 meV.[25] Such an amount, while appearing to be small, can accommodate τ_{fiss} = 5 ps without a driving force (appropriate because K ~ 1) when the reorganization energy is low, but entirely reasonable, at λ = 0.18 eV. Subsequent theory would be useful to refine these numbers but it is becoming clear that only modest diabatic couplings are needed to enable efficient ^{1}TT formation in competition to other radiative and non-radiative decay pathways, in large part because of the small reorganization energies associated with highly delocalized acetylene-substituted acene chromophores engaging in SF. A final point is made about TIPS-BT1′ in relation to the lifetime of the ^{1}TT that might be relied upon for subsequent generation of states like the ^{5}TT or separated

triplets. In this tetracenic system the ^{1}TT energy is poised to limit the non-radiative decay to ground state (encompassed in the rate constant k_{TT}) compared to pentacenic systems like TIPS-BP1′ that exhibit ^{1}TT lifetimes of order 100 ns. Unfortunately, excited state equilibrium with the singlet exciton state undermines this potential gain.

The second notable specific finding concerns the observation that ^{1}TT formation in the pentacenic TIPS-BP1′ (4.4 ps) is not substantially faster than in TIPS-BT1′ (5.0 ps) despite the significantly larger (exergonic) reaction driving force of 200 – 350 meV (giving the ^{1}TT an energy above the ground-state of ~1.58 – 1.73 eV). This can be partially understood now in the context of Marcus theory where the reaction in TIPS-BP1′ should be slowed by placement in the inverted region. However, other effects are also expected to be in play. Namely, we anticipate reductions in both λ and V_{eff} for the more π-delocalized and excitonically separated TIPS-BP1′ relative to TIPS-BT1′ to contribute to the observed similarity in ^{1}TT formation rate constants.

The final notable specific finding concerns the comparison between TIPS-BT1′ and the close constitutional isomer TIPS-BT1 and the fact that despite nearly identical singlet exciton energies, these two molecules exhibit markedly different ^{1}TT yields. We are intrigued by the possibility that we are observing the effect of exchange interactions between triplets in the multiexcitonic TT manifold where subtle structural changes – i.e., the placement of the TIPS-acetylene substituents in TIPS-BT1′ versus TIPS-BT1 – are controlling its magnitude and where the comparative observation is revealing its sign. The ^{1}TT yields in TIPS-BT1′ versus TIPS-BT1 are consistent with a scenario where exchange interactions raise the energy of the ^{1}TT relative to higher multiplicities ^{3}TT and ^{5}TT. In TIPS-BT1′, the relative placement of the acetylene side groups draws the triplet excitons further away from one another thereby lowering the overall energy of the ^{1}TT and enabling its substantial participation ($K \sim 1$) in equilibrium with the S_1

singlet exciton state. The mechanistic details revealed in these comparative studies can be used in the design and interpretation of new systems and architectures to exploit the ^{1}TT as a gateway to the ^{5}TT or separate triplets.

3.9 References

(1) Smith, M. B.; Michl, J. Singlet Fission *Chem. Rev.* **2010**, *110*, 6891-6936.

(2) Smith, M. B.; Michl, J. Recent Advances in Singlet Fission *Annu. Rev. Phys. Chem.* **2013**, *64*, 361-386.

(3) Hanna, M. C.; Nozik, A. J. Solar Conversion Efficiency of Photovoltaic and Photoelectrolysis Cells with Carrier Multiplication Absorbers *J. Appl. Phys.* **2006**, *100*, 074510.

(4) Müller, A. M.; Avlasevich, Y. S.; Schoeller, W. W.; Müllen, K.; Bardeen, C. J. Exciton Fission and Fusion in Bis(Tetracene) Molecules with Different Covalent Linker Structures. *J. Am. Chem. Soc.* **2007**, *129*, 14240-14250.

(5) Sanders, S. N.; Kumarasamy, E.; Pun, A. B.; Trinh, M. T.; Choi, B.; Xia, J. L.; Taffet, E. J.; Low, J. Z.; Miller, J. R.; Roy, X.; Zhu, X. Y.; Steigerwald, M. L.; Sfeir, M. Y.; Campos, L. M. Quantitative Intramolecular Singlet Fission in Bipentacenes *J. Am. Chem. Soc.* **2015**, *137*, 8965-8972.

(6) Lukman, S.; Musser, A. J.; Chen, K.; Athanasopoulos, S.; Yong, C. K.; Zeng, Z. B.; Ye, Q.; Chi, C. Y.; Hodgkiss, J. M.; Wu, J. S.; Friend, R. H.; Greenham, N. C. Tuneable Singlet Exciton Fission and Triplet-Triplet Annihilation in an Orthogonal Pentacene Dimer *Adv. Funct. Mater.* **2015**, *25*, 5452-5461.

(7) Zirzlmeier, J.; Lehnherr, D.; Coto, P. B.; Chernick, E. T.; Casillas, R.; Basel, B. S.; Thoss, M.; Tykwinski, R. R.; Guldi, D. M. Singlet Fission in Pentacene Dimers *Proc. Natl. Acad. Sci. USA* **2015**, *112*, 5325-5330.

(8) Korovina, N. V.; Das, S.; Nett, Z.; Feng, X.; Joy, J.; Haiges, R.; Krylov, A. I.; Bradforth, S. E.; Thompson, M. E. Singlet Fission in a Covalently Linked Cofacial Alkynyltetracene Dimer *J. Am. Chem. Soc.* **2016**, *138*, 617-627.

(9) Cook, J.; Carey, T. J.; Damrauer, N. H. Solution-Phase Singlet Fission in a Structurally Well-Defined Norbornyl-Bridged Tetracene Dimer *J. Phys. Chem. A* **2016**, *120*, 4473−4481.

(10) Lukman, S.; Chen, K.; Hodgkiss, J. M.; Turban, D. H. P.; Hine, N. D. M.; Dong, S. Q.; Wu, J. S.; Greenham, N. C.; Musser, A. J. Tuning the Role of Charge-Transfer States in Intramolecular Singlet Exciton Fission through Side-Group Engineering *Nat. Commun.* **2016**, *7*, 13622.

(11) Sakuma, T.; Sakai, H.; Araki, Y.; Mori, T.; Wada, T.; Tkachenko, N. V.; Hasobe, T. Long-Lived Triplet Excited States of Bent-Shaped Pentacene Dimers by Intramolecular Singlet Fission *J. Phys. Chem. A* **2016**, *120*, 1867-1875.

(12) Zirzlmeier, J.; Casillas, R.; Reddy, S. R.; Coto, P. B.; Lehnherr, D.; Chernick, E. T.; Papadopoulos, I.; Thoss, M.; Tykwinski, R. R.; Guldi, D. M. Solution-Based Intramolecular Singlet Fission in Cross-Conjugated Pentacene Dimers *Nanoscale* **2016**, *8*, 10113-10123.

(13) Cook, J. D.; Carey, T. J.; Arias, D. H.; Johnson, J. C.; Damrauer, N. H. Solvent-Controlled Branching of Localized Versus Delocalized Singlet Exciton States and Equilibration with Charge Transfer in a Structurally Well-Defined Tetracene Dimer *J. Phys. Chem. A* **2017**, *121*, 9229-9242.

(14) Kumarasamy, E.; Sanders, S. N.; Tayebjee, M. J. Y.; Asadpoordarvish, A.; Hele, T. J. H.; Feummeler, E. G.; Pun, A. B.; Yablon, L. M.; Low, J. Z.; Paley, D. W.; Dean, J. C.; Choi, B.; Scholes, G. D.; Steigerwald, M.; Ananth, N.; McCamey, D. R.; Sfeir, M. Y.; Campos, L. M. Tuning Singlet Fission in Pi-Bridge-Pi Chromophores *J. Am. Chem. Soc* **2017**, *139*, 12488–12494.

(15) Basel, B. S.; Zirzlmeier, J.; Hetzer, C.; Phelan, B. T.; Krzyaniak, M. D.; Reddy, S. R.; Coto, P. B.; Horwitz, N. E.; Young, R. M.; White, F. J.; Hampel, F.; Clark, T.; Thoss, M.;

Tykwinski, R. R.; Wasielewski, M. R.; Guldi, D. M. Unified Model for Singlet Fission within a Non-Conjugated Covalent Pentacene Dimer *Nat. Commun.* **2017**, *8*, 15171.

(16) Dean, J. C.; Zhang, R.; Hallani, R. K.; Pensack, R. D.; Sanders, S. N.; Oblinsky, D. G.; Parkin, S. R.; Campos, L. M.; Anthony, J. E.; Scholes, G. D. Photophysical Characterization and Time-Resolved Spectroscopy of a Anthradithiophene Dimer: Exploring the Role of Conformation in Singlet Fission *Phys. Chem. Chem. Phys.* **2017**, *19*, 23162-23175.

(17) Yamakado, T.; Takahashi, S.; Watanabe, K.; Matsumoto, Y.; Osuka, A.; Saito, S. Conformational Planarization versus Singlet Fission: Distinct Excited-State Dynamics of Cyclooctatetraene-Fused Acene Dimers *Angew. Chem. Int. Edit. Eng.* **2018**, *57*, 5438-5443.

(18) Carey, T. J.; Miller, E. G.; Gilligan, A. T.; Sammakia, T.; Damrauer, N. H. Modular Synthesis of Rigid Polyacene Dimers for Singlet Fission *Org. Lett.* **2018**, *20*, 457-460.

(19) Basel, B. S.; Zirzlmeier, J.; Hetzer, C.; Reddy, S. R.; Phelan, B. T.; Krzyaniak, M. D.; Volland, M. K.; Coto, P. B.; Young, R. M.; Clark, T.; Thoss, M.; Tykwinski, R. R.; Wasielewski, M. R.; Gulditla, D. M. Evidence for Charge-Transfer Mediation in the Primary Events of Singlet Fission in a Weakly Coupled Pentacene Dimer *Chem* **2018**, *4*, 1092-1111.

(20) Korovina, N. V.; Joy, J.; Feng, X. T.; Feltenberger, C.; Krylov, A. I.; Bradforth, S. E.; Thompson, M. E. Linker-Dependent Singlet Fission in Tetracene Dimers *J. Am. Chem. Soc.* **2018**, *140*, 10179-10190.

(21) Margulies, E. A.; Miller, C. E.; Wu, Y.; Ma, L.; Schatz, G. C.; Young, R. M.; Wasielewski, M. R. Enabling Singlet Fission by Controlling Intramolecular Charge Transfer in π-Stacked Covalent Terrylenediimide Dimers *Nat. Chem.* **2016**, *8*, 1120-1125.

(22) Johnson, J. C.; Akdag, A.; Zamadar, M.; Chen, X.; Schwerin, A. F.; Paci, I.; Smith, M. B.; Havlas, Z.; Miller, J. R.; Ratner, M. A.; Nozik, A. J.; Michl, J. Toward Designed Singlet

Fission: Solution Photophysics of Two Indirectly Coupled Covalent Dimers of 1,3-Diphenylisobenzofuran *J. Phys. Chem. B* **2013**, *117*, 4680−4695.

(23) Schrauben, J. N.; Akdag, A.; Wen, J.; Havlas, Z.; Ryerson, J. L.; Smith, M. B.; Michl, J.; Johnson, J. C. Excitation Localization/Delocalization Isomerism in a Strongly Coupled Covalent Dimer of 1,3-Diphenylisobenzofuran *J. Phys. Chem. A* **2016**, *120*, 3473-3483.

(24) Sanders, S. N.; Kumarasamy, E.; Pun, A. B.; Steigerwald, M. L.; Sfeir, M. Y.; Campos, L. M. Intramolecular Singlet Fission in Oligoacene Heterodimers *Angew. Chem. Int. Edit. Eng.* **2016**, *55*, 3373-3377.

(25) Alguire, E. C.; Subotnik, J. E.; Damrauer, N. H. Exploring Non-Condon Effects in a Covalent Tetracene Dimer: How Important Are Vibrations in Determining the Electronic Coupling for Singlet Fission? *J. Phys. Chem. A* **2015**, *119*, 299-311.

(26) Sanders, S. N.; Kumarasamy, E.; Pun, A. B.; Appavoo, K.; Steigerwald, M. L.; Campos, L. M.; Sfeir, M. Y. Exciton Correlations in Intramolecular Singlet Fission *J. Am. Chem. Soc.* **2016**, *138*, 7289-7297.

(27) Tayebjee, M. J. Y.; Sanders, S. N.; Kumarasamy, E.; Campos, L. M.; Sfeir, M. Y.; McCamey, D. R. Quintet Multiexciton Dynamics in Singlet Fission *Nat. Phys.* **2017**, *13*, 182-188.

(28) Trinh, M. T.; Pinkard, A.; Pun, A. B.; Sanders, S. N.; Kumarasamy, E.; Sfeir, M. Y.; Campos, L. M.; Roy, X.; Zhu, X. Y. Distinct properties of the triplet pair state from singlet fission *Sci. Adv.* **2017**, *3*.

(29) Fuemmeler, E. G.; Sanders, S. N.; Pun, A. B.; Kumarasamy, E.; Zeng, T.; Miyata, K.; Steigerwald, M. L.; Zhu, X. Y.; Sfeir, M. Y.; Campos, L. M.; Ananth, N. A Direct Mechanism of Ultrafast Intramolecular Singlet Fission in Pentacene Dimers *ACS Cent. Sci.* **2016**, *2*, 316-324.

(30) Berkelbach, T. C.; Hybertsen, M. S.; Reichman, D. R. Microscopic Theory of Singlet Exciton Fission. II. Application to Pentacene Dimers and the Role of Superexchange *J. Chem. Phys.* **2013**, *138*, 114103.

(31) Yost, S. R.; Lee, J.; Wilson, M. W. B.; Wu, T.; McMahon, D. P.; Parkhurst, R. R.; Thompson, N. J.; Congreve, D. N.; Rao, A.; Johnson, K.; Sfeir, M. Y.; Bawendi, M. G.; Swager, T. M.; Friend, R. H.; Baldo, M. A.; Van Voorhis, T. A Transferable Model for Singlet-Fission Kinetics *Nat. Chem.* **2014**, *6*, 492-497.

(32) Liu, H. Y.; Wang, R.; Shen, L.; Xu, Y. Q.; Xiao, M.; Zhang, C. F.; Li, X. Y. A Covalently Linked Tetracene Trimer: Synthesis and Singlet Exciton Fission Property *Org. Lett.* **2017**, *19*, 580-583.

(33) Liu, H. Y.; Wang, Z. W.; Wang, X. M.; Shen, L.; Zhang, C. F.; Xiao, M.; Li, X. Y. Singlet exciton fission in a linear tetracene tetramer *J. Mater. Chem. C* **2018**, *6*, 3245-3253.

(34) Vallett, P. J.; Snyder, J. L.; Damrauer, N. H. Tunable Electronic Coupling and Driving Force in Structurally Well-Defined Tetracene Dimers for Molecular Singlet Fission: A Computational Exploration Using Density Functional Theory *J. Phys. Chem. A* **2013**, *117*, 10824-10838.

(35) Damrauer, N. H.; Snyder, J. L. Symmetry-Directed Control of Electronic Coupling for Singlet Fission in Covalent Bis-Acene Dimers *J. Phys. Chem. Lett.* **2015**, *6*, 4456-4462.

(36) Pace, N. A.; Arias, D. H.; Granger, D. B.; Christensen, S.; Anthony, J. E.; Johnson, J. C. Dynamics of Singlet Fission and Electron Injection in Self-Assembled Acene Monolayers on Titanium Dioxide *Chem. Sci.* **2018**, *9*, 3004-3013.

(37) Bayliss, S. L.; Weiss, L. R.; Rao, A.; Friend, R. H.; Chepelianskii, A. D.; Greenham, N. C. Spin signatures of exchange-coupled triplet pairs formed by singlet fission *Phys. Rev. B* **2016**, *94*.

(38) Weiss, L. R.; Bayliss, S. L.; Kraffert, F.; Thorley, K. J.; Anthony, J. E.; Bittl, R.; Friend, R. H.; Rao, A.; Greenham, N. C.; Behrends, J. Strongly exchange-coupled triplet pairs in an organic semiconductor *Nat. Phys.* **2017**, *13*, 176-181.

(39) Burdett, J. J.; Piland, G. B.; Bardeen, C. J. Magnetic field effects and the role of spin states in singlet fission *Chem. Phys. Lett.* **2013**, *585*, 1-10.

(40) Lewis, J. E.; Maroncelli, M. On the (Uninteresting) Dependence of the Absorption and Emission Transition Moments of Coumarin 153 on Solvent *Chem. Phys. Lett.* **1998**, *282*, 197.

(41) Sens, R.; Drexhage, K. H. Fluorescence Quantum Yield of Oxazine and Carbazine Laser-Dyes *J. Lumin.* **1981**, *24-5*, 709-712.

(42) Scholes, G. D.; Ghiggino, K. P.; Oliver, A. M.; Paddon-Row, M. N. Through-Space and Through-Bond Effects on Exciton Interactions in Rigidly Linked Dinaphthyl Molecules *J. Am. Chem. Soc.* **1993**, *115*, 4345-4349.

(43) Spano, F. C. The Spectral Signatures of Frenkel Polarons in H- and J-Aggregates *Acc. Chem. Res.* **2010**, *43*, 429-439.

(44) It is noted that Saito and coworkers report a nearly quantitative triplet yield of 180%. In our view, this is difficult to reconcile with the reported spectra that show a significant ESA band at ~460 nm as well as significant stimulated emission at ~610 nm, thus signifying the presence of a large amount of excitonic singlet. These workers mention that to account for the dissociation of triplets into independent species from the ^{1}TT, the calculated excited-state concentration must be doubled. We believe that this step is unnecessary and that it leads to a

triplet yield overestimation while significant amounts of singlets remain. We suspect that the triplet yield in Saito's system is likely closer to the 100% that we report here.

(45) As desribed later, we find K ~ 0.1 in TIPS-BT1 and this means that we are underestimating these k_r and k_{nr} values by a small amount in this molecule by assuming K is very small, as per our original interpretation (c.f. 13). We recover the observed decay with the K = 0.1 in place by setting $k_{tot} = k_r + k_{nr} = 4.5\times10^7$ rather than 4.2×10^7. But this translates to a modest difference in lifetime (22.2ns versus 23.8 ns) and the overall conclusion holds.

(46) For example, setting ΔG = -0.34 eV (c.f. 7) while leaving λ = 0.18 eV, one obtains this value of k_{fiss} when V_{eff} is modestly decreased from 5.5 meV to 4.8 meV.

(47) Paddon-Row, M. N.; Shephard, M. J. Through-bond orbital coupling, the parity rule, and the design of "superbridges" which exhibit greatly enhanced electronic coupling: A natural bond orbital analysis *J. Am. Chem. Soc.* **1997**, *119*, 5355-5365.

(48) Clayton, A. H. A.; Scholes, G. D.; Ghiggino, K. P.; Paddon-Row, M. N. Through-Bond and Through-Space Coupling in Photoinduced Electron and Energy Transfer: An ab Initio and Semiempirical Study *J. Phys. Chem.* **1996**, *100*, 10912-10918.

(49) Scholes, G. D.; Ghiggino, K. P.; Oliver, A. M.; Paddon-Row, M. N. Intramolecular Electronic-Energy Transfer between Rigidly Linked Naphthalene and Anthracene Chromophores *J. Phys. Chem.* **1993**, *97*, 11871-11876.

Chapter 4: Dynamics of the Charge-Transfer State during Singlet Fission in a Rigid Molecular Dimer

4.1 Introduction

Chapter 3 has established the viability of studying singlet fission through the platform of molecular dimers, TIPS-BT1′ and TIPS-BP1′. In toluene, TIPS-BP1′ demonstrated unity conversion from the S_1 to ^{1}TT whereas TIPS-BT1′ showed only a partial conversion (~50 %) to form an excited-state equilibrium (K = 1).[1] While the rapid formation of the coupled triplet state in TIPS-BT1′ (τ = 2.5 ps) can obfuscate many important details, the equivalent excited state populations between S_1/^{1}TT provides a highly sensitive tool to observe and perturb the singlet fission process.

As previously mentioned in **Chapter 1** the formation of two independent triplets from a photoexcited singlet requires an intermediate, referred to as the coupled triplet state. The process of the formation of this coupled triplet state is itself the focus of significant investigation. In the simple system of weakly-coupled molecular dimers the formation of ^{1}TT from S_1 can be simply described as two diabatic states with a four frontier orbital basis set, representing the HOMO/LUMO of two chromophores.[2] The formation of the ^{1}TT state directly from the S_1 is referred to as the direct mechanism, represented by the Hamiltonian matrix element $\langle\, ^1TT|H_{el}|S_1S_0\rangle$ or $\langle\, ^1TT|H_{el}|S_0S_1\rangle$ depending on which chromophore arm the exciton is localized. As depicted in Fig. 4.1 going from the initial S_1 to the final ^{1}TT product directly requires two electron transfer events to occur simultaneously. These matrix elements are expected to be small resulting in small electronic coupling values that fail to explain the ultrafast observation of singlet fission.[3]

An alternative description is therefore required to overcome this obstacle. Using the previously describe orbital space two new states can be conceived of $|CA\rangle$ and $|AC\rangle$, referred to as charge-transfer states, hereafter referred to as the CT state. With two unpaired electrons (one in each chromophore, one arm is oxidized and referred to as the cation C, the other reduced to an anion A, a charge imbalance is created hence the name. Using the CT states as intermediates, second-order perturbation theory can be invoked to generate new matrix products ($\langle {}^1TT|H_{el}|CA\rangle \times \langle CA|H_{el}|S_0S_1\rangle$ and $\langle {}^1TT|H_{el}|AC\rangle \times \langle AC|H_{el}|S_0S_1\rangle$. Returning to the orbital space now, for the first step in the mediated mechanism both $\langle AC|H_{el}|S_0S_1\rangle$ and $\langle CA|H_{el}|S_0S_1\rangle$ can be well represented as "horizontal" electron transfers. What this describes is a HOMO-HOMO or LUMO-LUMO electron transfer from one chromophore arm to the other and they're expected to have a reasonable magnitude. The second step, $\langle {}^1TT|H_{el}|CA\rangle$ and $\langle {}^1TT|H_{el}|AC\rangle$ can also be described orbitally as "non-horizontal" HOMO-LUMO electron transfer from one arm to the other. These matrix elements when approximated for the orbital space depend heavily on chromophore orientation to produce sufficient matrix elements.[4] In the case of previously discussed norbornyl bridged dimers they're expected to be small. Given this treatment the CT state plays an important, but versatile role in singlet fission.[5] In tetracene based systems the CT state is expected to be several hundred meV above the S_1 & ^{1}TT states in a non-polar environment,[4] meaning no significant population buildup that can be observed by spectroscopic measurement can occur. The CT state is thus expected to facilitate singlet fission through virtual coupling. A more polar medium is expected to stabilize the cation/anion pair on the organic chromophores, lowering the CT state energy enough that it can be populated. Indeed, a vast body literature has been produced in the last few years studying the CT in a number of singlet fission systems, such as diimide,[6–8] dibenzofuran[9] and acene dimers.[10,11]

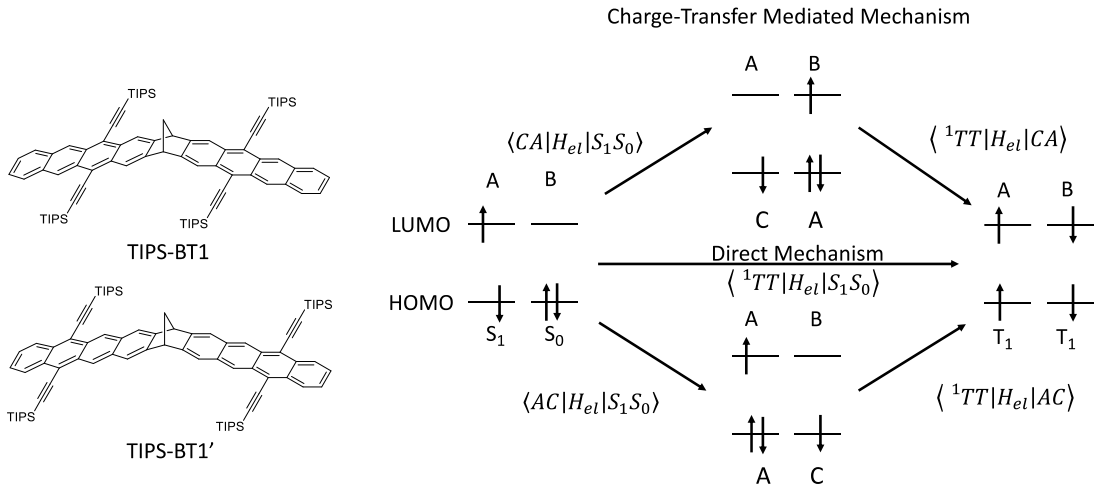

Figure 4.1 Chemical structures of TIPS-BT1 & TIPS-BT1´ (left). Representation of the direct & charge-transfer mediated paths for singlet fission (right).

For this work TIPS-BT1´ was again studied, but this time using the solvent of benzonitrile rather than toluene. With a dielectric constant of 25.2[12], compared to 2.38[13] for toluene, benzonitrile can help stabilize any present charge imbalance, energetically lowering the charge-transfer state. Previous work in the research group with the constitutional isomer dimer TIPS-BT1 in benzonitrile showed benzonitrile was indeed able to stabilize the CT state enough to allow it to be experimentally observed.[14] Time-resolved measurements determined that the formation of the CT state occurred in 50 ps with no additional dynamics observed before ground-state recovery. In addition, TIPS-BT1 also showed an excited-state bifurcation on excitation into an arm-localized and delocalized singlet states. It was the arm-delocalized S_1 that was able to undergo formation of the CT state while the arm localized S_1 decayed directly back to the ground state.

4.2 Results

4.2.1 Steady-State Measurements:

Stead-state absorption and emission measurements of TIPS-BT1´ were performed in room temperature benzonitrile. The absorption spectrum of TIPS-BT1´ shows a vibronic progression, characteristic of tetracenic molecules, with a 0-0 absorption peak at 534 nm (Fig. 4.2). This often characterized the S_0 to S_1 transition of acene systems. The vibronic progression undergoes a slight bathochromic shift of ~4 nm compared to the absorption spectrum measured in toluene/chloroform in **Chapter 3** similar to what was observed in TIPS-BT1. Compared to the monomer model of TIPS-Tc the 0-0 transition shows a slight blueshift of ~5 nm in benzonitrile. Unfortunately, the broad solvent absorption window of benzonitrile prevents observation of the Davydov split S_3 absorption feature. A lack of solubility prevented the use of the UV-transparent solvent acetonitrile to observed differences in the S_3 absorption. The emission spectrum showed a vibronic progression in its emission as well, with the 0-0 emission peak at 548 nm. As was the case with the absorption spectrum, the emission features experience a bathochromic shift as well in benzonitrile, compared to data collected in toluene. The quantum yield of TIPS-BT1´ in benzonitrile is ~40 % compared to the standard Coumarin 540A in methanol. This is lower than the reported quantum yield for TIPS-BT1 in benzonitrile at 54 %. This is also lower than both TIPS-BT1 & TIPS-BT1´ in toluene, with a reported quantum yield of ~72 %.

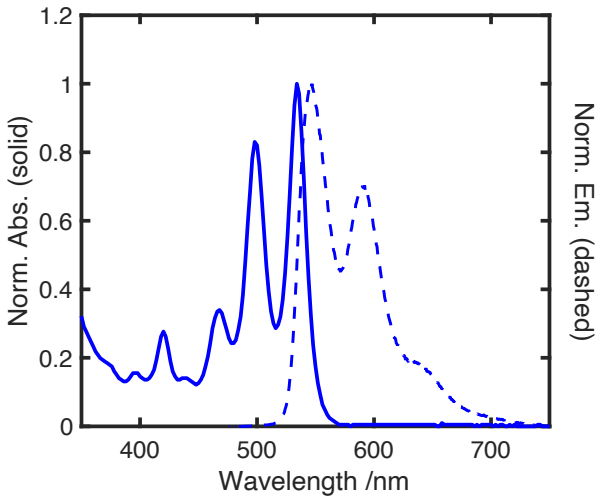

Figure 4.2 Absorption and emission spectra of TIPS-BT1′ in room temperature benzonitrile.

To further investigate this drastic change in the quantum yield for TIPS-BT1′ in benzonitrile compared to toluene, a temperature-dependent study of the emission was performed. The fluorescence was taken at six independent temperature points (0 °C to 50 °C in 10 °C increments) and the fluorescence spectrum and quantum yield were measured to observe any significant changes. Raw emission spectra in Fig. 4.3 show a steady increase in the emission intensity as the temperature is increased. The quantum yield increases from ~25 % at 0 °C to ~50 % at 50 °C for TIPS-BT1′ in benzonitrile. In TIPS-BT1 this was shown to be primarily due to the depopulation of the bright S_1 to a lower energy dark CT state.[14]

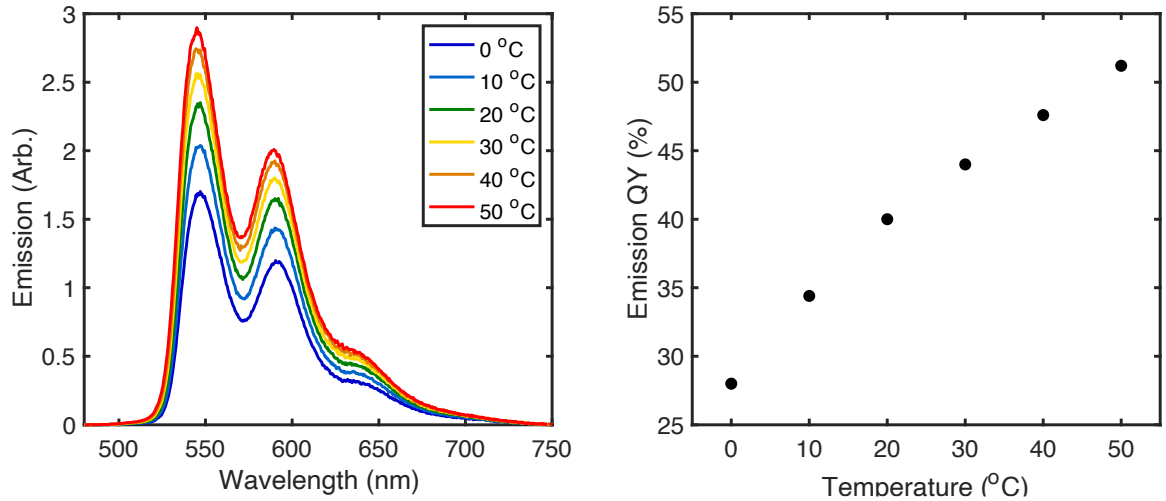

Figure 4.3 Temperature-dependent emission spectra of TIPS-BT1′ in benzonitrile (left). Temperature-dependent quantum yields of TIPS-BT1′ in benzonitrile (right).

4.2.2 Nanosecond Measurements:

Nanosecond transient absorption and time-correlated single photon counting (TCSPC) were used to observe and record excited-state dynamics on the timescale of ~500 ps after excitation until full ground-state recovery, ~200 ns later. Nanosecond transient absorption spectra were recorded in the visible range to monitor the excited state populations of any long-lived species present after excitation. TCSPC was also recorded allowing for the measurement of any fluorescent species present after excitation.

Prominent features of nanosecond transient absorption spectra in Fig. 4.4 (a) include from 390 nm to 520 nm an excited state absorption (ESA) band punctuated by features from the ground-state bleach. To the red of 550 nm is a continuous ESA band that extends past 900 nm, into the near-infrared region. Spectral slices show decay back to the ground-state with a time constant of ~40 ns.

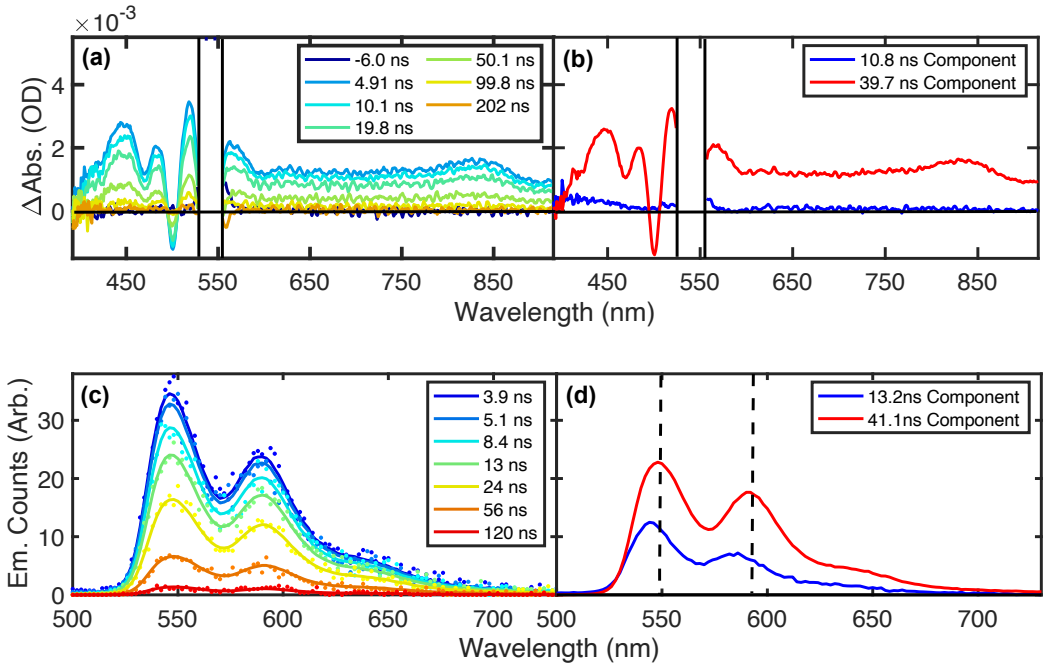

Figure 4.4 Nanosecond transient absorption of TIPS-BT1′ in benzonitrile. Spectral slices (a) and retrieved basis spectra from global analysis (b). Time-resolved fluorescence spectra of TIPS-BT1′ in benzonitrile (c) with retrieved basis spectra (d). Dashed lines in figure (d) are to clarify the dissimilar peak emission wavelengths between the two resolved basis spectra.

To better understand the observed dynamics collected using nanosecond TA, global analysis was performed to retrieve the basis spectra of the data set and their associated time constants. The data were fit to a two-exponential component model that decayed back to baseline (see Fig. 4.4 (b)). The retrieved basis spectra had time constants of 11 ns and 40 ns, with the majority of the signal coming from the 40 ns component. Given the small signal and relative lack of distinguishing features of the 11 ns component, TCSPC was performed due to its greater sensitivity. Time-resolved spectra collected from TCSPC at early times are highly similar to the steady-state photoluminescence spectrum (see Fig. 4.4 (c)). Single wavelength kinetic traces taken at a variety of wavelengths show bi-exponential decay back to baseline with retrieved time constants of ~13 ns and 40 ns.

To better understand the nature of these two observed time constants, global analysis was also performed on the full spectral and time resolved TCSPC data set using the same parameters as described for the nanosecond TA analysis. Global analysis returned two highly similar basis spectra with time constants of 13 ns & 41 ns (see Fig. 4.4 (d)). The greater intensity of the 41 ns component suggests it to be the major decay channel, similar to the nsTA global analysis results. This emission behavior has been seen previously with the compound TIPS-BT1 in benzonitrile. It was determined that after initial excitation a bifurcation of TIPS-BT1 occurred from its Franck-Condon state into localized & delocalized S_1 states that did not interconvert and had different photophysical characteristics. The highly similar structure and photophysical behavior of TIPS-BT1´ suggests that it is acting similarly to TIPS-BT1.

4.2.3 Femtosecond Measurements:

Early-time dynamics of TIPS-BT1´ were interrogated by femtosecond transient absorption spectroscopy. At early times the observed photo-induced absorption features appear similar to those observed previously with TIPS-BT1 in benzonitrile (see Fig. 4.5 for summarized TA results). A broad excited-state absorption feature is present from 370 nm out to 620 nm. This ESA overlaps with ground-state bleach features at 464 nm, 500 nm & 534 nm as well as stimulated emission at 580 nm to create distinct and unique transient absorption features. This initial excitation into the S_1 state provides the starting point for discussing observed spectral dynamics. Two sets of spectral dynamics are observed in the collected TA data. The first set occurs within 10 ps after initial excitation, while the second set of dynamics are finished after 400 ps. There appears to be no evolution in the spectral slices past 400 ps out to 1.5 ns, the end point of the experiment. The early time dynamics are characterized by several changes in the spectral slices as shown in Fig. 4.5 (a).

The primary changes include a reduction in the ESA band from ~400 – 460 nm and the loss of signal from stimulated emission at ~590 nm. The ultrafast nature of these changes as the small increase in the ESA at 520 nm excludes the idea of ground state recovery and suggest the population of a new state. The late time dynamics shown in Fig. 4.5 (b) are primarily characterized by an increase in the ground state bleach signal from ~460 – 530 nm and continued loss of stimulated emission signal. The observed signal continues into a broad ESA shoulder that continues out past 630 nm, the limit of this experiment. This presumably is the ESA shoulder observed in the previous nanosecond TA experiment. The final observed change to note is an increase in the ESA signal observed from 370 – 400 nm.

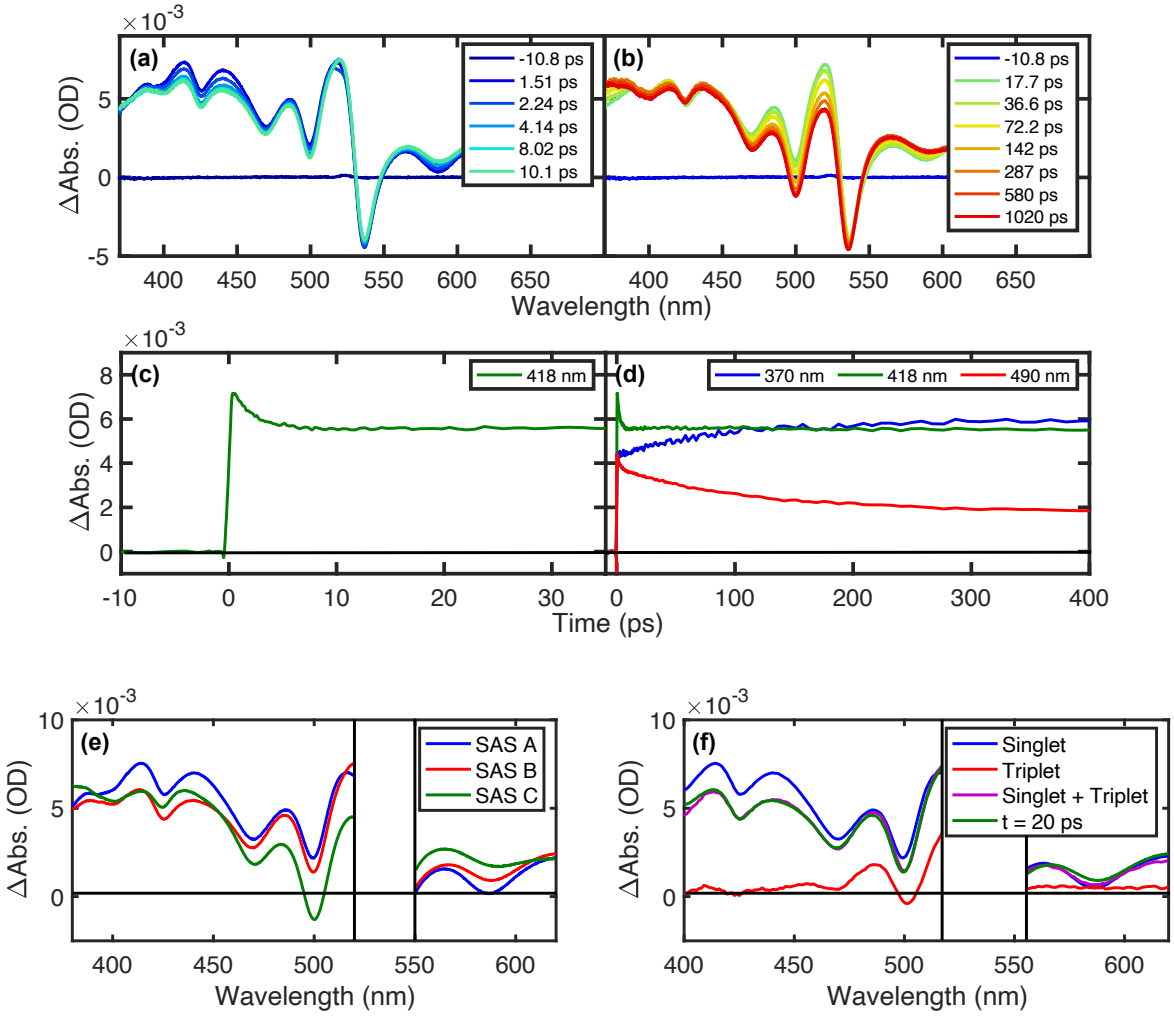

Figure 4.5 Femtosecond transient absorption measurements of TIPS-BT1´ in benzonitrile. Early-time spectra and kinetics (a/c) with late-time spectra and kinetics (b/d). Retrieved species associated spectra from global analysis (e). Reconstruction of spectral splice from singlet and sensitized triplet spectra compared to spectral slice at t = 20 ps (f).

To understand the excited-state dynamics of TIPS-BT1´ observed in fsTA global analysis was performed to retrieve species associated spectra as well as the associated time constants. The data set was fit to a three-basis set model with two-time constants and a long-lived shelf that continued past the limits of this experiment into the tens of nanoseconds. The residual of the raw data with model from global analysis suggests no other components or time constants are present within the data set. The retrieved species associated spectra (SAS) shown in Fig. 4.5 (e) show the

initially formed SAS A transitions with a time constant of 2 ps into SAS B through a series of spectral changes matching the early time dynamics previously described. SAS B itself then transitions into species C with a time constant of 92 ps.

The spectral dynamics observed on the timescale of 10 – 400 ps show significant similarities to those observed for TIPS-BT1 in benzonitrile.[14] The conclusions of that work were that TIPS-BT1 in benzonitrile, the CT state was stabilized enough energetically by the polar solvent to be populated after initial excitation, based on difference absorption spectra from spectral-electrochemical measurements taken of TIPS-BT1 in benzonitrile that matched the transient absorption features. The observed time constant for CT formation in TIPS-BT1 (50 ps) is of the same order of magnitude as the dynamics observed in TIPS-BT1′ (92 ps). Based on the similar spectral changes and lifetimes it appears likely that SAS C is showing CT state formation.

We now return to the earliest observed dynamics, from 0 – 10 ps. The 2 ps transition between SAS A & B whose primary characteristics are the loss of ESA signal from 400 – 460 nm and the decrease in stimulated emission signal. While not as pronounced, this bears a significant similarity to what was observed in TIPS-BT1′ in toluene in **Chapter 3**. The conclusion of that work was that TIPS-BT1′ was entering into an excited-state equilibrium between the S_1 & ^{1}TT. The observed spectral dynamics were due to the loss of S_1 population and the rise of ^{1}TT. This presents the question about whether the same evolution is occurring, but in benzonitrile.

To confirm this hypothesis a triplet sensitization experiment was performed where TIPS-BT1′ was sensitized with anthracene triplets to determine the triplet spectrum of TIPS-BT1′ in benzonitrile. The triplet spectrum of TIPS-BT1′ was retrieved though global analysis and bears significant similarity to the triplet spectrum observed in toluene (see Chapter 4 SI, Fig. 4.6.7 for comparison and triplet sensitization details). Using the same methodology to determine the singlet

fission yield for TIPS-BT1′ in toluene in **Chapter 3** the yield was calculated for benzonitrile. The superposition of S_1 and T_1 spectra was compared to measured spectra at 20 ps as shown in Fig. 4.5 (f) when the $S_1/^1TT$ equilibrium is expected to be established, but before significant CT formation is observed. The combination singlet/triplet spectra is well able to reproduce the spectrum at 20 ps. A T_1 yield of 50 % was calculated based on the calculation of initial excited state concentration and the excited triplet concentration. This corresponds to ^1TT of 25 %, half of the singlet fission yield observed in toluene. The calculated K_{SF} therefore is also reduced from 1.0 (toluene) to 0.33 (benzonitrile).

It is worth noting the unusual observation of CT state formation after the singlet fission event has occurred. A significant body of literature has shown the CT state to facilitate singlet fission as a virtual or real state, or to act as a trap state when low enough in energy.[10,15,16] In the case of TIPS-BT1′ in benzonitrile though singlet fission appears to be occurring before the appearance of the CT state. It provides compelling evidence though that singlet fission is occurring and not charge-transfer assisted intersystem crossing that can also generate triplets.[17] To further probe these dynamics the variable of temperature was invoked in measuring the impact on TIPS-BT1′ in benzonitrile.

4.2.4 Temperature-Dependent Femtosecond Measurements:

Previous experiments with TIPS-BT1 have shown the effect of temperature on the lifetimes of $S_{1,\,loc}$ and $S_{1,\,deloc}$, but not on the initial appearance of the CT state itself.[14] To further interrogate the role of both the ^1TT and CT in TIPS-BT1′ temperature-dependent femtosecond transient absorption measurements were performed. Spectra were collected at several different temperature points (between 10 °C and 50 °C in 10 °C increments, see Chapter 4 SI, section 4.6.6 for data and

spectral analysis), to determine the impact on the observed formation of the CT state. CT state formation will be discussed first. Using the same methods as previously described in section 4.2.3, global analysis showed a reduction in the formation lifetime of the CT state. The maximum lifetime observed was 120 ps at 10 °C while at 50 °C it had been reduced to 40 ps. Additionally there were several noticeable changes in SAS C. The most apparent is the decrease in the ESA feature observed at ~370 nm and a decreased intensity of the ground-state bleach feature, particularly at 498 nm as the temperature is increased. Both of these features are highly associated with the CT state and point to a disturbance in the CT equilibrium population.

As for the time-constant describing the initial dynamics. The retrieved time constant for the $S_1/^1TT$ formation was ~2 ps for all temperature points (see Table 4.6.2 for compiled data). While there was an apparent insensitivity in the first lifetimes from the five temperature points, small spectral changes were observed between samples. Both SAS A/B showed nearly identical retrieved spectra as shown in Fig. 4.6.12 for the temperature range covered. The ^1TT yield based on the S_1 spectral decay during equilibrium formation was also ~25 % for all temperature points. The lack of apparent spectral or temporal variation suggests no significant change in the equilibrium populations, unlike what was observed with the CT state. Definitive resolution of a change in lifetime would likely require cryogenic temperatures.

4.3 Discussion

In benzonitrile the observed 0-0 transition peak of TIPS-BT1´ at 534 nm, while slightly redshifted of the same transition in TIPS-BT1 (at 532 nm), is still blueshifted relative to the monomer model TIPS-Tc (at 535 nm). In simple acene systems the lowest energy excitation consists of a HOMO-LUMO transition, with a transition dipole aligned along the chromophores

short axis. The norbornyl bridging group electronically donates into the HOMO, destabilizing it and raising the S_1 energy.[4] Alignment of the transition dipole along the short-axis of each chromophore arm means that the two dipoles will lie in a parallel geometry, giving the molecular transition an H-type aggregate description.[18] The coupling of two chromophores to form a dimer will result in two possible singlet state (a previous computational work on these norbornyl bridged acenes referred to these as S_{1b} and S_{1a}).[4] S_{1b} represents the in-phase dipole allowed transition and S_{1a} is the out of phase transition. Splitting between S_{1b}/ S_{1a} is expected to be proportional to the Davydov splitting. Since the antiparallel dipole orientations destructively interfere completely, the redshifted S_{1a} lower energy transition is not observed, S_{1b} with constructive interference between dipoles is the brightly observed transition. What's curious is the greater blueshift that is observed in TIPS-BT1 vs TIPS-BT1´, compared to TIPS-Tc, suggesting stronger interaction between the transition dipoles via the placement of the TIPS groups on the core tetracene system. The observed emission 0-0 transition also experiences the same trend as described in absorption measurements for TIPS-BT1 vs TIPS-BT1´. Taken together this results in an S_1 energy that is slightly lower in TIPS-BT1´ vs TIPS-BT1, but to a negligible degree that the S_1 energy can be calculated to be 2.29 eV for both molecules. These steady-state measurements also suggest slightly lower interchromophore coupling for TIPS-BT1´ compared to TIPS-BT1, which at face-value would hurt the process of singlet fission. As was observed in toluene, TIPS-BT1´ still readily formed the ^{1}TT state despite this lower coupling due the reduced exchange interaction making the ^{1}TT more accessible energetically. While this is primarily expected to impact the SF rate, it can also be extended to CT state formation where lower coupling might impact the amount of CT state formed, although the effect should be minor. The steady-state measurements provide a qualitive means of

interrogating the chromophore coupling, ultimately time-resolved measurements are necessary to monitor excited-state population transfer.

We now turn to the transient absorption and time-resolved photoluminescence nanosecond measurements to look at the observed biexponential behavior seen in both experiments. Global analysis retrieved two lifetimes from both experiments, a short ~12 ns lifetime and a longer 40 ns one. This shorter lifetime matches well with the observed lifetime for the decay of TIPS-Tc in benzonitrile, suggesting as was observed with TIPS-BT1 that after initial excitation the TIPS-BT1′ excited-state population is getting partitioned into two separate S_1 states, $S_{1,\,loc}$ & $S_{1,\,deloc}$, with $S_{1,\,deloc}$ being the energetically lower of the two. We can further support this claim by looking at the retrieved spectra from TRES. Figure 4.4 (d) shows a slight redshift in the emission of the longer-lived lifetime that's hypothesized to be $S_{1,\,deloc}$, compared to the blueshifted spectrum of the shorter-lived lifetime (emphasized by the dashed lines placed in Fig. 4.4 (d)). This redshift comes from the stabilization of the excited-state across the entire molecule, slightly reducing the state energy as opposed to localizing it on one arm. Another point to consider is the relative intensity of the 0-1 emission peak to 0-0 emission peak in both spectra. The longer-lived lifetime shows a greater relative peak intensity between the 0-0 and 0-1 transitions compared to the shorter-lived lifetime (0.8 vs 0.5). The lack of suppression of the 0-0 transition, relative to the 0-1 transition suggests a lack of H-type aggregate state character.[19] Both of these behaviors were observed in TIPS-BT1 and determined to come from the fact that two S_1 states were being observed. With the determination of their state character we can also use these data to determine the relative population yields of $S_{1,\,loc}$ & $S_{1,\,deloc}$.

From retrieved spectra from global analysis, integrated photon counts along both the spectral and temporal axes were used to determine that ~12 % of emitted photons come from $S_{1,}$

$_{loc}$ vs ~88 % for $S_{1,\,deloc}$ (see Chapter 4, section 4.6.2 Supporting Information for full data analysis). While this suggests that most excited molecules end up in $S_{1,\,deloc}$ state, it doesn't conclusively prove the hypothesis that $S_{1,\,deloc}$ is the major population after initial excitation since non-radiative population loss isn't accounted for. In order to determine the relative excited-state populations of $S_{1,\,loc}$ & $S_{1,\,deloc}$ a careful examination of the radiative & non-radiative decay pathways available for each state will be required. It's been previously reported that TIPS-Tc in benzonitrile has a near unity quantum yield of fluorescence (90%). This suggests that the localized S_1 state does not decay by a significant amount through non-radiative processes. On the other hand, the measured quantum yield for TIPS-BT1′ in benzonitrile (40 %), with most of this emission coming from $S_{1,\,deloc}$, this suggests significant non-radiative decay processes present from the dimer delocalized state. This means that the relative concentration of $S_{1,\,deloc}$ is likely higher than 88 %. Using the reported quantum yield of TIPS-Tc as a proxy for $S_{1,\,loc}$ gives a likely $S_{1,\,deloc}$ yield of ~95% (see Chapter 4 SI, section 4.6.2 for details). The small yield of $S_{1,\,loc}$ makes its contribution to the observed femtosecond and nanosecond dynamics negligible. The results match well with nsTA global analysis where the ~11 ns component is shown to be a fraction of the larger 40 ns component suggesting it holds only a minimal amount of the excited state population.

The CT state energy was calculated to be ~2.18 eV based on DFT calculations of the cation/anion monomer energies (see Chapter 4 SI, section 4.6.1 for full details). A Coulomb attraction term was applied to account for the energetic stabilization of the adjacent cation/anion charges on separate dimer arms. The CT state energy is ~110 meV lower than $S_{1,\,deloc}$, with the CT state at ~2.18 eV or $\Delta E_{CT} = -110\ meV$. Per the Boltzmann factor at room temperature, most of this excited-state population from $S_{1,\,deloc}$ will transfer to the CT state (~98 %). As for ^{1}TT, based on the measured triplet yield the singlet fission equilibrium constant was calculated (K_{SF} = 0.33),

the Boltzmann factor was again applied to find $\Delta E_{SF} = 30\ meV$ and retrieve a E(^{1}TT) of 2.32 eV, the same E(^{1}TT) as reported for toluene. Relative state populations were calculated with the canonical partition function using the known energies for $S_{1,\ deloc}$, ^{1}TT and CT (see Chapter 4 SI, section 4.6.7). A kinetic model of parallel ^{1}TT and CT formation from the S_1 (see Chapter 4 Supporting Information, section 4.6.7) was constructed from coupled differential equations. Rate equations were fit to the retrieved global analysis lifetimes and relative populations. The CT formation rate constant $k_{CT} = 1.4\times10^{10}$ s^{-1} and SF formation rate constant $k_{fis} = 1.2\times10^{10}$ s^{-1} were retrieved from the model. Table 4.1 summarizes important photophysics of TIPS-BT1´ in benzonitrile compared to results taken in toluene in **Chapter 3**.

Solvent	S_1 (eV)	CT (eV)	^{1}TT (eV)	k_{fis} (s^{-1})	k_{CT} (s^{-1})
Toluene	2.32	2.71	~2.32	2.0×10^{11}	-
Benzonitrile	2.29	2.21	~2.32	$\sim1.2\times10^{11}$	1.4×10^{10}

Table 4.1: State energies and rate constants for TIPS-BT1´ in benzonitrile and toluene.

For the temperature-dependent fsTA state populations were calculated for each temperature point with the canonical partition function again. From the calculated state populations and observed lifetime, rate constants for the formation of the CT state (k_{CT}) were calculated through kinetic modeling of the system previously described for the room-temperature result. As expected by the shortening of the observed lifetime, the rate constant for the formation of the CT state significantly increases as the temperature is increased from 10 °C with $k_{CT} = 1.1\times10^{10}$ s^{-1} to 50 °C with $k_{CT} = 3.3\times10^{10}$ s^{-1} (k_{CT} results compiled in Table 4.6.4).

Given the observed temperature-dependence of k_{CT} this relationship can be used to further probe fundamental variables that compose it. We return to Marcus Analysis first visited in

Chapter 3, used to rationalize the rate of observed population transfer between two weakly-coupled diabatic states (S_1 and ^1TT) in TIPS-BT1, TIPS-BT1′ & TIPS-BP1′. Here it can be applied to the S_1/CT state dynamics. The classic Marcus expression (see Chapter 4 SI, section 4.6.9) contains only two unknown variables V_{eff} and λ (the electronic coupling between the states and solvent reorganization energy). The S_1/CT state energy difference ΔG having previously been determined from computations was also applied. Rate constant k_{CT} was plotted against the experimental temperature and fit to the Marcus expression to retrieve values for the solvent reorganization energy and electronic coupling, shown in Fig. 4.6. A value of 1150 meV was retrieved for λ and gave a corresponding value of ~86 meV for V_{eff}. A solvent reorganization energy of ~1 eV is expected for charge transfer state formation due to the large solvent motions required to stabilize the state in polar solvent.[20] With such a large reorganization energy a high coupling value is required in order to calculate a rate constant that matches with the observed formatiom.

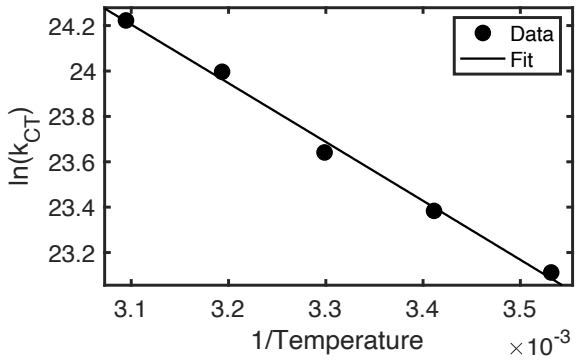

Figure 4.6 Plot of calculated rate constant k_{CT} from temperature-dependent fsTA data with fit to Marcus equation.

This brings up an interesting comparison with the previous values of solvent reorganization energy and coupling for the singlet fission rate constant for TIPS-BT1′ in toluene. In both cases of reorganization energy and coupling the retrieved values are much larger for CT state formation

in TIPS-BT1´ in benzonitrile than formation of the ^{1}TT in toluene. We shall first discuss the solvent reorganization energy. With a calculated reorganization energy of 1150 meV, this is much larger than the reasonable guess singlet fission value of 180 meV used previously in **Chapter 3**. This is unsurprising given the nature of the two states involved, the ^{1}TT and CT states. The CT state involves the charge separation of an electron and hole pair to separate arms of the molecule that can be effectively stabilized due to the large dielectric constant of benzonitrile (25.9). Such a large dielectric constant will make the solvent molecules susceptible to realignment to lower the energy of the charge-dipole interaction, and with large phenyl groups requires a large energetic expenditure on the part of the solvent molecules. This is opposed to the spin-paired coupled triplet state formed in singlet fission. With no charges requiring substantial reorientation of the solvent molecules, the reorganization energy is expected to be much lower. The CT state in benzonitrile, as opposed to toluene, moves from a virtual state to a real, populated state as solvent dipoles reorient during the charge-transfer process.

Now to consider the other half of the classical Marcus equation; the effective coupling (V_{eff}). The calculated coupling for the formation of the CT state (86 meV) is significantly larger than the considered value for singlet fission at 5.5 meV. These values suggest that formation of the CT state is significantly more favorable to form than the ^{1}TT. An easily approachable explanation that can reconcile this requires us to return to the simple two chromophore representation of singlet fission. At its simplest expression singlet fission proceeds via a direct mechanism (not currently favored due to low coupling terms) or indirect mechanism that includes a virtual or real charge-transfer state. If we consider the widely utilized second-order perturbation theory singlet fission coupling picture, the unique symmetry considerations of TIPS-BT1´ (the same C_{2v} symmetry of dimer BT1 where this was first discussed)[4] significantly hamper the

necessary diagonal matrix element to form ^{1}TT through both the electron and hole transfer mechanisms. The "first step" coupling values (to form the charge-transfer state) and are an intermediate of the indirect mechanism report significantly larger coupling values than for the second step which are nominally zero due to symmetry but can be non-zero due to symmetry breaking vibrations.[21] Ultimately the coupling to the ^{1}TT from the CT is expected to be smaller than compared to the first step. This provides a rationale for the difference in the magnitude of the coupling values. As for the determined S_1/CT state coupling, 86 meV is a large enough value to question whether S_1/CT can be considered diabatic states. The nonadiabatic Marcus expression is generally considered appropriate only when the coupling is small $V_{eff} << kT$. While 86 meV is greater than this limit the large reorganization should still mean that S_1 and CT are still fairly distinct electronically since $V_{eff} << \lambda$.[22]

Despite similar CT state energies, the formation of said state takes nearly twice as long in TIPS-BT1´ vs TIPS-BT1 (~90 ps vs ~50 ps). To understand this large difference, it's important to consider the structural difference of TIPS-BT1 vs. TIPS-BT1´: the placement of the TIPS acetylene groups. Computational results and physical observations have shown that the acetylene groups impact the excited-state localization due to their expansion of the conjugated tetracene molecule. With their placement in TIPS-BT1 vs. TIPS-BT1´ the net effect is excited-states in TIPS-BT1´ are localized farther away from each other in TIPS-BT1´ vs. TIPS-BT1. With charge-transfer described as a one electron transfer process from one chromophore to another it stands to reason that the larger distance between the conjugated π systems that constitute donor/acceptor in TIPS-BT1´ would reduce the rate of electron transfer compared to TIPS-BT1. To understand the difference in the rate of formation of the CT state between TIPS-BT1 & TIPS-BT1´ in the Marcus picture requires looking at the coupling between chromophores as well as the reorganization

energy. Reorganization energy in Marcus Theory has both the inner-sphere λ_i and out outer-sphere λ_o contributions. The impact on λ_o was calculated to be ~45 meV lower in TIPS-BT1 vs TIPS-BT1′ based on equation 4.6.38 (see Chapter 4 SI, section 4.6.9 for full discussion on Marcus Analysis of the CT state) at 1.10 eV. Using this new value of λ_o along with other necessary Marcus parameters (ΔG and V_{eff} were taken to be the same as in TIPS-BT1′) the rate constant for CT formation was calculated for TIPS-BT1. This minor change to λ_o (~5 %) significantly impacts the rate constant for CT formation with it being 50 % higher in TIPS-BT1 vs. TIPS-BT1′ at 1.7×10^{10} s^{-1}. Using the same methodology to calculate the rate constant for the reverse process, the reformation of $S_{1,\,deloc}$ from the CT state finds similar results with rate constant being ~50 % higher in TIPS-BT1 vs TIPS-BT1′. These two rate constants were summed to approximate the observed rate constant for CT formation (50 ps experimental, 58 ps calculated). The calculated reduction in the CT state formation lifetime matches well with experimental results suggesting that TIPS-BT1 does likely benefit from a lower λ_o energy.

With a calculated rate constant of $\sim1.4\times10^{10}$ s^{-1}, the rate constant for the formation of the CT state is approximately an order of magnitude smaller than the value calculated for the singlet fission rate constant at $\sim1.2\times10^{11}$ s^{-1}. As previously discussed, while the S_1 to CT rate constant shows an inherently larger coupling value than S_1 to ^{1}TT as well as more favorable energetics, the significantly larger reorganization energy delays its formation. It's important to consider the physical basis of this solvent reorganization and its impact on the singlet fission process. After initial excitation into the S_1 state the benzonitrile solvent shell, must reorder itself to account for the small changes in the molecular geometry of the excited-state of TIPS-BT1′. This reordering is generally thought to be non-instantaneous in the case of benzonitrile due to the bulk nature of the core phenyl rings. Without the stabilizing effect of the solvent environment the CT state acts as a

virtual state that can still serve to couple the S_1 to ^{1}TT and mediate singlet fission. As time further passes the solvent dipoles are able to reorient, producing an energetically stable CT state that can be observed. With the ^{1}TT positioned uphill energetically of both the S_1 & the CT state its population is drained as the low energy CT state becomes available. Ultimately due to thermodynamic considerations the CT state serves as a parasitic pathway that transfers population out of the ^{1}TT after facilitating its formation.

As for the ^{1}TT itself, its formation is of similar lifetime as observed in toluene, but with a smaller yield. The reported yield of ^{1}TT formation for TIPS-BT1´, was 50 %, whereas in benzonitrile it's ~25 %. The significant difference between the ^{1}TT yields of TIPS-BT1´ in toluene & benzonitrile provides an interesting case study on solvent interactions with the ^{1}TT. A lower ^{1}TT yield is expected given the small redshift of $S_{1,\,deloc}$ as the solvent is changed from toluene to benzonitrile only if the ^{1}TT state energy doesn't change by a similar amount. To fully understand why this may be the case we can return to the charge-transfer mediated singlet fission mechanism. As previously discussed there isn't expected to be significant coupling in the $\langle\, ^1TT|H_{el}|CA\rangle$ matrix element for TIPS-BT1´. This suggests little mixing between the ^{1}TT and the CT state. Returning to the S_1 state, the bathochromic shift in the absorption and emission spectra suggest a small measure of mixing of the S_1 and CT states.[23] This mixing allows for the reduction in S_1 energy without significantly affecting the ^{1}TT energy, disturbing the symmetric equilibrium that was established in toluene. Ultimately this mixture of the CT state into the S_1 serves to disfavor the formation of ^{1}TT even before population is transferred into the lower energy CT state. With a goal of increasing the ^{1}TT yield these results suggest that achieving less mixture with the CT state is desirable.

With a ΔG = 29 meV, singlet fission can now be considered endergonic and is expected to impact both k_{fis} and k_{fus} (k_{fus}, the triplet fusion rate constant, was determined to be 3.8×10^{11} s^{-1} from the kinetic model). Compared to in toluene where $k_{fis} = k_{fus}$, in benzonitrile k_{fus} is now favored by a factor of three over k_{fis}. As observed in the fsTA, a small buildup of ^{1}TT occurs but rapidly disappears as the S_1 is depopulated to the CT state and k_{fus} replenishes it. Applying the same reasonable guesses for V_{eff} = 5.5 meV and λ = 180 meV, used in the Marcus expression in **Chapter 3** with the new ΔG gives values of 1.1×10^{11} s^{-1} and 3.5×10^{11} s^{-1} for k_{fis} and k_{fus}, suggesting that ΔG is the significant contributing factor to differences in the singlet fission rate constant between toluene and benzonitrile. With singlet fission now endergonic, potential applications would now require a means for exciton separation like spatial separation of triplet excitons so favorable recombination doesn't occur.[24]

A final point to consider with $S_1/^1$TT equilibrium for TIPS-BT1´ is the results obtained from temperature-dependent fsTA and where it fits in the adiabatic/diabatic framework. The absence of variation in the retrieved time constants and SAS points suggests that the population is insensitive to the temperature change, pointing towards a mixed $S_1/^1$TT state adiabatic picture. However, applying the same reasonable guess values previously to the observed temperature range shows the change to k_{SF} is relatively minimal (see Chapter 4 SI, section 4.6.10). Over the given temperature range k_{SF} only increases by ~30 %, much smaller than the factor of three observed with k_{CT}. This minimal change in k_{SF} will likely extend to a minimal change in an observed lifetime that's difficult to observe. While adiabatic SF has been observed those systems were composed of face-stacked PDI[8] and orthogonal pentacene dimers[11] that suggested to be strongly coupled. Indeed, the extent of state mixing in those cases was such that the molar extinction coefficient of the dimers was significantly lower compared to monomer versions. Given the behavior observed

in chloroform in **Chapter 3** where TIPS-BT1′ showed a molar extinction coefficient twice that of the monomer, points to only very weak mixing. These points together favor the diabatic representation as still being valid, though confirmation from cryogenic TA would still be required.

4.4 Conclusion

In summary, a photophysical study of TIPS-BT1′ was conducted in the polar solvent benzonitrile. These findings are similar to those reported for the molecule TIPS-BT1, but to build off them to look at more fundamental underlying physics for these similar molecules. After initial photoexcitation the excited-state population is partitioned into localized & delocalized singlet states. The localized singlet state appears to relax to the ground-state after ~13 ns, with no further dynamics. The delocalized singlet state on the other hand undergoes significant dynamics. After ~2 ps an equilibrium is established between S_1 & ^{1}TT, similar to behavior seen toluene. This equilibrium is short-lived as after ~92 ps excited-state population is transferred to the CT state where it then decays to the ground state.

The CT state serves as a virtual coupling pathway to the ^{1}TT while also being occupied in an explicit manner after the fact in the case of TIPS-BT1′ in benzonitrile. It plays both a virtual and real role in the dynamics of the molecule depending on the timescale of observation after excitation. This comes from the significant solvent reorganization energy calculated for TIPS-BT1′ in benzonitrile that serves to hamper the rapid formation of the CT state, even though it's energetically favored. This reorganization energy is expected to be lower in TIPS-BT1 due to lower charge separation from the placement of the TIPS groups, enough to explain the difference in apparent onset of CT formation in both molecules.

The results show that important consideration be given to not only forming the ^{1}TT, but making sure alternative pathways remain unavailable to siphon off excited-state population. These

efforts can include molecular engineering of functional groups on the tetracene chromophores themselves to stabilize/destabilize electronic states, as the TIPS groups have done, or select a more suitable solvent. A final note should be given to pentacene dimers like TIPS-BP1´. In benzonitrile, both the ^{1}TT & CT states are significantly lower in energy than the S_1, creating considerable driving force for both states. In-depth study would provide information on whether the CT state is low enough in energy to outcompete the ^{1}TT and whether or not population transfer to the CT state is observed before the ^{1}TT. The results of this study have shown the impact of solvent on the relevant electronic states for singlet fission to occur and provide a framework for fine tuning the process in future tetracene dimers.

4.5 References

(1) Gilligan, A. T.; Miller, E. G.; Sammakia, T.; Damrauer, N. H. Using Structurally Well-Defined Norbornyl-Bridged Acene Dimers to Map a Mechanistic Landscape for Correlated Triplet Formation in Singlet Fission. *J. Am. Chem. Soc.* **2019**.

(2) Smith, M. B.; Michl, J. Singlet Fission. *Chem. Rev.* **2010**, *110* (11), 6891–6936.

(3) Berkelbach, T. C.; Hybertsen, M. S.; Reichman, D. R. Microscopic Theory of Singlet Exciton Fission. II. Application to Pentacene Dimers and the Role of Superexchange. *J. Chem. Phys.* **2013**, *138* (11).

(4) Vallett, P. J.; Snyder, J. L.; Damrauer, N. H. Tunable Electronic Coupling and Driving Force in Structurally Well-Defined Tetracene Dimers for Molecular Singlet Fission: A Computational Exploration Using Density Functional Theory. *J. Phys. Chem. A* **2013**, *117* (42), 10824–10838.

(5) Monahan, N.; Zhu, X.-Y. Charge Transfer–Mediated Singlet Fission. *Annu. Rev. Phys. Chem.* **2015**, *66* (1), 601–618.

(6) Mandal, A.; Chen, M.; Foszcz, E. D.; Schultz, J. D.; Kearns, N. M.; Young, R. M.; Zanni, M. T.; Wasielewski, M. R. Two-Dimensional Electronic Spectroscopy Reveals Excitation Energy-Dependent State Mixing during Singlet Fission in a Terrylenediimide Dimer. *J. Am. Chem. Soc.* **2018**, *140* (51), 17907–17914.

(7) Margulies, E. A.; Miller, C. E.; Wu, Y.; Ma, L.; Schatz, G. C.; Young, R. M.; Wasielewski, M. R. Enabling Singlet Fission by Controlling Intramolecular Charge Transfer in π-Stacked Covalent Terrylenediimide Dimers. *Nat. Chem.* **2016**, *8* (12), 1120–1125.

(8) Chen, M.; Bae, Y. J.; Mauck, C. M.; Mandal, A.; Young, R. M.; Wasielewski, M. R. Singlet Fission in Covalent Terrylenediimide Dimers: Probing the Nature of the Multiexciton State

Using Femtosecond Mid-Infrared Spectroscopy. *J. Am. Chem. Soc.* **2018**, *140* (29), 9184–9192.

(9) Johnson, J. C.; Akdag, A.; Zamadar, M.; Chen, X.; Schwerin, A. F.; Paci, I.; Smith, M. B.; Havlas, Z.; Miller, J. R.; Ratner, M. A.; et al. Toward Designed Singlet Fission: Solution Photophysics of Two Indirectly Coupled Covalent Dimers of 1,3-Diphenylisobenzofuran. *J. Phys. Chem. B* **2013**, *171* (16), 4680–4695.

(10) Alvertis, A. M.; Lukman, S.; Hele, T. J. H.; Fuemmeler, E. G.; Feng, J.; Wu, J.; Greenham, N. C.; Chin, A. W.; Musser, A. J. Switching between Coherent and Incoherent Singlet Fission via Solvent-Induced Symmetry Breaking. *J. Am. Chem. Soc.* **2019**, *141* (44), 17558–17570.

(11) Lukman, S.; Chen, K.; Hodgkiss, J. M.; Turban, D. H. P.; Hine, N. D. M.; Dong, S.; Wu, J.; Greenham, N. C.; Musser, A. J. Tuning the Role of Charge-Transfer States in Intramolecular Singlet Exciton Fission through Side-Group Engineering. *Nat. Commun.* **2016**, *7*, 13622.

(12) Ball, A. O. LXXX.—The measurement of the dielectric constants of organic liquids *J. Chem. Soc.,* **1930**, 570–596.

(13) Rltzoulls, G.; Papadopoulos, N.; Jannakoudakls, D. Densities, Viscosities, and Dielectric Constants of Acetonitrile + Toluene at 15, 25, and 35 °C. *J. Chem. Eng. Data* **1986**, *31*, 146–148.

(14) Cook, J. D.; Carey, T. J.; Arias, D. H.; Johnson, J. C.; Damrauer, N. H. Solvent-Controlled Branching of Localized versus Delocalized Singlet Exciton States and Equilibration with Charge Transfer in a Structurally Well-Defined Tetracene Dimer. *J. Phys. Chem. A* **2017**, *121* (48), 9229–9242.

(15) Mauck, C. M.; Bae, Y. J.; Chen, M.; Powers-Riggs, N.; Wu, Y.-L.; Wasielewski, M. R. Charge-Transfer Character in a Covalent Diketopyrrolopyrrole Dimer: Implications for Singlet Fission. *ChemPhotoChem* **2018**, *2*, 223.

(16) Lukman, S.; Musser, A. J.; Chen, K.; Athanasopoulos, S.; Yong, C. K.; Zeng, Z.; Ye, Q.; Chi, C.; Hodgkiss, J. M.; Wu, J.; et al. Tuneable Singlet Exciton Fission and Triplet-Triplet Annihilation in an Orthogonal Pentacene Dimer. *Adv. Funct. Mater.* **2015**, *25* (34), 5452–5461.

(17) Sartor, S. M.; McCarthy, B. G.; Pearson, R. M.; Miyake, G. M.; Damrauer, N. H. Exploiting Charge-Transfer States for Maximizing Intersystem Crossing Yields in Organic Photoredox Catalysts. *J. Am. Chem. Soc.* **2018**, *140* (14), 4778–4781.

(18) Schwoerer, M.; Wolf, H. C. Organic Molecular Solids. Wiley. **2008**, DOI: 10.1002/9783527618651.

(19) Spano, F. C. The Spectral Signatures of Frenkel Polarons in H- and J-Aggregates. *Acc. Chem. Res.* **2010**, *43* (3), 429–439.

(20) Sartor, S. M.; Lattke, Y. M.; McCarthy, B. G.; Miyake, G. M.; Damrauer, N. H. Effects of Naphthyl Connectivity on the Photophysics of Compact Organic Charge-Transfer Photoredox Catalysts. *J. Phys. Chem. A* **2019**, *123* (22), 4727–4736.

(21) Alguire, E. C.; Subotnik, J. E.; Damrauer, N. H. Exploring Non-Condon Effects in a Covalent Tetracene Dimer: How Important Are Vibrations in Determining the Electronic Coupling for Singlet Fission. *J. Phys. Chem. A* **2015**, *119*, 299–311.

(22) Brunschwig, B. S.; Creutz, C.; Sutin, N. Optical Transitions of Symmetrical Mixed-Valence Systems in the Class II-III Transition Regime †. *Chem. Soc. Rev.* **2002**, *31*, 168–184.

(23) Reichardt, C. Solvatochromic Dyes as Solvent Polarity Indicators. *Chem. Rev.* **1994**, *94* (8),

2319–2358.

(24) Korovina, N. V.; Chang, C. H.; Johnson, J. C. Spatial Separation of Triplet Excitons Drives Endothermic Singlet Fission. *Nat. Chem.* **2020**, *12* 391–398.

Chapter 5: Enhancement of Triplet-Triplet Upconversion in a Rigidly Coupled Tetracene Dimer

5.1 Introduction

Chapter 3 was an in-depth examination of rigidly coupled dimers for singlet fission. The focus of **Chapter 4** was elucidating the role the CT state served in the singlet fission process. Both focus on the partition of higher energy singlets into lower energy states. The reverse process should also be discussed, the formation of higher energy states from lower ones, the process of upconversion.

Generation and application of Anti-Stokes shifted electronic states relative to their excitation source to drive photophysical or chemical processes is an area of interest for both fundamental science and a blossoming field of potential commercial technologies such as solar energy conversion,[1–3] photoredox catalysis,[4,5] bioimaging[6,7] and 3D printing[8,9] to name a few. One method of Anti-Stokes generation is triplet-triplet annihilation upconversion (TTA-UC). TTA-UC commonly consists of a bi-molecular system where a molecule with a low energy singlet (S_1) state (referred to as the sensitizer, S) is photoexcited and rapidly undergoes intersystem crossing into its triplet (T_1) state.[10] The energy is then transferred via Dexter energy transfer from the T_1 of the sensitizer molecule to the T_1 of a harvesting molecule (referred to as the annihilator, A). Collisions between two excited triplet annihilators generate an S_1 that can photoluminesce with photon energy greater than the excitation source (see Fig. 5.1 for full TTA-UC process). The study of upconversion requires careful selection of both sensitizer and annihilator and an understanding of their key attributes. A good sensitizer should be a strong absorber, have a large intersystem crossing yield and have a long-lived triplet state. The annihilator should fulfill the energy

requirement that $2\times T_1 > S_1$, itself have a long-lived T_1 state, and have a large fluorescence quantum yield. When considering a sensitizer/annihilator pair together, care should be taken matching the T_1 energies of the sensitizer and annihilator so that efficient triplet energy transfer (TET) occurs.

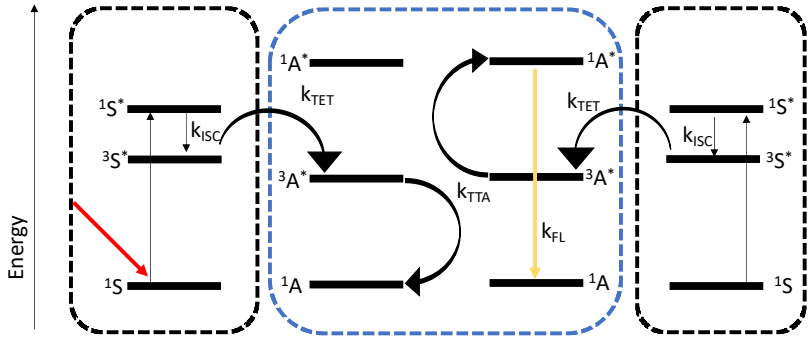

$$\Phi_{UC} = \Phi_{ISC}\Phi_{TTET}\Phi_{TTA}\Phi_{Fl} \tag{5.1}$$

Figure 5.1 Schematic representation of TTA-UC with relevant states and rate constants. Equation 5.1 for upconversion quantum yield from constituent quantum yields.

While upconversion has been studied in a wide range of systems, for solution phase the leading system generally consists of the annihilator 9,10-diphenylanthracene (DPA) and a metal porphyrin species (Zn, Pd or Pt octaethylporphyrin for example).[11–16] Indeed, a growing body of literature on DPA has reported upconversion quantum yields of up to ~26 %.[17] However, usage of DPA restricts upconversion photoluminescence to the blue-green portion of the visible spectrum and excitation must be ~520 nm. For many cases these restrictions can severely impact practical application. In solar energy conversion, upconversion would ideally be used to harvest sub-bandgap photons, not the ~3.0 eV excitons generated by DPA. With the Si bandgap at ~1.1 eV designing an upconversion system that has the required energetics to enhance efficiency is difficult due to a lack of suitable sensitizers/annihilators. In recent years the growing field of perovskite solar cells has seen enormous gains in efficiency, up to 25.2 %.[18] Often the perovskite systems

have higher energy bandgaps than silicon that would fit better with many previously designed upconversion systems. For bioimaging and 3D printing higher photon energy excitation sources run into issues of scattering and tissue penetration.[19,20] It would therefore be more beneficial if upconversion could move to redder emitting annihilators and excitation sources.[21]

The electronic core of DPA, anthracene, belongs to a subset of molecules referred to as polycyclic aromatic hydrocarbons, the acene series, that consist of fused benzene rings and whose electronic properties are well defined along the series. The next acene in the series, tetracene fulfills the fundamental requirements for upconversion while offering redder emission compared to anthracene-based systems. However, tetracene based upconversion systems studied previously have reported upconversion quantum yields significantly lower than DPA at similar sensitizer/annihilator concentrations (often <1 %).[22,23] Such a significant reduction in the useful photoproduct will severely inhibit adoption to previously described applications. It's therefore necessary to improve the competitiveness of the TTA process itself. In systems of simple monomeric annihilators operating on the basis of a collisional environment, the generation of photoproduct via triplet-triplet collision $T_1 + T_1 \rightarrow S_1$ can be restricted via reasons such as incorrect chromophore orientation or the collision product having the incorrect spin value that can reduce the efficiency of the TTA process. Our group has begun to consider that the coupling of two monomeric species together in a dimer allows for direct electronic coupling from the T_1 state to more readily access the S_1 via an intermediate multiexciton spin-manifold $T_1 + T_1 \rightarrow [^1TT \rightleftharpoons {}^3TT \rightleftharpoons {}^5TT] \rightarrow S_1$, potentially facilitating the formation of useful product and increasing the TTA efficiency.[24] Dimers have demonstrated previously success in enhancing upconversion yields in tetracene based systems.[22,23]

In this work, a dimerized version of TIPS-Tc (a triisopropylsilyl acetyl functionalized version of tetracene) was synthesized, referred to as TIPS-BTX′, to study if an enhancement of the TTA-UC process was observed in a weakly-coupled dimeric system (structures shown in Fig. 5.2 (a)). TIPS-BTX′ consists of two norbornyl functionalized TIPS-Tc units coupled together via a *para*-xylene linker. The additional of another norbornyl unit and the *para*-xylene results in significantly morechromophore separation compared to the dimers studied in **Chapters 3 & 4**. The norbornyl bridge that couples the two TIPS-Tc units together also limits the chromophore orientations to a single geometry, preventing rotational sampling that can impact experimental observations. TIPS-BTX′ was photophysically characterized to establish viability as an upconversion annihilator relative to TIPS-Tc. The metal phthalocyanine species Palladium(II) octabutoxyphthalocyanine (PdPc, structure shown in Fig. 5.2 (a)) was chosen as the sensitizer due to its previously established ability to sensitize tetracenic molecules.[22,23] Several samples of TIPS-Tc & TIPS-BTX′ were prepared covering a concentration range of 0.095 mM to 1.67 mM for TIPS-Tc and 0.39 mM to 0.392 mM for TIPS-BTX′ in toluene. Upconversion quantum yields and TET efficiencies were measured for each sample and used to determine TTA efficiency. These results and the experimental conditions were then applied to a model for TTA to retrieve the TTA rate constant for both TIPS-Tc & TIPS-BTX′. Additionally, time-resolved steady-state decay experiments showed the presence of a second-order decay pathway consistent with excimer formation in the TIPS-Tc samples.

5.2 Results

Previous studies have well characterized the photophysical behavior of TIPS-Tc upon excitation. While TIPS-BTX′ is expected to share properties with TIPS-Tc given common chromophoric units, it's important to characterize several photophysical parameters such as the quantum yield and triplet lifetime as these parameters can significantly impact observed upconversion behavior. All solutions were prepared in de-oxygenated toluene with an absorbance of ~0.1 at the excitation wavelength.

5.2.1 Direct Excitation

Results from direct excitation of TIPS-Tc and TIPS-BTX′ are shown in Fig 5.2 and summarized below. The absorption spectrum of TIPS-BTX′ shows a vibronic progression from ~ 450 – 550 nm, a typical characteristic of tetracenic molecules with a 0 – 0 absorbance peak maximum observed at 532 nm. This represents a slight (3 nm) blue shift compared to the monomer TIPS-Tc and has been observed in previous dimeric systems in **Chapters 3 & 4**. The observed emission of TIPS-BTX′ is also highly similar to that of TIPS-Tc with a small (~10 nm) Stokes shift and highly structured vibronic progression. The quantum yield of TIPS-BTX′ was measured to be 72 % against the fluorescence standard Coumarin 540A, only slightly lower than the measured quantum yield for TIPS-Tc at 74 %. Again, all this photophysical behavior suggests only weak coupling between the two chromophores in TIPS-BTX′.

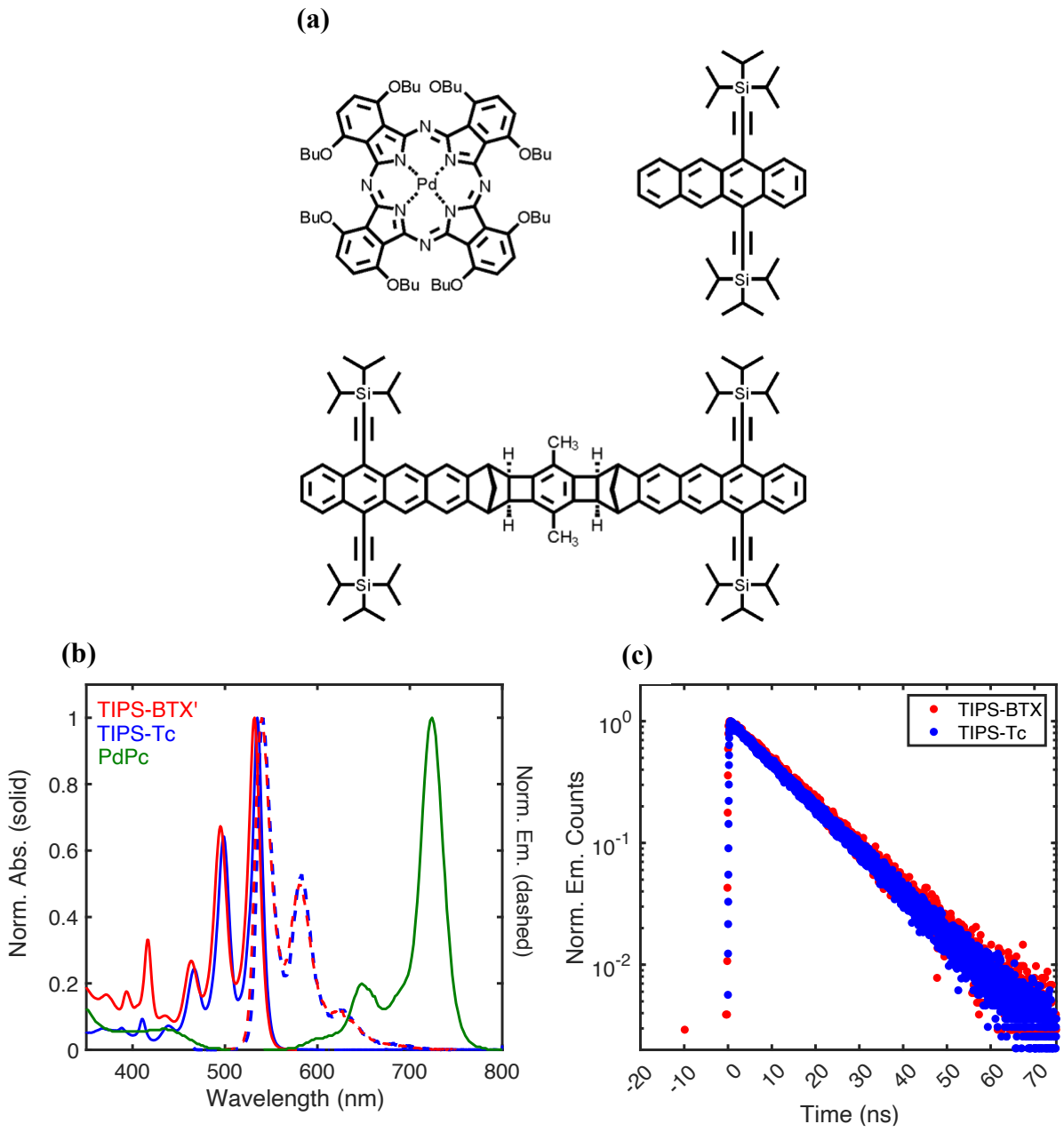

Figure 5.2 (a) Chemical structures of annihilators TIPS-BTX′ & TIPS-Tc and sensitizer PdPc. (b) Absorption and emission spectra of TIPS-BTX′, TIPS-Tc and PdPc in toluene. (c) TCSPC decay traces of TIPS-BTX′ & TIPS-Tc in toluene.

While this steady state behavior suggests significant similarity to TIPS-Tc and overall monomeric behavior, additional measurements are required. Time-correlated single photon counting (TCSPC) was performed to measure the excited-state lifetime of TIPS-BTX′. A lifetime of 12.7 ns monoexponential decay was observed for TIPS-BTX′, highly similar to the reported

12.4 ns lifetime for TIPS-Tc.[25] The similar photophysics of TIPS-BTX′ compared to TIPS-Tc suggests there is only weak interchromophore coupling in the dimer. Additionally, triplet sensitization of the annihilators via the sensitizer anthracene was performed to determine their triplet lifetimes. A 290 μs lifetime was observed for TIPS-Tc and a 410 μs for TIPS-BTX′. While the longer triplet lifetime in TIPS-BTX′ versus TIPS-Tc is beneficial for its prospects as a good upconversion annihilator, it's still an order of magnitude shorter than the ~4 ms triplet lifetime of champion annihilator DPA.

PdPc is characterized by a strongly absorbing Q band from ~ 600 – 750 nm (see Fig. 5.2.b) with minimal absorption and emission overlap with the S_1 of the annihilators. Additionally, PdPc shows a significant suppression of the Soret band typical of most metal porphyrin species used as upconversion sensitizers. This is beneficial since it has been observed in metal porphyrin systems that Soret band absorption can absorb upconversion emission, reducing the total observed upconversion intensity. PdPc allows this to be avoided. The most important quality of a prospective sensitizer though is its intersystem crossing (ISC) yield. For PdPc it's been reported as 0.77 in deaerated benezene.[26] In the solvet toluene a value of 0.75 was used for upconversion kinetic modeling as a lower-limit value given the presence of phosphoresence from PdPc and will be the value used in this work.[22] Results for sensitizer and annihilator are summarized in table 5.1.

	Molecule	S_1 (eV)	T_1 (eV)	τ_S (ns)	τ_T (μs)	QY (%)
Annihilator	TIPS-Tc	2.30	1.21[27]	12.4	290	74
	TIPS-BTX′	2.32	1.21[27]	13	410	72
Sensitizer	PdPc	1.71	1.13[22]	-	3.42	-

Table 5.1: Summary of relevant photophysical parameters for sensitizer and annihilators in toluene. Triplet energies are reported values from phosphorescence of TIPS-Tc touene/polystyrene thin film (ref. 27) and PdPc phosphorescence in solution (ref. 22).

5.2.2 Indirect Excitation

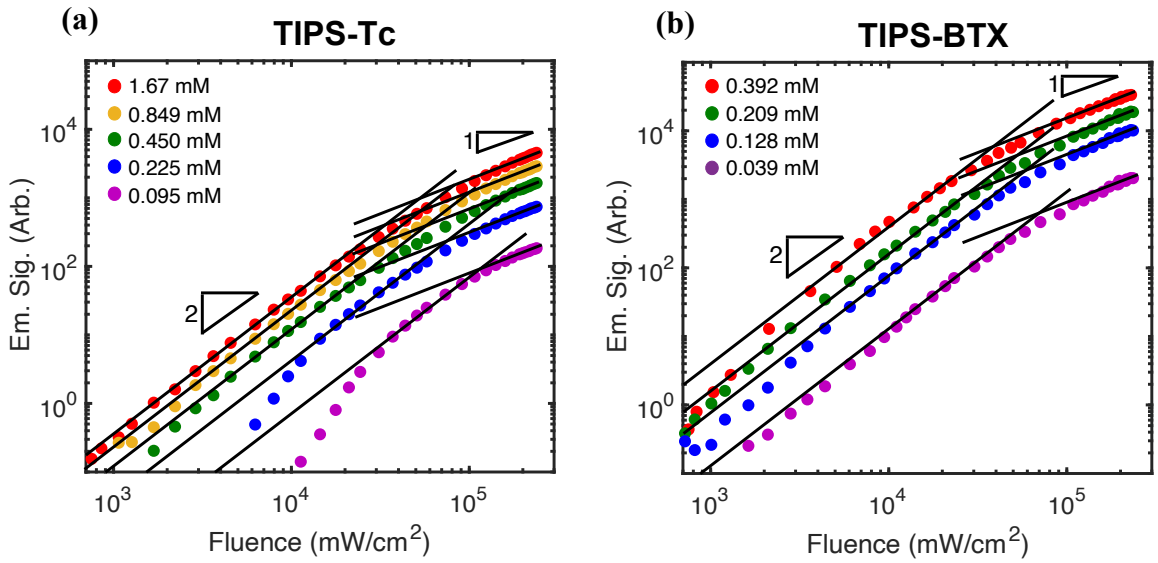

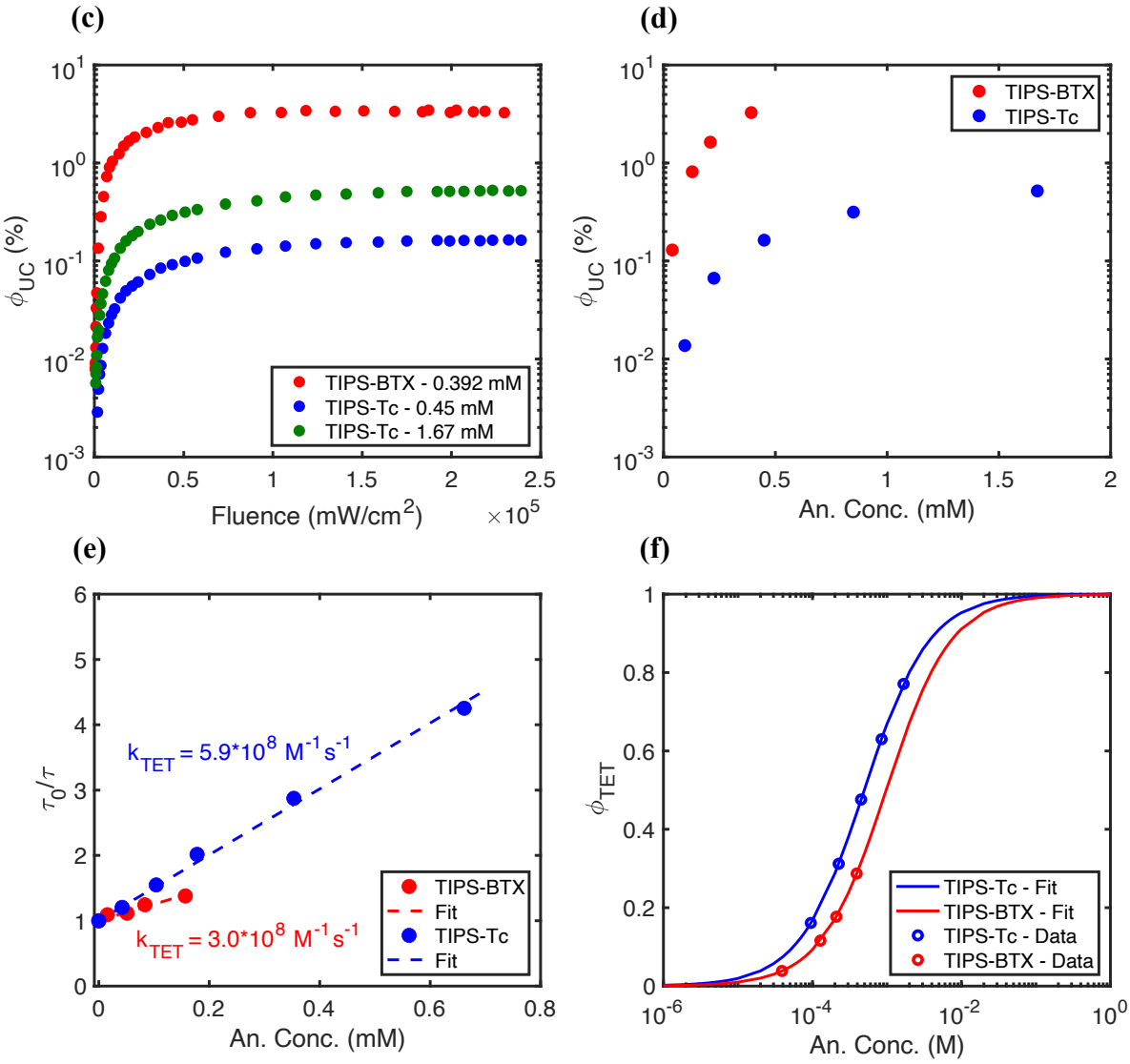

Figure 5.3 (a) Integrated emission intensity of four TIPS-BTX′ in toluene upconversion samples. (b) Integrated emission intensity of five TIPS-Tc in toluene upconversion samples. Applied quadratic (2) and linear (1) fits to figures a/b. (c) Fluence dependent UCQY for TIPS-BTX (0.392 mM) and TIPS-Tc (1.67 & 0.45 mM). (d) Concentration dependent upconversion quantum yields for TIPS-BTX′ & TIPS-Tc in toluene. (e) Stern-Volmer plot for TIPS-BTX′ & TIPS-Tc in toluene. (f) Calculated TET yields for monomer/dimer upconversion samples based on equation 5.6.4.

Upconversion samples of ~1.3 μM PdPc and annihilators were prepared in de-oxygenated toluene and excited with a 730 nm diode laser (from Thorlabs). Samples were excited with fluences ranging from ~500 – 250000 mW/cm^2. Emission data were collected from 480 – 680 nm and integrated to determine total upconversion signal. The upconversion emission for both

monomer/dimer shows two separate regimes. At low fluences the emission signal increases quadratically with fluence (marked with slope of 2 in Fig. 5.3 (a/b)) and at high fluences emission signal is increasing linearly (marked with slope of 1 in Fig. 5.3 (a/b)). Such behavior is observed in many upconversion systems and is due to the triplet annihilator concentration having reached saturation.[28] This crossing point between quadratic and linear behavior is considered to be the point where TTA is a competitive decay process compared to triplet decay for the excited state triplet annihilator concentration. The upconversion emission spectra were observed to have the characteristic vibronic progression seen in direct excitation measurements (see Chapter 5 Supporting Information, Fig. 5.6.8 for upconversion emission spectra). Self-absorption of the 0 – 0 emission peak was observed in all prepared samples, with higher concentration samples showing greater suppression of the peak.

To measure the upconversion quantum yield (UCQY) a standard of TIPS-Tc in toluene was excited with a 405 nm diode laser (from Thorlabs) and the collected emission was compared to the upconversion emission using the following formula.[29]

$$\Phi_{UC} = \Phi_{ref} \frac{I_{UC}}{I_{ref}} \frac{(1 - 10^{-Abs_{ref}})}{(1 - 10^{-Abs})} \frac{\eta_{UC}^2}{\eta_{ref}^2} \frac{\phi_{ref}}{\phi_{UC}} \tag{5.2}$$

Equation 5.2 is the normal fluorescent quantum yield formula where an experimental sample is compared to a known reference with the addition of the accounting for the photon fluence applied to the sample. Here, Φ is the quantum yield, I is the integrated emission signal, Abs is the sample absorbance at the excitation wavelength, η^2 is the refractive index of the solvent (this term cancels since toluene was solvent of both upconversion and reference sample) and ϕ is the photon flux. The photon flux was determined from the measured fluence, the excitation power W_{pump} divided by the pump area A, divided by the pump wavelength E_{photon} (shown in equation 5.3).

$$\phi = \frac{W_{pump}}{AE_{photon}} \tag{5.3}$$

Equation 5.2 was used to calculate the upconversion quantum yield for all samples (Equation 5.2 was use to show the unnormalized UCQY[30] as a function of fluence). As shown in Fig. 5.6.5 the quantum yield steadily increases at lower fluences, corresponding to a quadratic increase of upconversion emission intensity before leveling off at higher fluences and reaching a steady value. These were the values used to report the upconversion quantum yield. Correction for self-absorption in the samples was done by comparing upconversion emission spectra to a reference annihilator emission spectrum (see Chapter 5 Supporting Information, Fig. 5.6.8 for reference spectrum). As shown in Fig. 5.3 (d) the maximum upconversion quantum yield was measured to be 3.3 % for TIPS-BTX′ and 0.52 % for TIPS-Tc at the highest reported concentrations. These values represent the "unnormalized" upconversion quantum yield, where for a normalized upocnversion quantum yield two input photons converting to one output photons represents 100 % efficiency. The low measured quantum yields suggest significant inefficiency occurring in either the triplet-triplet energy transfer or triplet-triplet annihilation processes.

A Stern-Volmer study was performed to calculate the efficiency of triplet energy transfer (TET) between PdPc and the two annihilators. Nanosecond transient absorption spectroscopy of PdPc with the annihilators in toluene was used to determine the quenching of the triplet lifetime to determine triplet energy transfer efficiency. PdPc was photoexcited at 650 nm and monitored at 600 nm where the PdPc triplet has a broad excited state absorption. Unquenched PdPc was observed to have a monoexponential decay corresponding to a triplet lifetime of 3.42 μs (lifetime retrieved from nsTA, see Fig. 5.6.4); this matches well with previous literature.[26] Samples with either TIPS-BTX′ or TIPS-Tc showed a reduction of the PdPc triplet lifetime.

$$\frac{\tau_0}{\tau} = 1 + \tau_0 k_q[Q] = 1 + \tau_0 k_{TET}[An.] \quad (5.4)$$

Fitting the plotted data (Fig. 5.3.e) to the classic Stern-Volmer equation (equation 5.4) allows for the calculation of the quenching constant k_q (k_q is considered to be solely due to TET and thus $k_q \approx k_{TET}$) and the efficiency of TET. TIPS-Tc was calculated to have a k_q of 5.9×10^8 $M^{-1}s^{-1}$ while TIPS-BTX′ was calculated to have k_q of 3.0×10^8 $M^{-1}s^{-1}$ (rate constants compiled in table 5.2). The TET efficiency was calculated for all upconversion samples and shown in Fig. 5.3 (f) based on equation 5.6.4. As expected from the calculated quenching constants, TIPS-BTX′ at equimolar concentrations shows less efficient transfer of the triplet from the sensitizer to the annihilator. This behavior has been seen in several previous dimeric systems and is explained by the larger molecular volume of dimers slowing diffusion in the solvent medium.

5.2.3 Pulsed Diode Experiment:

To further probe the large difference between dimer and monomer upconversion samples, a pulsed diode laser experiment was performed to measure the upconversion kinetics. As described in **Chapter 2**, a pulsed diode was used to pump the upconversion samples for several milliseconds up to their steady-state limit and then switched off. The corresponding emission decay was then observed in a time-resolved manner. This is referred to as the steady-state decay. As discussed in **Chapter 2**, the observed emission decay traces corresponded to the excited triplet annihilator concentration (referred to as $[^3A^*]$ for rest of chapter). Each dimer and monomer sample were pumped across a fluence range of approximately similar to those used for determining the UCQY and the measured kinetic traces were globally analyzed according to equation 2.1.

Equation 2.1 contains two fit parameters, the annihilator triplet lifetime (τ_T) and the fraction of excited state population that decays through the second order pathway (β). Global

modeling was performed to return a constant value for τ_T across the fluence range while allowing β to float. For the dimer series a lifetime of 410 μs was measured while for the monomer series the triplet lifetime was measured as 315 μs. These lifetimes match well compared to the triplet lifetimes from triplet sensitization, providing good evidence that the experiment is factually monitoring $[^3A^*]$. As for β, the monomer series shall be discussed first (see S.I. section 5.6.11 for monomer & dimer kinetic traces fit to equation 2.1 and retrieved β from global analysis, see Fig. 5.6.11 for all dimer/monomer values for β as a function of fluence). Starting at low fluences all monomer samples reported a beta of ~0.1 (0.1 seems to be the limit of the experiment as global analysis had difficulty below this value) and steadily increasing as fluence was increased. Additionally higher concentration samples returned larger betas than lower concentration samples at similar fluences. At the highest measured fluence the 1.67 mM sample reported the largest measured beta at 0.35. Without further consideration this value suggests that 35 % of $[^3A^*]$ is decaying through a second-order pathway. The dimer series presents a more complicated picture. Like the monomer series, the three highest concentration samples showed a general trend of increasing beta as fluence increased. At the highest fluence the 0.392 mM sample returned a beta of ~0.33. The low concentration sample did not return the expected trend for beta as the low fluence measurements returned larger betas that then gradually decreased as the fluence was increased. Additionally, the significant variance of the retrieved betas suggests insufficient emission signal could be collected from the sample to resolve differences within the kinetic traces. The final complication for the dimer series is that at the lowest fluences, global analysis returned large values for beta that decreased with increasing fluence before steadying at β of ~0.1 before increasing, as expected. Again, this suggests sensitivity issues at low fluences/concentration where insufficient signal is present to cleanly resolve a kinetic trace. Potential upconversion systems should first be

determined to have a sufficient upconversion QY to generate enough signal to generate clean stead-state decay traces. While low signal samples present challenges, high fluence/concentration data presents an undeniable trend that a second-order pathway is becoming a significant contributor to the decay of the excited triplet annihilator population.

5.3 Discussion

Using the previously determined quenching constants, the efficiency of TET was determined over the concentration range of the tested samples. The TIPS-Tc TET was calculated to be 16 % (at 0.095 mM) and 77 % (at 1.672 mM). TET for TIPS-BTX´ was determined to be 3.9 % (at 0.039 mM) and 29 % (at 392 mM). These data highlight two important conclusions about the two upconversion systems. First, the chosen annihilators are failing to saturate the triplet sensitizer, allowing a significant portion of sensitizer triplets to relax to the ground state before undergoing TET. Compared to systems built around the champion annihilator DPA that achieve near unity TET at similar annihilator concentrations, TET of PdPc to TIPS-BTX´/TIPS-Tc is inefficient.[13-14] Two possible reasons for this are 1. the endoergic nature of the TET process between PdPC and TIPS-BTX´/TIPS-Tc and 2. the short triplet lifetime of PdPc. Phosphorescence measurements of PdPc suggest a triplet energy of 1.17 eV, while the triplet energy of TIPS-Tc has been reported as 1.21 eV. Using the two values creates 40 meV gradient that will inhibit the energy transfer process. With similar electronic behavior to TIPS-Tc, TIPS-BTX´ is not expected to have a T_1 energy significantly different to that of TIPS-Tc. The second point is that despite less efficient TET, TIPS-BTX´ still outperforms TIPS-Tc with a significantly greater UCQY. With similar QY efficiencies this leaves ϕ_{TTA} as the only possible source to explain the greater UCQY in TIPS-BTX´ compared to TIPS-Tc.

With the previously reported quantum yields for ISC, TET and Fl, we can calculate the efficiency of the triplet-triplet annihilation process. As shown in Fig. 5.4 TIPS-BTX′ shows a significant advantage in upconversion emission over monomeric TIPS-Tc over all concentrations. With TIPS-BTX′ shown to have little interchromophore coupling and a lower quenching rate constant it presents the question of why it shows significant improvement in facilitating upconversion compared to the monomeric TIPS-Tc.

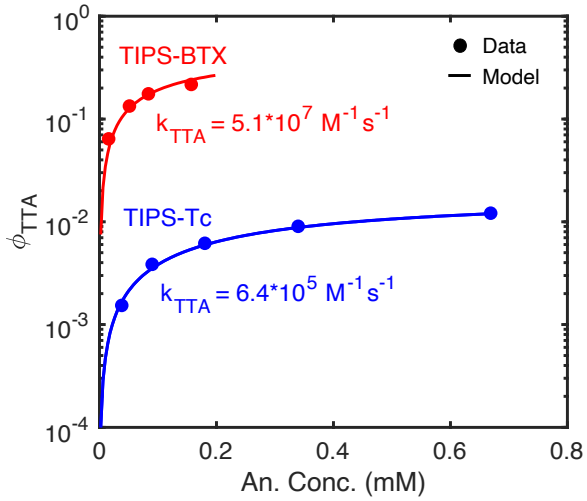

Figure 5.4 Kinetic modeling results for ϕ_{TTA} plotted against annihilator concentration with plotted values used for k_{TTA} along with experimental data.

To determine whether the increased TTA efficiency of TIPS-BTX′ is due to more favorable TTA or just a longer triplet lifetime, kinetic modeling was employed to retrieve the rate constant k_{TTA} for both TIPS-BTX′ & TIPS-Tc. The k_{TTA} rate constant (a second-order rate constant for how competitive singlet formation from $[^3A^*]$ is) serves as a good metric for comparison as it will be insensitive to sample concentrations, unlike ϕ_{UC} & ϕ_{TTA}. A system of equations previously laid out by Wilson et al. (see Chapter 5 Supporting Information section 5.6.9),[22] that consists of calculating excited state concentrations from the photon flux and other parameters was used to

find k_{TTA} and retrieve a best fit to the data (solid line in Fig. 5.4). It was calculated to be 5.1×10^7 $M^{-1}s^{-}1$ in TIPS-BTX′ and 6.4×10^5 $M^{-1}s^{-1}$ in TIPS-Tc (rate constants compiled in table 5.2). The difference in magnitude of k_{TTA} between TIPS-Tc and the dimeric system is similar to the difference reported by Campos et al. in their tetracenic upconversion systems.[4]

The greater value of k_{TTA} in TIPS-BTX′ compared to TIPS-Tc can be rationalized as TIPS-BTX′ having an intramolecular upconversion pathway as a dimer to facilitate the formation singlets from sensitized triplets. This can impact TTA in several different ways. First is that in traditional monomeric systems, triplet collisions can result in a distribution of spin states with the coveted singlet state forming in only ~11.1 % of all collisions and the remainder potentially serving as a significant loss pathway, though many monomer systems appear capable of exceeding this limit.[10] In a weakly-coupled dimer like TIPS-BTX′ triplets can be directly coupled to the singlet state through the multi-exciton manifold. This manifold allows for interconversion between different spin-states for triplets or quintets the opportunity to transfer to the singlet via the interconversion to the first ^{1}TT, unlike the monomer case. Second is that monomeric collisions can diffuse apart after an unproductive annihilation event. While in a dimeric species with both arms sensitized can reattempt annihilation in the event of spin-dephasing to independent triplets again from the multi-exciton manifold since they can't diffuse away from each other. This allows for multiple attempts at annihilation before the triplets decay. The monomer is also allowed to reattempt collision before decay, but the dimer is more favorable since triplets maintain close proximity if on both arms. Allowing for re-collision is especially important for TIPS-BTX′ & TIPS-Tc due to their comparatively short triplet lifetimes.

From the upconversion quantum yields and subsequent kinetic modeling TIPS-BTX′ was shown to have a much larger k_{TTA} compared to TIPS-Tc, suggesting the dimeric TIPS-BTX′ will

always outcompete monomer TIPS-Tc. It is therefore worthwhile to consider the merits of a dimer vs monomeric upconversion annihilator in a more general sense. The library of tetracene based dimers used for upconversion is relatively small, but enough to compare to TIPS-BTX′. For the sake of comparison on the upconversion QY will be used as it's the ultimate end product of any upconversion system and disregards the different kinetic models used to determine k_{TTA}. The other dimer comparisons in the literature are by Wilson who studied the rigid dimer TIPS-BT1′ and Campos whose dimers consisted of two TIPS-Tc units connected by phenyl space units (n = 0, 1, 2 & 4). Starting with Wilson, at similar concentrations as those reported here, TIPS-BT1′ was shown to have a greater upconversion QY compared to TIPS-Tc, though not to the extent reported here with TIPS-BTX′. By contrast Campos reported a maximum UCQY where one phenyl spacer unit was present between TIPS-Tc units, the dimer BT1. The observed trend showed a decreasing UCQY as the number of phenyl spacers increased (with the zero-phenyl spaced dimer BT0 having a negligible UCQY). Thus, we can draw some conclusions about TIPS-BTX′ from this behavior. To determine the extent of electronic coupling a TD-DFT calculation was performed on TIPS-BTX′ to look at the energetic splitting of paired states resulting from the interchromophore coupling. The transitions to the first six excited states were determined (see Chapter 5 Supporting Information, section 5.6.14 for full TD-DFT results) and show three sets of paired states with an energy difference of less than 5 meV. This suggests that there appears to be very little electronic coupling in TIPS-BTX′, and much less than TIPS-BT1′ given the elongation of the norbornyl bridge. While for the Campos dimers the more strongly coupled BT0 showed negligible upconversion, the following dimer BT1 reported the greatest upconversion QY with diminishing results for subsequently elongated dimers. This presents a case of too much chromophore spatial separation being detrimental while close chromophore interaction is also detrimental. A possible

explanation for this is that if TTA proceeds through the multiexcitonic TT manifold, at higher electronic couplings ^{1}TT, ^{3}TT and ^{5}TT are no longer degenerate with each other due to greater inter-chromophore exchange (term J in the JDE model).[31] Interconversion within this manifold therefore may be inhibited, preventing repopulation of the spin favorable product ^{1}TT, reducing the upconversion QY in the more strongly coupled dimers. With too much spatial separation, triplet annihilation is unfavorable, reducing the upconversion QY. These results suggest an "island" exists in terms of chromophore spatial separation where too much can lead to insufficient triplet annihilation and too little can impart unwanted electronic contributions. To determine this contribution would require being able to directly probe the multiexcitonic spin-manifold.

While k_{TTA} was successfully obtained by the standard upconversion reference method, the large number of independent variables can introduce substantial uncertainty into the final values, particularly the annihilator triplet lifetime. Measuring long triplet lifetimes can pose a challenge due to oxygen contamination and molecular collisions at high concentrations can artificially lower the observed triplet lifetime. In the subsequent kinetic modeling this can lead to a higher value of k_{TTA}. Independent verification of k_{TTA} is therefore prudent. We return to the steady-state decay traces from the pulsed diode experiment to determine this. To retrieve the coveted k_{TTA} rate constant, global modeling was again employed to solve for the two unknown variables in the beta expression, k_{TTA} and $[^3A^*]$ using the system of equations in Chapter 5 Supporting Information, section 5.6.9. Based on recorded experimental parameters, $[^3A^*]$ was calculated for each dimer/monomer sample. Both k_{TTA} and $[^3A^*]$ were then determined from a system of two equations across the concertation series. The k_{TTA} that gave the model the best global fit to experimental data was retrieved and used to plot β as a function of fluence along with experimental data as shown in

Fig. 5.5. The lowest concentration sample of each series wasn't used in the model due to either their poor compatibility with the rest of the concentration series or a low number of data points.

The global model returned a rate constant for TTA-UC of 2.8×10^7 $M^{-1}s^{-1}$ for the TIPS-BTX′ series and 2.7×10^7 $M^{-1}s^{-1}$ for the TIPS-Tc series (rate constants compiled in table 5.2). While returning reasonable numbers for the rate constant, the beta fits appear to underestimate beta at lower fluences and overestimate it at higher fluences. In the work by Albinsson et al that used this experiment to determine triplet lifetimes they commented that only the region $0.3 < \beta < 0.7$ during initial analysis to find τ_T should be fit to find k_{TTA} to due to numeric instability.[32] Based on this, low resolution of the lower fluence kinetic traces to find τ_T can introduce significant uncertainty in the determination of β, potentially causing this deviation compared to the global modeling. Ideally data sets observe the inflection point at $\beta = 0.5$ to fully capture system behavior. Increasing the fluences would allow this, but was not considered due to experimental and sample considerations.

	k_{TET} ($M^{-1}s^{-1}$)	k_{TTA} ($M^{-1}s^{-1}$)	k_{TTA} ($M^{-1}s^{-1}$) (pulsed diode)
TIPS-Tc	5.9×10^8	6.4×10^5	2.7×10^7
TIPS-BTX′	3.0×10^8	5.1×10^7	2.8×10^7

Table 5.2: Retrieved TET and upconversion rate constants for TIPS-BTX′ & TIPS-Tc in toluene.

For the dimer series, a k_{TTA} of 2.8×10^7 $M^{-1}s^{-1}$ is similar to, if smaller, the value calculated from modeling upconversion quantum yields at 5.1×10^7 $M^{-1}s^{-1}$. This serves as good confirmation of both the measured upconversion quantum yields for TIPS-BTX′ and the ability of the steady-state decay experiment to measure and model upconversion kinetics. As for the monomer series a

value for k_{TTA} of 2.7×10^{7} $M^{-1}s^{-1}$ was returned from the model as the best fit value. This is considerably larger than the value of 6.4×10^{5} $M^{-1}s^{-1}$ that was calculated from upconversion quantum yields. In fact, when β is modeled with the latter value for k_{TTA} in TIPS-Tc, at the highest concentration, β barely reached 0.03 (as shown in Fig. 5.5.13). As this is significantly lower than the observed 0.35, the TTA process is insufficient by itself to explain the depletion of $[^3A^*]$. Given the similar values reported for the dimer it seems unlikely that the discrepancy is due to experimental and modeling error. The fact that trend holds along the concentration series also reinforces this.

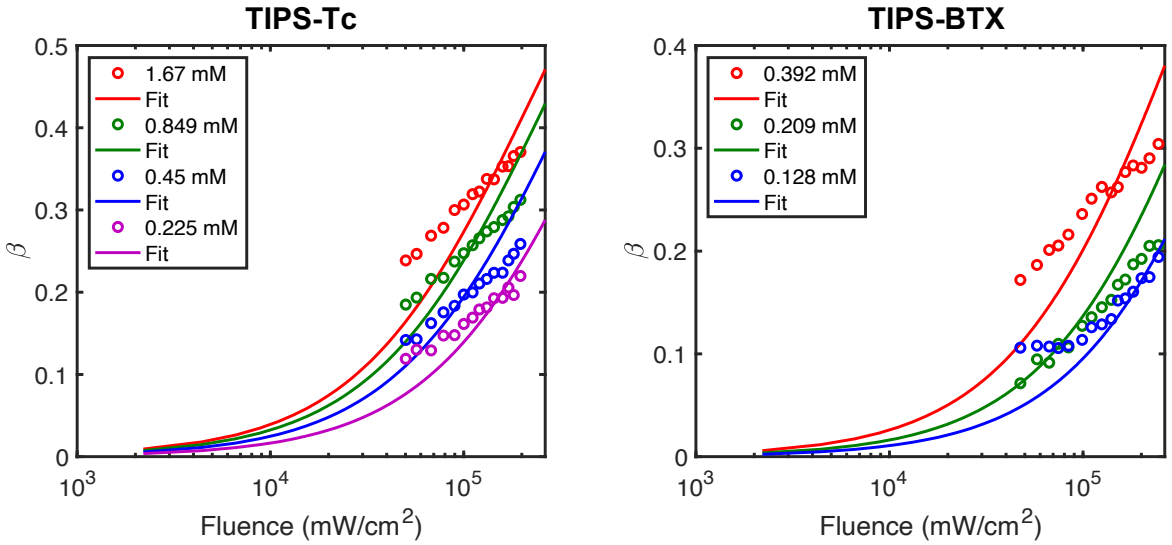

Figure 5.5 Fluence dependent β for TIPS-BTX´ (left) and TIPS-Tc (right) in toluene upconversion samples along with applied for β from kinetic modeling.

This of course necessitates the question of what is occurring in these TIPS-Tc samples to return such large value of β. To answer this requires returning to what is precisely being measured in these two experiments that could give such a large difference in k_{TTA}. With the upconversion quantum yields, only upconverted emission from the annihilator singlet is being observed and

quantified, and as such modeling will be of just the TTA-UC process itself. For the steady-state decay experiment, while singlet emission serves as the observable the experiment is still tracking the decay of $[^3A^*]$ through a second-order channel. In the global model upconversion is the only second-order channel present with no additional second-order decay channels considered. Therefore, any second-order decay would be misattributed to TTA, artificially boosting k_{TTA} when in fact there could be an alternative pathway that isn't formally described in the kinetic modeling. This begs the question what that pathway could potentially be.

In a work by Schmidt et al in 2018[33], a concentrated sample of TIPS-Tc was studied for the purpose of ascertaining whether excimer formation served as an intermediate or parasitic pathway in the singlet fission process (the reverse of TTA-UC). In their work it was ultimately determined that the excimer state was in fact a parasitic pathway based on the delayed fluorescence profile, kinetic modeling, and careful interpretation of fsTA of the sample. In their global model both singlets and excimers can form from two triplets in a ratio slightly favoring excimer formation based on the modeled rate constants, but not enough to explain the discrepancy observed for k_{TTA} between the UCQY's and the steady-state decays. However, upon formation from the S_1, the rate constant for excimer formation is over two orders of magnitude larger than the reverse rate constant, attesting to the nature of the excimer as a trap state. Reformation of the triplet state is considered insignificant since in the model it's ten times less than its reverse conjugate from the singlet and ten thousand times less from the excimer. Explicit confirmation would require observation of excimer emission, but given the sample used was ~50 mM this was beyond experimental limits. The question now becomes why excimer formation doesn't appear to be inhibiting TTA in the dimer compared to the monomer. There are two possible explanations to consider. The first is that TTA is simply able to outcompete excimer formation through the use of

the multiexcitonic spin-manifold. The second is that the structure of TIPS-BTX´ prevents access to excimer geometry. Given how well the UCQY and steady-state decay results agree with each other for the dimer showing the enhancement of k_{TTA}, it seems likely that the multi-excitonic manifold allows the dimer to bypass the initial excimer forming step by using intermolecular TTA instead that doesn't require two separate annihilators that can form an excimer structure. Once in the singlet there also appears to be a lack of excimer formation. Given that tetracene excimers tend to require a stacked geometry between the two chromophores the addition of the norbornyl bridgehead likely interferes with this more compared to the monomer, further inhibiting excimer formation.[34] This work demonstrates the usefulness of the steady-state decay measurement and its ability to observe difficult or dark states even if only implicitly and should be considered during kinetics discussion of upconversion annihilators.

One final aspect of the studied upconversion systems to consider is the "quality" of observed emitted photons from the annihilator singlet state. Significant effort has been spent in the upconversion field trying to increase the quantity of observed photons, without as much thought being given to their character. Under ideal circumstances for all upconversion systems, the upconverted photons would have exactly twice the energy of the absorbed photons to maintain perfect conservation of energy. Such efficiency is impossible to achieve, but still worthwhile to consider when evaluating upconversion systems

To evaluate the upconversion "quality" efficiency of the experimental systems, the relevant state energies (the sensitizer absorbing state and annihilator emitting state) were compared as a ratio to each other. In an ideal system (where energy is perfectly conserved) this ratio between annihilator and sensitizer singlet state energies would equal 2. Using the state energies reported in table 5.1, we find the upconversion efficiency to be ~1.35 for both TIPS-BTX´ and TIPS-Tc. To

put this in context in the broader upconversion field, the champion system (sensitizer: platinum(II) octaethylporphyrin and annihilator: DPA) has a measured gain factor of ~1.35. The highest reported upconversion anti-Stokes gain is ~1.1 eV in systems of platinum(II) meso-tetraphenyltetrabenzoporphine (PtTPBP) or $Os(phen)_3$ complex as the sensitizer and DPA as the annihilator has a gain factor of 1.76 due the use of directly exciting a low absorptive T_1 state in PtTPBP.[35,36] With the initial absorbing state at 1.71 eV and the upconverted product state at ~2.3 eV PdPc & TIPS-Tc/ TIPS-BTX′ would not be suitable to use in tandem with silicon for solar energy. Returning to other solar cell materials such as perovskites offers potential though. In the case of a mixed halide perovskite solar cells the bandgap was measured to be ~1.75 eV with efficiencies of ~16 %,[37] TIPS-Tc/ TIPS-BTX′ could serve as a potential annihilator to upconvert photons to this solar cell. PdPc with a 1.71 eV S_1 wouldn't serve as a good sensitizer pair though as the fraction of sub-bandgap photons that could be captured would be small. This reinforces both the merit of near-IR upconversion and the need to find appropriate sensitizers for this wavelength region as well.

5.4 Conclusion

In summary, a weakly coupled tetracenic dimer, TIPS-BTX′, was shown to have facilitated upconversion through enhancement of the triplet-triplet annihilation process compared to the monomer model TIPS-Tc. Direct excitation of TIPS-Tc & TIPS-BTX′ showed nearly identical photophysical characterization, suggesting that TIPS-BTX′ doesn't undergo significant additional photophysics like singlet fission. With the addition of the sensitizer PdPc, TIPS-BTX′ reported a UCQY of ~3 % compared to ~0.5 % for TIPS-Tc, with TTA efficiencies of ~20 % and ~1 % at the highest annihilator concentrations respectively. Kinetic modeling determined this was due to a

nearly two orders of magnitude increase in k_{TTA} for TIPS-BTX′ compared to TIPS-Tc. Additional improvements in this upconversion system would most likely come from the selection of an alternative sensitizer, ideally one with a longer triplet lifetime to saturate the TET efficiency compared to the calculated 77 % & 29 % for TIPS-Tc & TIPS-BTX′.

In addition, TIPS-Tc was shown to have a second-order decay channel other than upconversion through monitoring of steady-state decay traces, serving as a parasitic pathway for the excited state annihilator concentration. Excimer formation would be a reasonable explanation for this observation as it has been observed in TIPS-Tc previously. While the experiment was unable to observe excimers the ability to monitor decay through second-order channels is invaluable to learn about dark states that may be difficult to track directly. Global modeling was able to retrieve a similar value for k_{TTA} for TIPS-BTX′, strengthening the results achieved through measuring the UCQY.

This work adds to a growing body of literature that seeks to take advantage of near-IR upconversion. While the low UCQY of TIPS-Tc damages its viability as a useful annihilator, dimers offer a path for increasing yields that would be necessary in any potential commercial application. More work needs to be done to understand why such a dramatic increase in k_{TTA} is occurring. Such efforts would involve directly probing the multi-excitonic spin-manifold that is thought to serve as an intermediate. Maximizing efficiency of the TTA process is essential should upconversion ever be harnessed for solar energy conversion.

5.5 References

(1) Schulze, T. F.; Schmidt, T. W. Photochemical Upconversion: Present Status and Prospects for Its Application to Solar Energy Conversion. *Energy Environ. Sci.* **2014**, *8* (1), 103–125.

(2) Ghazy, A.; Safdar, M.; Lastusaari, M.; Savin, H.; Karppinen, M. Advances in Upconversion Enhanced Solar Cell Performance. *Sol. Energy Mater. Sol. Cells* **2021**, *230*, 111234.

(3) Liu, M.; Lu, Y.; Xie, Z. B.; Chow, G. M. Enhancing Near-Infrared Solar Cell Response Using Upconverting Transparentceramics. *Sol. Energy Mater. Sol. Cells* **2011**, *95* (2), 800–803.

(4) Ravetz, B. D.; Pun, A. B.; Churchill, E. M.; Congreve, D. N.; Rovis, T.; Campos, L. M. Photoredox Catalysis Using Infrared Light via Triplet Fusion Upconversion. *Nature* **2019**, *565* (7739), 343–346.

(5) Huang, L.; Wu, W.; Li, Y.; Huang, K.; Zeng, L.; Lin, W.; Han, G. Highly Effective Near-Infrared Activating Triplet–Triplet Annihilation Upconversion for Photoredox Catalysis. *J. Am. Chem. Soc.* **2020**, *142* (43), 18460–18470.

(6) Zhou, J.; Liu, Q.; Feng, W.; Sun, Y.; Li, F. Upconversion Luminescent Materials: Advances and Applications. *Chem. Rev.* **2015**, *115* (1), 395–465.

(7) Park, Y. Il; Lee, K. T.; Suh, Y. D.; Hyeon, T. Upconverting Nanoparticles: A Versatile Platform for Wide-Field Two-Photon Microscopy and Multi-Modal in Vivo Imaging. *Chem. Soc. Rev.* **2015**, *44* (6), 1302–1317.

(8) Sanders, S. N.; Schloemer, T. H.; Gangishetty, M. K.; Anderson, D.; Seitz, M.; Gallegos, A. O.; Stokes, R. C.; Congreve, D. N. Triplet Fusion Upconversion Nanocapsules for Volumetric 3D Printing. *Nature* **2022**, *604* (7906), 474–478.

(9) Park, J. M.; Lee, H.; Choe, H. S.; Ahn, S. K.; Seong, K. Y.; Yang, S. Y.; Kim, J. H. Highly

Efficient Triplet–Triplet Annihilation Upconversion in Polycaprolactone: Application to 3D Printable Architectures and Microneedles. *J. Mater. Chem. C* **2022**, *10* (12), 4584–4589.

(10) Singh-Rachford, T. N.; Castellano, F. N. Photon Upconversion Based on Sensitized Triplet-Triplet Annihilation. *Coordination Chemistry Reviews*. **2010**, *254* (21-22), 2560–2573.

(11) Morteza Gholizadeh, E.; Frazer, L.; Macqueen, R. W.; Gallaher, J. K.; Schmidt, T. W. Photochemical Upconversion Is Suppressed by High Concentrations of Molecular Sensitizers Photochemical Upconversion Is Suppressed by High Concentrations of Molecular Sensitizers †. *J. Phys. Chem. Chem. Phys.* **2018**, *20*, 19500–19506.

(12) Hwang, S. Y.; Song, D.; Seo, E. J.; Hollmann, F.; You, Y.; Park, J. B. Triplet–Triplet Annihilation-Based Photon-Upconversion to Broaden the Wavelength Spectrum for Photobiocatalysis. *Sci. Reports* **2022**, *12* (1), 1–7.

(13) Olesund, A.; Gray, V.; Mårtensson, J.; Albinsson, B. Diphenylanthracene Dimers for Triplet-Triplet Annihilation Photon Upconversion: Mechanistic Insights for Intramolecular Pathways and the Importance of Molecular Geometry. *J. Am. Chem. Soc.* **2021**, *143* (15), 5745–5754.

(14) Gray, V.; Dzebo, D.; Lundin, A.; Alborzpour, J.; Abrahamsson, M.; Albinsson, B.; Moth-Poulsen, K. Photophysical Characterization of the 9,10-Disubstituted Anthracene Chromophore and Its Applications in Triplet–Triplet Annihilation Photon Upconversion. *J. Mater. Chem. C* **2015**, *3* (42), 11111–11121.

(15) Kanoh, M.; Matsui, Y.; Honda, K.; Kokita, Y.; Ogaki, T.; Ohta, E.; Ikeda, H. Elongation of Triplet Lifetime Caused by Intramolecular Energy Hopping in Diphenylanthracene Dyads Oriented to Undergo Efficient Triplet–Triplet Annihilation Upconversion. *J. Phys. Chem. B* **2021**, *125* (18), 4831–4837.

(16) Gao, C.; Prasad, S. K. K.; Zhang, B.; Dvořák, M.; Tayebjee, M. J. Y.; McCamey, D. R.; Schmidt, T. W.; Smith, T. A.; Wong, W. W. H. Intramolecular Versus Intermolecular Triplet Fusion in Multichromophoric Photochemical Upconversion. *J. Phys. Chem. C* **2019**, *123* (33), 20181–20187.

(17) Monguzzi, A.; Tubino, R.; Hoseinkhani, S.; Campione, M.; Meinardi, F. Low Power, Non-Coherent Sensitized Photon up-Conversion: Modelling and Perspectivesw. *Phys. Chem. Chem. Phys.* **2012**, *14*, 4322–4332.

(18) Kim, J. Y.; Lee, J.-W.; Jung, H. S.; Shin, H.; Park, N.-G. High-Efficiency Perovskite Solar Cells. *Chem. Rev.* **2020**, *120* (15), 7867–7918.

(19) Kwon, O. S.; Kim, J.-H.; Cho, J. K.; Kim, J.-H. Triplet–Triplet Annihilation Upconversion in CdS-Decorated SiO2 Nanocapsules for Sub-Bandgap Photocatalysis. *ACS Appl. Mater. Interfaces* **2015**, *7* (1), 318–325.

(20) Dou, Q. Q.; Guo, H. C.; Ye, E. Near-Infrared Upconversion Nanoparticles for Bio-Applications. *Mater. Sci. Eng. C* **2015**, *45*, 635–643.

(21) Bharmoria, P.; Bildirir, H.; Moth-Poulsen, K. Triplet–Triplet Annihilation Based near Infrared to Visible Molecular Photon Upconversion. *Chem. Soc. Rev.* **2020**, *49* (18), 6529–6554.

(22) Imperiale, C. J.; Green, P. B.; Miller, E. G.; Damrauer, N. H.; Wilson, M. W. B. Triplet-Fusion Upconversion Using a Rigid Tetracene Homodimer. *J. Phys. Chem. Lett* **2019**, *10* (23), 7463–7469.

(23) Pun, A. B.; Sanders, S. N.; Sfeir, M. Y.; Campos, L. M.; Congreve, D. N. Annihilator Dimers Enhance Triplet Fusion Upconversion †. *Chem. Sci.* **2019**, *10*, 3969-3975.

(24) Bossanyi, D. G.; Sasaki, Y.; Wang, S.; Chekulaev, D.; Kimizuka, N.; Yanai, N.; Clark, J.

Spin Statistics for Triplet–Triplet Annihilation Upconversion: Exchange Coupling, Intermolecular Orientation, and Reverse Intersystem Crossing. *JACS Au* **2021**, *1* (12), 2188–2201.

(25) Cook, J. D.; Carey, T. J.; Arias, D. H.; Johnson, J. C.; Damrauer, N. H. Solvent-Controlled Branching of Localized versus Delocalized Singlet Exciton States and Equilibration with Charge Transfer in a Structurally Well-Defined Tetracene Dimer. *J. Phys. Chem. A* **2017**, *121* (48), 9229–9242.

(26) Rihter, B. D.; Kenney, M. E.; Ford, W. E.; Rodgers, M. A. J. Synthesis and Photoproperties of Diamagnetic Octabutoxyphthalocyanines with Deep Red Optical Absorbance. *J. Am. Chem. Soc.* **1990**, *112* (22), 8064–8070.

(27) Stern, H. L.; Musser, A. J.; Gelinas, S.; Parkinson, P.; Herz, L. M.; Bruzek, M. J.; Anthony, J.; Friend, R. H.; Walker, B. J. Identification of a Triplet Pair Intermediate in Singlet Exciton Fission in Solution. *Proc. Natl. Acad. Sci. U. S. A.* **2015**, *112* (25), 7656–7661.

(28) Haefele, A.; Blumhoff, J.; Khnayzer, R. S.; Castellano, F. N. Getting to the (Square) Root of the Problem: How to Make Noncoherent Pumped Upconversion Linear. *J. Phys. Chem. Lett.* **2012**, *3* (3), 299–303.

(29) Yanai, N.; Suzuki, K.; Ogawa, T.; Sasaki, Y.; Harada, N.; Kimizuka, N. Absolute Method to Certify Quantum Yields of Photon Upconversion via Triplet−Triplet Annihilation. *J. Phys. Chem. A* **2019**, *123*, 10197–10203.

(30) Zhou, Y.; Castellano, F. N.; Schmidt, T. W.; Hanson, K. On the Quantum Yield of Photon Upconversion via Triplet-Triplet Annihilation. *ACS Energy Lett.* **2020**, *5* (7), 2322–2326.

(31) Smyser, K. E.; Eaves, J. D. Singlet Fission for Quantum Information and Quantum Computing: The Parallel JDE Model. *Sci. Reports 2020 101* **2020**, *10* (1), 1–10.

(32) Olesund, A.; Johnsson, J.; Edhborg, F.; Ghasemi, S.; Moth-Poulsen, K.; Albinsson, B. Approaching the Spin-Statistical Limit in Visible-to-Ultraviolet Photon Upconversion. *J. Am. Chem. Soc.* **2022**, *144* (8), 3706–3716.

(33) Dover, C. B.; Gallaher, J. K.; Frazer, L.; Tapping, P. C.; Petty, A. J.; Crossley, M. J.; Anthony, J. E.; Kee, T. W.; Schmidt, T. W. Endothermic Singlet Fission Is Hindered by Excimer Formation. *Nat. Chem.* **2018**, *10*, 305 – 310.

(34) Hoche, J.; Flock, M.; Miao, X.; Philipp, L. N.; Wenzel, M.; Fischer, I.; Mitric, R. Excimer Formation Dynamics in the Isolated Tetracene Dimer. *Chem. Sci.* **2021**, *12* (36), 11965–11975.

(35) Fan, C.; Wei, L.; Niu, T.; Rao, M.; Cheng, G.; Chruma, J. J.; Wu, W.; Yang, C. Efficient Triplet-Triplet Annihilation Upconversion with an Anti-Stokes Shift of 1.08 EV Achieved by Chemically Tuning Sensitizers. *J. Am. Chem. Soc.* **2019**, *141* (38), 15070–15077.

(36) Wei, Y.; Li, Y.; Zheng, M.; Zhou, X.; Zou, Y.; Yang, C. Simultaneously High Upconversion Efficiency and Large Anti-Stokes Shift by Using Os(II) Complex Dyad as Triplet Photosensitizer. *Adv. Opt. Mater.* **2020**, *8* (9), 1902157.

(37) Gil-Escrig, L.; Dreessen, C.; Palazon, F.; Hawash, Z.; Moons, E.; Albrecht, S.; Sessolo, M.; Bolink, H. J. Efficient Wide-Bandgap Mixed-Cation and Mixed-Halide Perovskite Solar Cells by Vacuum Deposition. *ACS Energy Lett.* **2021** *6* (2), 827 – 836.

Bibliography

Chapter 1

(1) IPCC, 2021: *Climate Change 2021: The Physical Science Basis. Contribution of Working Group I to the Sixth Assessment Report of the Intergovernmental Panel on Climate Change*[Masson-Delmotte, V., P. Zhai, A. Pirani, S.L. Connors, C. Péan, S. Berger, N. Caud, Y. Chen, L. Goldfarb, M.I. Gomis, M. Huang, K. Leitzell, E. Lonnoy, J.B.R. Matthews, T.K. Maycock, T. Waterfield, O. Yelekçi, R. Yu, and B. Zhou (eds.)]. Cambridge University Press, Cambridge, United Kingdom and New York, NY, USA, In press, doi:10.1017/9781009157896.

(2) IPCC, 2018: Summary for Policymakers. In: *Global Warming of 1.5°C. An IPCC Special Report on the impacts of global warming of 1.5°C above pre-industrial levels and related global greenhouse gas emission pathways, in the context of strengthening the global response to the threat of climate change, sustainable development, and efforts to eradicate poverty* [Masson-Delmotte, V., P. Zhai, H.-O. Pörtner, D. Roberts, J. Skea, P.R. Shukla, A. Pirani, W. Moufouma-Okia, C. Péan, R. Pidcock, S. Connors, J.B.R. Matthews, Y. Chen, X. Zhou, M.I. Gomis, E. Lonnoy, T. Maycock, M. Tignor, and T. Waterfield (eds.)]. Cambridge University Press, Cambridge, UK and New York, NY, USA, pp. 3-24, doi:10.1017/9781009157940.001.

(3) IPCC, 2022*:* Summary for Policymakers. In: *Climate Change 2022: Mitigation of Climate Change. Contribution of Working Group III to the Sixth Assessment Report of the Intergovernmental Panel on Climate Change* [P.R. Shukla, J. Skea, R. Slade, A. Al Khourdajie, R. van Diemen, D. McCollum, M. Pathak, S. Some, P. Vyas, R. Fradera, M. Belkacemi, A. Hasija, G. Lisboa, S. Luz, J. Malley, (eds.)]. Cambridge University Press,

Cambridge, UK and New York, NY, USA. doi: 10.1017/9781009157926.001.

(4) Electric Power Annual 2020. *Energy Information Administration, U.S.* **2022**.

(5) Woodhouse, M.; Feldman, D.; Fu, R.; Horowitz, K.; Chung, D.; Jordan, D.; Kurtz, S.; Jones-Albertus, R.; Department of Energy, U. On the Path to SunShot: The Role of Advancements in Solar Photovoltaic Efficiency, Reliability, and Costs. **2015**.

(6) Shockley, W.; Queisser, H. J. Detailed Balance Limit of Efficiency of P-n Junction Solar Cells. *J. Appl. Phys.* **1961**, *32* (3), 510–519.

(7) Heidarzadeh, H.; Rostami, A.; Dolatyari, M. Management of Losses (Thermalization-Transmission) in the Si-QDs inside 3C–SiC to Design an Ultra-High-Efficiency Solar Cell. *Mater. Sci. Semicond. Process.* **2020**, *109*, 104936.

(8) De Vos, A.; Desoete, B. On the Ideal Performance of Solar Cells with Larger-than-Unity Quantum Efficiency. *Sol. Energy Mater. Sol. Cells* **1998**, *51* (3–4), 413–424.

(9) Hanna, M. C.; Nozik, A. J. Solar Conversion Efficiency of Photovoltaic and Photoelectrolysis Cells with Carrier Multiplication Absorbers. *J. Appl. Phys.* **2006**, *100* (7), 074510.

(10) Zhu, X. Exceeding the Limit in Solar Energy Conversion with Multiple Excitons. *Acc. Chem. Res.* **2013**, *46* (6), 1239–1241.

(11) Smith, M. B.; Michl, J. Singlet Fission. *Chem. Rev.* **2010**, *110* (11), 6891–6936.

(12) Miyata, K.; Conrad-Burton, F. S.; Geyer, F. L.; Zhu, X.-Y. Triplet Pair States in Singlet Fission. *Chem. Rev.* **2019**, *119* (6), 4261–4292.

(13) Alvertis, A. M.; Lukman, S.; Hele, T. J. H.; Fuemmeler, E. G.; Feng, J.; Wu, J.; Greenham, N. C.; Chin, A. W.; Musser, A. J. Switching between Coherent and Incoherent Singlet Fission via Solvent-Induced Symmetry Breaking. *J. Am. Chem. Soc.* **2019**, *141* (44), 17558–

17570.

(14) Walker, B. J.; Musser, A. J.; Beljonne, D.; Friend, R. H. Singlet Exciton Fission in Solution. *Nat. Chem.* **2013**, *5*, 1019–1024.

(15) Stern, H. L.; Musser, A. J.; Gelinas, S.; Parkinson, P.; Herz, L. M.; Bruzek, M. J.; Anthony, J.; Friend, R. H.; Walker, B. J. Identification of a Triplet Pair Intermediate in Singlet Exciton Fission in Solution. *Proc. Natl. Acad. Sci. U. S. A.* **2015**, *112* (25), 7656–7661.

(16) Johnson, J. C.; Nozik, A. J.; Michl, J. High Triplet Yield from Singlet Fission in a Thin Film of 1,3-Diphenylisobenzofuran. *J. Am. Chem. Soc.* **2010**, *132* (46), 16302–16303.

(17) Jundt, C.; Klein, G.; Sipp, B.; Le Moigne, J.; Joucla, M.; Villaeys, A. A. Exciton Dynamics in Pentacene Thin Films Studied by Pump-Probe Spectroscopy. *Chem. Phys. Lett.* **1995**, *241* (1–2), 84–88.

(18) Le, A. K.; Bender, J. A.; Roberts, S. T. Slow Singlet Fission Observed in a Polycrystalline Perylenediimide Thin Film. *J. Phys. Chem. Lett.* **2016**, *7* (23), 4922–4928.

(19) Müller, A. M.; Avlasevich, Y. S.; Müllen, K.; Bardeen, C. J. Evidence for Exciton Fission and Fusion in a Covalently Linked Tetracene Dimer. *Chem. Phys. Lett.* **2006**, *421* (4–6), 518–522.

(20) Dover, C. B.; Gallaher, J. K.; Frazer, L.; Tapping, P. C.; Petty, A. J.; Crossley, M. J.; Anthony, J. E.; Kee, T. W.; Schmidt, T. W. Endothermic Singlet Fission Is Hindered by Excimer Formation. *Nat. Chem.* **2018**, *10*, 305–310.

(21) Singh, S.; Jones, W. J.; Siebrand, W.; Stoicheff, B. P.; Schneider, W. G. Laser Generation of Excitons and Fluorescence in Anthracene Crystals. *J. Chem. Phys.* **1965**, *42* (1), 330–342.

(22) Schulze, T. F.; Schmidt, T. W. Photochemical Upconversion: Present Status and Prospects

for Its Application to Solar Energy Conversion. *Energy Environ. Sci.* **2014**, *8* (1), 103–125.

(23) Trupke, T.; Green, M. A.; Würfel, P. Improving Solar Cell Efficiencies by Up-Conversion of Sub-Band-Gap Light. *J. Appl. Phys.* **2002**, *92* (7), 4117.

(24) Singh-Rachford, T. N.; Castellano, F. N. Photon Upconversion Based on Sensitized Triplet-Triplet Annihilation. *Coordination Chemistry Reviews*. **2010**, *254* (21–22), 2560–2573.

(25) Chen, M.; Bae, Y. J.; Mauck, C. M.; Mandal, A.; Young, R. M.; Wasielewski, M. R. Singlet Fission in Covalent Terrylenediimide Dimers: Probing the Nature of the Multiexciton State Using Femtosecond Mid-Infrared Spectroscopy. *J. Am. Chem. Soc.* **2018**, *140* (29), 9184–9192.

(26) Basel, B. S.; Zirzlmeier, J.; Hetzer, C.; Reddy, S. R.; Phelan, B. T.; Krzyaniak, M. D.; Volland, M. K.; Coto, P. B.; Young, R. M.; Clark, T.; et al. Evidence for Charge-Transfer Mediation in the Primary Events of Singlet Fission in a Weakly Coupled Pentacene Dimer. *Chem* **2018**, *4* (5), 1092–1111.

(27) Margulies, E. A.; Miller, C. E.; Wu, Y.; Ma, L.; Schatz, G. C.; Young, R. M.; Wasielewski, M. R. Enabling Singlet Fission by Controlling Intramolecular Charge Transfer in π-Stacked Covalent Terrylenediimide Dimers. *Nat. Chem.* **2016**, *8* (12), 1120–1125.

(28) Mandal, A.; Chen, M.; Foszcz, E. D.; Schultz, J. D.; Kearns, N. M.; Young, R. M.; Zanni, M. T.; Wasielewski, M. R. Two-Dimensional Electronic Spectroscopy Reveals Excitation Energy-Dependent State Mixing during Singlet Fission in a Terrylenediimide Dimer. *J. Am. Chem. Soc.* **2018**, 140 (51), 17907–17914.

(29) Johnson, J. C.; Akdag, A.; Zamadar, M.; Chen, X.; Schwerin, A. F.; Paci, I.; Smith, M. B.; Havlas, Z.; Miller, J. R.; Ratner, M. A.; et al. Toward Designed Singlet Fission: Solution Photophysics of Two Indirectly Coupled Covalent Dimers of 1,3-Diphenylisobenzofuran.

J. Phys. Chem. B **2013**, *117* (16), 4680–4695.

(30) Buchanan, E. A.; Kaleta, J.; Wen, J.; Lapidus, S. H.; Císařová, I.; Havlas, Z.; Johnson, J. C.; Michl, J. Molecular Packing and Singlet Fission: The Parent and Three Fluorinated 1,3-Diphenylisobenzofurans. *J. Phys. Chem. Lett.* **2019**, *10* (8), 1947–1953.

(31) Kaur, I.; Jazdzyk, M.; Stein, N. N.; Prusevich, P.; Miller, G. P. Design, Synthesis, and Characterization of a Persistent Nonacene Derivative. *J. Am. Chem. Soc.* **2010**, *132* (4), 1261–1263.

(32) Zhou, J.; Liu, Q.; Feng, W.; Sun, Y.; Li, F. Upconversion Luminescent Materials: Advances and Applications. *Chem. Rev.* **2015**, *115* (1), 395–465.

(33) Michl, J.; Thulstrup, E. W. Why Is Azulene Blue and Anthracene White? A Simple Mo Picture. *Tetrahedron* **1976**, *32* (2), 205–209.

(34) Murov, S., Carmichael, I., Prodi, L., & Hug, G.L. Handbook of Photochemistry (2nd ed.). CRC Press. **1993**, DOI: 10.1201/9781420015195.

(35) Haefele, A.; Blumhoff, J.; Khnayzer, R. S.; Castellano, F. N. Getting to the (Square) Root of the Problem: How to Make Noncoherent Pumped Upconversion Linear. *J. Phys. Chem. Lett.* **2012**, *3* (3), 299–303.

(36) Olesund, A.; Gray, V.; Mårtensson, J.; Albinsson, B. Diphenylanthracene Dimers for Triplet-Triplet Annihilation Photon Upconversion: Mechanistic Insights for Intramolecular Pathways and the Importance of Molecular Geometry. *J. Am. Chem. Soc.* **2021**, *143* (15), 5745–5754.

(37) Matsui, Y.; Kanoh, M.; Ohta, E.; Ogaki, T.; Ikeda, H. Triplet–Triplet Annihilation-Photon Upconversion Employing an Adamantane-Linked Diphenylanthracene Dyad Strategy. *J. Photochem. Photobiol. A Chem.* **2020**, *387*, 112107.

(38) Fan, C.; Wei, L.; Niu, T.; Rao, M.; Cheng, G.; Chruma, J. J.; Wu, W.; Yang, C. Efficient Triplet-Triplet Annihilation Upconversion with an Anti-Stokes Shift of 1.08 EV Achieved by Chemically Tuning Sensitizers. *J. Am. Chem. Soc.* **2019**, *141* (38), 15070–15077.

(39) Rao, A.; Wilson, M. W. B.; Albert-Seifried, S.; Di Pietro, R.; Friend, R. H. Photophysics of Pentacene Thin Films: The Role of Exciton Fission and Heating Effects. *Phys. Rev. B - Condens. Matter Mater. Phys.* **2011**, *84* (19), 195411.

(40) Arbuzov, Y. A. THE DIELS–ALDER REACTION WITH MOLECULAR OXYGEN AS DIENOPHILE. *Russ. Chem. Rev.* **1965**, *34* (8), 558.

(41) Anthony, J. E.; Brooks, J. S.; Eaton, D. L.; Parkin, S. R. Functionalized Pentacene: Improved Electronic Properties from Control of Solid-State Order [20]. *J. Am. Chem. Soc.* **2001**, *123* (38), 9482–9483.

(42) Scholes, G. D.; Ghiggino, K. P.; Oliver, A. M.; Paddon-Row, M. N. Through-Space and Through-Bond Effects on Exciton Interactions in Rigidly Linked Dinaphthyl Molecules. *J. Am. Chem. Soc.* **1993**, *115* (10), 4345–4349.

(43) Gerson, F.; Wellauer, T.; Oliver, A. M.; Paddon-Row, M. N. Long-Range Intramolecular Electron Transfer between Two Naphthalene Π-Moieties Attached to a Rigid Norbornylogous Spacer of Variable Length: An ESR and ENDOR Study. *Helv. Chim. Acta* **1990**, *73* (6), 1586–1601.

(44) Clayton, A. H. A.; Scholes, G. D.; Ghiggino, K. P.; Paddon-Row, M. N. Through-Bond and Through-Space Coupling in Photoinduced Electron and Energy Transfer: An *Ab Initio* and Semiempirical Study. *J. Phys. Chem.* **1996**, *100* (26), 10912–10918.

(45) Paddon-Row, M. N.; Shephard, M. J. Through-Bond Orbital Coupling, the Parity Rule, and the Design of “superbridges” Which Exhibit Greatly Enhanced Electronic Coupling: A

Natural Bond Orbital Analysis. *J. Am. Chem. Soc.* **1997**, *119* (23), 5355–5365.

(46) Kroon, J.; Verhoeven, J. W.; Oliver, A. M.; Paddon-Row, M. N. Observation of a Remarkable Dependence of the Rate of Singlet-Singlet Energy Transfer on the Configuration of the Hydrocarbon Bridge in Bichromophoric Systems. *J. Am. Chem. Soc.* **1990**, *112* (12), 4868–4873.

(47) Cook, J. D.; Carey, T. J.; Damrauer, N. H. Solution-Phase Singlet Fission in a Structurally Well-Defined Norbornyl-Bridged Tetracene Dimer. *J. Phys. Chem. A* **2016**, *120* (26), 4473–4481.

(48) Cook, J. D.; Carey, T. J.; Arias, D. H.; Johnson, J. C.; Damrauer, N. H. Solvent-Controlled Branching of Localized versus Delocalized Singlet Exciton States and Equilibration with Charge Transfer in a Structurally Well-Defined Tetracene Dimer. *J. Phys. Chem. A* **2017**, *121* (48), 9229–9242.

Chapter 2

(1) Carey, T. J.; Snyder, J. L.; Miller, E. G.; Sammakia, T.; Damrauer, N. H. Synthesis of Geometrically Well-Defined Covalent Acene Dimers for Mechanistic Exploration of Singlet Fission. *J. Org. Chem.* **2017**, *82* (9), 4866–4874.

(2) Miller, E. G.; Singh, M.; Parkin, S. R.; Sammakia, T.; Damrauer, N. Preparation of a Rigid and Nearly Coplanar Bis-Tetracene Dimer through Application of the CANAL Reaction. *ChemRxiv* Cambridge: Cambridge Open Engage; **2021**; This content is a preprint and has not been subject to peer review.

(3) Edhborg, F.; Olesund, A.; Albinsson, B. Best Practice in Determining Key Photophysical Parameters in Triplet–Triplet Annihilation Photon Upconversion. *Photochem. Photobiol.*

Sci. **2022**, *21* (7), 1143–1158.

(4) Olesund, A.; Johnsson, J.; Edhborg, F.; Ghasemi, S.; Moth-Poulsen, K.; Albinsson, B. Approaching the Spin-Statistical Limit in Visible-to-Ultraviolet Photon Upconversion. *J. Am. Chem. Soc.* **2022**, *144* (8), 3706–3716.

(5) Olesund, A.; Gray, V.; Mårtensson, J.; Albinsson, B. Diphenylanthracene Dimers for Triplet-Triplet Annihilation Photon Upconversion: Mechanistic Insights for Intramolecular Pathways and the Importance of Molecular Geometry. *J. Am. Chem. Soc.* **2021**, *143* (15), 5745–5754.

Chapter 3

(1) Smith, M. B.; Michl, J. Singlet Fission *Chem. Rev.* **2010**, *110*, 6891-6936.

(2) Smith, M. B.; Michl, J. Recent Advances in Singlet Fission *Annu. Rev. Phys. Chem.* **2013**, *64*, 361-386.

(3) Hanna, M. C.; Nozik, A. J. Solar Conversion Efficiency of Photovoltaic and Photoelectrolysis Cells with Carrier Multiplication Absorbers *J. Appl. Phys.* **2006**, *100*, 074510.

(4) Müller, A. M.; Avlasevich, Y. S.; Schoeller, W. W.; Müllen, K.; Bardeen, C. J. Exciton Fission and Fusion in Bis(Tetracene) Molecules with Different Covalent Linker Structures. *J. Am. Chem. Soc.* **2007**, *129*, 14240-14250.

(5) Sanders, S. N.; Kumarasamy, E.; Pun, A. B.; Trinh, M. T.; Choi, B.; Xia, J. L.; Taffet, E. J.; Low, J. Z.; Miller, J. R.; Roy, X.; Zhu, X. Y.; Steigerwald, M. L.; Sfeir, M. Y.; Campos, L. M. Quantitative Intramolecular Singlet Fission in Bipentacenes *J. Am. Chem. Soc.* **2015**, *137*, 8965-8972.

(6) Lukman, S.; Musser, A. J.; Chen, K.; Athanasopoulos, S.; Yong, C. K.; Zeng, Z. B.; Ye, Q.; Chi, C. Y.; Hodgkiss, J. M.; Wu, J. S.; Friend, R. H.; Greenham, N. C. Tuneable Singlet Exciton Fission and Triplet-Triplet Annihilation in an Orthogonal Pentacene Dimer *Adv. Funct. Mater.* **2015**, *25*, 5452-5461.

(7) Zirzlmeier, J.; Lehnherr, D.; Coto, P. B.; Chernick, E. T.; Casillas, R.; Basel, B. S.; Thoss, M.; Tykwinski, R. R.; Guldi, D. M. Singlet Fission in Pentacene Dimers *Proc. Natl. Acad. Sci. USA* **2015**, *112*, 5325-5330.

(8) Korovina, N. V.; Das, S.; Nett, Z.; Feng, X.; Joy, J.; Haiges, R.; Krylov, A. I.; Bradforth, S. E.; Thompson, M. E. Singlet Fission in a Covalently Linked Cofacial Alkynyltetracene Dimer *J. Am. Chem. Soc.* **2016**, *138*, 617-627.

(9) Cook, J.; Carey, T. J.; Damrauer, N. H. Solution-Phase Singlet Fission in a Structurally Well-Defined Norbornyl-Bridged Tetracene Dimer *J. Phys. Chem. A* **2016**, *120*, 4473−4481.

(10) Lukman, S.; Chen, K.; Hodgkiss, J. M.; Turban, D. H. P.; Hine, N. D. M.; Dong, S. Q.; Wu, J. S.; Greenham, N. C.; Musser, A. J. Tuning the Role of Charge-Transfer States in Intramolecular Singlet Exciton Fission through Side-Group Engineering *Nat. Commun.* **2016**, *7*, 13622.

(11) Sakuma, T.; Sakai, H.; Araki, Y.; Mori, T.; Wada, T.; Tkachenko, N. V.; Hasobe, T. Long-Lived Triplet Excited States of Bent-Shaped Pentacene Dimers by Intramolecular Singlet Fission *J. Phys. Chem. A* **2016**, *120*, 1867-1875.

(12) Zirzlmeier, J.; Casillas, R.; Reddy, S. R.; Coto, P. B.; Lehnherr, D.; Chernick, E. T.; Papadopoulos, I.; Thoss, M.; Tykwinski, R. R.; Guldi, D. M. Solution-Based Intramolecular Singlet Fission in Cross-Conjugated Pentacene Dimers *Nanoscale* **2016**, *8*, 10113-10123.

(13) Cook, J. D.; Carey, T. J.; Arias, D. H.; Johnson, J. C.; Damrauer, N. H. Solvent-Controlled Branching of Localized Versus Delocalized Singlet Exciton States and Equilibration with Charge Transfer in a Structurally Well-Defined Tetracene Dimer *J. Phys. Chem. A* **2017**, *121*, 9229-9242.

(14) Kumarasamy, E.; Sanders, S. N.; Tayebjee, M. J. Y.; Asadpoordarvish, A.; Hele, T. J. H.; Feummeler, E. G.; Pun, A. B.; Yablon, L. M.; Low, J. Z.; Paley, D. W.; Dean, J. C.; Choi, B.; Scholes, G. D.; Steigerwald, M.; Ananth, N.; McCamey, D. R.; Sfeir, M. Y.; Campos, L. M. Tuning Singlet Fission in Pi-Bridge-Pi Chromophores *J. Am. Chem. Soc* **2017**, *139*, 12488–12494.

(15) Basel, B. S.; Zirzlmeier, J.; Hetzer, C.; Phelan, B. T.; Krzyaniak, M. D.; Reddy, S. R.; Coto, P. B.; Horwitz, N. E.; Young, R. M.; White, F. J.; Hampel, F.; Clark, T.; Thoss, M.; Tykwinski, R. R.; Wasielewski, M. R.; Guldi, D. M. Unified Model for Singlet Fission within a Non-Conjugated Covalent Pentacene Dimer *Nat. Commun.* **2017**, *8*, 15171.

(16) Dean, J. C.; Zhang, R.; Hallani, R. K.; Pensack, R. D.; Sanders, S. N.; Oblinsky, D. G.; Parkin, S. R.; Campos, L. M.; Anthony, J. E.; Scholes, G. D. Photophysical Characterization and Time-Resolved Spectroscopy of a Anthradithiophene Dimer: Exploring the Role of Conformation in Singlet Fission *Phys. Chem. Chem. Phys.* **2017**, *19*, 23162-23175.

(17) Yamakado, T.; Takahashi, S.; Watanabe, K.; Matsumoto, Y.; Osuka, A.; Saito, S. Conformational Planarization versus Singlet Fission: Distinct Excited-State Dynamics of Cyclooctatetraene-Fused Acene Dimers *Angew. Chem. Int. Edit. Eng.* **2018**, *57*, 5438-5443.

(18) Carey, T. J.; Miller, E. G.; Gilligan, A. T.; Sammakia, T.; Damrauer, N. H. Modular Synthesis of Rigid Polyacene Dimers for Singlet Fission *Org. Lett.* **2018**, *20*, 457-460.

(19) Basel, B. S.; Zirzlmeier, J.; Hetzer, C.; Reddy, S. R.; Phelan, B. T.; Krzyaniak, M. D.; Volland, M. K.; Coto, P. B.; Young, R. M.; Clark, T.; Thoss, M.; Tykwinski, R. R.; Wasielewski, M. R.; Gulditla, D. M. Evidence for Charge-Transfer Mediation in the Primary Events of Singlet Fission in a Weakly Coupled Pentacene Dimer *Chem* **2018**, *4*, 1092-1111.

(20) Korovina, N. V.; Joy, J.; Feng, X. T.; Feltenberger, C.; Krylov, A. I.; Bradforth, S. E.; Thompson, M. E. Linker-Dependent Singlet Fission in Tetracene Dimers *J. Am. Chem. Soc.* **2018**, *140*, 10179-10190.

(21) Margulies, E. A.; Miller, C. E.; Wu, Y.; Ma, L.; Schatz, G. C.; Young, R. M.; Wasielewski, M. R. Enabling Singlet Fission by Controlling Intramolecular Charge Transfer in π-Stacked Covalent Terrylenediimide Dimers *Nat. Chem.* **2016**, *8*, 1120-1125.

(22) Johnson, J. C.; Akdag, A.; Zamadar, M.; Chen, X.; Schwerin, A. F.; Paci, I.; Smith, M. B.; Havlas, Z.; Miller, J. R.; Ratner, M. A.; Nozik, A. J.; Michl, J. Toward Designed Singlet Fission: Solution Photophysics of Two Indirectly Coupled Covalent Dimers of 1,3-Diphenylisobenzofuran *J. Phys. Chem. B* **2013**, *117*, 4680−4695.

(23) Schrauben, J. N.; Akdag, A.; Wen, J.; Havlas, Z.; Ryerson, J. L.; Smith, M. B.; Michl, J.; Johnson, J. C. Excitation Localization/Delocalization Isomerism in a Strongly Coupled Covalent Dimer of 1,3-Diphenylisobenzofuran *J. Phys. Chem. A* **2016**, *120*, 3473-3483.

(24) Sanders, S. N.; Kumarasamy, E.; Pun, A. B.; Steigerwald, M. L.; Sfeir, M. Y.; Campos, L. M. Intramolecular Singlet Fission in Oligoacene Heterodimers *Angew. Chem. Int. Edit. Eng.* **2016**, *55*, 3373-3377.

(25) Alguire, E. C.; Subotnik, J. E.; Damrauer, N. H. Exploring Non-Condon Effects in a Covalent Tetracene Dimer: How Important Are Vibrations in Determining the Electronic Coupling for Singlet Fission? *J. Phys. Chem. A* **2015**, *119*, 299-311.

(26) Sanders, S. N.; Kumarasamy, E.; Pun, A. B.; Appavoo, K.; Steigerwald, M. L.; Campos, L. M.; Sfeir, M. Y. Exciton Correlations in Intramolecular Singlet Fission *J. Am. Chem. Soc.* **2016**, *138*, 7289-7297.

(27) Tayebjee, M. J. Y.; Sanders, S. N.; Kumarasamy, E.; Campos, L. M.; Sfeir, M. Y.; McCamey, D. R. Quintet Multiexciton Dynamics in Singlet Fission *Nat. Phys.* **2017**, *13*, 182-188.

(28) Trinh, M. T.; Pinkard, A.; Pun, A. B.; Sanders, S. N.; Kumarasamy, E.; Sfeir, M. Y.; Campos, L. M.; Roy, X.; Zhu, X. Y. Distinct properties of the triplet pair state from singlet fission *Sci. Adv.* **2017**, *3*.

(29) Fuemmeler, E. G.; Sanders, S. N.; Pun, A. B.; Kumarasamy, E.; Zeng, T.; Miyata, K.; Steigerwald, M. L.; Zhu, X. Y.; Sfeir, M. Y.; Campos, L. M.; Ananth, N. A Direct Mechanism of Ultrafast Intramolecular Singlet Fission in Pentacene Dimers *ACS Cent. Sci.* **2016**, *2*, 316-324.

(30) Berkelbach, T. C.; Hybertsen, M. S.; Reichman, D. R. Microscopic Theory of Singlet Exciton Fission. II. Application to Pentacene Dimers and the Role of Superexchange *J. Chem. Phys.* **2013**, *138*, 114103.

(31) Yost, S. R.; Lee, J.; Wilson, M. W. B.; Wu, T.; McMahon, D. P.; Parkhurst, R. R.; Thompson, N. J.; Congreve, D. N.; Rao, A.; Johnson, K.; Sfeir, M. Y.; Bawendi, M. G.; Swager, T. M.; Friend, R. H.; Baldo, M. A.; Van Voorhis, T. A Transferable Model for Singlet-Fission Kinetics *Nat. Chem.* **2014**, *6*, 492-497.

(32) Liu, H. Y.; Wang, R.; Shen, L.; Xu, Y. Q.; Xiao, M.; Zhang, C. F.; Li, X. Y. A Covalently Linked Tetracene Trimer: Synthesis and Singlet Exciton Fission Property *Org. Lett.* **2017**, *19*, 580-583.

(33) Liu, H. Y.; Wang, Z. W.; Wang, X. M.; Shen, L.; Zhang, C. F.; Xiao, M.; Li, X. Y. Singlet exciton fission in a linear tetracene tetramer *J. Mater. Chem. C* **2018**, *6*, 3245-3253.

(34) Vallett, P. J.; Snyder, J. L.; Damrauer, N. H. Tunable Electronic Coupling and Driving Force in Structurally Well-Defined Tetracene Dimers for Molecular Singlet Fission: A Computational Exploration Using Density Functional Theory *J. Phys. Chem. A* **2013**, *117*, 10824-10838.

(35) Damrauer, N. H.; Snyder, J. L. Symmetry-Directed Control of Electronic Coupling for Singlet Fission in Covalent Bis-Acene Dimers *J. Phys. Chem. Lett.* **2015**, *6*, 4456-4462.

(36) Pace, N. A.; Arias, D. H.; Granger, D. B.; Christensen, S.; Anthony, J. E.; Johnson, J. C. Dynamics of Singlet Fission and Electron Injection in Self-Assembled Acene Monolayers on Titanium Dioxide *Chem. Sci.* **2018**, *9*, 3004-3013.

(37) Bayliss, S. L.; Weiss, L. R.; Rao, A.; Friend, R. H.; Chepelianskii, A. D.; Greenham, N. C. Spin signatures of exchange-coupled triplet pairs formed by singlet fission *Phys. Rev. B* **2016**, *94*.

(38) Weiss, L. R.; Bayliss, S. L.; Kraffert, F.; Thorley, K. J.; Anthony, J. E.; Bittl, R.; Friend, R. H.; Rao, A.; Greenham, N. C.; Behrends, J. Strongly exchange-coupled triplet pairs in an organic semiconductor *Nat. Phys.* **2017**, *13*, 176-181.

(39) Burdett, J. J.; Piland, G. B.; Bardeen, C. J. Magnetic field effects and the role of spin states in singlet fission *Chem. Phys. Lett.* **2013**, *585*, 1-10.

(40) Lewis, J. E.; Maroncelli, M. On the (Uninteresting) Dependence of the Absorption and Emission Transition Moments of Coumarin 153 on Solvent *Chem. Phys. Lett.* **1998**, *282*, 197.

(41) Sens, R.; Drexhage, K. H. Fluorescence Quantum Yield of Oxazine and Carbazine Laser-Dyes *J. Lumin.* **1981**, *24-5*, 709-712.

(42) Scholes, G. D.; Ghiggino, K. P.; Oliver, A. M.; Paddon-Row, M. N. Through-Space and Through-Bond Effects on Exciton Interactions in Rigidly Linked Dinaphthyl Molecules *J. Am. Chem. Soc.* **1993**, *115*, 4345-4349.

(43) Spano, F. C. The Spectral Signatures of Frenkel Polarons in H- and J-Aggregates *Acc. Chem. Res.* **2010**, *43*, 429-439.

(44) It is noted that Saito and coworkers report a nearly quantitative triplet yield of 180%. In our view, this is difficult to reconcile with the reported spectra that show a significant ESA band at ~460 nm as well as significant stimulated emission at ~610 nm, thus signifying the presence of a large amount of excitonic singlet. These workers mention that to account for the dissociation of triplets into independent species from the ^{1}TT, the calculated excited-state concentration must be doubled. We believe that this step is unnecessary and that it leads to a triplet yield overestimation while significant amounts of singlets remain. We suspect that the triplet yield in Saito's system is likely closer to the 100% that we report here.

(45) As desribed later, we find K ~ 0.1 in TIPS-BT1 and this means that we are underestimating these k_r and k_{nr} values by a small amount in this molecule by assuming K is very small, as per our original interpretation (c.f. 13). We recover the observed decay with the K = 0.1 in place by setting $k_{tot} = k_r + k_{nr} = 4.5\times10^7$ rather than 4.2×10^7. But this translates to a modest difference in lifetime (22.2ns versus 23.8 ns) and the overall conclusion holds.

(46) For example, setting ΔG = -0.34 eV (c.f. 7) while leaving λ = 0.18 eV, one obtains this value of k_{fiss} when V_{eff} is modestly decreased from 5.5 meV to 4.8 meV.

(47) Paddon-Row, M. N.; Shephard, M. J. Through-bond orbital coupling, the parity rule, and the design of "superbridges" which exhibit greatly enhanced electronic coupling: A natural bond orbital analysis *J. Am. Chem. Soc.* **1997**, *119*, 5355-5365.

(48) Clayton, A. H. A.; Scholes, G. D.; Ghiggino, K. P.; Paddon-Row, M. N. Through-Bond and Through-Space Coupling in Photoinduced Electron and Energy Transfer: An ab Initio and Semiempirical Study *J. Phys. Chem.* **1996**, *100*, 10912-10918.

(49) Scholes, G. D.; Ghiggino, K. P.; Oliver, A. M.; Paddon-Row, M. N. Intramolecular Electronic-Energy Transfer between Rigidly Linked Naphthalene and Anthracene Chromophores *J. Phys. Chem.* **1993**, *97*, 11871-11876.

Chapter 4

(1) Gilligan, A. T.; Miller, E. G.; Sammakia, T.; Damrauer, N. H. Using Structurally Well-Defined Norbornyl-Bridged Acene Dimers to Map a Mechanistic Landscape for Correlated Triplet Formation in Singlet Fission. *J. Am. Chem. Soc.* **2019**.

(2) Smith, M. B.; Michl, J. Singlet Fission. *Chem. Rev.* **2010**, *110* (11), 6891–6936.

(3) Berkelbach, T. C.; Hybertsen, M. S.; Reichman, D. R. Microscopic Theory of Singlet Exciton Fission. II. Application to Pentacene Dimers and the Role of Superexchange. *J. Chem. Phys.* **2013**, *138* (11).

(4) Vallett, P. J.; Snyder, J. L.; Damrauer, N. H. Tunable Electronic Coupling and Driving Force in Structurally Well-Defined Tetracene Dimers for Molecular Singlet Fission: A Computational Exploration Using Density Functional Theory. *J. Phys. Chem. A* **2013**, *117* (42), 10824–10838.

(5) Monahan, N.; Zhu, X.-Y. Charge Transfer–Mediated Singlet Fission. *Annu. Rev. Phys. Chem.* **2015**, *66* (1), 601–618.

(6) Mandal, A.; Chen, M.; Foszcz, E. D.; Schultz, J. D.; Kearns, N. M.; Young, R. M.; Zanni, M. T.; Wasielewski, M. R. Two-Dimensional Electronic Spectroscopy Reveals Excitation

Energy-Dependent State Mixing during Singlet Fission in a Terrylenediimide Dimer. *J. Am. Chem. Soc.* **2018**, *140* (51), 17907–17914.

(7) Margulies, E. A.; Miller, C. E.; Wu, Y.; Ma, L.; Schatz, G. C.; Young, R. M.; Wasielewski, M. R. Enabling Singlet Fission by Controlling Intramolecular Charge Transfer in π-Stacked Covalent Terrylenediimide Dimers. *Nat. Chem.* **2016**, *8* (12), 1120–1125.

(8) Chen, M.; Bae, Y. J.; Mauck, C. M.; Mandal, A.; Young, R. M.; Wasielewski, M. R. Singlet Fission in Covalent Terrylenediimide Dimers: Probing the Nature of the Multiexciton State Using Femtosecond Mid-Infrared Spectroscopy. *J. Am. Chem. Soc.* **2018**, *140* (29), 9184–9192.

(9) Johnson, J. C.; Akdag, A.; Zamadar, M.; Chen, X.; Schwerin, A. F.; Paci, I.; Smith, M. B.; Havlas, Z.; Miller, J. R.; Ratner, M. A.; et al. Toward Designed Singlet Fission: Solution Photophysics of Two Indirectly Coupled Covalent Dimers of 1,3-Diphenylisobenzofuran. *J. Phys. Chem. B* **2013**, *171* (16), 4680–4695.

(10) Alvertis, A. M.; Lukman, S.; Hele, T. J. H.; Fuemmeler, E. G.; Feng, J.; Wu, J.; Greenham, N. C.; Chin, A. W.; Musser, A. J. Switching between Coherent and Incoherent Singlet Fission via Solvent-Induced Symmetry Breaking. *J. Am. Chem. Soc.* **2019**, *141* (44), 17558–17570.

(11) Lukman, S.; Chen, K.; Hodgkiss, J. M.; Turban, D. H. P.; Hine, N. D. M.; Dong, S.; Wu, J.; Greenham, N. C.; Musser, A. J. Tuning the Role of Charge-Transfer States in Intramolecular Singlet Exciton Fission through Side-Group Engineering. *Nat. Commun.* **2016**, *7*, 13622.

(12) Ball, A. O. LXXX.—The measurement of the dielectric constants of organic liquids *J. Chem. Soc.,* **1930**, 570–596.

(13) Rltzoulls, G.; Papadopoulos, N.; Jannakoudakls, D. Densities, Viscosities, and Dielectric Constants of Acetonitrile + Toluene at 15, 25, and 35 °C. *J. Chem. Eng. Data* **1986**, *31*, 146–148.

(14) Cook, J. D.; Carey, T. J.; Arias, D. H.; Johnson, J. C.; Damrauer, N. H. Solvent-Controlled Branching of Localized versus Delocalized Singlet Exciton States and Equilibration with Charge Transfer in a Structurally Well-Defined Tetracene Dimer. *J. Phys. Chem. A* **2017**, *121* (48), 9229–9242.

(15) Mauck, C. M.; Bae, Y. J.; Chen, M.; Powers-Riggs, N.; Wu, Y.-L.; Wasielewski, M. R. Charge-Transfer Character in a Covalent Diketopyrrolopyrrole Dimer: Implications for Singlet Fission. *ChemPhotoChem* **2018**, *2*, 223.

(16) Lukman, S.; Musser, A. J.; Chen, K.; Athanasopoulos, S.; Yong, C. K.; Zeng, Z.; Ye, Q.; Chi, C.; Hodgkiss, J. M.; Wu, J.; et al. Tuneable Singlet Exciton Fission and Triplet-Triplet Annihilation in an Orthogonal Pentacene Dimer. *Adv. Funct. Mater.* **2015**, *25* (34), 5452–5461.

(17) Sartor, S. M.; McCarthy, B. G.; Pearson, R. M.; Miyake, G. M.; Damrauer, N. H. Exploiting Charge-Transfer States for Maximizing Intersystem Crossing Yields in Organic Photoredox Catalysts. *J. Am. Chem. Soc.* **2018**, *140* (14), 4778–4781.

(18) Schwoerer, M.; Wolf, H. C. Organic Molecular Solids. Wiley. **2008**, DOI: 10.1002/9783527618651.

(19) Spano, F. C. The Spectral Signatures of Frenkel Polarons in H- and J-Aggregates. *Acc. Chem. Res.* **2010**, *43* (3), 429–439.

(20) Sartor, S. M.; Lattke, Y. M.; McCarthy, B. G.; Miyake, G. M.; Damrauer, N. H. Effects of Naphthyl Connectivity on the Photophysics of Compact Organic Charge-Transfer

Photoredox Catalysts. *J. Phys. Chem. A* **2019**, *123* (22), 4727–4736.

(21) Alguire, E. C.; Subotnik, J. E.; Damrauer, N. H. Exploring Non-Condon Effects in a Covalent Tetracene Dimer: How Important Are Vibrations in Determining the Electronic Coupling for Singlet Fission. *J. Phys. Chem. A* **2015**, *119*, 299–311.

(22) Brunschwig, B. S.; Creutz, C.; Sutin, N. Optical Transitions of Symmetrical Mixed-Valence Systems in the Class II-III Transition Regime †. *Chem. Soc. Rev.* **2002**, *31*, 168–184.

(23) Reichardt, C. Solvatochromic Dyes as Solvent Polarity Indicators. *Chem. Rev.* **1994**, *94* (8), 2319–2358.

(24) Korovina, N. V.; Chang, C. H.; Johnson, J. C. Spatial Separation of Triplet Excitons Drives Endothermic Singlet Fission. *Nat. Chem.* **2020**, *12* 391–398.

Chapter 5

(1) Schulze, T. F.; Schmidt, T. W. Photochemical Upconversion: Present Status and Prospects for Its Application to Solar Energy Conversion. *Energy Environ. Sci.* **2014**, *8* (1), 103–125.

(2) Ghazy, A.; Safdar, M.; Lastusaari, M.; Savin, H.; Karppinen, M. Advances in Upconversion Enhanced Solar Cell Performance. *Sol. Energy Mater. Sol. Cells* **2021**, *230*, 111234.

(3) Liu, M.; Lu, Y.; Xie, Z. B.; Chow, G. M. Enhancing Near-Infrared Solar Cell Response Using Upconverting Transparentceramics. *Sol. Energy Mater. Sol. Cells* **2011**, *95* (2), 800–803.

(4) Ravetz, B. D.; Pun, A. B.; Churchill, E. M.; Congreve, D. N.; Rovis, T.; Campos, L. M. Photoredox Catalysis Using Infrared Light via Triplet Fusion Upconversion. *Nature* **2019**, *565* (7739), 343–346.

(5) Huang, L.; Wu, W.; Li, Y.; Huang, K.; Zeng, L.; Lin, W.; Han, G. Highly Effective Near-

Infrared Activating Triplet–Triplet Annihilation Upconversion for Photoredox Catalysis. *J. Am. Chem. Soc.* **2020**, *142* (43), 18460–18470.

(6) Zhou, J.; Liu, Q.; Feng, W.; Sun, Y.; Li, F. Upconversion Luminescent Materials: Advances and Applications. *Chem. Rev.* **2015**, *115* (1), 395–465.

(7) Park, Y. Il; Lee, K. T.; Suh, Y. D.; Hyeon, T. Upconverting Nanoparticles: A Versatile Platform for Wide-Field Two-Photon Microscopy and Multi-Modal in Vivo Imaging. *Chem. Soc. Rev.* **2015**, *44* (6), 1302–1317.

(8) Sanders, S. N.; Schloemer, T. H.; Gangishetty, M. K.; Anderson, D.; Seitz, M.; Gallegos, A. O.; Stokes, R. C.; Congreve, D. N. Triplet Fusion Upconversion Nanocapsules for Volumetric 3D Printing. *Nature* **2022**, *604* (7906), 474–478.

(9) Park, J. M.; Lee, H.; Choe, H. S.; Ahn, S. K.; Seong, K. Y.; Yang, S. Y.; Kim, J. H. Highly Efficient Triplet–Triplet Annihilation Upconversion in Polycaprolactone: Application to 3D Printable Architectures and Microneedles. *J. Mater. Chem. C* **2022**, *10* (12), 4584–4589.

(10) Singh-Rachford, T. N.; Castellano, F. N. Photon Upconversion Based on Sensitized Triplet-Triplet Annihilation. *Coordination Chemistry Reviews*. **2010**, *254* (21-22), 2560–2573.

(11) Morteza Gholizadeh, E.; Frazer, L.; Macqueen, R. W.; Gallaher, J. K.; Schmidt, T. W. Photochemical Upconversion Is Suppressed by High Concentrations of Molecular Sensitizers Photochemical Upconversion Is Suppressed by High Concentrations of Molecular Sensitizers †. *J. Phys. Chem. Chem. Phys.* **2018**, *20*, 19500–19506.

(12) Hwang, S. Y.; Song, D.; Seo, E. J.; Hollmann, F.; You, Y.; Park, J. B. Triplet–Triplet Annihilation-Based Photon-Upconversion to Broaden the Wavelength Spectrum for Photobiocatalysis. *Sci. Reports* **2022**, *12* (1), 1–7.

(13) Olesund, A.; Gray, V.; Mårtensson, J.; Albinsson, B. Diphenylanthracene Dimers for

Triplet-Triplet Annihilation Photon Upconversion: Mechanistic Insights for Intramolecular Pathways and the Importance of Molecular Geometry. *J. Am. Chem. Soc.* **2021**, *143* (15), 5745–5754.

(14) Gray, V.; Dzebo, D.; Lundin, A.; Alborzpour, J.; Abrahamsson, M.; Albinsson, B.; Moth-Poulsen, K. Photophysical Characterization of the 9,10-Disubstituted Anthracene Chromophore and Its Applications in Triplet–Triplet Annihilation Photon Upconversion. *J. Mater. Chem. C* **2015**, *3* (42), 11111–11121.

(15) Kanoh, M.; Matsui, Y.; Honda, K.; Kokita, Y.; Ogaki, T.; Ohta, E.; Ikeda, H. Elongation of Triplet Lifetime Caused by Intramolecular Energy Hopping in Diphenylanthracene Dyads Oriented to Undergo Efficient Triplet–Triplet Annihilation Upconversion. *J. Phys. Chem. B* **2021**, *125* (18), 4831–4837.

(16) Gao, C.; Prasad, S. K. K.; Zhang, B.; Dvořák, M.; Tayebjee, M. J. Y.; McCamey, D. R.; Schmidt, T. W.; Smith, T. A.; Wong, W. W. H. Intramolecular Versus Intermolecular Triplet Fusion in Multichromophoric Photochemical Upconversion. *J. Phys. Chem. C* **2019**, *123* (33), 20181–20187.

(17) Monguzzi, A.; Tubino, R.; Hoseinkhani, S.; Campione, M.; Meinardi, F. Low Power, Non-Coherent Sensitized Photon up-Conversion: Modelling and Perspectivesw. *Phys. Chem. Chem. Phys.* **2012**, *14*, 4322–4332.

(18) Kim, J. Y.; Lee, J.-W.; Jung, H. S.; Shin, H.; Park, N.-G. High-Efficiency Perovskite Solar Cells. *Chem. Rev.* **2020**, *120* (15), 7867–7918.

(19) Kwon, O. S.; Kim, J.-H.; Cho, J. K.; Kim, J.-H. Triplet–Triplet Annihilation Upconversion in CdS-Decorated SiO2 Nanocapsules for Sub-Bandgap Photocatalysis. *ACS Appl. Mater. Interfaces* **2015**, *7* (1), 318–325.

(20) Dou, Q. Q.; Guo, H. C.; Ye, E. Near-Infrared Upconversion Nanoparticles for Bio-Applications. *Mater. Sci. Eng. C* **2015**, *45*, 635–643.

(21) Bharmoria, P.; Bildirir, H.; Moth-Poulsen, K. Triplet–Triplet Annihilation Based near Infrared to Visible Molecular Photon Upconversion. *Chem. Soc. Rev.* **2020**, *49* (18), 6529–6554.

(22) Imperiale, C. J.; Green, P. B.; Miller, E. G.; Damrauer, N. H.; Wilson, M. W. B. Triplet-Fusion Upconversion Using a Rigid Tetracene Homodimer. *J. Phys. Chem. Lett* **2019**, *10* (23), 7463–7469.

(23) Pun, A. B.; Sanders, S. N.; Sfeir, M. Y.; Campos, L. M.; Congreve, D. N. Annihilator Dimers Enhance Triplet Fusion Upconversion †. *Chem. Sci.* **2019**, *10*, 3969-3975.

(24) Bossanyi, D. G.; Sasaki, Y.; Wang, S.; Chekulaev, D.; Kimizuka, N.; Yanai, N.; Clark, J. Spin Statistics for Triplet–Triplet Annihilation Upconversion: Exchange Coupling, Intermolecular Orientation, and Reverse Intersystem Crossing. *JACS Au* **2021**, *1* (12), 2188–2201.

(25) Cook, J. D.; Carey, T. J.; Arias, D. H.; Johnson, J. C.; Damrauer, N. H. Solvent-Controlled Branching of Localized versus Delocalized Singlet Exciton States and Equilibration with Charge Transfer in a Structurally Well-Defined Tetracene Dimer. *J. Phys. Chem. A* **2017**, *121* (48), 9229–9242.

(26) Rihter, B. D.; Kenney, M. E.; Ford, W. E.; Rodgers, M. A. J. Synthesis and Photoproperties of Diamagnetic Octabutoxyphthalocyanines with Deep Red Optical Absorbance. *J. Am. Chem. Soc.* **1990**, *112* (22), 8064–8070.

(27) Stern, H. L.; Musser, A. J.; Gelinas, S.; Parkinson, P.; Herz, L. M.; Bruzek, M. J.; Anthony, J.; Friend, R. H.; Walker, B. J. Identification of a Triplet Pair Intermediate in Singlet Exciton

Fission in Solution. *Proc. Natl. Acad. Sci. U. S. A.* **2015**, *112* (25), 7656–7661.

(28) Haefele, A.; Blumhoff, J.; Khnayzer, R. S.; Castellano, F. N. Getting to the (Square) Root of the Problem: How to Make Noncoherent Pumped Upconversion Linear. *J. Phys. Chem. Lett.* **2012**, *3* (3), 299–303.

(29) Yanai, N.; Suzuki, K.; Ogawa, T.; Sasaki, Y.; Harada, N.; Kimizuka, N. Absolute Method to Certify Quantum Yields of Photon Upconversion via Triplet−Triplet Annihilation. *J. Phys. Chem. A* **2019**, *123*, 10197–10203.

(30) Zhou, Y.; Castellano, F. N.; Schmidt, T. W.; Hanson, K. On the Quantum Yield of Photon Upconversion via Triplet-Triplet Annihilation. *ACS Energy Lett.* **2020**, *5* (7), 2322–2326.

(31) Smyser, K. E.; Eaves, J. D. Singlet Fission for Quantum Information and Quantum Computing: The Parallel JDE Model. *Sci. Reports 2020 101* **2020**, *10* (1), 1–10.

(32) Olesund, A.; Johnsson, J.; Edhborg, F.; Ghasemi, S.; Moth-Poulsen, K.; Albinsson, B. Approaching the Spin-Statistical Limit in Visible-to-Ultraviolet Photon Upconversion. *J. Am. Chem. Soc.* **2022**, *144* (8), 3706–3716.

(33) Dover, C. B.; Gallaher, J. K.; Frazer, L.; Tapping, P. C.; Petty, A. J.; Crossley, M. J.; Anthony, J. E.; Kee, T. W.; Schmidt, T. W. Endothermic Singlet Fission Is Hindered by Excimer Formation. *Nat. Chem.* **2018**, *10*, 305 – 310.

(34) Hoche, J.; Flock, M.; Miao, X.; Philipp, L. N.; Wenzel, M.; Fischer, I.; Mitric, R. Excimer Formation Dynamics in the Isolated Tetracene Dimer. *Chem. Sci.* **2021**, *12* (36), 11965–11975.

(35) Fan, C.; Wei, L.; Niu, T.; Rao, M.; Cheng, G.; Chruma, J. J.; Wu, W.; Yang, C. Efficient Triplet-Triplet Annihilation Upconversion with an Anti-Stokes Shift of 1.08 EV Achieved by Chemically Tuning Sensitizers. *J. Am. Chem. Soc.* **2019**, *141* (38), 15070–15077.

(36) Wei, Y.; Li, Y.; Zheng, M.; Zhou, X.; Zou, Y.; Yang, C. Simultaneously High Upconversion Efficiency and Large Anti-Stokes Shift by Using Os(II) Complex Dyad as Triplet Photosensitizer. *Adv. Opt. Mater.* **2020**, *8* (9), 1902157.

(37) Gil-Escrig, L.; Dreessen, C.; Palazon, F.; Hawash, Z.; Moons, E.; Albrecht, S.; Sessolo, M.; Bolink, H. J. Efficient Wide-Bandgap Mixed-Cation and Mixed-Halide Perovskite Solar Cells by Vacuum Deposition. *ACS Energy Lett.* **2021** *6* (2), 827 – 836.

Appendix

Chapter 3 Supporting Information

3.10.1 Steady-State Absorption and Emission

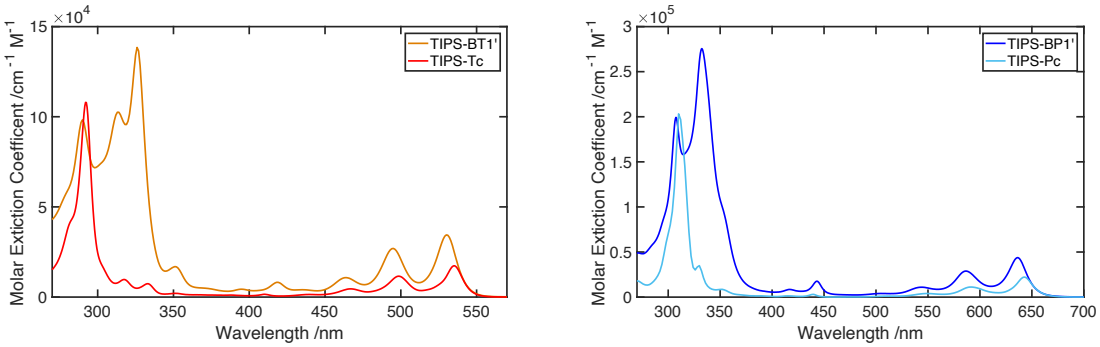

Figure 3.10.1 Molar Extinction Coefficients for dimers TIPS-BT1′ with monomer TIPS-Tc (left) & TIPS-BP1′ with monomer TIPS-Pc (right) in room temperature chloroform to show the Davydov-split UV features that cannot be resolved in toluene due to the solvent absorption cutoff.

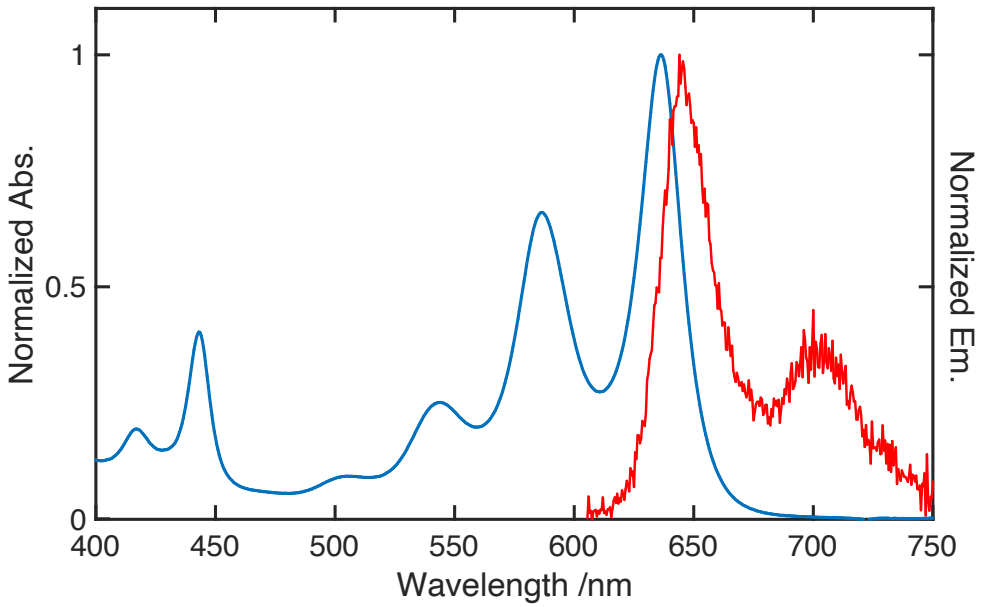

Figure 3.10.2 Normalized steady-state absorption and emission for TIPS-BP1′ in room temperature toluene. The photoluminescence is weak with an emissive quantum yield of ~ 0.5%.

3.10.2 Time-Correlated Single Photon Counting

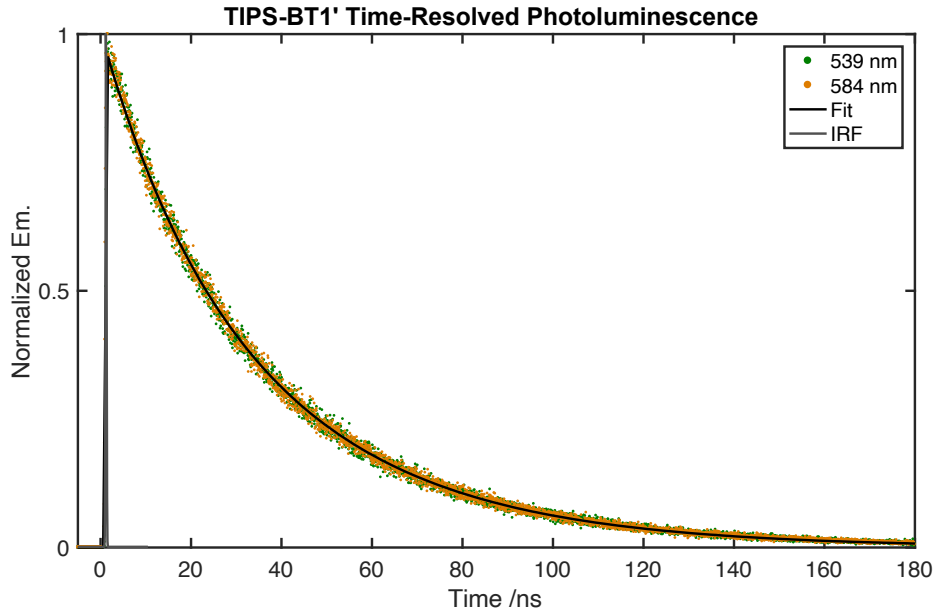

Figure 3.10.3 Time-resolved fluorescence of TIPS-BT1′in room temperature toluene. Sample was pumped at 402 nm with fluorescence collected at 539 nm. Data were fit to Gaussian convoluted single exponential decay to retrieve the time constant.

3.10.3 Global Analysis

Results acquired from fsTA were analyzed using global analysis from homebuilt MATLAB code. Analysis through decay associated spectra (DAS) was used to determine the lowest number of observed evolving components of TIPS-BT1′ & TIPS-BP1′ and their observed lifetimes. Both molecules were fit to two exponentially decaying basis functions. Of these, one component decayed over the course of the experiment while the other long-lived component showed a decay beyond the limits of the experiment. A simple kinetic model of A→B was chosen to retrieve the species associated spectra (SAS) that represent the involved excited states. Supplementary figures 3.10.4 & 3.10.5 correspond to the retrieved SAS for TIPS-BT1′ & TIPS-BP1′.

3.10.3.1 Femtosecond Transient Absorption Spectroscopy

a.

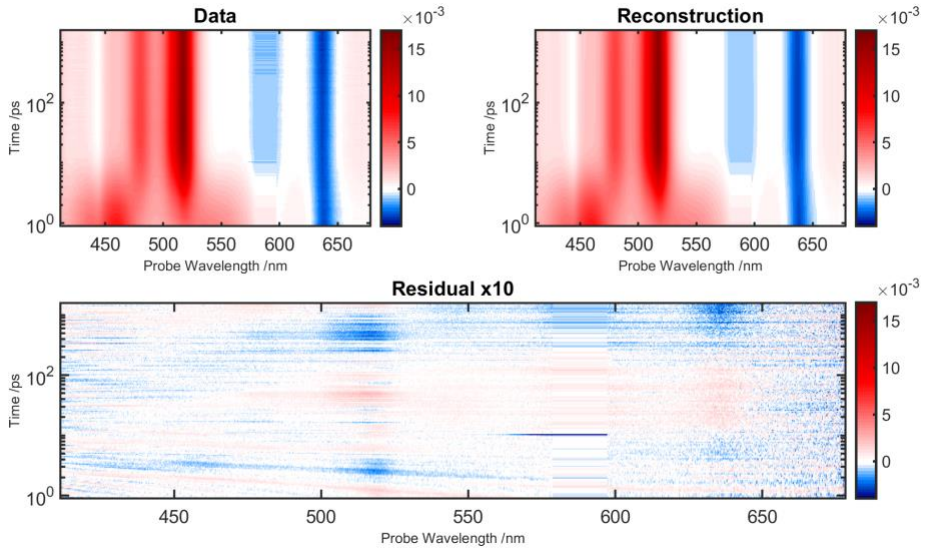

b.

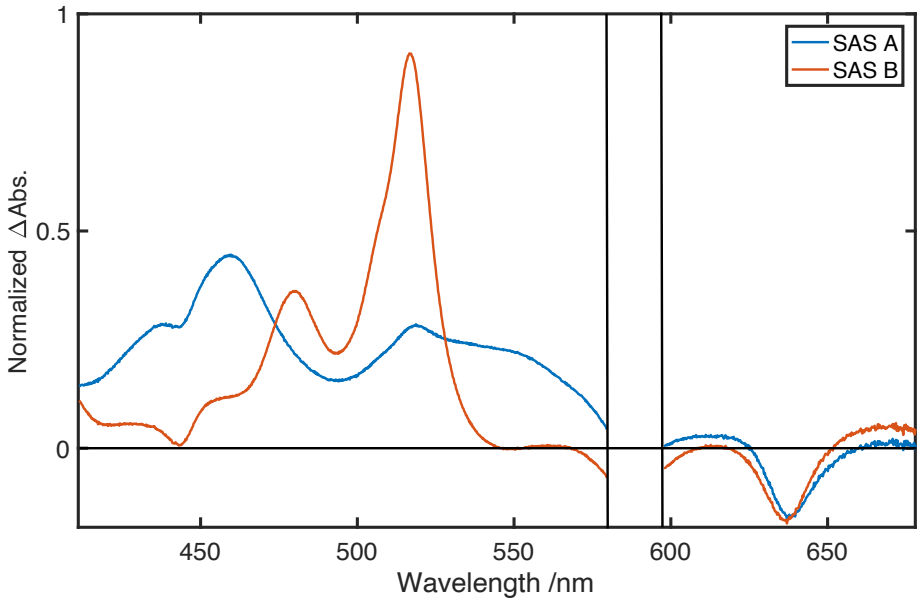

Figure 3.10.4 (a) Raw fsTA data collected for TIPS-BP1′ in room temperature toluene (left) along with a reconstructed global analysis model (right) comprised of a sequential A→B process (B does not decay during the time window of this fit). (b) Two-state species associated spectra (SAS) retrieved from global analysis mentioned above.

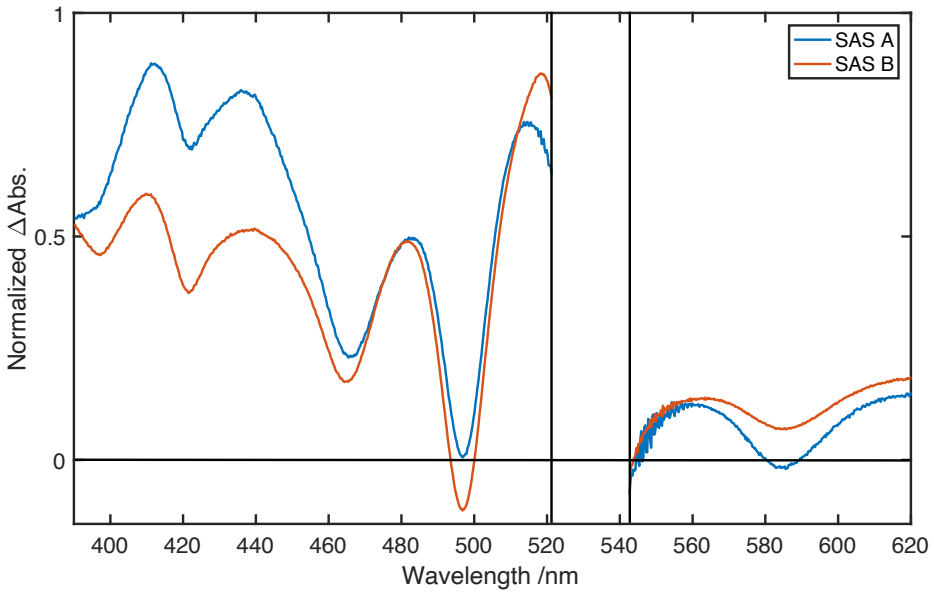

Figure 3.10.5 Two-state species associated spectra (SAS) retrieved from global analysis for fsTA of TIPS-BT1′ in room temperature toluene.

3.10.3.2 Nanosecond Transient Absorption Spectroscopy

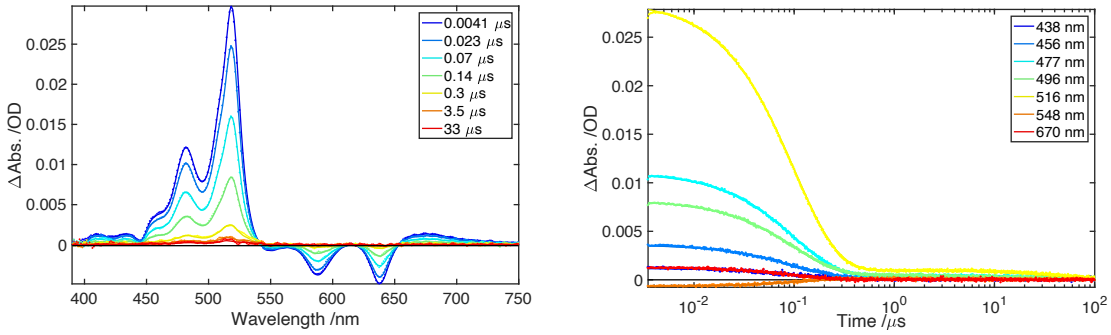

Figure 3.10.6 Nanosecond transient absorption spectra (left) and kinetics (right) for TIPS-BP1′ in room temperature toluene. Both spectra and kinetics show raw data overlain with a fit from global analysis.

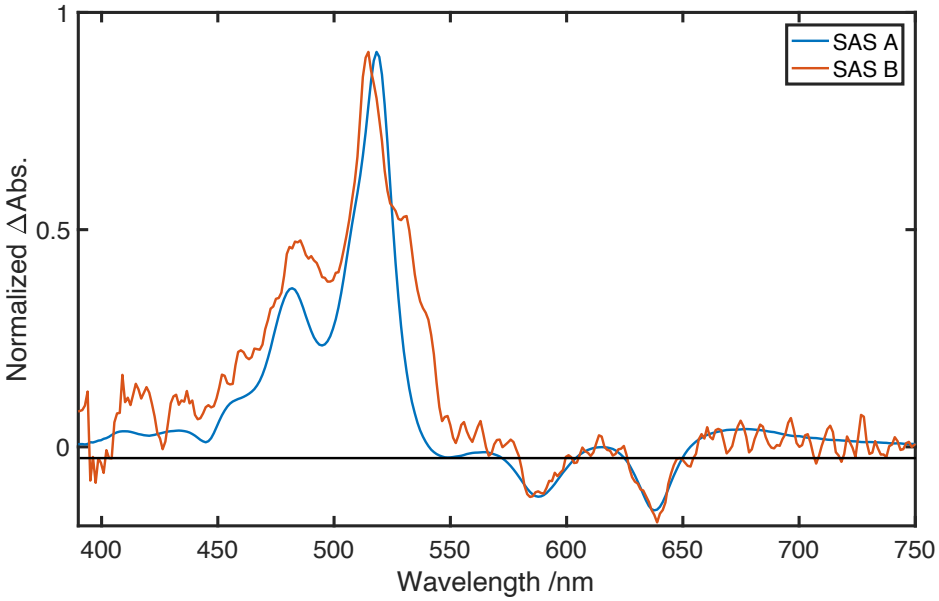

Figure 3.10.7 Two-state species associated spectra (SAS) retrieved from global analysis for nsTA of TIPS-BP1′.

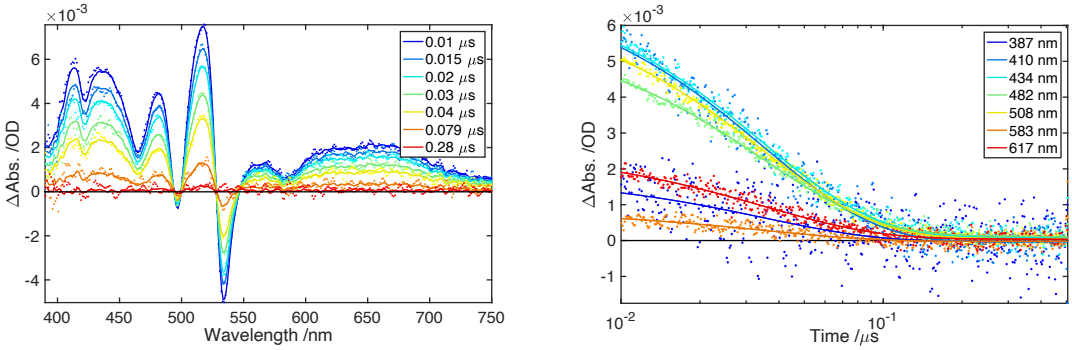

Figure 3.10.8 Nanosecond transient absorption spectra (left) and kinetics (right) for TIPS-BT1′ in room temperature toluene. Both spectra and kinetics show raw data overlain with a fit from global analysis.

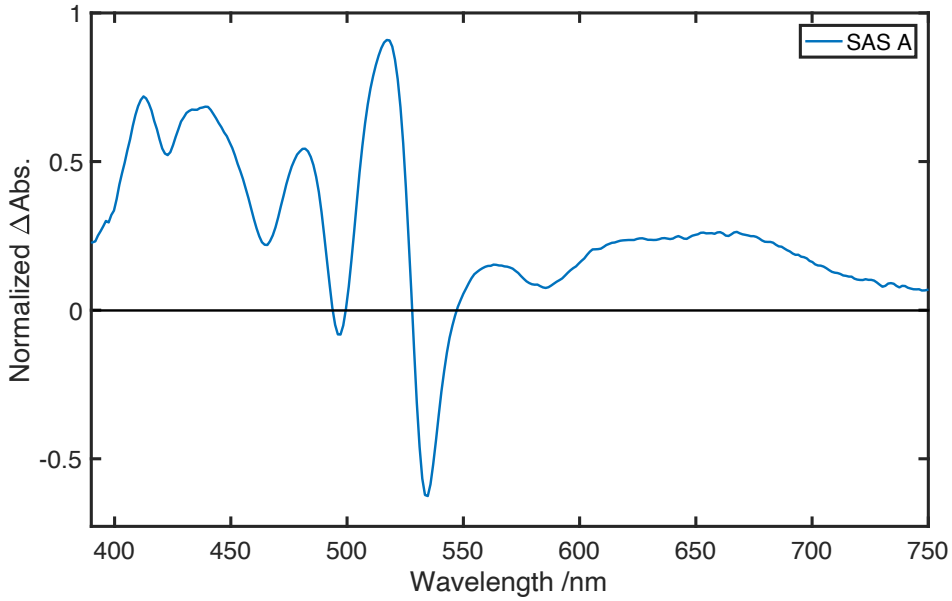

Figure 3.10.9 Single-state species associated spectra (SAS) retrieved from global analysis for nsTA of TIPS-BT1′.

3.10.4 Power Dependent Measurements

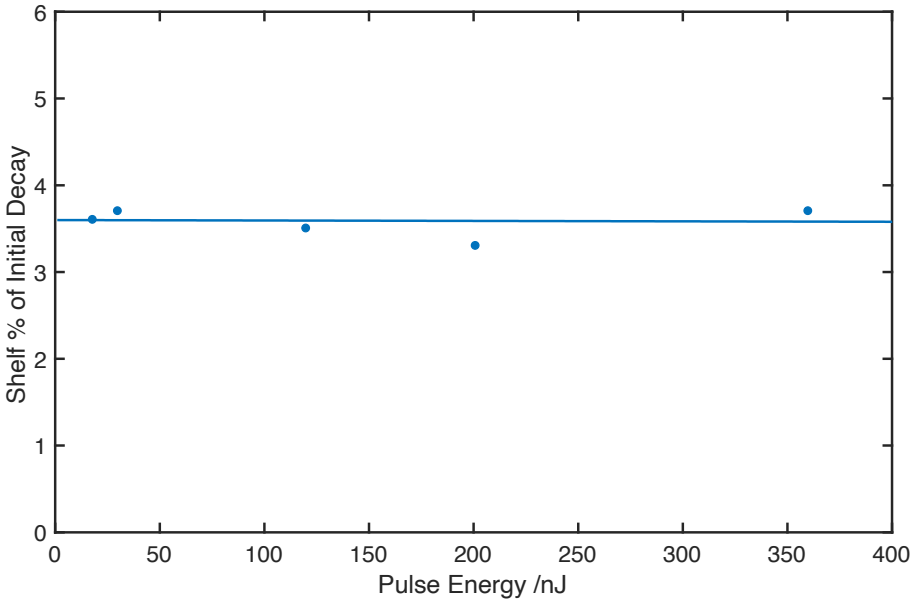

Figure 3.10.10 Power dependent nsTA measurements of TIPS-BP1′ in toluene show the long-lived shelf remaining constant relative to the initial amplitude of the TA signal.

3.10.5 Triplet Sensitization of TIPS-BT1′ & TIPS-BP1′

Nanosecond transient absorption spectroscopy was used in triplet sensitization experiments to characterize the T_1 of both dimer species. Data sets were analyzed through global fitting with four exponential functions to retrieve decay associated spectra (DAS). Species associated spectra were retrieved using a model with two decay pathways to fit the data, similar to what was used during the analysis of TIPS-BT1.[2] These two pathways are comprised of the following: (1) The sensitization pathway wherein excited anthracene undergoes intersystem crossing to form its lowest energy triplet population that can transfer to the dimer; i.e. $S_{1,\,An} \rightarrow T_{1,\,An} \rightarrow T_{1,\,Dim}$. And (2), a small amount of dimer population is generated due to direct photoexcitation.

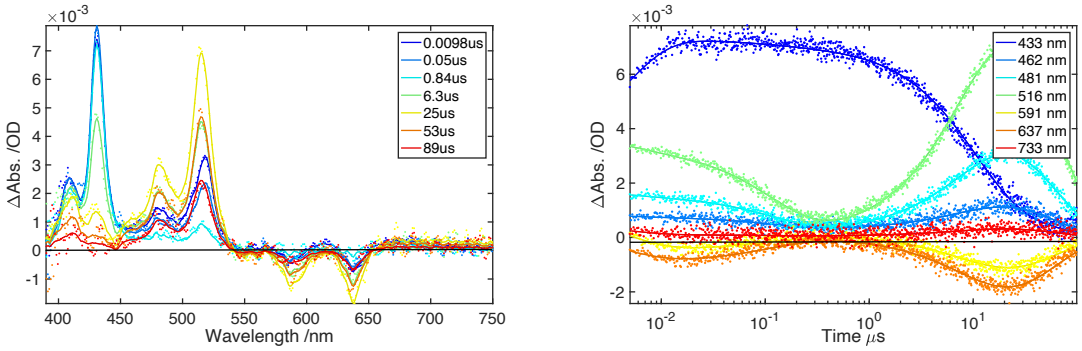

Figure 3.10.11 Nanosecond transient absorption spectra (left) and kinetics (right) for triplet sensitization of TIPS-BP1′ with anthracene in room temperature toluene. Data fit with applied model described in the text above.

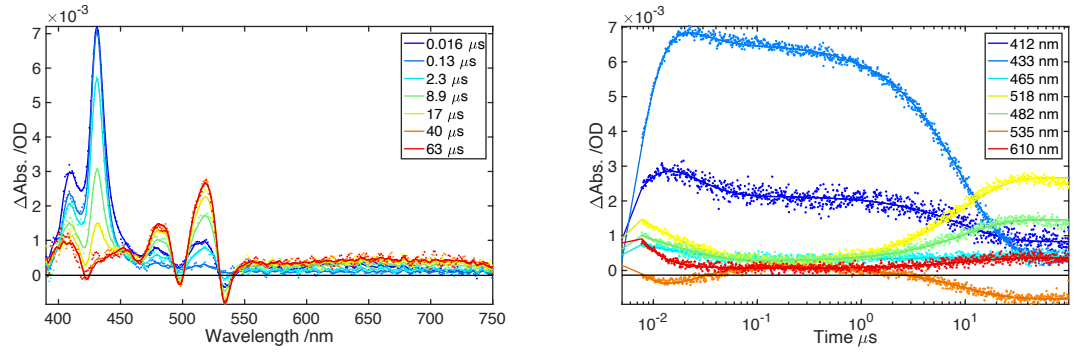

Figure 3.10.12 Nanosecond transient absorption spectra (left) and kinetics (right) for triplet sensitization of TIPS-BT1′ with anthracene in room temperature toluene. Data fit with applied model described in the text above.

Sample	Sample Abs. (Anthracene)	Pump Power (μJ/pulse)	An. Triplet Lifetime (μs)	Dimer Triplet Lifetime (μs)
Sensitized TIPS-BT1′	0.264	200	9.33	714
Sensitized TIPS-BP1′	1.20	66	10.3	55

Table 3.10.1: Table of dimer specific lifetime data collected during triplet sensitization to calculate the triplet epsilon for TIPS-BT1′ & TIPS-BP1′.

The excited state delta epsilons for both dimer species were calculated using pump fluence, photon energy (E_{photon} = 5.52×10^{-19} J; corresponding to 360 nm) and sample anthracene absorption at 360 nm to calculate an anthracene excited state population. The total number of triplets transferred to dimer species could then be calculated by using anthracene's intersystem crossing yield (0.7)[1] and the triplet transfer efficiency ($\Phi_{Transfer}$) measured in relation to pure anthracene in toluene (a lifetime $\tau = 123$ μs was measured in degassed toluene). The following expression was used.

$$N_{triplet} = (1 - 10^{-Abs.}) \frac{E_{pump}}{E_{photon}} \Phi_{ISC} \Phi_{Transfer} \tag{3.10.1}$$

$$N_{triplet} = (1 - 10^{-Abs.}) \frac{E_{pump}}{E_{photon}} \Phi_{ISC} \frac{1/\tau_{sens}}{1/\tau_{sens} + 1/\tau} \tag{3.10.2}$$

The concentration of sensitized dimer was then calculated using the population from the expression above along with the pump spot size (d = 247 μm) and cuvette length (L = 0.2 cm) to calculate the volume, based on the following equation.

$$V = \pi(\frac{d}{2})^2 \times L \tag{3.10.3}$$

The $\Delta\varepsilon$ for TIPS-BT1′ and TIPS-BP1′ was then calculated from the concentration and ΔAbs. Due to some of the signal already starting to decay before all triplets are transferred (particularly in TIPS-BP1′) we use a correction factor to get the true signal based on the observed transfer and decay lifetimes.[2]

$$\Delta Abs = \Delta Abs(t_{max}) \times e^{-k_{Dim}t} \tag{3.10.4}$$

The quantity t_{max} is the time where the TA signal reaches its maximum amplitude before it starts to decay to the ground state again and k_{Dim} is the observed decay rate constant of the sensitized dimer species.

$$\Delta\varepsilon = \frac{\Delta Abs.}{(\frac{N_{triplet}}{V \times N_A}) \times L} \tag{3.10.5}$$

These calculations were performed to produce the delta epsilon T_1 spectra for TIPS-BT1′ and TIPS-BP1′ as shown below.

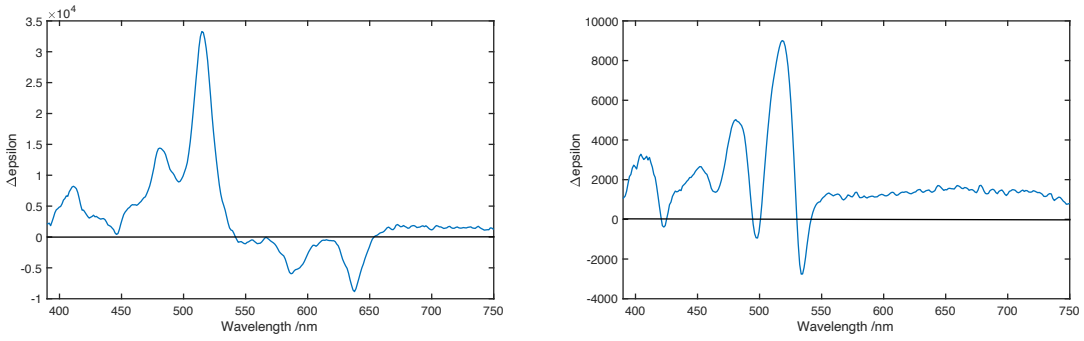

Figure 3.10.13 Retrieved delta epsilon spectra for TIPS-BP1′ (left) and TIPS-BT1′ (right; also shown in Fig. 3.5(a)) in room temperature toluene.

3.10.6 Error Propagation in Triplet Yield

Error bars for the calculated triplet yield in the main text were determined from experimental uncertainty and propagated through to the uncertainty associated with the excited-state singlet and

triplet concentrations according to methods previously described.[3] Experimental uncertainty was based off of measured standard deviation for absorbance and spot size and reported instrument uncertainties for pump wavelength and power.

Initial Singlet Concentration:

$$\frac{\delta[S_1]}{[S_1]} = \sqrt{\left(\frac{\delta\left(I/I_0\right)}{I/I_0}\right)^2 + \left(\frac{\delta(E_{Total})}{E_{Total}}\right)^2 + \left(\frac{\delta(E_{Photon})}{E_{Photon}}\right)^2 + \left(\frac{\delta(Area)}{Area}\right)^2 + \left(\frac{\delta(d)}{d}\right)^2} \tag{3.10.6}$$

where,

$$\frac{\delta\left(I/I_0\right)}{I/I_0} = Abs. * ln(10) * \delta Abs. \tag{3.10.7}$$

Triplet Concentration:

$$\frac{\delta[T_1]}{[T_1]} = \sqrt{\left(\frac{\delta(\Delta Abs)}{\Delta Abs}\right)^2 + \left(\frac{\delta(\varepsilon)}{\varepsilon}\right)^2 + \left(\frac{\delta(d)}{d}\right)^2} \tag{3.10.8}$$

where,

$$\frac{\delta(\varepsilon)}{\varepsilon} = \sqrt{\left(\frac{\delta\left(I/I_0\right)}{I/I_0}\right)^2 + \left(\frac{\delta(E_{Total})}{E_{Total}}\right)^2 + \left(\frac{\delta(E_{Photon})}{E_{Photon}}\right)^2 + \left(\frac{\delta(Area)}{Area}\right)^2 + \left(\frac{\delta(d)}{d}\right)^2 + \left(\frac{\delta(\Phi_{ISC})}{\Phi_{ISC}}\right)^2 + \left(\frac{\delta\left(\Phi_{Transfer}\right)}{\Phi_{Transfer}}\right)^2} \tag{3.10.9}$$

and where,

$$\frac{\delta(\Phi_{Transfer})}{\Phi_{Transfer}} = \sqrt{\left(\frac{\delta(k_{An+Dim.})}{k_{An+Dim.}}\right)^2 + \left(\frac{\delta(k_{Total})}{k_{Total}}\right)^2} \quad (3.10.10)$$

and where,

$$\delta(k_{Total}) = \sqrt{\left(\delta(k_{An+Dim})\right)^2 + \left(\delta(k_{An})\right)^2} \quad (3.10.11)$$

Singlet Fission Yield:

$$\frac{\delta(SF\ Yield)}{(SF\ Yield)} = \sqrt{\left(\frac{\delta[S_1]}{[S_1]}\right)^2 + \left(\frac{\delta[T_1]}{[T_1]}\right)^2} \quad (3.10.12)$$

3.10.7 TIPS-BT1′ Spectral Deconstruction

The singlet and triplet populations for TIPS-BT1′ were fit to the globally analyzed transient absorption data as a linear combination of two independent TA spectra.

$$\Delta A_{Total}(t) = \Delta A_{singlet}(t) + \Delta A_{Triplet}(t) \quad (3.10.13)$$

This equation can be further decomposed into individual transient epsilons and excited state concentrations of the singlet and correlated triplet pair species.

$$\Delta A_{Total}(t) = \Delta\varepsilon_{Singlet} * c_{singlet}(t) + \Delta\varepsilon_{Triplet} * c_{Triplet}(t) \quad (3.10.14)$$

The initial excited state concentration of the singlet species was calculated based on sample absorbance, pump power and spot size. The singlet Δε was calculated based on the earliest

retrieved species from global analysis. For triplet characterization the Δε determined from triplet sensitization was used. The excited triplet concentration of TIPS-BT1′ was modeled using the constraint that overall population is conserved during the course of the experiment ($S_1(t) + {}^1TT(t) = S_1(0)$). Within this constraint, species concentrations were varied until ΔA_{Total} matched the raw data at 120 ps (a least-squares analysis was run to minimize the difference between the raw data and the reconstruction).

3.10.8 Kinetic Modeling

From the kinetic model presented in the main body text, we can model the change in the population of the S_1 and ${}^1TT$ through two coupled differential equations as presented.

$$\frac{dS_1}{dt} = -\left(k_{fiss} + k_r + k_{nr}\right)S_1 + k_{fus}\ {}^1TT \tag{3.10.15}$$

$$\frac{d\ {}^1TT}{dt} = -\left(k_{fus} + k_{TT}\right)\ {}^1TT + k_{fiss}S_1 \tag{3.10.16}$$

Kinetic modeling can be used to retrieve rate constants from observed lifetimes.[4] The model can either be solved numerically or it can be simplified since k_{fus} & k_{fiss} >> k_r, k_{nr}, & k_{TT} and the early time dynamics will solely be determined by k_{fus} & k_{fiss}. This simplifies the system of differential equations to the following expressions.

$$\frac{dS_1}{dt} = -k_{fiss}S_1 + k_{fus}\ {}^1TT \tag{3.10.17}$$

$$\frac{d\ {}^1TT}{dt} = -k_{fus}\ {}^1TT + k_{fiss}S_1 \tag{3.10.18}$$

We can diagonalize for the eigenvalues-eigenvectors for this matrix and fit to the observed lifetimes and amplitudes.

$$K = \begin{pmatrix} -k_{fiss} & k_{fus} \\ k_{fiss} & -k_{fus} \end{pmatrix} \tag{3.10.19}$$

A general solution for solving this is a known n-exponential equation. General solutions for these equations are provided.

$$[S_1(t)] = (A_1 e^{-k_1 t} + A_2 e^{-k_2 t}) * [S_1(0)] \tag{3.10.20}$$

where,

$$A_1 = \frac{k_{fus}}{k_{fiss} + k_{fus}},\ A_2 = \frac{k_{fiss}}{k_{fiss} + k_{fus}}, k_1 = 0, k_2 = k_{fiss} + k_{fus} \tag{3.10.21}$$

Substitutions provide the following expression for the population of S_1 during early time kinetics.

$$[S_1(t)] = \frac{k_{fus} + k_{fiss} e^{-(k_{fiss}+k_{fus})t}}{k_{fiss} + k_{fus}} [S_1(0)] \tag{3.10.22}$$

The above expression can also be used to solve for the population of ^{1}TT during early time kinetics as well based on the constraint $S_1(0) = S_1(t) + {}^1TT(t)$.

$$\left[{}^1TT(t) \right] = \frac{k_{fiss} - k_{fiss} e^{-(k_{fiss}+k_{fus})t}}{k_{fiss} + k_{fus}} [S_1(0)] \tag{3.10.23}$$

Using the observed lifetimes retrieved from global analysis and the initial excited state concentration, the derived expressions were used fit the kinetic traces of TIPS-BT1′ to extract the rate constants. These extracted rate constants are provided in Table 3.1 of the main text.

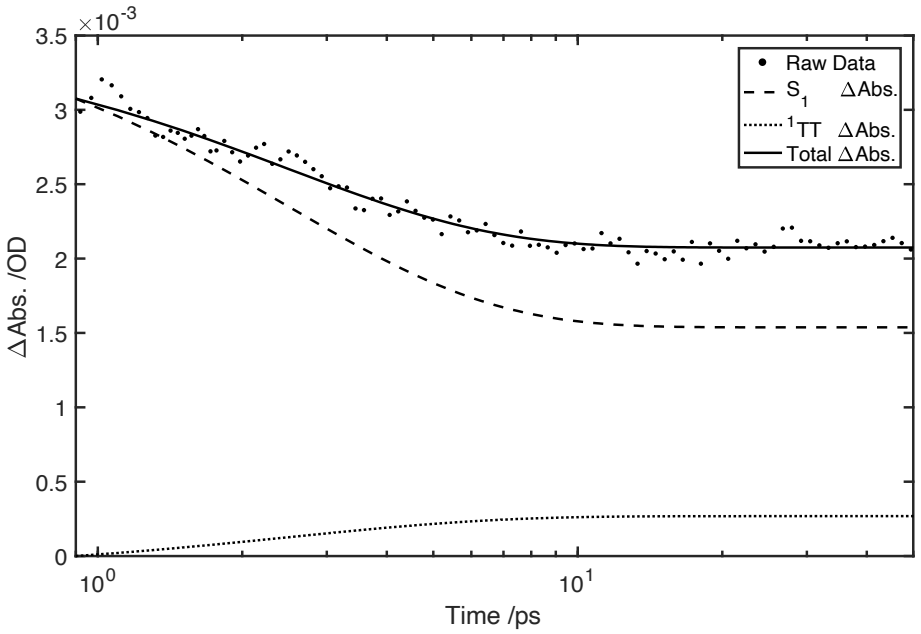

Figure 3.10.14 A kinetic trace collected at 410 nm reconstructed with individual contributions from the S_1 and ^{1}TT fit to raw data for TIPS-BT1′ in toluene.

3.10.9 Singlet Fission Yields

Singlet fission yields were measured using the calculated from the triplet excited state concentration at steady-state and singlet excited state concentration from excitation. First the number of excited singlets was calculated with equation 3.10.24. This was used to calculate moles of excited singlets.

$$N_{singlet} = (1 - 10^{-Abs.}) \frac{E_{pump}}{E_{photon}} \tag{3.10.24}$$

The excitation volume was calculated using equation 3.10.3 and the measured spot size. Along with the moles of singlets the initial excited singlet concentration was calculated. Using the $\Delta\varepsilon$ measured from triplet sensitization and ΔA of the observed triplet feature from fsTA the excited triplet concentration was calculated for TIPS-BP1′. TIPS-BT1′ the excited triplet concentration was found based on the kinetic modeling results from the previous section.

$$\frac{[T_1]}{[S_1]} = SF\ Yield \tag{3.10.25}$$

TIPS-BP1':

$$\frac{[T_1]}{[S_1]} = \frac{(2.50 \pm 0.22) \times 10^{-6} M}{(1.28 \pm 0.09) \times 10^{-6} M} = 1.94 \pm 0.22$$

TIPS-BT1':

$$\frac{[T_1]}{[S_1]} = \frac{(8.95 \pm 1.25) \times 10^{-7} M}{(9.02 \pm 0.69) \times 10^{-7} M} = 1.00 \pm 0.16$$

3.10.10 Marcus Analysis

As explained in the **Chapter 3** main text Marcus Theory underpinned by the classic Marcus expression in equation 3.10.26 can be used to analyze fundamental electron and energy transfer processes in systems with weak electronic coupling between two diabatic states.

$$k_{ET} = \sqrt{\frac{4\pi^3}{h^2 \lambda kT}} {V_{eff}}^2 e^{\frac{-(\Delta G + \lambda)^2}{4\lambda kT}} \tag{3.10.26}$$

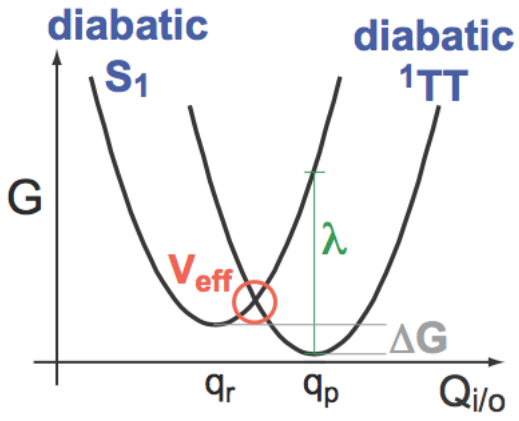

Figure 3.10.15 and Equation 3.10.26 Representation of diabatic states S_1 and ^1TT with coupling parameter (V_{eff}) and reorganization energy (λ) used in Marcus analysis of k_{sf} in TIPS-BT1′ & TIPS-BP1′.

In the expression h, T and k are physical constants representing Planck's constant (h), temperature (T) and the Boltzmann constant (k). The system dependent variables are V_{eff} the diabatic coupling between states, λ the solvent reorganization energy and ΔG the free energy difference between states. The rate constant k_{ET} is the rate of transfer between the two states.

3.10.11 TIPS-Pentacene

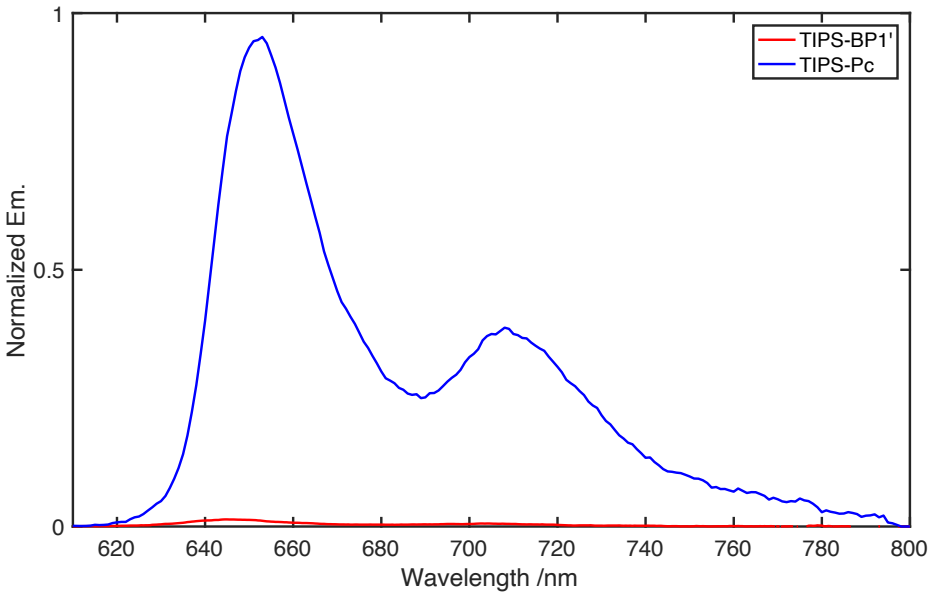

Figure 3.10.16 Relative emission of TIPS-Pc (monomer) and TIPS-BP1 (dimer) in room temperature toluene.

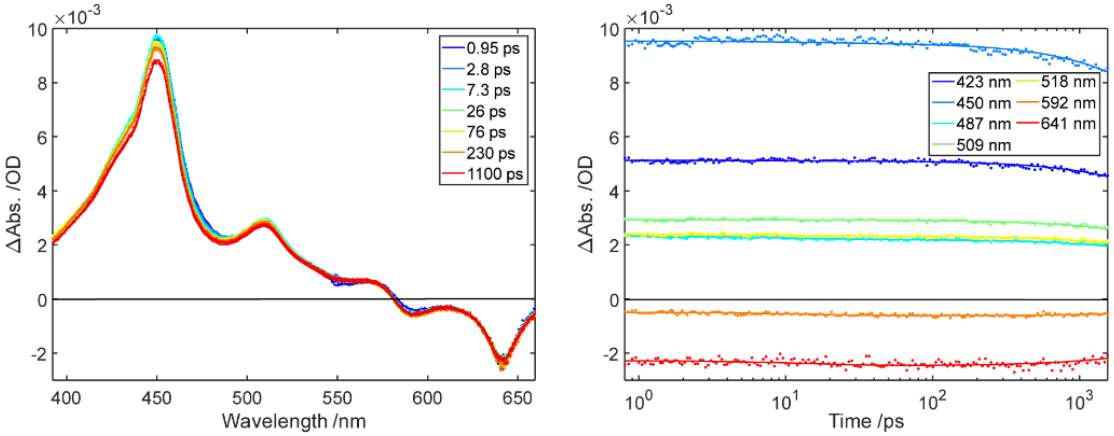

Figure 3.10.17 Femtosecond transient absorption spectra (left) and kinetics (right) of TIPS-Pc in toluene.

3.10.12 References

(1) Nijegorodov, N.; Ramachandran, V.; Winkoun, D. P. The Dependence of the Absorption and Fluorescence Parameters, the Intersystem Crossing and Internal Conversion Rate Constants on the Number of Rings in Polyacene Molecules. *Spectrochim. Acta Part A Mol. Biomol. Spectrosc.* **1997**, *53*, 1813–1824.

(2) Carmichael, I.; Hug, G. L. Triplet-Triplet Absorption Spectra of Organic Molecules in Condensed Phases. *J. Phys. Chem. Ref. Data* **1986**, *15*, 1–250.

(3) Walker, B. J.; Musser, A. J.; Beljonne, D.; Friend, R. H. Singlet Exciton Fission in Solution. *Nat. Chem.* **2013**, *5*, 1019–1024.

(4) Cook, J. D.; Carey, T. J.; Damrauer, N. H. Solution-Phase Singlet Fission in a Structurally Well-Defined Norbornyl-Bridged Tetracene Dimer. *J. Phys. Chem. A* 2016, *120* (26), 4473-4481.

Chapter 4 Supporting Information

4.6.1 Computations

The energy of the CT state of TIPS-BT1′ was determined via calculating the cation and anion energies of the monomeric species TMS-Tc-Nb (Trimethylsilylacetylene tetracene with an attached norbornyl bridge used in the dimeric TIPS-BT1′) and compared to the neutral ground-state monomer to determine cation/anion energies. The functional w97xd was used along with the basis set 6 - 31G for all calculations along with a solvent continuum model that account for benzonitrile solvation. A neutral species dimer was ground-state geometry optimization was performed to calculate the interchromophore distance as well. Results are compiled in Table 4.6.1

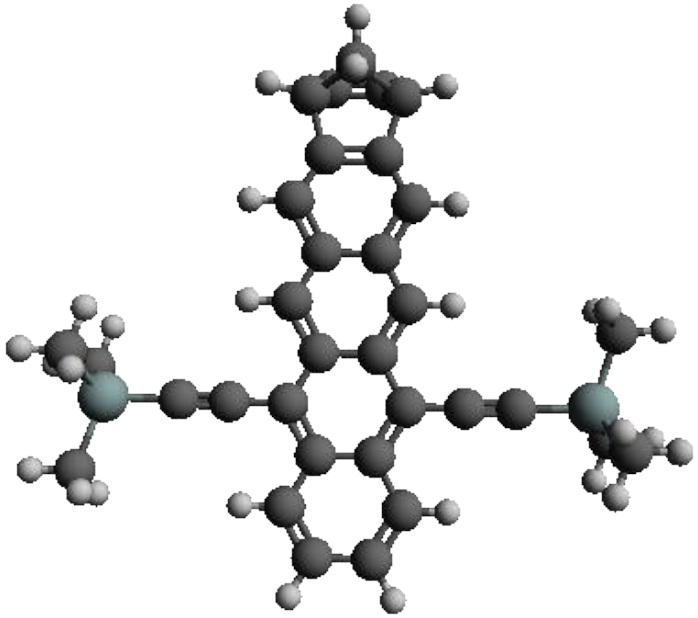

Figure 4.6.1 Structure of TMS-Tc-Nb used in computations to determine CT state energy.

Species	Relative Energy (meV)
Neutral	0
Cation	-2.825
Anion	5.052

Table 4.6.1 Compiled energies from computations for cation/anion species of TMS-Tc-Nb.

The energy of the CT state itself was calculated using the Weller formula,[1] which consists of the sum of the calculated cation/anion energies and a coulombic stabilization term.

$$E(CT) = E(Cat.) + E(An.) - k_e \frac{e^2}{\varepsilon r_c} \tag{4.6.1}$$

The sum cation/anion energies were calculated to be 2.277 eV. For the coulombic stabilization a r_c of 11.317 A was used by finding the centroid distance between the two conjugated dimer arms representing the cation/anion that compose the CT state. Using benzonitriles dielectric constant of 25.9 the stabilization factor was calculated to be 49 meV, The CT state energy was therefore calculated to be 2.178 eV. This gives ΔE_{CT} a value of 110 meV relative to S_1. Given the large energy difference the CT state is expected to act as a sink in the excited state dynamics with ~98 % of the population expected to transfer here based on the Boltzmann factor.

4.6.2 Temperature-dependent steady-state emission measurements and quantum yield

Temperature-dependent measurements were performed with the same experimental setup as previous fluorescence measurements. The fluorescence standard used was TIPS-BT1′ in benzonitrile as the quantum yield had previously been determined.

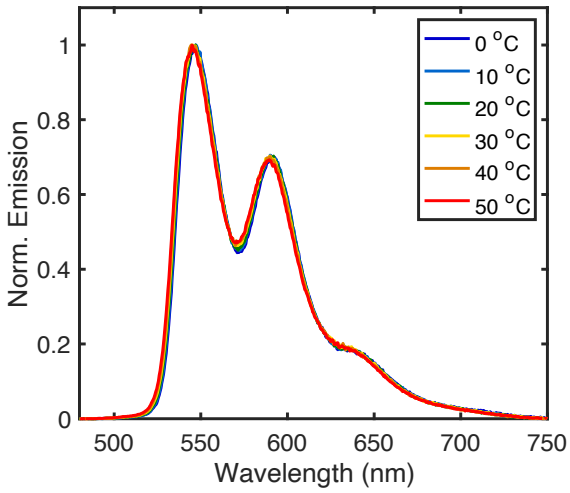

Figure 4.6.2 Normalized emission spectra of TIPS-BT1´ in benzonitrile from 0 ºC to 50 ºC.

Since TIPS-BT1´ is partitioning into localized and delocalized states upon excitation it's important to determine the relative fraction for each state. This information can be calculated from the measured quantum yield and the global analysis of the TRES data. Starting with the TRES global analysis, the spectrally and temporally integrated fraction of emission was 12 % for localized singlets and 88 % for delocalized singlets respectively.

$$Em_{tot} = Em_{loc} + Em_{deloc} = 1 \tag{4.6.2}$$

The quantum yield though is partitioned into localized and delocalized based their relative fraction.

$$\phi_{loc} + \phi_{deloc} = 40\ \% \tag{4.6.3}$$

With a measured quantum yield of 40 % for TIPS-BT1´ in benzonitrile, 4% is coming from the arm localized state and 36 % from the arm delocalized state. The relative fraction quantum yield itself is the product of the intrinsic quantum yield of localized/delocalized state and the relative population fraction for the two states.

$$\phi_{loc} = \phi_{QY,loc} * \frac{S_{1,loc}}{S_{1,tot}} = 4\% \tag{4.6.4}$$

$$\phi_{deloc} = \phi_{QY,deloc} * \frac{S_{1,deloc}}{S_{1,tot}} = 35.2\ \% \tag{4.6.5}$$

Determining the species quantum yield or relative population fraction requires knowing the other. Measuring $\phi_{QY,loc}$ or $\phi_{QY,deloc}$ directly is a challenging task, but fortunately we can turn to the monomer model of TIPS-Tc for assistance. Given the highly similar emission profiles between TIPS-Tc and $S_{1,loc}$ it can serve as a substitute. The quantum yield of TIPS-Tc in benzonitrile was previously measured to 90 %. Substituting this value into equation 4.6.4 for $\phi_{QY,loc}$ gives relative fraction of 5 % for $S_{1,\,loc}$. Therefore, the remaining 95 % fraction belongs to $S_{1,\,deloc}$, making it the vast majority of the excited state population. Additionally, $\phi_{QY,deloc}$ is calculated to be 35 %, suggesting a significant depletion pathway is available in $S_{1,\,deloc}$.

4.6.3 Time-Correlated Singlet Photon Counting Kinetic Traces

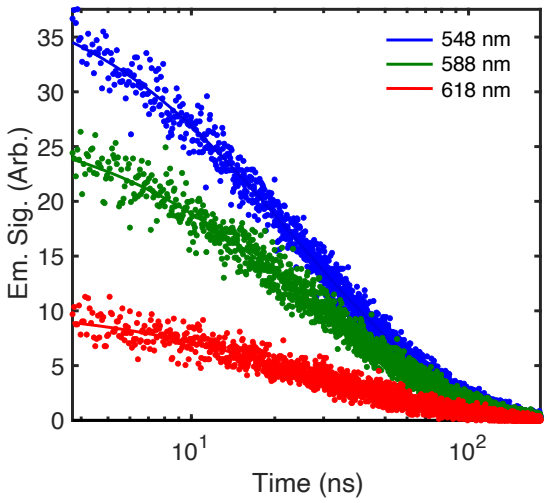

Figure 4.6.3 Time-resolved fluorescence of TIPS-BT1′ in benzonitrile. Sample was pumped at 405 nm with fluorescence collected at 548 nm, 588 nm and 618 nm. Data were fit to a two exponential decay to retrieve the time constants.

4.6.4 Triplet Sensitization of TIPS-BT1´ in benzonitrile

Triplet sensitization of TIPS-BT1´ in benzonitrile was performed with the same procedure as used in **Chapter 3** to determine the triplet delta epsilon spectrum for quantifying the SF yield. To briefly summarize, the sensitizer anthracene was added to a sample of TIPS-BT1´ in benzonitrile and excited at 360 nm. Excited anthracene molecules can undergo intersystem crossing in high yield (reported to be 70 % in toluene) and undergo a Dexter Energy Transfer to transfer the triplet from anthracene to TIPS-BT1´. This triplet energy transfer could be observed and quantified by nanosecond transient absorption after several microseconds. Both anthracene and TIPS-BT1´ absorption was kept to ~0.1 OD.

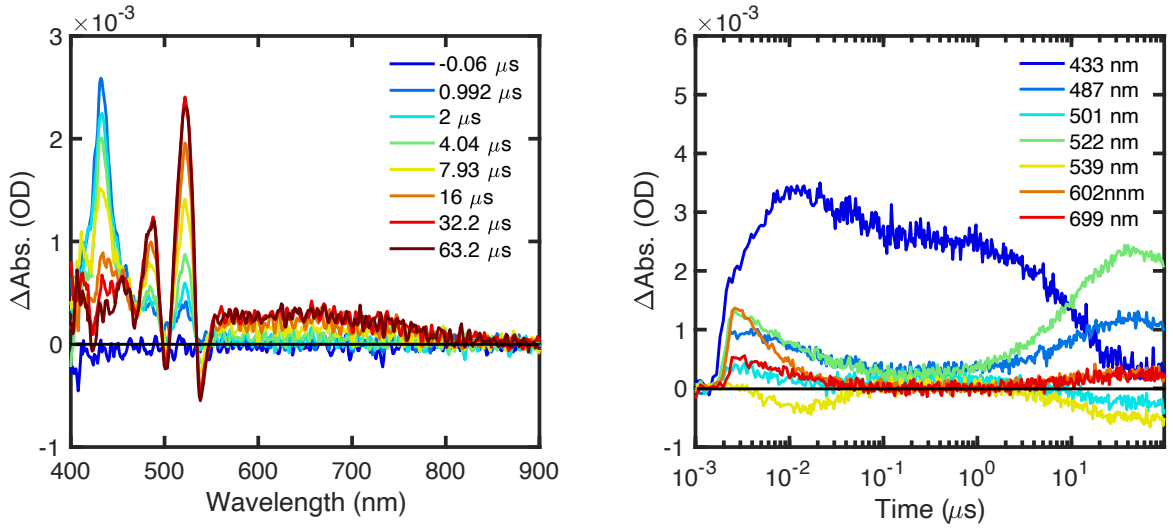

Figure 4.6.4 Nanosecond transient absorption spectra (left) and kinetics (right) for triplet sensitization of TIPS-BT1´ with anthracene in room temperature toluene.

However, while the crucial metric of intersystem crossing yield for anthracene in toluene is known, there isn't a reported literature value for benzonitrile. To determine the intersystem crossing yield in benzonitrile, requires knowing the relative yields for radiative (Φ_r) and non-radiative (Φ_{nr}) decay from the excited singlet state, as shown in equation 4.6.6.

$$\Phi_r + \Phi_{nr} + \Phi_{ISC} = 1 \quad (4.6.6)$$

Starting with Φ_r, the fluorescence quantum yield of anthracene in benzonitrile was measured against a standard of anthracene in toluene. Anthracene has a reported quantum yield of 30 %.[2] Anthracene in benzonitrile was measured to have a quantum yield of ~25 %, only slightly lower than the reference value. Energy gap law was used to determine the impact of non-radiative decay on anthracenes total decay. It's observed that the non-radiative rate constant becomes a diminishing pathway as the energy difference between two electronic states increases, due to reduced Franck-Condon overlap. In the original work by Englman and Jortner the non-radiative rate constant of anthracene is discussed and was ~1/10th of the radiative decay.[3] With that in mind we can return to the issue of Φ_{nr} for anthracene in benzonitrile. With a fluorescence quantum yield of 25 % and a non-radiative rate constant that's an order of magnitude smaller, then Φ_{nr} should be ~2.5 %. With both Φ_r and Φ_{nr} known, Φ_{ISC} for anthracene in benzonitrile can be calculated to ~72.5 %, less than a 5 % difference compared to the value for toluene.

With Φ_{ISC} determined, the last parameter needed to determine the triplet transfer yield to TIPS-BT1´ is the triplet lifetime itself. Anthracene in benzonitrile was excited at 355 nm and monitored at 430 nm where anthracene is known to have a triplet ESA. The triplet decay was fit to a mono-exponential decay of 330 μs. The excited state delta epsilons for both dimer species were calculated using pump fluence, photon energy (E_{photon} = 5.52×10^{-19} J; corresponding to 360 nm) and sample anthracene absorption at 360 nm to calculate an anthracene excited state population. The concentration of sensitized dimer was then calculated using the population from the expression above along with the pump spot size (d = 247 μm) and cuvette length (L = 0.2 cm) to calculate the excitation volume.

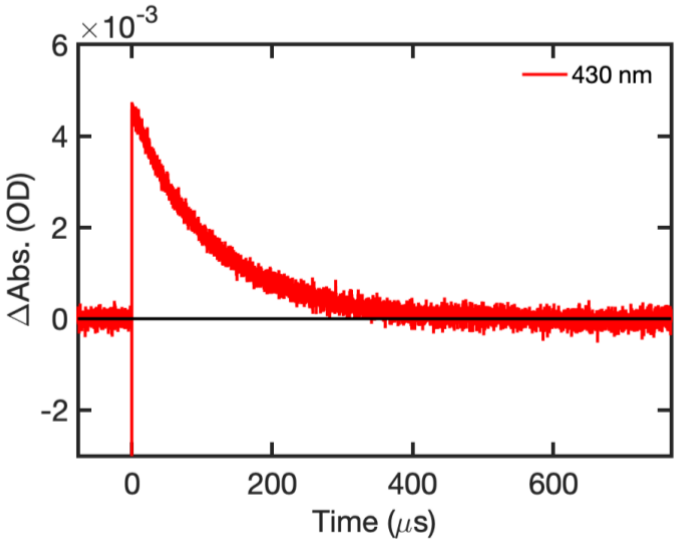

Figure 4.6.5 Nanosecond transient absorption kinetics trace at 430 nm for TIPS-BT1′ in benzonitrile.

These calculations were performed to produce the delta epsilon T_1 spectra for TIPS-BT1′ in benzonitrile.

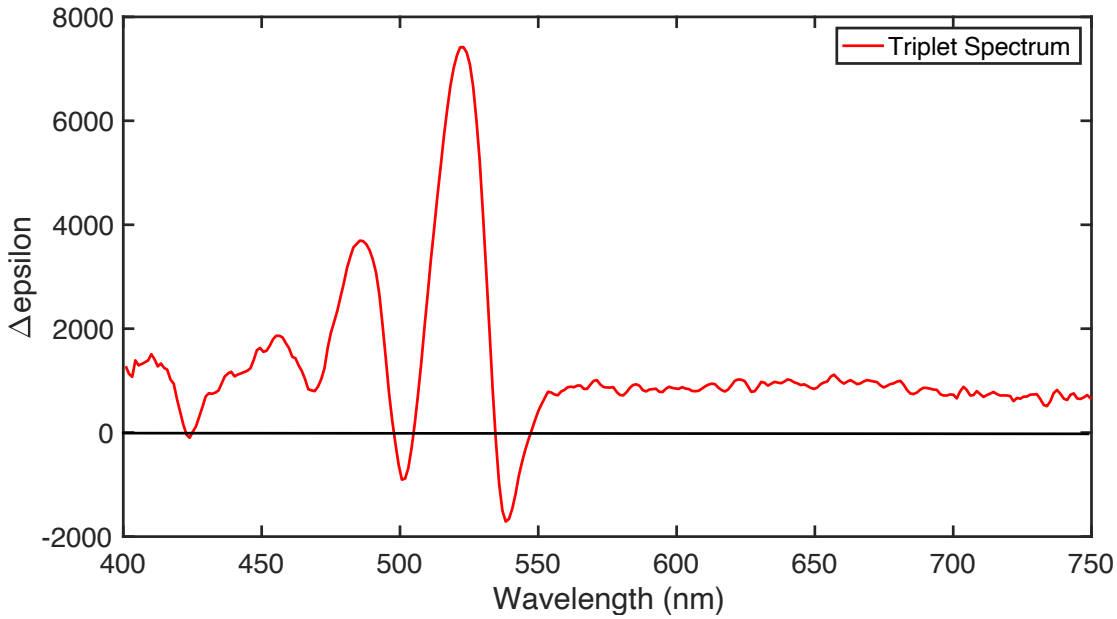

Figure 4.6.6 Sensitized triplet spectrum of TIPS-BT1′ in benzonitrile retrieved from global analysis.

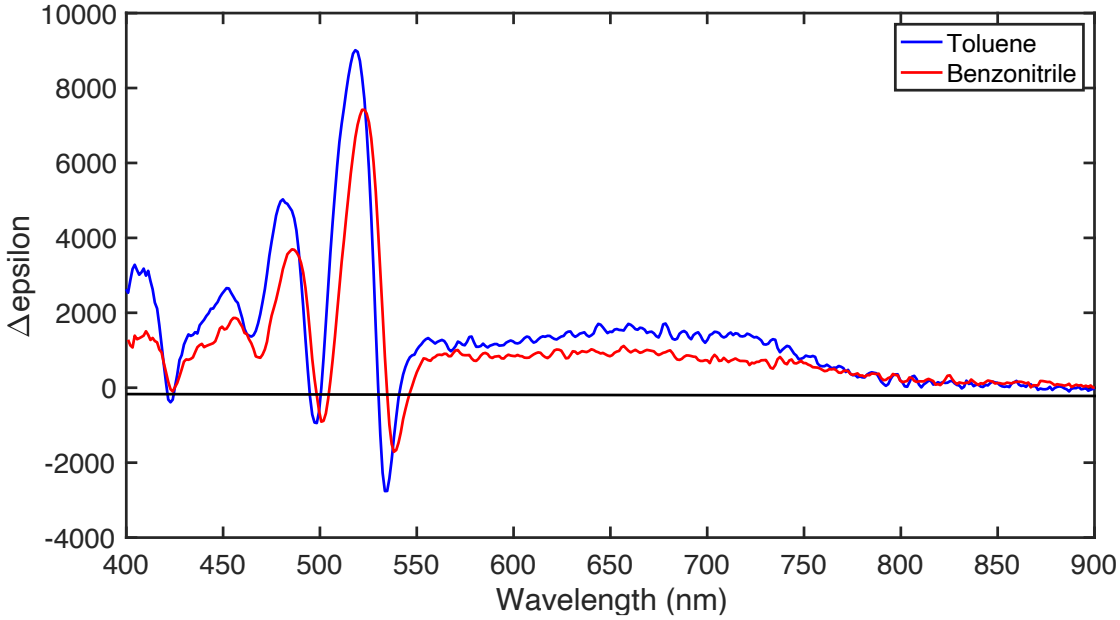

Figure 4.6.7 Comparison of sensitized triplet spectra from triplet sensitization for TIPS-BT1′ in toluene and benzonitrile.

4.6.5 Singlet Fission Yield

The same methodology previous used in **Chapter 3** was applied again to find the excited singlet/triplet concentrations based on experimental parameters and therefore the triplet yield.

$$SF\ Yield = \frac{[T_1]}{[S_1]} = 0.50 \tag{4.6.7}$$

A triplet yield of 0.50 (or 50 %) corresponds to a ^{1}TT yield of 25 %, suggesting ~75 % of S_1 still remains present. The SF equilibrium is therefore 0.33 and can be used to find the energy difference between the S_1 and ^{1}TT states using the Boltzmann factor.

$$-ln\left(K_{S_1/^1TT}\right) \times kT = \Delta E_{S_1/^1TT} \tag{4.6.8}$$

With kT = 25.85 meV at room temperature ΔE_{SF} was calculated to be 29 meV. Using 2.29 eV from stead-state measurments ^{1}TT is therefore 2.32 eV. This SF yield will be discussed in further context in section 4.6.7 since there are three observed states.

4.6.6 Temperature-dependent fsTA Results and Global Analysis

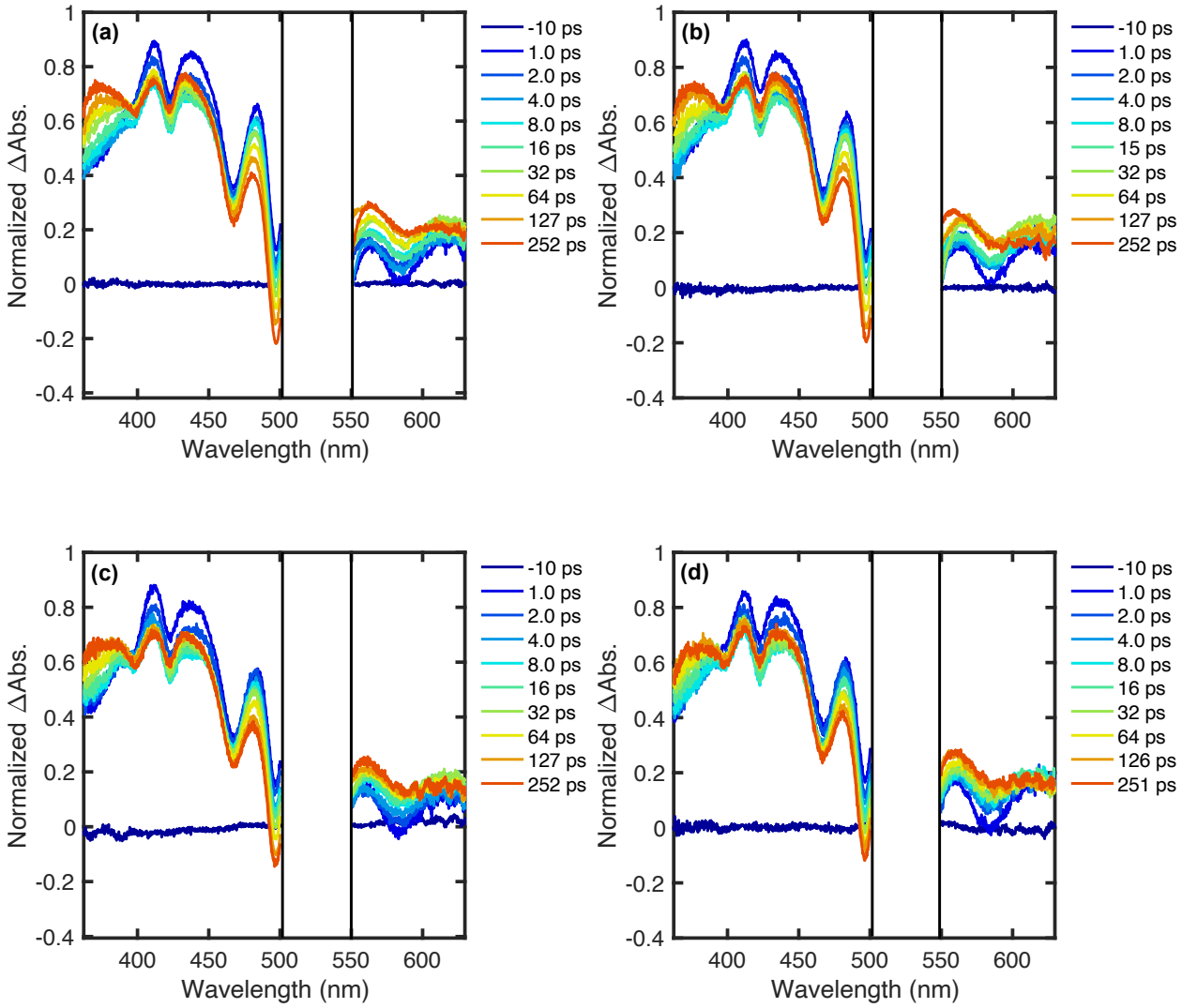

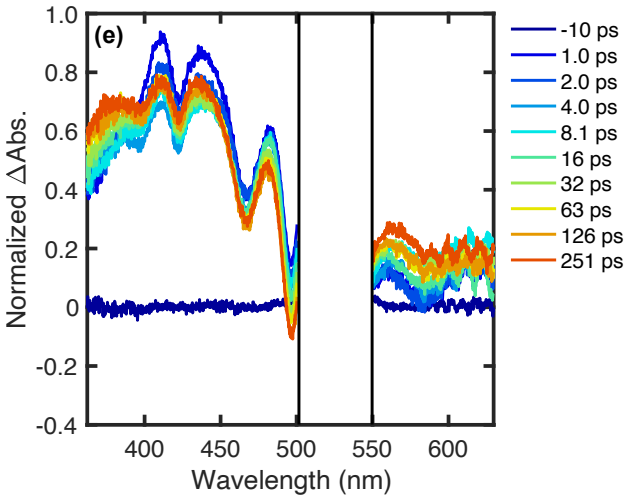

Figures 4.6.8 a – e. Temperature dependent femtosecond transient absorption spectral slices of TIPS-BT1´ in benzonitrile at (a) 10 ºC, (b) 20 ºC, (c) 30 ºC, (d) 40 ºC, and (e) 50 ºC.

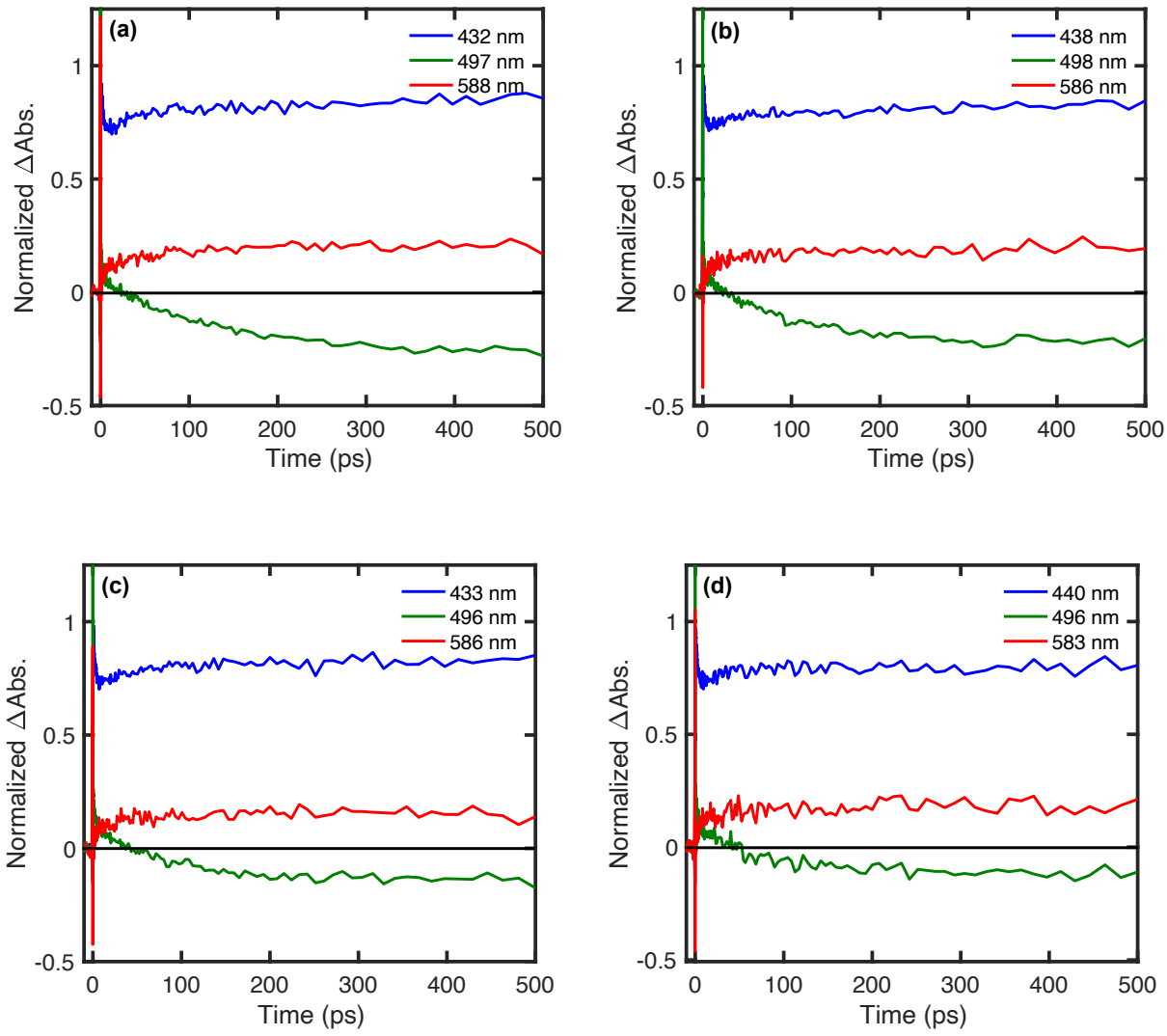
(a)
432 nm
497 nm
588 nm
Normalized ΔAbs.
Time (ps)
(b)
438 nm
498 nm
586 nm
Normalized ΔAbs.
Time (ps)
(c)
433 nm
496 nm
586 nm
Normalized ΔAbs.
Time (ps)
(d)
440 nm
496 nm
583 nm
Normalized ΔAbs.
Time (ps)

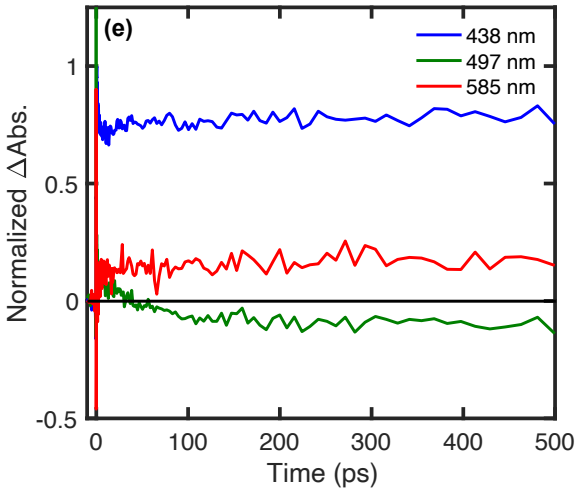

Figures 4.6.9 a – e. Temperature dependent femtosecond transient absorption kinetic traces of TIPS-BT1´ in benzonitrile at (a) 10 ºC, (b) 20 ºC, (c) 30 ºC, (d) 40 ºC, and (e) 50 ºC.

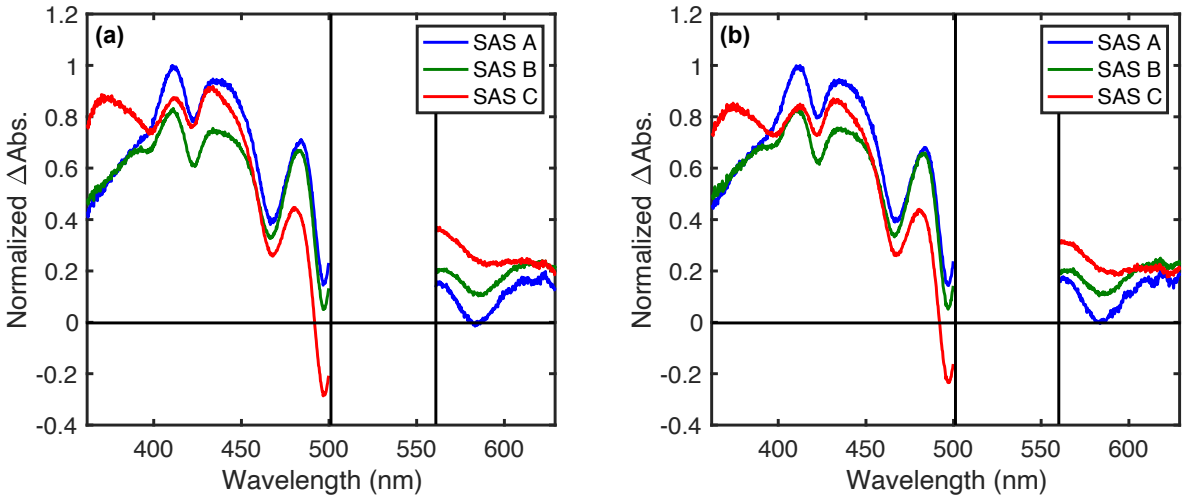

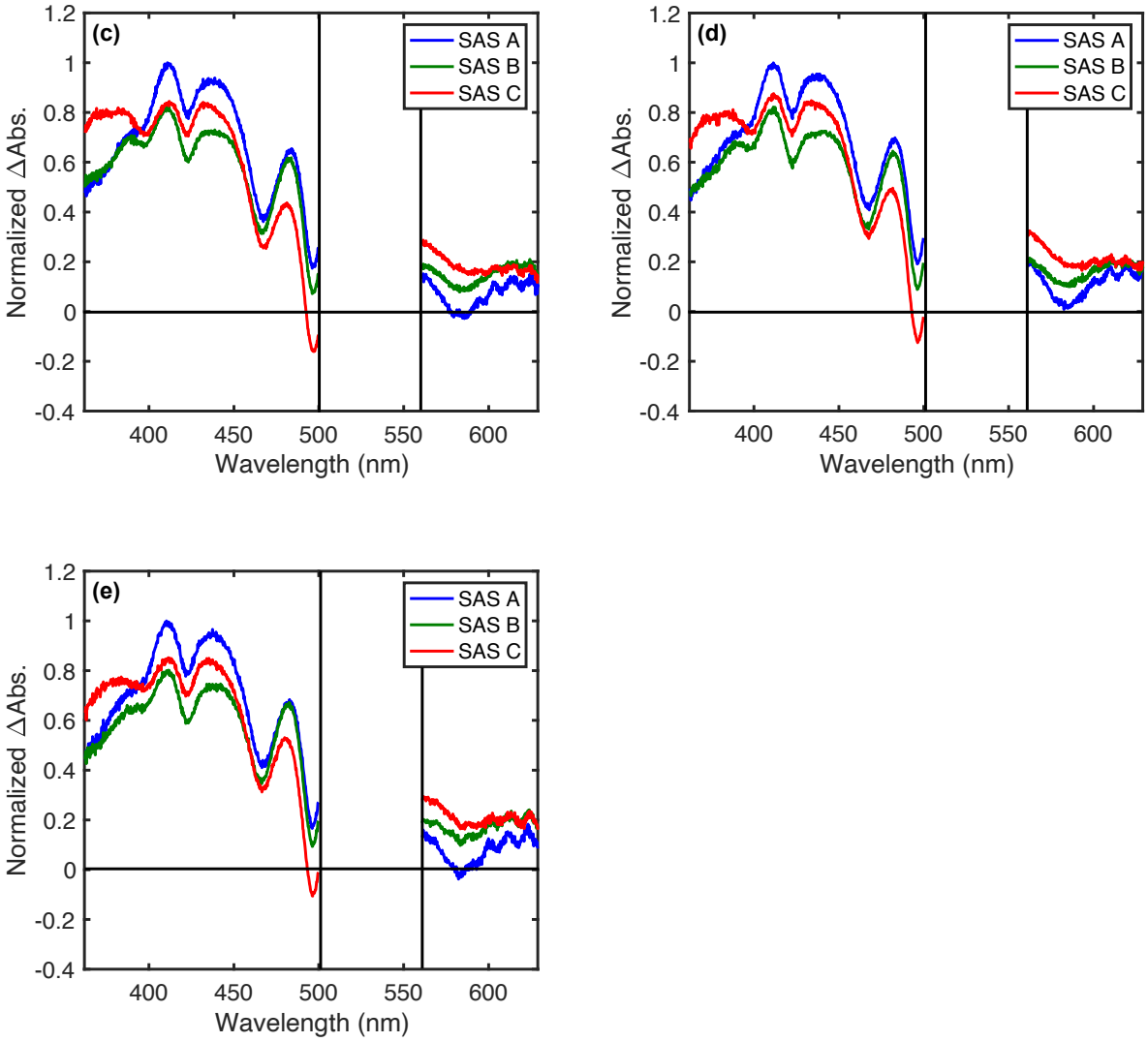

Figures 4.6.10 a – e. Retrieved species associated spectra of TIPS-BT1′ in benzonitrile at (a) 10 ºC, (b) 20 ºC, (c) 30 ºC, (d) 40 ºC, and (e) 50 ºC.

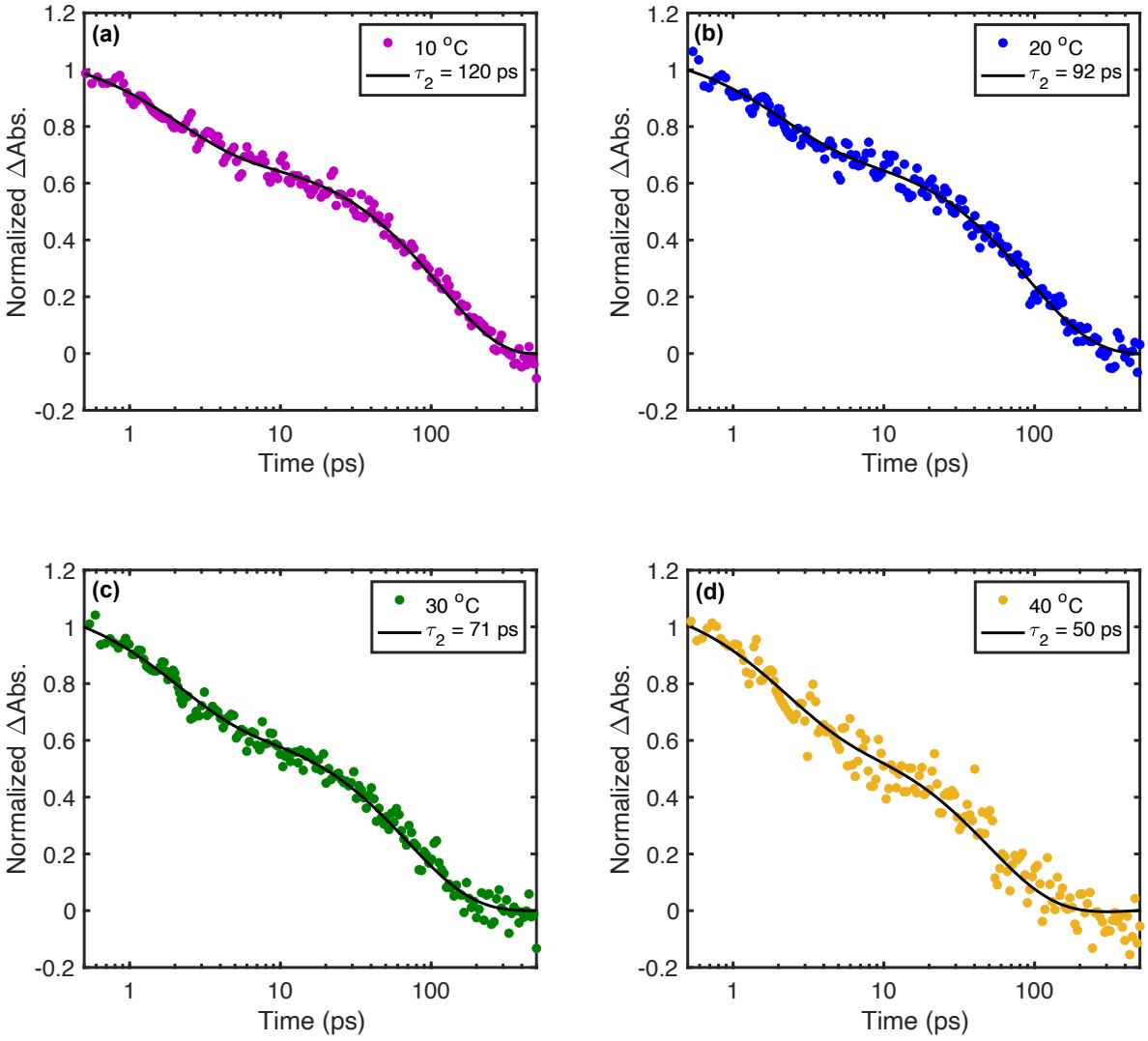
(a)
10 °C
τ2 = 120 ps
(b)
20 °C
τ2 = 92 ps
(c)
30 °C
τ2 = 71 ps
(d)
40 °C
τ2 = 50 ps
Normalized ΔAbs.
Time (ps)
1.2
1
0.8
0.6
0.4
0.2
0
-0.2
1
10
100

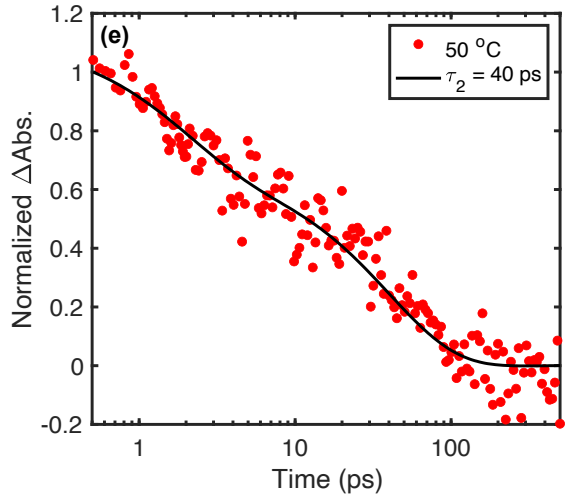

Figures 4.6.11 a – e. Temperature dependent femtosecond transient absorption kinetic traces of TIPS-BT1´ in benzonitrile at 497 nm with an applied two exponential and shelf fit with retrieved time-constants from global analysis at(a) 10 ºC, (b) 20 ºC, (c) 30 ºC, (d) 40 ºC, and (e) 50 ºC.

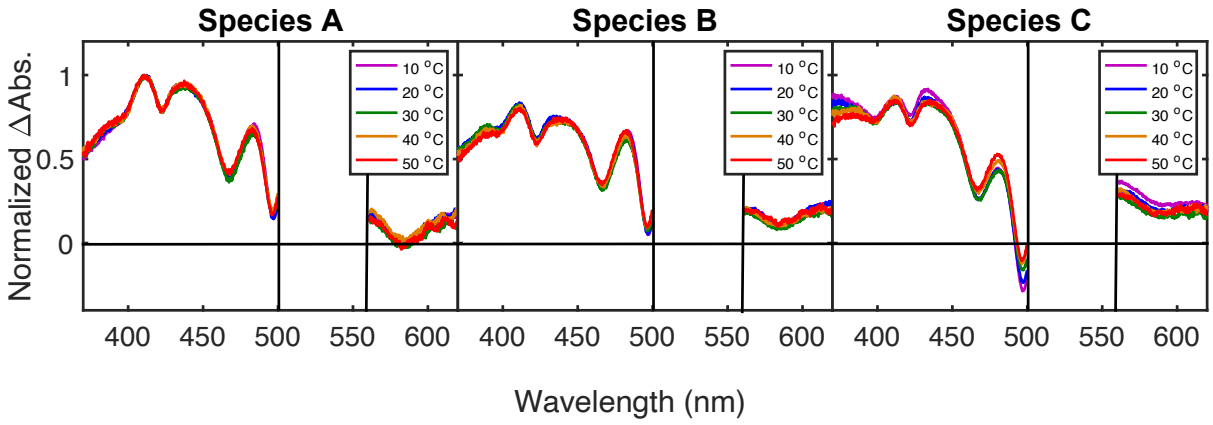

Figures 4.6.12 Comparison of retrieved species associated spectra of TIPS-BT1´ in benzonitrile as a function of temperature.

Temperature (°C)	A → B Time Constant (ps)	B → C Time Constant (ps)
10	2.0	120
20	1.9	92
30	2.0	71
40	2.0	50
50	1.9	40

Table 4.6.2 Retrieved time constants from global analysis of temperature-dependent femtosecond transient absorption of TIPS-BT1´ in benzonitrile.

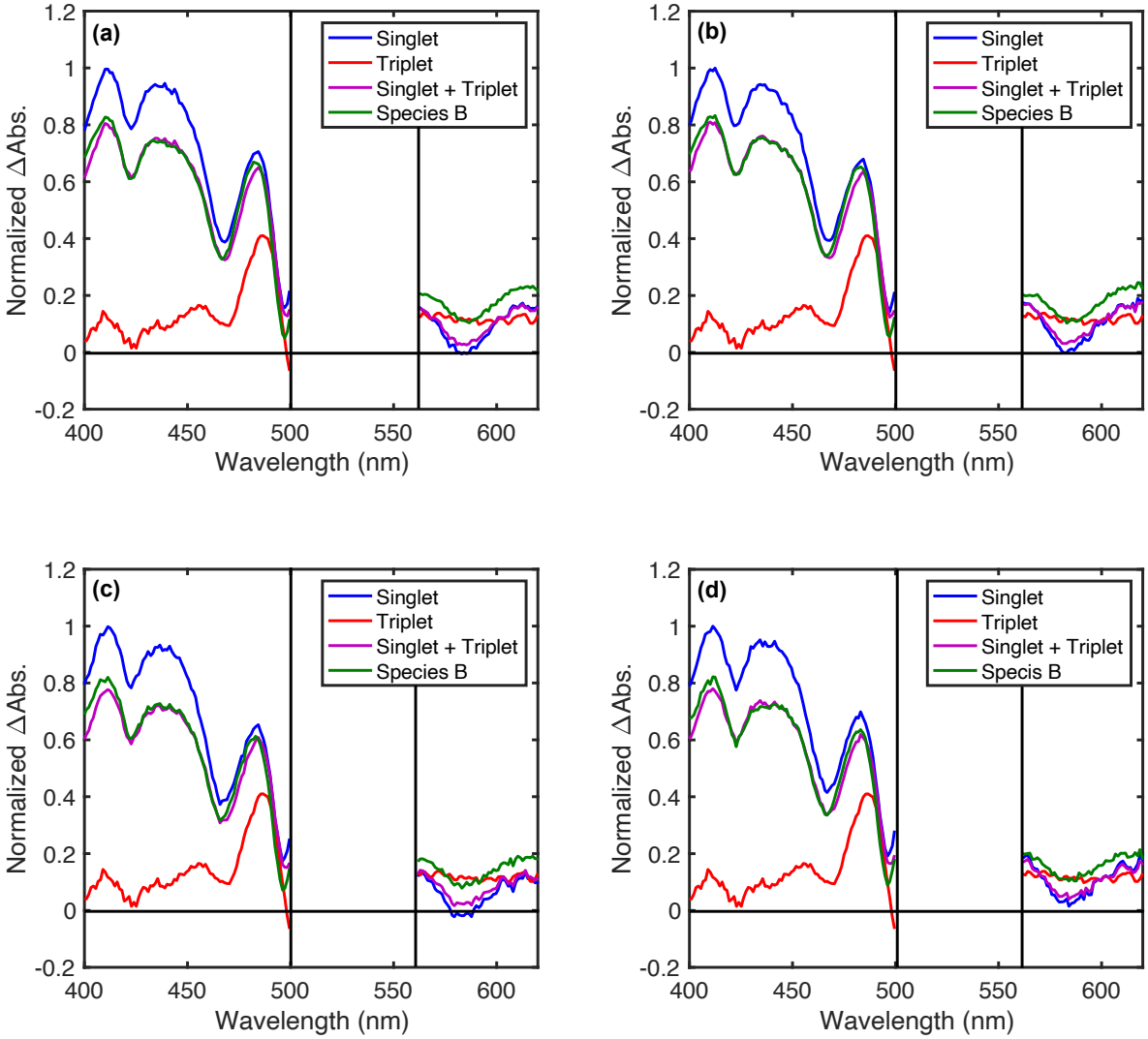

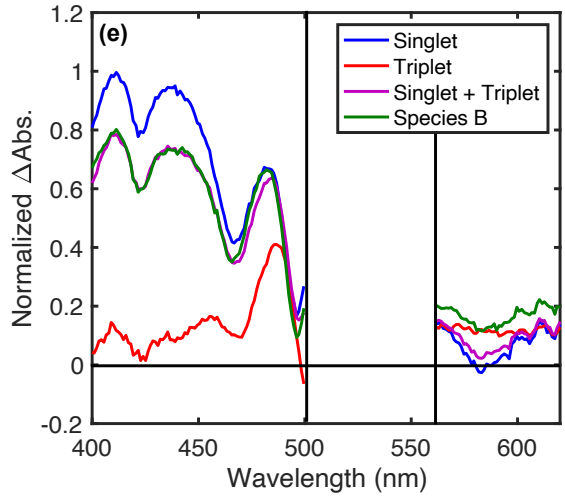

Figures 4.6.13 a – e. Spectral reconstructions of species B from the retrieved singlet and sensitized triplet spectra of TIPS-BT1´ in benzonitrile at (a) 10 ºC, (b) 20 ºC, (c) 30 ºC, (d) 40 ºC, and (e) 50 ºC.

4.6.7 Kinetic Modeling – Parallel Model

A kinetic model was developed to help inform the results observed in femtosecond transient absorption of TIPS-BT1´ in benzonitrile and calculate the coveted rate constants for ^{1}TT and CT formation from the time constants retrieved from global analysis. Given the rapid formation of triplet features, similar to what was observed in toluene in **Chapter 3** and the later onset of spectral features that define the CT state, a parallel model was chosen to describe the chemical dynamics of the system. Wherein population from the initially excited S_1 can begin transferring to both ^{1}TT and the CT state, as shown in Fig. 4.6.14. Rate constants k_{fis}/k_{fus} (represent singlet fission and triplet fusion) couple S_1 to the ^{1}TT while the S_1 and CT state are coupled by k_{ct}/k_{bct} (the charge transfer and back-charge transfer rate constants).

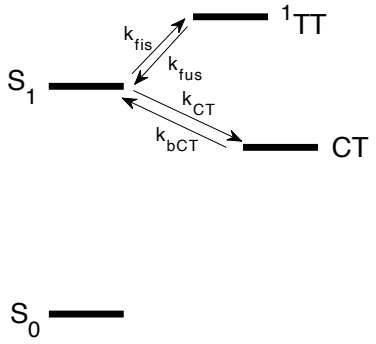

Figure 4.6.14 Parallel three state kinetic model for S_1, ^{1}TT and CT state formation.

The following set of coupled differential equations were used to represent the kinetic scheme presented in Fig. 4.6.14. While similar to the kinetic model used in **Chapter 3** the addition of a third state will significantly increase the complexity of solving and fitting to an analytical expression for state populations.

$$\frac{d[S_1]}{dt} = -k_{fis}[S_1] - k_{CT}[S_1] + k_{fus}[^1TT] + k_{bCT}[CT] \tag{4.6.9}$$

$$\frac{d[^1TT]}{dt} = k_{fis}[S_1] - k_{fus}[^1TT] \tag{4.6.10}$$

$$\frac{d[CT]}{dt} = k_{CT}[S_1] - k_{bCT}[CT] \tag{4.6.11}$$

The differential equations can be rewritten in matrix form as:

$$\frac{dP(t)}{dt} = \boldsymbol{K}P(t) \tag{4.6.12}$$

Where *P(t)* represents the populations for S_1, ^{1}TT and CT states and $\boldsymbol{K}$ is the rate matrix that contains the rate constants for the transitions between the associated states. The full master equation for the kinetic scheme in Fig. 4.6.14 is:

$$\frac{d}{dt}\begin{pmatrix}[S_1]\\ [^1TT]\\ [CT]\end{pmatrix}=\begin{pmatrix}-(k_{fis}+k_{CT}) & k_{fus} & k_{bCT}\\ k_{fis} & -k_{fus} & 0\\ k_{CT} & 0 & k_{bCT}\end{pmatrix}\begin{pmatrix}[S_1]\\ [^1TT]\\ [CT]\end{pmatrix} \tag{4.6.13}$$

The general solution for this system of n-equations is a sum of n-exponentials corresponding to the size of matrix ***K*** (in this case 3).

$$P(t)=c_1V_1e^{\lambda_1 t}+c_2V_2e^{\lambda_2 t}+c_3V_3e^{\lambda_3 t} \tag{4.6.14}$$

The state populations can thus be determined as the following:

$$S_1(t)=c_1V_{11}e^{\lambda_1 t}+c_2V_{12}e^{\lambda_2 t}+c_3V_{13}e^{\lambda_3 t} \tag{4.6.15}$$

$$^1TT(t)=c_1V_{21}e^{\lambda_1 t}+c_2V_{22}e^{\lambda_2 t}+c_3V_{23}e^{\lambda_3 t} \tag{4.6.16}$$

$$CT(t)=c_1V_{31}e^{\lambda_1 t}+c_2V_{32}e^{\lambda_2 t}+c_3V_{33}e^{\lambda_3 t} \tag{4.6.17}$$

The rate matrix ***K*** was diagonalized to find the associated eigenvalues and eigenvectors for the above system. As a size n = 3 matrix, two non-zero eigenvalues are expected to be returned, representing the major dynamics of the system while the $\lambda_1 = 0$ represents the populations of S_1, ^{1}TT and CT once steady-state has been achieved since no decay pathways were adopted in the model.

$$det\begin{pmatrix}-(k_{fis}+k_{CT})-\lambda & k_{fus} & k_{bCT}\\ k_{fis} & -k_{fus}-\lambda & 0\\ k_{CT} & 0 & k_{bCT}-\lambda\end{pmatrix}=0 \tag{4.6.18}$$

The following expressions were returned for eigenvalues λ_1, λ_2 and λ_3.

$$\lambda_1 = 0 \tag{4.6.19}$$

$$\lambda_2=\frac{1}{2}(-\text{kbct}-\text{kct}-\text{kfis}-\text{kfus}-\sqrt{(\text{kbct}+\text{kct}+\text{kfis}+\text{kfus})^2-4(\text{kbctkfis}+\text{kbctkfus}+\text{kctkfus})}) \tag{4.6.20}$$

$$\lambda_3=\frac{1}{2}(-\text{kbct}-\text{kct}-\text{kfis}-\text{kfus}+\sqrt{(\text{kbct}+\text{kct}+\text{kfis}+\text{kfus})^2-4(\text{kbctkfis}+\text{kbctkfus}+\text{kctkfus})}) \tag{4.6.21}$$

Along with corresponding eigenvectors v_1, v_2 and v_3.

$$v_1 = \begin{Bmatrix} \frac{\text{kbct}}{\text{kct}}, \\ \frac{\text{kbctkfis}}{\text{kctkfus}}, \\ 1 \end{Bmatrix} \tag{4.6.22}$$

$$v_2 = \begin{Bmatrix} -\frac{1}{2\text{kct}}\left(-\text{kbct} + \text{kct} + \text{kfis} + \text{kfus} + \sqrt{\text{kbct}^2 + 2\text{kbctkct} + \text{kct}^2 - 2\text{kbctkfis} + 2\text{kctkfis} + \text{kfis}^2 - 2\text{kbctkfus} - 2\text{kctkfus} + 2\text{kfiskfus} + \text{kfus}^2}\right) \\ -\frac{1}{2\text{kct}}\left(\text{kbct} + \text{kct} - \text{kfis} - \text{kfus} - \sqrt{\text{kbct}^2 + 2\text{kbctkct} + \text{kct}^2 - 2\text{kbctkfis} + 2\text{kctkfis} + \text{kfis}^2 - 2\text{kbctkfus} - 2\text{kctkfus} + 2\text{kfiskfus} + \text{kfus}^2}\right) \\ 1 \end{Bmatrix} \tag{4.6.23}$$

$$v_3 = \begin{Bmatrix} -\frac{1}{2\text{kct}}\left(-\text{kbct} + \text{kct} + \text{kfis} + \text{kfus} - \sqrt{\text{kbct}^2 + 2\text{kbctkct} + \text{kct}^2 - 2\text{kbctkfis} + 2\text{kctkfis} + \text{kfis}^2 - 2\text{kbctkfus} - 2\text{kctkfus} + 2\text{kfiskfus} + \text{kfus}^2}\right) \\ -\frac{1}{2\text{kct}}\left(\text{kbct} + \text{kct} - \text{kfis} - \text{kfus} + \sqrt{\text{kbct}^2 + 2\text{kbctkct} + \text{kct}^2 - 2\text{kbctkfis} + 2\text{kctkfis} + \text{kfis}^2 - 2\text{kbctkfus} - 2\text{kctkfus} + 2\text{kfiskfus} + \text{kfus}^2}\right) \\ 1 \end{Bmatrix} \tag{4.6.24}$$

Expressions for eigenvalues λ_{1-3} and v_{1-3} were plugged into the equations for S_1, ^1TT and CT populations. The system of equations was solved in Mathematica with the initial condition that $S_1(0) = 1$ and $^1TT(0) = CT(0) = 0$. The non-zero eigenvalues are the retrieved lifetimes from global analysis ($\lambda_2 = -\frac{1}{\tau_1}$) and ($\lambda_3 = -\frac{1}{\tau_2}$). The additional condition of c_1V_1 being the steady-state populations of S_1, ^1TT and CT was calculated and applied based on the canonical partition function, as shown below. $\beta = \frac{1}{k_B T}$ and E_i is the energy of the respective state. All calculations were done at 298.15 K.

$$Z = \sum_i e^{-\beta E_i} \tag{4.6.25}$$

The S_1 relative population was calculated based on the DFT results which showed the S_1 to be 110 meV above the CT state. Finally, based on the ^{1}TT yield and the equilibrium constant K_{SF} calculated, the $^1TT/S_1$ energy difference was determined to be 2.32 eV. The CT state being lowest in energy was set as the zero point on the energy scale. State populations were normalized such that Z = 1. Relative state populations along with measured lifetimes were used to solve the system of equations 4.6.15-17. Table 4.6.3 lists the values for the rate constants retrieved from the kinetic model.

Retrieved rate constants	Rate Constant (s^{-1})
k_{fis}	1.2×10^{11}
k_{fus}	3.8×10^{11}
k_{CT}	1.4×10^{10}
k_{bCT}	1.9×10^{8}

Table 4.6.3: Retrieved rate constants from three state parallel model from global analysis time constants.

Plugging these values for the rates constants back into equations 4.6.9-11 generates the time evolution profiles for S_1, ^{1}TT and CT, shown in Fig. 4.6.10.

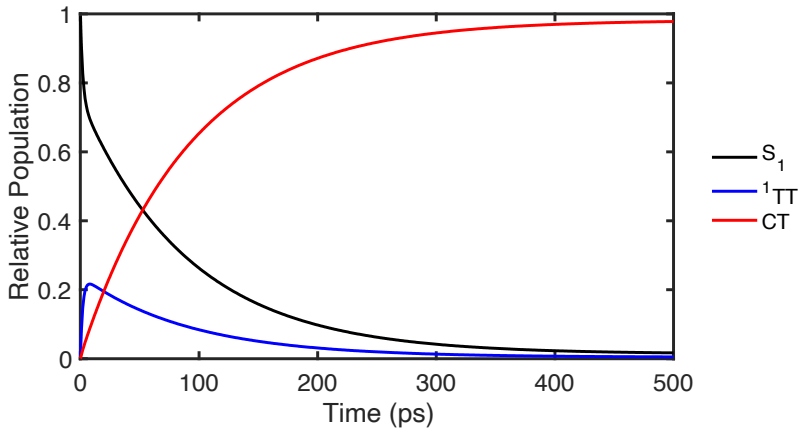

Figure 4.6.15 Time evolution populations for S_1, ^{1}TT and CT state from parallel three state model.

In the model all initial population starts in the S_1, but quickly begins decaying. After this initial decay a second decay of the S_1 is observed until the population reaches a steady-state value of less than 5 %. For the ^{1}TT a rise in population occurs, corresponding the initial decay observed for the S_1, up to a maximum value of ~20 %. This ^{1}TT population the begins decaying to a negligible steady-state value. For the CT state it is observed slowly being populated as well up to its steady-state value of ~95 %. The population profiles match well with the observations in the fsTA data and analysis. For the temperature-dependent fsTA analysis all modeling parameters were the same except τ_2, which was substituted with the observed lifetime at each temperature point (B $\rightarrow$ C Time Constant in Table 4.6.2). Results for k_{CT} from kinetic modeling are compiled in Table 4.6.4.

Temperature (°C)	k_{CT} (s^{-1})
10	1.1×10^{10}
20	1.4×10^{10}
30	1.8×10^{10}
40	2.6×10^{10}
50	3.3×10^{10}

Table 4.6.4: Temperature dependent rate constants for k_{CT} retrieved from kinetic modeling

4.6.8 Kinetic Modeling – Sequential Model

An alternative kinetic model was considered to explain the fsTA results in the main text compared to the parallel model in the previous section. This model used sequential steps for CT and ^{1}TT formation and is shown in Fig. 4.6.16.

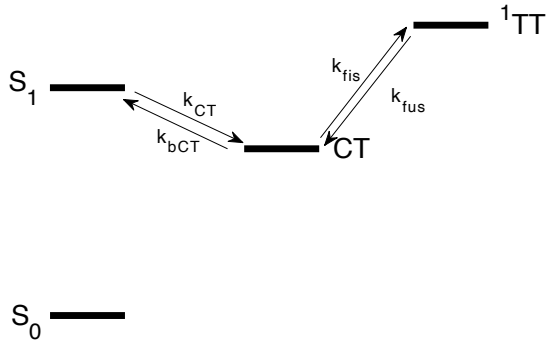

Figure 4.6.16 Sequential three state kinetic model for S_1, ^{1}TT and CT state formation.

The following set of coupled differential equations were used to describe the dynamics of this sequential step model. The same modeling and fitting procedure from section 4.6.7 was used with the sequential model to retrieve the relevant rate constants.

$$\frac{d[S_1]}{dt} = -k_{CT}[S_1] + k_{bCT}[CT] \tag{4.6.26}$$

$$\frac{d[^1TT]}{dt} = k_{fis}[CT] - k_{fus}[^1TT] \tag{4.6.27}$$

$$\frac{d[CT]}{dt} = k_{CT}[S_1] + k_{fus}[^1TT] - k_{bCT}[CT] - k_{fis}[CT] \tag{4.6.28}$$

The rate matrix ***K*** was diagonalized to find the associated eigenvalues and eigenvectors for the above system.

$$det\begin{pmatrix} -k_{CT} - \lambda & 0 & k_{bCT} \\ 0 & -k_{fus} - \lambda & k_{fis} \\ k_{CT} & k_{fus} & -(k_{fis} + k_{bCT}) - \lambda \end{pmatrix} = 0 \tag{4.6.29}$$

The following expressions were returned for eigenvalues λ_1, λ_2 and λ_3.

$$\lambda_1 = 0 \tag{4.6.30}$$

$$\lambda_2 = \frac{1}{2}(-\text{kbct} - \text{kct} - \text{kfis} - \text{kfus} - \sqrt{(\text{kbct} + \text{kct} + \text{kfis} + \text{kfus})^2 - 4(\text{kctkfis} + \text{kbctkfus} + \text{kctkfus})}) \tag{4.6.31}$$

$$\lambda_3 = \frac{1}{2}(-\text{kbct} - \text{kct} - \text{kfis} - \text{kfus} + \sqrt{(\text{kbct} + \text{kct} + \text{kfis} + \text{kfus})^2 - 4(\text{kbctkfis} + \text{kbctkfus} + \text{kctkfus})})$$

Along with corresponding eigenvectors v_1, v_2 and v_3.

$$v_1 = \begin{Bmatrix} \frac{\text{kbct}}{\text{kct}}, \\ \frac{\text{kfis}}{\text{kfus}}, \\ 1 \end{Bmatrix} \tag{4.6.32}$$

$$v_2 \tag{4.6.33}$$

$$= \begin{Bmatrix} -\left(\frac{\left(\sqrt{\text{kbct}^2 + 2\text{kbctkct} + \text{kct}^2 + 2\text{kbctkfis} - 2\text{kctkfis} + \text{kfis}^2 - 2\text{kbctkfus} - 2\text{kctkfus} + 2\text{kfiskfus} + \text{kfus}^2}\right)}{\text{kbct} + \text{kct} + \text{kfis} - \text{kfus} + \sqrt{\text{kbct}^2 + 2\text{kbctkct} + \text{kct}^2 + 2\text{kbctkfis} - 2\text{kctkfis} + \text{kfis}^2 - 2\text{kbctkfus} - 2\text{kctkfus} + 2\text{kfiskfus} + \text{kfus}^2}}\right), \\ -\left(\frac{2\text{kfis}}{\text{kbct} + \text{kct} + \text{kfis} - \text{kfus} + \sqrt{\text{kbct}^2 + 2\text{kbctkct} + \text{kct}^2 + 2\text{kbctkfis} - 2\text{kctkfis} + \text{kfis}^2 - 2\text{kbctkfus} - 2\text{kctkfus} + 2\text{kfiskfus} + \text{kfus}^2}}\right), \\ 1 \end{Bmatrix}$$

$$v_3 \tag{4.6.34}$$

$$= \left\{ \begin{array}{c} -\left(\frac{\left(\sqrt{\mathrm{kbct}^2 + 2\mathrm{kbctkct} + \mathrm{kct}^2 + 2\mathrm{kbctkfis} - 2\mathrm{kctkfis} + \mathrm{kfis}^2 - 2\mathrm{kbctkfus} - 2\mathrm{kctkfus} + 2\mathrm{kfiskfus} + \mathrm{kfus}^2} \right)}{\mathrm{kbct} + \mathrm{kct} + \mathrm{kfis} - \mathrm{kfus} - \sqrt{\mathrm{kbct}^2 + 2\mathrm{kbctkct} + \mathrm{kct}^2 + 2\mathrm{kbctkfis} - 2\mathrm{kctkfis} + \mathrm{kfis}^2 - 2\mathrm{kbctkfus} - 2\mathrm{kctkfus} + 2\mathrm{kfiskfus} + \mathrm{kfus}^2}} \right), \\ -\left(\frac{2\mathrm{kfis}}{\mathrm{kbct} + \mathrm{kct} + \mathrm{kfis} - \mathrm{kfus} - \sqrt{\mathrm{kbct}^2 + 2\mathrm{kbctkct} + \mathrm{kct}^2 + 2\mathrm{kbctkfis} - 2\mathrm{kctkfis} + \mathrm{kfis}^2 - 2\mathrm{kbctkfus} - 2\mathrm{kctkfus} + 2\mathrm{kfiskfus} + \mathrm{kfus}^2}} \right), \\ 1 \end{array} \right\}$$

The system of equations was solved in Mathematica with the initial condition that $S_1(0) = 1$ and $^1TT(0) = CT(0) = 0$. The additional condition of c_1V_1 being the steady-state populations of S_1, ^1TT and CT was calculated and applied based on the canonical partition function with the same energetic splitting between the three states, the same as in section 4.6.7. Table 4.6.5 lists the values for the rate constants retrieved from the model.

Retrieved rate constants	Rate Constant (s^{-1})
k_{fis}	2.1×10^{9}
k_{fus}	5.0×10^{11}
k_{CT}	1.1×10^{10}
k_{bCT}	1.5×10^{8}

Table 4.6.5: Retrieved rate constants from sequential three state model and global analysis time constants.

Plugging these values for the rates constants back into equations 4.6.26-28 generates the time evolution profiles for S_1, ^1TT and CT, shown in Fig. 4.6.17.

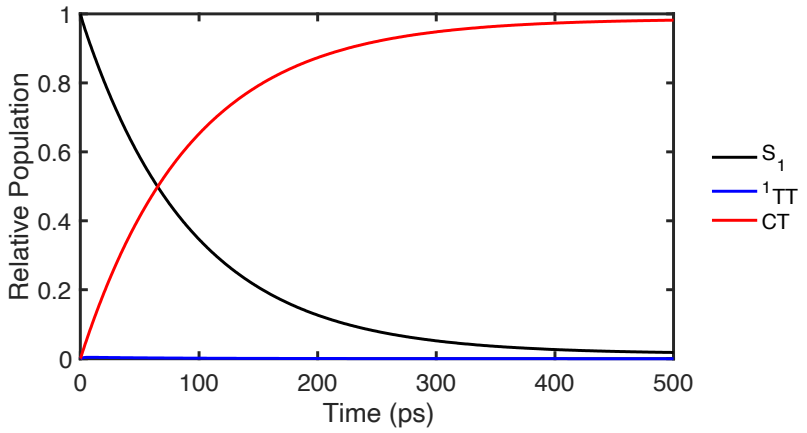

Figure 4.6.17 Time evolution populations for S_1, ^1TT and CT state from sequential three state model.

Similar to the population profiles in Fig. 4.6.15, all population starts in the S_1. However, no significant initial decay is observed in the S_1. Instead, a single decay dominates the S_1 profile corresponding to the rise in CT, up to their steady-state levels. An insignificant fraction of ^1TT is formed (less than 5 %), before decaying. This significantly deviates from the fsTA data and can therefore be ruled out as the kinetics model for describing TIPS-BT1´ in benzonitrile.

4.6.9 Marcus Analysis

We return to the classical Marcus expression first used in **Chapter 3**.

$$k_{ET} = \sqrt{\frac{4\pi^3}{h^2 \lambda kT}} {V_{eff}}^2 e^{\frac{-(\Delta G+\lambda)^2}{4\lambda kT}} \tag{4.6.35}$$

The reorganization energy λ consists of two separate components, the inner-sphere reorganization energy λ_i and the outer-sphere reorganization contribution λ_o. Inner-sphere contribution is expected to be negligible considering the rigid nature of TIPS-BT1 & TIPS-BT1´ prevents dihedral angle changes between the chromophores and the acene bond length changes are minimal in the excited state relative to the ground state. The outer-sphere reorganization

energy is expected to be the more significant component to explain the different observations in the two dimers.

$$\lambda = \lambda_i + \lambda_o \tag{4.6.36}$$

The following expression can be used to calculate λ_o based on the Marcus 2 sphere model.

$$\lambda_o = \frac{e^2}{4\pi\varepsilon_0}\left(\frac{1}{2R_D} + \frac{1}{2R_A} - \frac{1}{R_{DA}}\right)\left(\frac{1}{n^2} - \frac{1}{\varepsilon_s}\right) \tag{4.6.37}$$

The expression contains *e* as the elementary charge, ε_0 as the vacuum permittivity of space, n is the solvent index or refraction and ε_s is static dielectric constant. These are known values for benzonitrile. $R_{D/A}$ is the donor/acceptor radius and R_{DA} is the distance between donor/acceptor. Given both TIPS-BT1 & TIPS-BT1´ geometry an accurate estimate of $R_{D/A}$ can be difficult. With a known λ_o for TIPS-BT1´ and λ_i unlikely to change significantly between TIPS-BT1 & TIPS-BT1´, λ_o for TIPS-BT1 can be calculated by finding $\Delta\lambda_o$ between TIPS-BT1 & TIPS-BT1´. This has been done using equation 4.6.37 to derive the following expression, used to measure differences in outer-sphere reorganization energy.[4] Since TIPS-BT1 & TIPS-BT1´ share similar donor/acceptor moieties $R_{D/A}$ is expected to be the same for both molecules and cancel out in the expression, simplifying it.

$$\Delta\lambda_o = \lambda_{o,1} - \lambda_{o,2} = \frac{e^2}{4\pi\varepsilon_0}\left(\frac{1}{n^2} - \frac{1}{\varepsilon_s}\right)\left(\frac{1}{R_{DA,1}} - \frac{1}{R_{DA,2}}\right) \tag{4.6.38}$$

The only parameter left is R_{DA} the donor-acceptor distance. A distance of 11.317 angstroms for TIPS-BT1´, the same distance used in the Weller equation to determine the CT state energy, was used on the basis of the four orbital picture showing CT state formation being single electron HOMO-HOMO/LUMO-LUMO transfers from one chromophore arm to the other. For TIPS-BT1, a distance of 10.5 angstroms was used as that had previously been computed to be the chromophore-chromophore distance. Plugging in values for benzonitrile (n = 1.528[5] and ε_s = 25.9)

gives a value for $\Delta\lambda_o$= 45 meV. With the λ_o for TIPS-BT1′ measured to 1.15 eV, λ for TIPS-BT1 is expected to be ~1.10 eV.

4.6.10 Expected Temperature dependence of k_{SF}

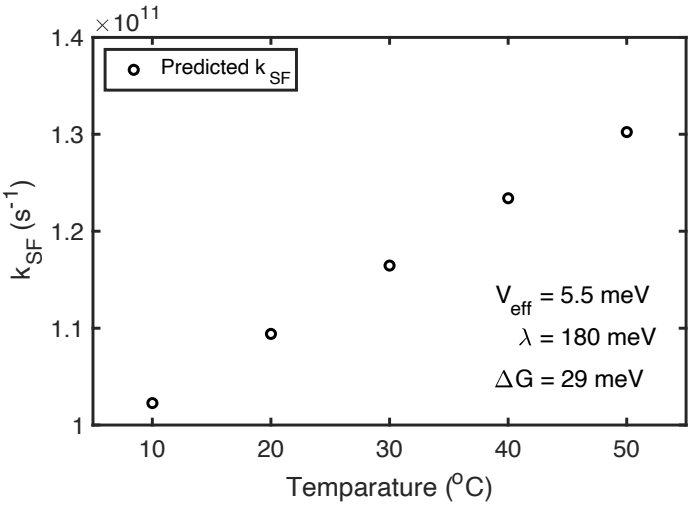

Figure 4.6.18 Predicted singlet fission rate constants for TIPS-BT1′ covering temperature range 10 °C to 50 °C.

4.6.11 TIPS-BT1′ Cartesian Coordinates

TMS-Tc-Nb Neutral Species – Molecular Coordinates

C	0.87270	-5.27895	0.09596
C	-0.55320	-5.32191	0.09664
C	1.52631	-4.08491	0.06388
C	0.80434	-2.84775	0.03040
C	-1.27726	-4.16929	0.06531
C	-0.63101	-2.89106	0.03130
C	1.46545	-1.60741	-0.00286
C	0.72955	-0.39086	-0.03592
C	-0.70527	-0.43422	-0.03449
C	-1.36598	-1.69320	-0.00067
C	1.37063	0.86491	-0.07075
C	0.66000	2.05144	-0.10204
C	-0.78438	2.00779	-0.09975
C	-1.42157	0.78031	-0.06719
C	1.32984	3.33130	-0.13969

C	0.58779	4.45862	-0.16236
C	-0.85867	4.41496	-0.15918
C	-1.53089	3.24466	-0.13422
C	0.95185	5.93966	-0.20387
C	-1.31142	5.87153	-0.19833
C	0.47351	6.50744	1.13562
C	-0.86156	6.46723	1.13890
C	-0.19823	6.44420	-1.11576
H	1.43575	-6.20665	0.12111
H	-1.05934	-6.28184	0.12229
H	2.61090	-4.04960	0.06311
H	-2.36201	-4.19883	0.06560
C	2.89208	-1.56172	-0.00318
C	-2.79276	-1.73158	0.00028
H	2.45634	0.89672	-0.07248
H	-2.50723	0.74615	-0.06610
H	2.41657	3.35591	-0.15380
H	-2.61719	3.20294	-0.14397
H	1.97613	6.16957	-0.49646
H	-2.34911	6.03938	-0.48586
H	1.13087	6.78655	1.95065
H	-1.53056	6.70638	1.95714
H	-0.23126	7.53458	-1.18940
H	-0.18720	5.99640	-2.11506
C	4.10953	-1.51428	-0.00321
C	-4.01098	-1.74889	0.00055
Si	5.95614	-1.44721	-0.00285
Si	-5.85859	-1.72962	-0.00353
C	6.51059	-0.49644	-1.52566
C	6.60093	-3.21132	-0.04698
C	6.51341	-0.57298	1.56426
C	-6.46422	-2.42212	1.63474
C	-6.45980	-2.78849	-1.43436
C	-6.40879	0.05443	-0.21605
H	6.17614	-0.99004	-2.44432
H	7.60456	-0.43299	-1.55441
H	6.11281	0.52405	-1.52259
H	6.26031	-3.73459	-0.94688
H	6.26140	-3.77863	0.82630
H	7.69703	-3.21541	-0.04773
H	6.11764	0.44719	1.61123
H	7.60753	-0.51319	1.59522
H	6.17858	-1.11015	2.45802
H	-6.12481	-3.45328	1.77981
H	-7.56004	-2.41943	1.66355
H	-6.10232	-1.82220	2.47650

H	-6.11618	-3.82359	-1.33389
H	-6.09893	-2.40088	-2.39299
H	-7.55555	-2.79724	-1.46362
H	-6.03781	0.68202	0.60147
H	-7.50302	0.11780	-0.22160
H	-6.04093	0.47166	-1.15960

TMS-Tc-Nb Anion – Molecular Coordinates

C	0.84372	-5.32448	0.08732
C	-0.56192	-5.36153	0.09155
C	1.49776	-4.11004	0.05524
C	0.79180	-2.88217	0.02637
C	-1.27892	-4.18315	0.06316
C	-0.63855	-2.91997	0.03035
C	1.46977	-1.61926	-0.00653
C	0.73256	-0.38497	-0.03606
C	-0.71197	-0.42324	-0.03161
C	-1.38255	-1.69487	0.00129
C	1.36662	0.86035	-0.07000
C	0.66046	2.07248	-0.09955
C	-0.77090	2.03460	-0.09415
C	-1.41150	0.78666	-0.06047
C	1.33228	3.34038	-0.13790
C	0.59634	4.48208	-0.16644
C	-0.83536	4.44424	-0.16029
C	-1.50943	3.26505	-0.12648
C	0.97164	5.96332	-0.20802
C	-1.28866	5.90377	-0.19790
C	0.49921	6.54945	1.12710
C	-0.83585	6.51422	1.13307
C	-0.17686	6.47449	-1.11951
H	1.41550	-6.24827	0.10905
H	-1.08414	-6.31414	0.11667
H	2.58394	-4.07953	0.05147
H	-2.36525	-4.20924	0.06599
C	2.88056	-1.58108	-0.00937
C	-2.79338	-1.72963	0.00364
H	2.45364	0.89162	-0.07397
H	-2.49859	0.76031	-0.05664
H	2.42037	3.36141	-0.14958
H	-2.59717	3.22808	-0.12938
H	1.99666	6.18898	-0.50403
H	-2.32677	6.07500	-0.48469
H	1.15872	6.83787	1.93759

H	-1.50239	6.76766	1.94949
H	-0.20598	7.56550	-1.19583
H	-0.16948	6.02413	-2.11775
C	4.10645	-1.53840	-0.01108
C	-4.01991	-1.74555	0.00459
Si	5.93298	-1.47300	-0.00157
Si	-5.84738	-1.72325	-0.00171
C	6.58268	-1.17573	-1.74519
C	6.60038	-3.11193	0.64386
C	6.50064	-0.06964	1.11991
C	-6.50947	-2.32990	1.65473
C	-6.49440	-2.83970	-1.37437
C	-6.42201	0.04591	-0.29975
H	6.28022	-1.98120	-2.42345
H	7.67838	-1.12950	-1.74272
H	6.20634	-0.23099	-2.15291
H	6.27416	-3.94793	0.01522
H	6.25762	-3.30363	1.66651
H	7.69678	-3.10306	0.65059
H	6.10909	0.89474	0.77746
H	7.59521	-0.00485	1.12879
H	6.16248	-0.22527	2.15021
H	-6.18101	-3.35423	1.86282
H	-7.60609	-2.32096	1.65486
H	-6.16634	-1.69113	2.47596
H	-6.16066	-3.87407	-1.23569
H	-6.14662	-2.50076	-2.35635
H	-7.59093	-2.83805	-1.38450
H	-6.05537	0.71798	0.48408
H	-7.51712	0.09891	-0.30495
H	-6.06086	0.42159	-1.26342

TMS-Tc-Nb Cation – Molecular Coordinates

C	0.81519	-5.27254	0.08336
C	-0.59206	-5.30222	0.08256
C	1.48584	-4.07060	0.05538
C	0.77416	-2.85035	0.02548
C	-1.31244	-4.12950	0.05403
C	-0.65263	-2.88048	0.02507
C	1.45791	-1.59597	-0.00444
C	0.72764	-0.37888	-0.03626
C	-0.71071	-0.40936	-0.03599
C	-1.38875	-1.65633	-0.00449
C	1.37905	0.85972	-0.06946

C	0.67419	2.06923	-0.10236
C	-0.76181	2.03874	-0.10124
C	-1.41436	0.80033	-0.06831
C	1.35845	3.32127	-0.14038
C	0.62091	4.46550	-0.16590
C	-0.81112	4.43511	-0.16372
C	-1.49912	3.26041	-0.13711
C	1.00562	5.93891	-0.20587
C	-1.25809	5.89108	-0.20178
C	0.53112	6.51153	1.13462
C	-0.80335	6.48329	1.13704
C	-0.13928	6.45542	-1.11903
H	1.37440	-6.20153	0.10608
H	-1.11159	-6.25400	0.10454
H	2.57009	-4.04864	0.05594
H	-2.39662	-4.15293	0.05327
C	2.87204	-1.57087	-0.00258
C	-2.80275	-1.68852	-0.00255
H	2.46454	0.88422	-0.06977
H	-2.49992	0.77853	-0.06815
H	2.44425	3.33746	-0.15306
H	-2.58471	3.22987	-0.14721
H	2.03314	6.15335	-0.49624
H	-2.29483	6.06183	-0.48837
H	1.19320	6.79344	1.94413
H	-1.47382	6.73704	1.94894
H	-0.16243	7.54563	-1.18862
H	-0.13167	6.01074	-2.11951
C	4.09105	-1.54680	-0.00038
C	-4.02185	-1.70599	-0.00069
Si	5.95416	-1.51211	0.00296
Si	-5.88522	-1.70895	0.00228
C	6.48959	-0.63888	-1.56829
C	6.54482	-3.29106	0.04516
C	6.48345	-0.56797	1.53482
C	-6.43049	-2.15211	1.74144
C	-6.44141	-2.99251	-1.24659
C	-6.43916	0.01626	-0.48100
H	6.13947	-1.17193	-2.45828
H	7.58351	-0.58865	-1.61201
H	6.10162	0.38435	-1.60539
H	6.19053	-3.84675	-0.82938
H	6.18998	-3.80445	0.94496
H	7.64021	-3.32397	0.04632
H	6.09794	0.45679	1.52247
H	7.57727	-0.51832	1.58183

H	6.12746	-1.05838	2.44669
H	-6.06640	-3.14318	2.03124
H	-7.52506	-2.16356	1.79560
H	-6.06290	-1.42354	2.47134
H	-6.07248	-3.98897	-0.98208
H	-6.08362	-2.74930	-2.25242
H	-7.53615	-3.03328	-1.27719
H	-6.06695	0.76416	0.22711
H	-7.53359	0.07210	-0.48862
H	-6.07989	0.28150	-1.48085

4.6.12 References

(1) Weller, A. Photoinduced Electron Transfer in Solution: Exciplex and Radical Ion Pair Formation Free Enthalpies and Their Solvent Dependence. *Zeitschrift fur Phys. Chemie* **1982**, *133* (1), 93–98.

(2) Triplet State Formation Efficiencies of Aromatic Hydrocarbons in Solution. *Proc. R. Soc. London. Ser. A. Math. Phys. Sci.* **1968**, *306* (1485), 257–273.

(3) Englman, R.; Jortner, J. The Energy Gap Law for Radiationless Transitions in Large Molecules. *Mol. Phys.* **1970**, *18* (2), 145–164.

(4) Sartor, S. M.; Lattke, Y. M.; McCarthy, B. G.; Miyake, G. M.; Damrauer, N. H. Effects of Naphthyl Connectivity on the Photophysics of Compact Organic Charge-Transfer Photoredox Catalysts. *J. Phys. Chem. A* **2019**, *123* (22), 4727–4736.

(5) Williams, M. The Merck Index: An Encyclopedia of Chemicals, Drugs, and Biologicals, 15th Edition Edited by M.J. O'Neil, Royal Society of Chemistry, Cambridge, UK ISBN 9781849736701;. *Drug Dev. Res.* **2013**, *74* (5), 339–339.

Chapter 5 Supporting Information

5.6.1 Molar Attenuation Coefficients

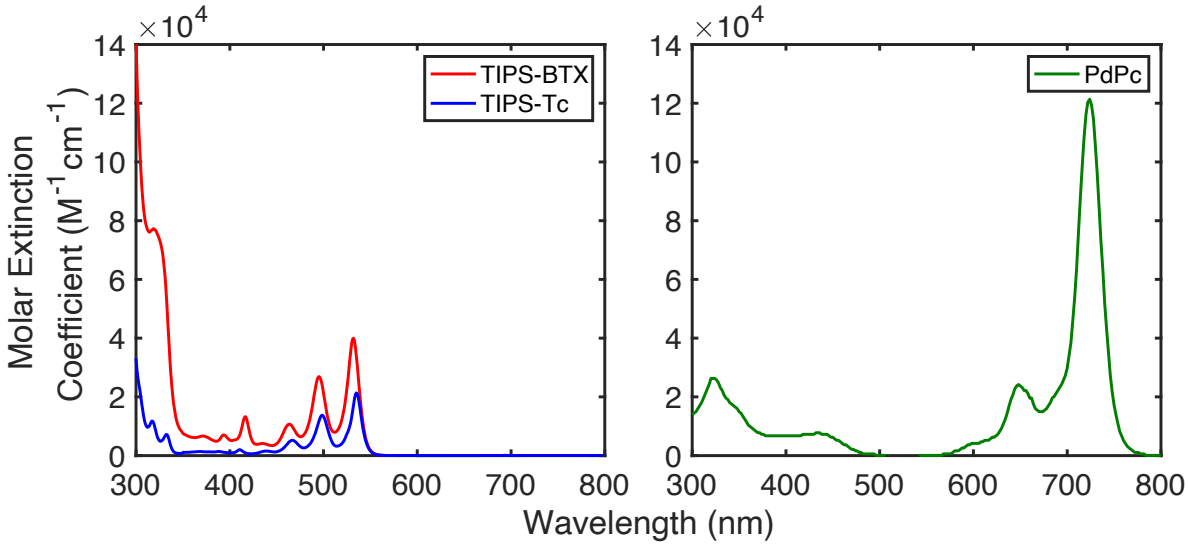

Figure 5.6.1 Molar extinction coefficients for TIPS-Tc & TIPS-BTX´ (left) and PdPc (right) in toluene. Molar extinction coefficient of PdPc at 730 nm was used to find absorption cross-section of sensitizer used in equation 5.6.7 in section 5.6.9.

5.6.2 Upconversion Sample Steady-State Absorption Spectra

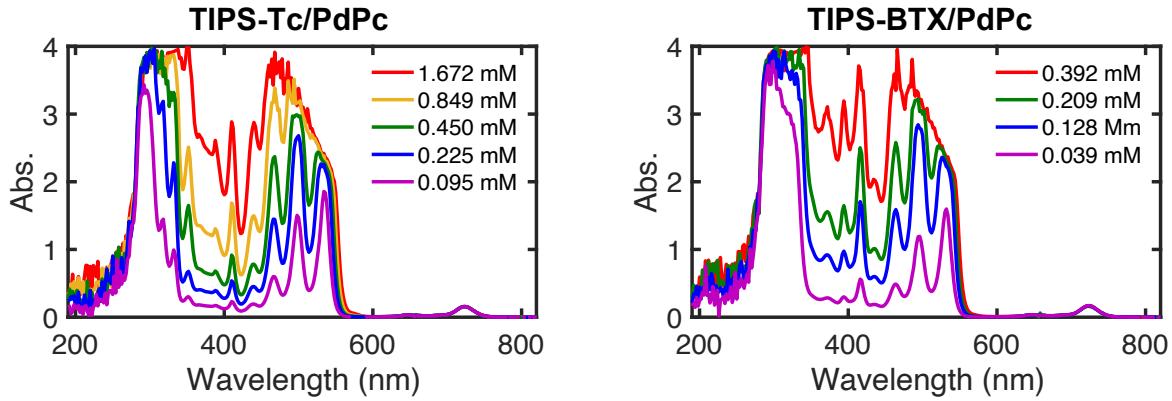

Figure 5.6.2 Steady-state absorption spectra for TIPS-Tc (left) and TIPS-BTX´ (right) upconversion samples.

5.6.3 Triplet Sensitization of Annihilator Species

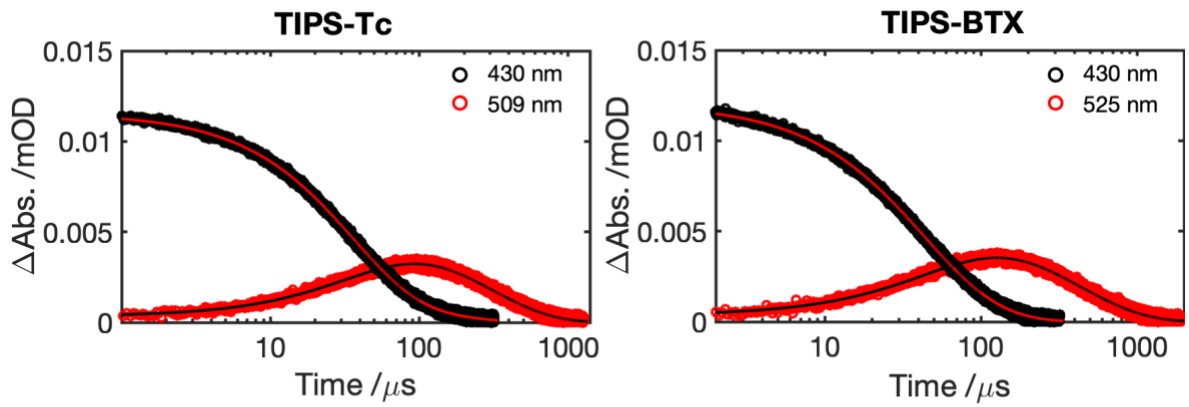

Figure 5.6.3 Kinetic traces with bi-exponential fit (solid lines) of anthracene and TIPS-Tc/TIPS-BTX´ in toluene. Decay of anthracene triplet (430 nm) corresponds with rise of sensitized triplet signal measured at 509 nm for TIPS-Tc and 525 nm for TIPS-BTX. Triplet lifetimes of TIPS-Tc/TIPS-BTX´ used in **Chapter 5** retrieved from the second lifetime in bi-exponential fit.

5.6.4 Triplet Lifetime of PdPc in Toluene

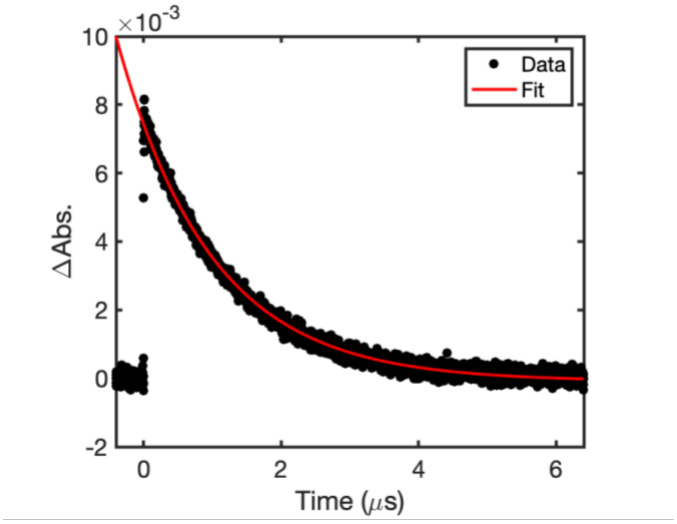

Figure 5.6.4 Kinetic trace of PdPc in toluene excited at 650 nm and observed at 600 nm. Fit to a 3.42 μs single exponential lifetime.

5.6.5 Raw Upconversion Quantum Yields

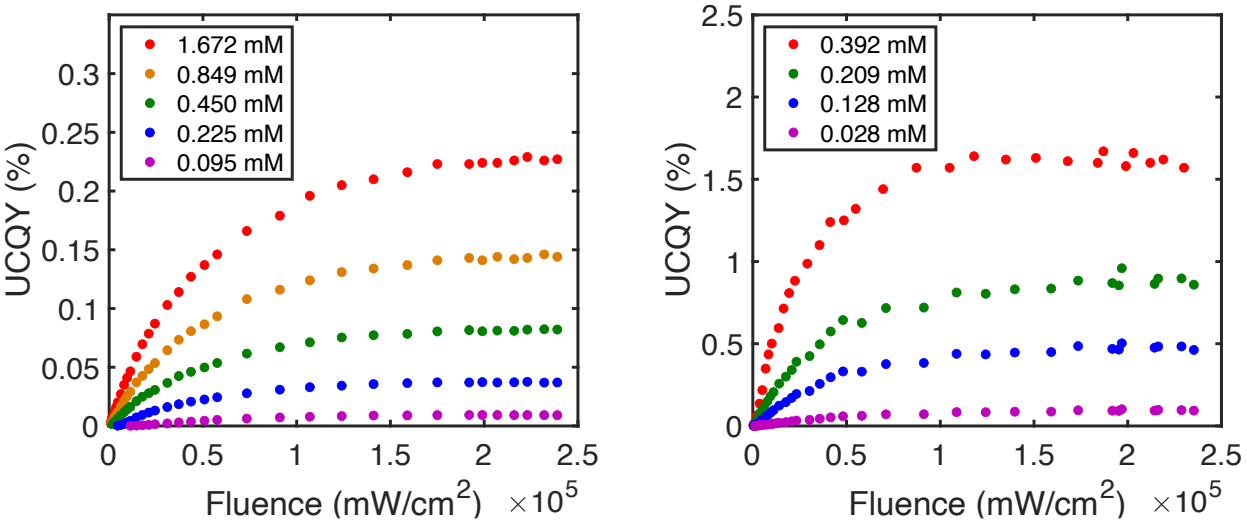

Figure 5.6.5 Fluence dependent upconversion QY for TIPS-Tc (left) and TIPS-BTX´ (right) upconversion samples (upconversion QY not corrected for sample self-absorption).

5.6.6 Crossing Points for TIPS-BTX´ and TIPS-Tc

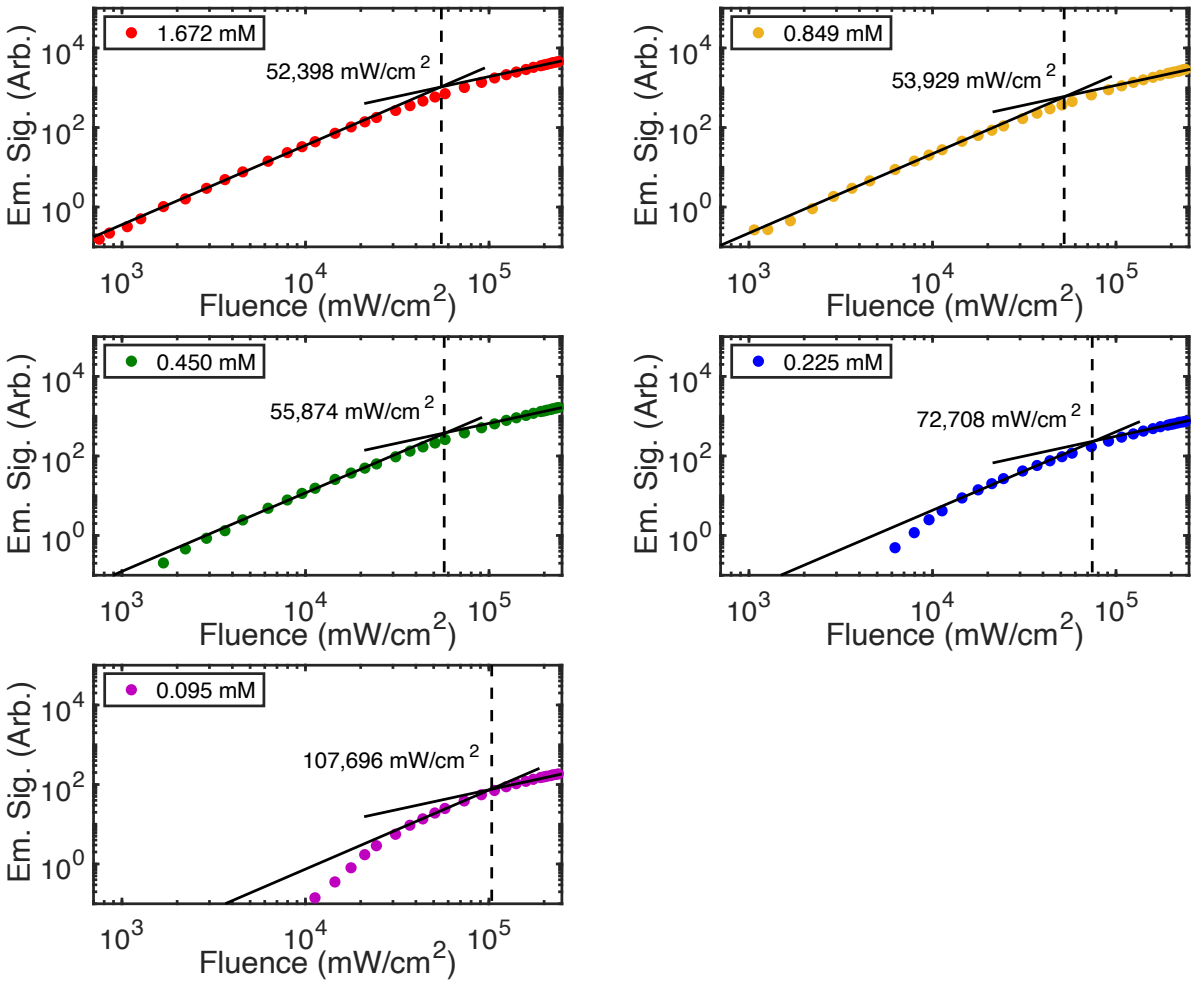

Figure 5.6.6 Measured quadratic-linear regime crossing points for TIPS-Tc upconversion samples.

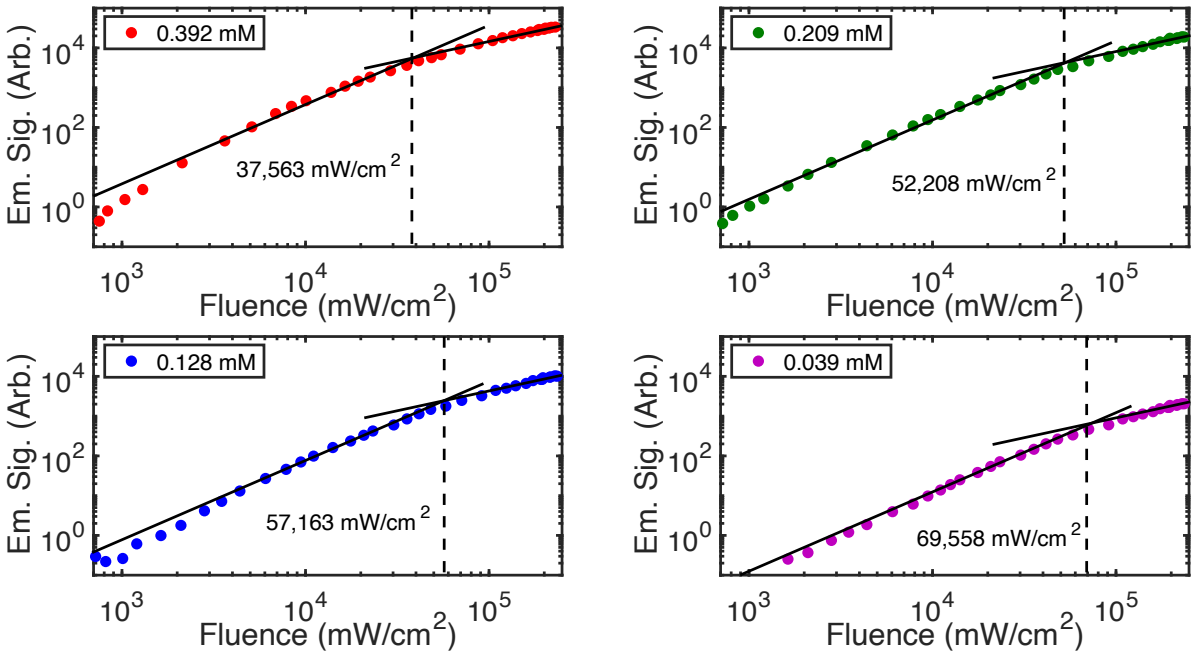

Figure 5.6.7 Measured quadratic-linear regime crossing points for TIPS-BTX′ upconversion samples.

5.6.7 Correction of Upconversion Spectra and UCQY

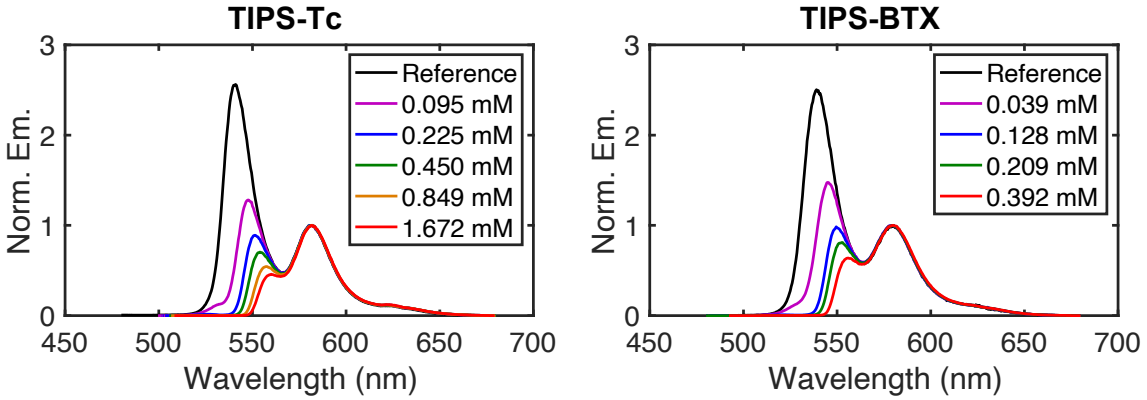

Figure 5.6.8 Upconversion emission spectra for TIPS-Tc (left) and TIPS-BTX′ (right) compared to direct emission spectra. Used to determine full UCQY.

To account for self-absorption in upconversion samples that would artificially lower the upconversion quantum yield equation 5.6.1 was employed to correct the yields. $\phi_{UC,raw}$ is the final UCQY fluence point in Fig. 5.6.4. This yield was then multiplied against the ratio of the integrated

emission intensity for the upconversion sample (Int_{Sample}) and a reference sample of just the annihilator in toluene directly excited ($Int_{Ref.}$).

$$\phi_{UC,corr.} = \phi_{UC,raw} \times \frac{Int_{Ref.}}{Int_{Sample}} \tag{5.6.1}$$

These correct UCQY values are the ones reported in the main text of **Chapter 5**.

5.6.8 Upconversion Efficiency Equations

Equation 5.6.2 is the four constituent yield processes that determine upconversion quantum yield (Φ_{UC}). 1. Sensitizer intersystem crossing yield (Φ_{ISC}, equation 5.6.3). 2. Triplet energy transfer yield from excited sensitizer to ground-state annihilator (Φ_{TET}, equation 5.6.4). 3. Triplet-triplet annihilation yield (Φ_{TTA}, equation 5.6.5). 4. Fluoresence quantum yield of annihilator (Φ_{Fl}, equation 5.6.6). Both Φ_{ISC} and Φ_{Fl} are first-order rate process and won't be impacted by sensitzer or annihilator concentration. Φ_{TET} and Φ_{TTA} are second-order rate processes and as such are dependent on sample concentrations.

$$\Phi_{UC} = \Phi_{ISC}\Phi_{TET}\Phi_{TTA}\Phi_{Fl} \tag{5.6.2}$$

$$\Phi_{ISC} = \frac{k_{ISC}}{k_{ISC} + k_{NR} + k_R} \tag{5.6.3}$$

$$\Phi_{TET} = \frac{k_{TET}[A_0]}{k_{TET}[A_0] + k_T} \tag{5.6.4}$$

$$\Phi_{TTA} = \frac{k_{TTA}[^3A^*]}{k_{TTA}[^3A^*] + k_T} \tag{5.6.5}$$

$$\Phi_{Fl} = \frac{k_R}{k_{ISC} + k_{NR} + k_R} \tag{5.6.6}$$

5.6.9 Kinetic Modeling of k_{TTA}

To determine k_{TTA} is equation 5.6.5 requires knowing the parameters Φ_{TTA}, k_T and $[^3A^*]$, the triplet excited state annihilator concentration. Both Φ_{TTA} and k_T are relatively easy to determine, Φ_{TTA} from measurement or literature values for equations 5.6.2-4, 5.6.6 and k_T from triplet sensitization. Determination of $[^3A^*]$ can be a more difficult task as direct observation can be difficult in typical upconversion samples and be prone to significant errors but can be modeled from experimental parameters the pump the upconversion system.

The following system of equation have been used previously for the purpose of modeling upconversion to determine $[^3A^*]$.[1] Equation 5.6.7 concerns the determination of $[^3S^*]$, the triplet excited state sensitizer concentration, under experimental conditions. Modeling was done on all monomer/dimer samples at the highest measured fluence.

$$\frac{d[^3S^*]}{dt} = \Phi_{laser}[S_0 - {}^3S^*]\sigma_{sens}\eta_{ISC} - k_{phos}[^3S^*] - k_{TET}[A_0][^3S^*] \tag{5.6.7}$$

The experimental parameters are the following:

1. Φ_{laser} – Photon fluence.
2. σ_{sens} – Absorption cross-section of sensitizer.
3. η_{ISC} – Sensitizer intersystem crossing yield.
4. k_{phos} – Sensitizer triplet decay rate constant.
5. k_{TET} – Triplet energy transfer rate constant.
6. $[A_0]$ – Annihilator ground state concentration.
7. $[S_0]$ – Sensitizer ground state concentration.

8. $[^3S^*]$ – Excited triplet sensitizer concentration.

The steady-state condition is applied equation 5.6.7, representing upconversion under constant excitation that experiments were performed at and produces equation 5.6.8.

$$0 = \Phi_{laser}[S_0 - {}^3S^*]\sigma_{sens}\eta_{ISC} - k_{phos}[^3S^*] - k_{TET}[A_0][^3S^*] \tag{5.6.8}$$

$[^3S^*]$ can be solved for now.

$$[^3S^*] = \frac{\Phi_{laser}[S_0]\sigma_{sens}\eta_{ISC}}{k_{phos} + k_{TET}[A_0] + \Phi_{laser}\sigma_{sens}\eta_{ISC}} \tag{5.6.9}$$

With $[^3S^*]$ determined the same approach can be used to determine $[^3A^*]$. Equation 5.6.10 is the differential equation used to model $[^3A^*]$. In equation S6, the only source of $[^3A^*]$ comes from TET, necessitating determination of $[^3S^*]$. $\left[\ {}^3A^*\ \right]$ has two decay channels, k_T representing decay from the triplet state and k_{TTA} as the TTA process and is a bi-molecular process.

$$\frac{d\left[\ {}^3A^*\ \right]}{dt} = -k_{TTA}[^3A^*]^2 - k_T[^3A^*] + k_{TET}[A_0][^3S^*] \tag{5.6.10}$$

The same steady-state condition is applied equation 5.6.10.

$$0 = -k_{TTA}[^3A^*]^2 - k_T[^3A^*] + k_{TET}[A_0][^3S^*] \tag{5.6.11}$$

Solving for $[^3A^*]$ with the quadratic formula gives the following expression with k_{TTA} being the only unknown parameter.

$$\left[\ {}^3A^*\ \right] = \frac{-k_T \pm \sqrt{{k_T}^2 - 4(-k_{TTA})(k_{TET}[A_0][^3S^*])}}{2(-k_{TTA})} \tag{5.6.12}$$

Equation 5.6.12 was along with equation 5.6.5 using determined Φ_{TTA} to solve a system of two equations with two unknowns to find k_{TTA} and $[^3A^*]$. Returned values are present in the main text.

5.6.10 Threshold Intensity

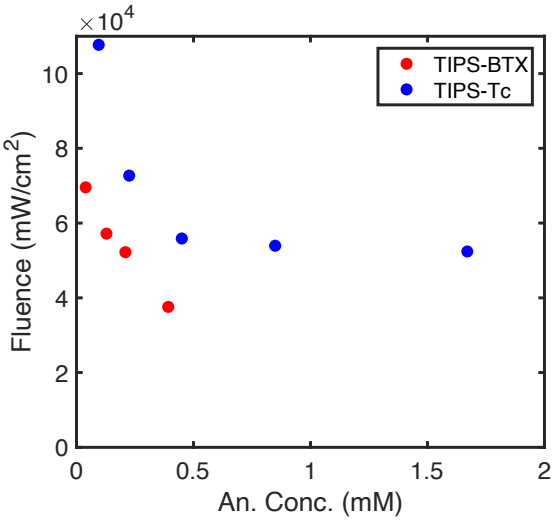

Figure 5.6.9 Annihilator concentration dependence of observed upconversion crossing points

5.6.11 Steady-State Decay Traces

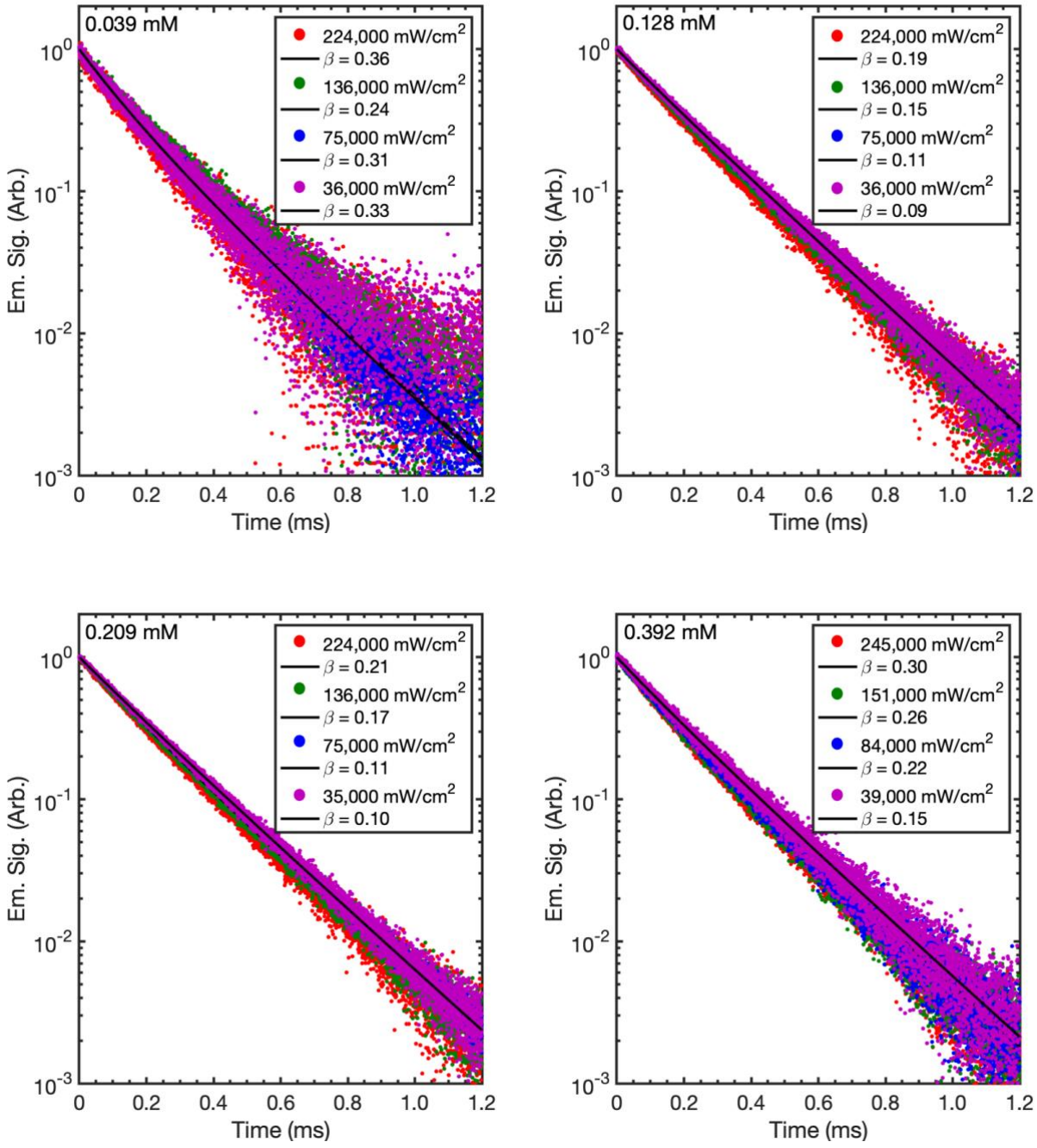

Figure 5.6.10 Steady-state decay kinetic traces for TIPS-BTX′ upconversion samples along with fit to equation 2.1. Kinetic traces include retrieved β from global analysis.

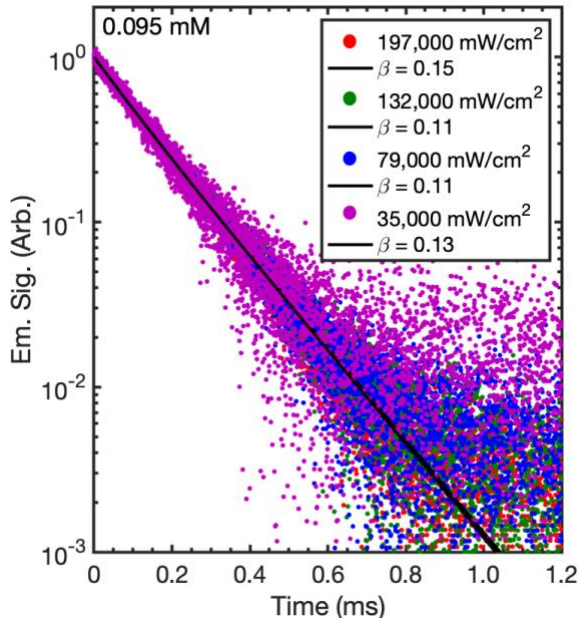
0.095 mM
197,000 mW/cm2
β = 0.15
132,000 mW/cm2
β = 0.11
79,000 mW/cm2
β = 0.11
35,000 mW/cm2
β = 0.13
Em. Sig. (Arb.)
Time (ms)

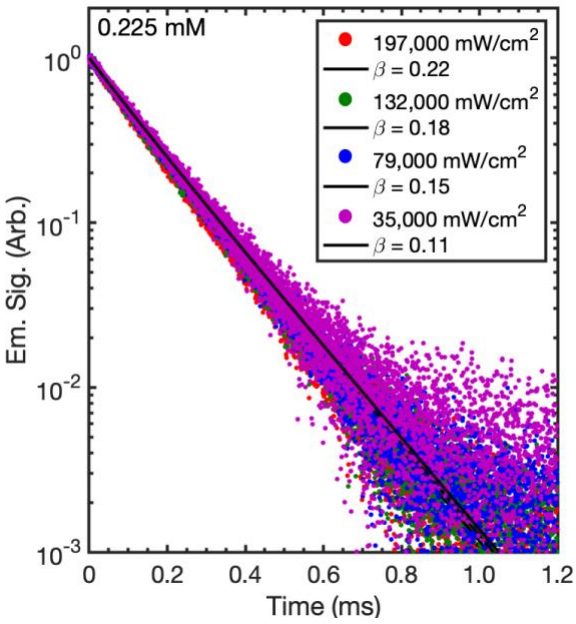
0.225 mM
197,000 mW/cm2
β = 0.22
132,000 mW/cm2
β = 0.18
79,000 mW/cm2
β = 0.15
35,000 mW/cm2
β = 0.11
Em. Sig. (Arb.)
Time (ms)

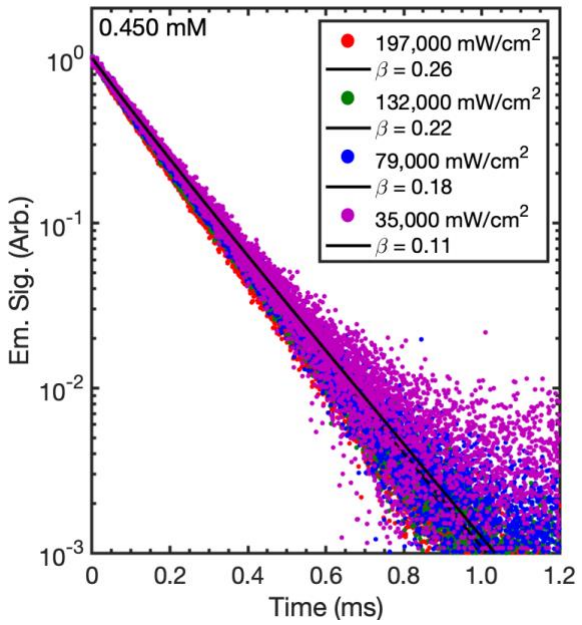
0.450 mM
197,000 mW/cm2
β = 0.26
132,000 mW/cm2
β = 0.22
79,000 mW/cm2
β = 0.18
35,000 mW/cm2
β = 0.11
Em. Sig. (Arb.)
Time (ms)

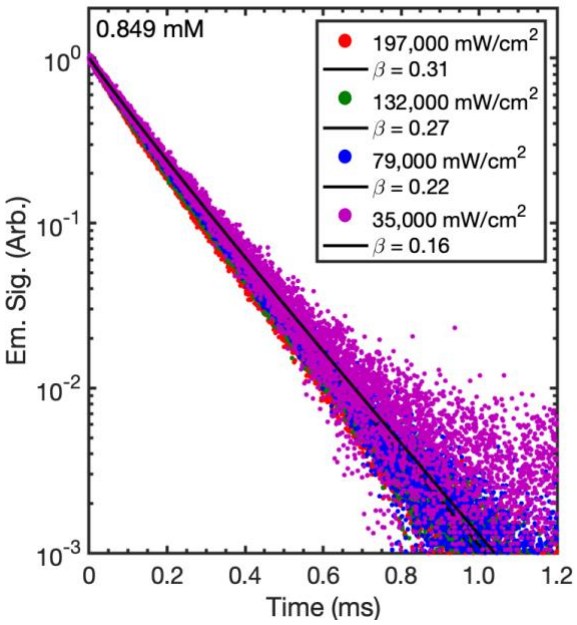
0.849 mM
197,000 mW/cm2
β = 0.31
132,000 mW/cm2
β = 0.27
79,000 mW/cm2
β = 0.22
35,000 mW/cm2
β = 0.16
Em. Sig. (Arb.)
Time (ms)

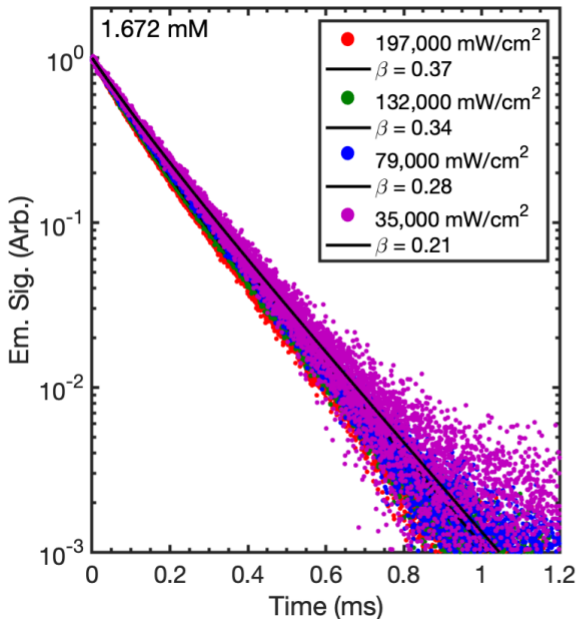

Figure 5.6.11 Steady-state decay kinetic traces for TIPS-Tc upconversion samples along with fit to equation 2.1. Kinetic traces include retrieved β from global analysis.

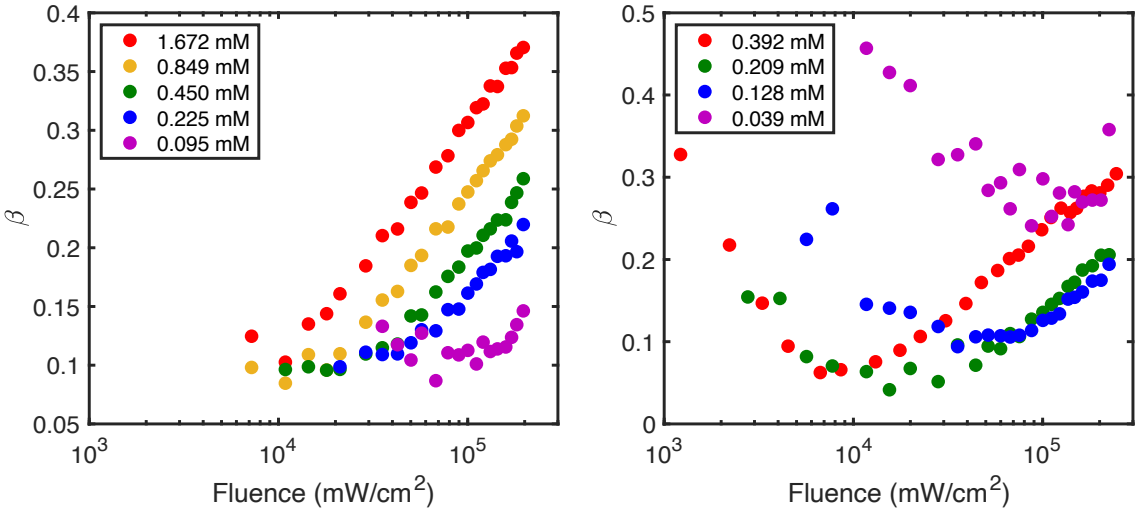

Figure 5.6.12 Fluence dependent β for TIPS-Tc (left) and TIPS-BTX′ (right) in toluene upconversion samples.

5.6.12 Kinetic Modeling of β

To model the second-order parameter β, the following set of differential equations taken from Albinsson et al were used. Equation 5.6.13 is the pumping equation to first determine $[^3S^*]$.[2,3]

$$\frac{d[^3S^*]}{dt} = k_{exc}\Phi_{ISC} - k_{Phos}[^3S^*] - k_{TET}[^3S^*][A_0] \tag{5.6.13}$$

The steady-state condition was applied to solve for $[^3S^*]$.

$$[^3S^*] = \frac{k_{exc}\Phi_{ISC}}{k_{Phos} + k_{TET}[A_0]} \tag{5.6.14}$$

With $[^3S^*]$ determined, $\left[\ ^3A^*\ \right]$ was calculated in a similar manner to section 5.6.10, starting with the differential rate equation.

$$\frac{d[^3A^*]}{dt} = -2 * k_{TTA}[^3A^*]^2 - k_T[^3A^*] + k_{TET}[^3S^*][A_0] \tag{5.6.15}$$

The steady-state condition was applied.

$$0 = -2 * k_{TTA}[^3A^*]^2 - k_T[^3A^*] + k_{TET}[^3S^*][A_0] \tag{5.6.16}$$

Equation 5.6.17 is the functional form to find β from $[^3A^*]$.

$$\beta = \frac{2 * k_{TTA}[^3A^*]}{2 * k_{TTA}[^3A^*] + k_T} \tag{5.6.17}$$

Both k_{TTA} and $\left[\ ^3A^*\ \right]$ were determined by modeling k_{TTA} in equations 5.6.16 and 5.6.17 to return a line of best-fit for β over a fluence corresponding to measured data.

$$k_{exc} = \frac{I_{exc}\lambda(1 - 10^{-A})}{hcN_AV_{exc}} \tag{5.6.18}$$

Equation 5.6.18 is the pumping rate constant used in equation 5.6.14 with the following experimental parameters:

1. I_{exc} – Excitation power.
2. λ – Wavelength of excitation.

3. A – Absorbance of sensitizer at excitation wavelength.
4. V_{exc} – Excitation volume of the pumping laser, determined from the beam spot size and cuvette length.

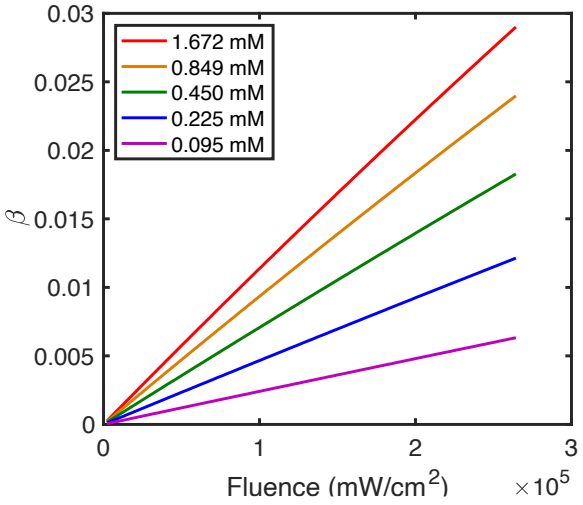

Figure 5.6.13 Predicted values for β over experimental fluence range with $k_{TTA} = 6.4\times10^5$ $M^{-1}s^{-1}$.

5.6.13 Computational Details

The performed computations used the same procedure and level of theory as those performed in **Chapter 4**. Calculations were performed in a solvent continuum model for toluene. The TIPS groups were removed for the geometry optimization to expedite the calculation. TD-DFT computations used the same basis set/functional as previous computations and were set to find the transitions to the six lowest energy singlet states.

5.6.14 TD-DFT Results

Excited State 1:	Singlet	2.6002 eV	476.82 nm	f = 0.0001	<S**2> = 0.000
204 → 207	HOMO – 1 →	LUMO + 1		0.49539	
205 → 206	HOMO →	LUMO		0.49873	

Excited State 2:	Singlet	2.6021 eV	476.47 nm	f = 0.5135	<S**2> = 0.000
204 → 206	HOMO – 1 →	LUMO		0.49830	
205 → 207	HOMO →	LUMO + 1		0.49596	
Excited State 3:	Singlet	3.6337 eV	341.20 nm	f = 0.3575	<S**2> = 0.000
198 → 206				0.31148	
200 → 207				0.39927	
203 → 206				–0.27394	
204 → 209				–0.25965	
205 → 211				0.26102	
Excited State 4:	Singlet	3.6399 eV	340.63 nm	f = 0.0015	<S**2> = 0.000
198 → 207				0.30839	
200 → 206				0.39673	
203 → 207				–0.26351	
204 → 211				0.27006	
205 → 209				–0.26913	
Excited State 5:	Singlet	3.9619 eV	312.94 nm	f = 0.0029	<S**2> = 0.000
199 → 207				–0.28798	
201 → 206				0.46200	
202 → 207				–0.35789	
204 → 210				0.14285	
205 → 208				–0.14234	
Excited State 6:	Singlet	3.9620 eV	312.93 nm	f = 0.0981	<S**2> = 0.000
199 → 206				–0.28954	
201 → 207				0.45900	
202 → 206				–0.36048	
204 → 208				–0.14185	
205 → 210				0.14323	

5.6.15 TIPS-BTX´ Cartesian Coordinates

C	4.74932	-0.72314	-0.58490
C	3.30217	-1.14179	-0.72274
C	3.30214	1.14186	-0.72254
C	2.78421	0.00011	-1.63000
H	1.69890	0.00010	-1.75762

H	3.26310	0.00020	-2.61310
C	2.65916	-0.79353	0.64653
C	2.65912	0.79334	0.64667
H	3.13319	-2.16409	-1.06614
H	3.13316	2.16422	-1.06575
C	5.89527	1.42798	-0.45214
C	5.89531	-1.42789	-0.45240
C	7.14573	0.72211	-0.31950
H	5.90363	2.51523	-0.45162
C	7.14575	-0.72201	-0.31963
H	5.90370	-2.51514	-0.45208
C	8.34790	1.39655	-0.19417
C	8.34794	-1.39644	-0.19441
C	9.57571	0.71809	-0.06344
C	9.57573	-0.71797	-0.06357
C	10.80762	1.41566	0.06771
C	10.80766	-1.41553	0.06746
C	12.01910	0.71845	0.19625
C	12.01912	-0.71831	0.19613
C	13.27156	-1.40216	0.32901
C	13.27152	1.40231	0.32924
C	4.74931	0.72322	-0.58476
C	-1.14529	0.69800	0.70863
C	0.00010	1.49299	0.69652
C	-1.14528	-0.69837	0.70855
C	1.14532	0.69818	0.70873
C	-0.00009	2.99551	0.68242
C	0.00018	-1.49329	0.69631
C	-2.65909	0.79323	0.64653
C	1.14533	-0.69841	0.70863
C	0.00003	-2.99581	0.68187
C	-2.65907	-0.79360	0.64655
C	-4.74934	-0.72333	-0.58472
C	-3.30220	-1.14204	-0.72262
C	-4.74929	0.72302	-0.58481
C	-3.30212	1.14160	-0.72271
H	3.15769	-1.28909	1.48367
H	3.15763	1.28878	1.48389
H	-0.02804	-3.39897	1.70122
H	-0.87369	-3.38633	0.15074
H	0.90071	-3.38677	0.19850
H	0.89240	3.38653	0.18406
H	-0.88256	3.38622	0.16619
H	-0.01063	3.39842	1.70221
H	-3.15759	1.28880	1.48369
H	-3.15749	-1.28916	1.48377

C	-2.78428	-0.00027	-1.63008
H	-3.26325	-0.00028	-2.61314
H	-1.69898	-0.00032	-1.75777
H	-3.13339	-2.16441	-1.06587
H	-3.13317	2.16393	-1.06605
C	14.43828	-0.71322	0.45278
C	14.43826	0.71338	0.45290
H	13.26823	2.48709	0.32900
H	13.26830	-2.48694	0.32859
C	10.80640	2.84567	0.06796
C	10.80649	-2.84554	0.06746
C	10.80205	-4.05352	0.06717
C	10.80191	4.05365	0.06779
H	8.34956	2.48244	-0.19508
H	8.34962	-2.48233	-0.19552
C	-5.89533	-1.42805	-0.45208
C	-7.14576	-0.72212	-0.31941
C	-7.14571	0.72200	-0.31953
C	-5.89523	1.42783	-0.45229
C	-8.34795	-1.39651	-0.19408
C	-9.57574	-0.71799	-0.06337
C	-9.57569	0.71807	-0.06352
C	-8.34787	1.39648	-0.19433
C	-10.80768	-1.41551	0.06776
C	-12.01913	-0.71824	0.19625
C	-10.80760	1.41569	0.06746
C	-12.01909	0.71852	0.19609
H	-8.34966	-2.48239	-0.19499
H	-8.34950	2.48237	-0.19545
H	-5.90374	-2.51529	-0.45160
H	-5.90357	2.51507	-0.45196
C	-10.80654	-2.84551	0.06804
C	-10.80636	2.84569	0.06742
C	-10.80185	4.05367	0.06701
C	-10.80212	-4.05349	0.06800
C	-13.27159	-1.40205	0.32922
C	-13.27151	1.40243	0.32891
C	-14.43830	-0.71306	0.45282
C	-14.43826	0.71354	0.45266
H	-13.26834	-2.48683	0.32902
H	-13.26820	2.48721	0.32845
H	15.37760	-1.24830	0.55234
H	15.37757	1.24847	0.55254
H	-15.37764	-1.24811	0.55245
H	-15.37757	1.24866	0.55216
H	10.79987	-5.12113	0.06721

H	10.79979	5.12125	0.06730
H	-10.79972	5.12128	0.06629
H	-10.80002	-5.12110	0.06814

5.6.16 References

(1) Imperiale, C. J.; Green, P. B.; Miller, E. G.; Damrauer, N. H.; Wilson, M. W. B. Triplet-Fusion Upconversion Using a Rigid Tetracene Homodimer. *J. Phys. Chem. Lett* **2019**, *10* (23), 7463–7469.

(2) Edhborg, F.; Olesund, A.; Albinsson, B. Best Practice in Determining Key Photophysical Parameters in Triplet–Triplet Annihilation Photon Upconversion. *Photochem. Photobiol. Sci.* **2022**, *21* (7), 1143–1158.

(3) Olesund, A.; Johnsson, J.; Edhborg, F.; Ghasemi, S.; Moth-Poulsen, K.; Albinsson, B. Approaching the Spin-Statistical Limit in Visible-to-Ultraviolet Photon Upconversion. *J. Am. Chem. Soc.* **2022**, *144* (8), 3706–3716.